

**NEXT GENERATION SEISMIC FRAGILITY CURVES FOR
CALIFORNIA BRIDGES INCORPORATING THE EVOLUTION IN
SEISMIC DESIGN PHILOSOPHY**

A Thesis
Presented to
The Academic Faculty

by

Karthik Narayan Ramanathan

In Partial Fulfillment
of the Requirements for the Degree
Doctor of Philosophy in the
School of Civil and Environmental Engineering

Georgia Institute of Technology
August 2012

Thesis Errata Sheet

Author Karthik Ramanathan

Primary Dept. Civil & Environmental Engineering

Degree Ph.D. **Graduation date** August, 2012

Thesis title

Next Generation Seismic Fragility Curves For California Bridges Incorporating the Evolution in Seismic Design Philosophy

Brief description of errata sheet

Although preliminary fragility models are presented in this report, they ARE NOT intended for deployment.

Planned subsequent project phases will complete validation work and adopt refined versions of both damage models and bridge taxonomy that are needed for deployment models.

Fragility Models presented in this report are preliminary and are not intended for deployment.

Supplemental analyses and discussion appear in the project report at <http://trid.trb.org/view/2012/M/1398010>.

Number of pages ¹_____ (15 maximum, including this page)

❖ **Author:** I request that the attached errata sheet be added to my thesis. I have attached two copies prepared as prescribed by the current *Specifications for Thesis Preparation*.

Signature of author _____ Date _____

❖ **Thesis Advisor or Dept. Chair:** I approve the attached errata sheet and recommend its addition to the student's thesis.

Signature _____ Date _____

Name _____ Thesis supervisor/Dept. Chair

❖ **VP for Graduate Education/Faculty Affairs:** I approve the attached errata sheet and direct the Institute Archives to insert it into all copies of the student's thesis held by the Georgia Tech Libraries, both print and electronic.

Signature _____ Date _____

Name _____

**NEXT GENERATION SEISMIC FRAGILITY CURVES FOR
CALIFORNIA BRIDGES INCORPORATING THE EVOLUTION IN
SEISMIC DESIGN PHILOSOPHY**

Approved by:

Dr. Reginald DesRoches, Co-advisor
School of Civil and Environmental
Engineering
Georgia Institute of Technology

Dr. Bruce R. Ellingwood
School of Civil and Environmental
Engineering
Georgia Institute of Technology

Dr. Barry Goodno
School of Civil and Environmental
Engineering
Georgia Institute of Technology

Dr. Jamie E. Padgett, Co-advisor
Department of Civil and Environmental
Engineering
Rice University

Dr. Lawrence F. Kahn
School of Civil and Environmental
Engineering
Georgia Institute of Technology

Dr. Seymour Goodman
The Sam Nunn School of International
Affairs
Georgia Institute of Technology

Date Approved: June 13, 2012

*I dedicate this research to my mother Shanthi, father Ramanathan, brother Vivek, and my
best friends*

ACKNOWLEDGEMENTS

I am extremely happy to record my profound gratitude to Dr. Reginald DesRoches and Dr. Jamie Padgett for their valuable guidance, sustained interest, keen encouragement and inspiring instruction. Putting to best use of their uncanny persuasive skills and scholarly erudition in tendering timely and valuable advice, they have been instrumental in bringing out this thesis in its present form. I thank them for all the patience and tremendous exposure given to me throughout my graduate career at Georgia Tech since August 2008.

I would like to thank my thesis committee Dr. Bruce Ellingwood, Dr. Barry Goodno, Dr. Lawrence Kahn and Dr. Seymour Goodman. They have provided encouragement, praise and guidance throughout my tenure at Georgia Tech. My special thanks to Dr. Ellingwood considering the many hours I spent in his office and his lectures discussing structural reliability and probability theory. I am grateful for the opportunity of working under the advisement of Dr. Seymour Goodman as a part of the Sam Nunn Security Fellowship and gaining key insight into aspects of science, technology and policy.

Georgia Tech has provided an excellent academic environment for education and research, and I would like to thank the support I have received from the California Department of Transportation to pursue my doctoral studies. I would like to express my sincere gratitude to Cliff Roblee, Mark Yashinsky, Mark Mahan, Loren Turner, and Tom Shantz for their time and patience in providing insight regarding bridge design

philosophy and seismic details which was instrumental in the presentation of this research.

I am extremely fortunate to be surrounded by a group of highly motivated and wonderful friends without whom life in Atlanta would have been miserable. I would like to sincerely thank my best friends Timothy Wright, Jieun Hur, Abdollah Shafieezadeh, Brittany Luken, and Nathan Mayercsik for all the encouragement and support over the last four years. Countless hours of laughter and lively discussions, travel, long and detailed discussions of technical aspects have reinforced the friendship and will never be forgotten. I would like to also thank my current officemates from Mason 522A and friends from the Structural Engineering group: Stephanie German, Jongsu Jeon, Laura Redmond, Jazalyn Dukes, Niki Fanouraki, Dapeng Zhu, Walter Yang, Reza Mirzaeifar, Amal Jayapalan, Chrish Shearer

I would be remiss if I did not acknowledge my best friends and true well wishers Malini Katta, Sandeep Degala, Karthik Chittepup, Harika Boga and Jyotirmoy Sircar, in no specific order, for all the support and encouragement. Over the years they have expressed tremendous confidence in my abilities ever since my first acquaintance with them during my undergraduate career in India. Their tremendous patience, countless hours of funny telephonic conversations and good wishes are instrumental in my pursuit of a doctoral degree.

Finally, I am extremely thankful to my parents and brother for their unconditional love, encouragement and support, without which I would not be here today. No words can explain how grateful I am and how fortunate I feel.

TABLE OF CONTENTS

	Page
ACKNOWLEDGEMENTS	iv
LIST OF TABLES	xi
LIST OF FIGURES	xv
SUMMARY	xxi
<u>CHAPTER</u>	
1 INTRODUCTION	1
1.1 Problem Description and Motivation	1
1.2 Research Objectives	5
1.3 Dissertation Outline	6
2 EXISTING RESEARCH ON HIGHWAY BRIDGE FRAGILITY – A STATE OF THE ART SUMMARY	8
2.1 Evolution in the Development of Fragility Curves	10
2.1.1 Response Spectrum Analysis (RSA)	14
2.1.2 Nonlinear Static Procedure (NSP) or Capacity Spectrum Method (CSM)	15
2.1.3 Nonlinear Time History Analysis (NLTHA)	16
2.1.4 Incremental Dynamic Analysis (IDA)	18
2.2 Structural Reliability Assessment Techniques for Bridges	20
2.3 Fragilities for Bridge Classes, HAZUS and the Necessity to go Beyond HAZUS	24
2.3.1 Emergence of Seismic Design Provisions for Bridges in California	27
2.4 Closure	29

3	CALIFORNIA BRIDGE DESIGN ATTRIBUTES	31
3.1	Bridge Classification Based on National Bridge Inventory and HAZUS	31
3.2	Bridge Class Statistics	35
3.3	Need for Sub-binning Beyond NBI	40
3.4	Bridge Design Eras and Typical Design Details	40
3.4.1	Pre 1971 Design Era	41
3.4.2	1971-1990 Design Era	42
3.4.3	Post 1990 Design Era	43
3.5	Bridge Components and Typical Details	45
3.5.1	Bridge Superstructure	45
3.5.2	Columns	48
3.5.3	Superstructure to Substructure Connectivity	53
3.5.4	Abutments	58
3.5.5	Foundation Systems	63
3.5.6	Seat, Bearings, Restrainers and Shear Keys	67
3.6	Conventional Bridge Classes and Seismic Performance Sub-bins	72
3.7	Closure	74
4	ANALYTICAL MODELING PROCEDURES AND DETERMINISTIC BRIDGE COMPONENT RESPONSES	75
4.1	Bridge Component Modeling Strategies	76
4.1.1	Substructure – Single and Multi Column Concrete Bents	76
4.1.2	Abutments	81
4.1.3	Deck Elements	85
4.1.4	Elastomeric Bearing Pads	86
4.1.5	Shear Keys	87

4.1.6 Restrainers	90
4.1.7 Impact or Pounding Elements	92
4.2 Global Bridge Finite Element Models	93
4.3 Analytical Bridge Models and Deterministic Responses	94
4.3.1 Multispan Continuous Concrete Single Frame Box Girder Bridges	96
4.3.2 Multispan Continuous Concrete Slab Bridges	110
4.3.3 Multispan Continuous Concrete Tee Girder Bridges	121
4.3.4 Multispan Continuous Concrete I-Girder Bridges	129
4.4 Closure	139
5 FRAGILITY FRAMEWORK	142
5.1 Ground Motion Suite	145
5.2 Parameterized Stochastic Finite Element Models and Propagation Of Uncertainty	148
5.2.1 Uncertainty in Material Parameters	149
5.2.2 Uncertainty in Geometric and Structural Parameters	150
5.2.3 Uncertainty in Other Parameters	155
5.2.4 Parameterized Stochastic Bridge Models	156
5.3 Probabilistic Seismic Demand Models	158
5.4 Choice of an Optimal Intensity Measure	160
5.4.1 Introduction and Characteristics of an Optimal Intensity Measures	160
5.4.2 Practicality, Efficiency and Proficiency	163
5.4.3 Sufficiency	164
5.4.4 Hazard Computability	167
5.4.5 Optimal IMs across Bridge Classes and Seismic Performance Sub-bins	168

5.5 Component Capacity or Limit State Models	168
5.5.1 Columns	175
5.5.2 Abutment Seat and Joint Seal	178
5.5.3 Superstructure Deck	180
5.5.4 Abutments – Passive, Active and Transverse Responses	180
5.5.5 Bent Foundation – Translation and Rotational Responses	181
5.5.6 Elastomeric Bearing Pads, Restrainers and Shear Keys	182
5.5.7 Component Limit States Summary	183
5.6 Closure	184
6 SYSTEM AND COMPONENT FRAGILITY CURVES	185
6.1 Multispan Continuous Concrete Slab Bridges	188
6.2 Multispan Continuous Concrete Single Frame Box-girder Bridges	193
6.2.1 Trends based on Diaphragm Abutments	194
6.2.2 Trends based on Seat Abutments	197
6.2.3 Trends based on the Design Era	199
6.2.4 Effect of Gap Size on the Fragility of Post 1990 MSCC-BG bridges	202
6.3 Multispan Continuous Concrete Tee-girder Bridges	206
6.3.1 Trends based on Diaphragm Abutments	209
6.3.2 Trends based on Seat Abutments	210
6.3.3 Trends based on the Design Era	211
6.4 Multispan Continuous Concrete I-girder Bridges	215
6.4.1 Trends based on Diaphragm Abutments	216
6.4.2 Trends based on Seat Abutments	217
6.4.3 Trends based on the Design Era	219
6.5 HAZUS Comparison	221

6.6 Closure	225
7 CONCLUSIONS AND FUTURE WORK	227
7.1 Summary and Conclusions	227
7.2 Research Impact	232
7.3 Recommendations for Future Work	233
APPENDIX A: COMPONENT ATTRIBUTES AND MODELING ASSUMPTIONS	236
APPENDIX B: PROBABILISTIC SEISMIC DEMAND MODELS AND CORRELATION MATRICES	250
APPENDIX C: OPTIMAL INTENSITY MEASURE INVESTIGATION	270
APPENDIX D: COMPONENT FRAGILITY CURVES FOR BRIDGE CLASSES AND SEISMIC PERFORMANCE SUB-BINS	277
APPENDIX E: COMPARISON OF THE BRIDGE CLASS SYSTEM FRAGILITIES WITH HAZUS	293
REFERENCES	296
VITA	307

LIST OF TABLES

	Page
Table 3.1: Kind of material and/or design listed in NBI	32
Table 3.2: Type of design and/or construction listed in NBI	33
Table 3.3: Bridge classes in California and their proportion in the overall inventory	34
Table 3.4: Bridge classes considered for fragility modeling	35
Table 3.5: General statistics for bridge class geometrical parameters	38
Table 3.6: Type of seals adopted in bridge joints	68
Table 3.7: Distribution of gap sizes in the California state bridge inventory	69
Table 3.8: Conventional bridge class codes (BC) adopted in the present study	73
Table 3.9: Seismic performance sub-bins (SPS) in each bridge class	73
Table 4.1: Deterministic bridge model attributes for MSCC single frame box-girder bridges	99
Table 4.2: First and second mode time periods for MSCC-BG bridges considered for deterministic analysis	100
Table 4.3: Modal time periods for MSCC-SL bridges	114
Table 4.4: Modal periods for MSCC-TG bridges with circular columns	124
Table 4.5: Modal periods for MSCC-TG bridges with integral pile columns	125
Table 4.6: Model time periods for MSCC-IG bridges with seat and diaphragm abutments	133
Table 5.1: Distributions for longitudinal and transverse reinforcement ratios in bridge columns	151
Table 5.2: Probability distributions for foundation translational and rotational spring stiffnesses	154
Table 5.3: Engineering demand parameters for bridge components monitored in NLTHA	157
Table 5.4: Intensity measures investigated for optimality	163

Table 5.5: Optimal IM across the bridge classes and the respective SPS considered in this study	168
Table 5.6: List of primary and secondary components in the bridge classes considered in this study	170
Table 5.7: General description of bridge system level damage states along with component damage thresholds	173
Table 5.8: Component level damage state descriptions – Component Damage Thresholds (CDT) for Primary Components	173
Table 5.9: Component level damage state descriptions – Component Damage Thresholds (CDT) for Secondary Components	174
Table 5.10: Median values of column CDTs along with damage description and likely emergency and permanent repair strategies	177
Table 5.11: Median values of CDT for abutment seat	179
Table 5.12: Median values of CDT for joint seal	179
Table 5.13: CDT values for maximum deck displacement	180
Table 5.14: CDT values for abutment passive, active and transverse response	181
Table 5.15: CDT values for translation and rotational foundation response	181
Table 5.16: CDT values for elastomeric bearing pads, restrainers and shear keys	183
Table 5.17: Summary of CDT values adopted in this study	183
Table 6.1: Multispan continuous slab bridge fragilities	189
Table 6.2: Details of the most vulnerable component across the SPS for MSCC-SL bridge class	193
Table 6.3: Multispan continuous concrete box-girder bridge fragilities	194
Table 6.4: Details of the most vulnerable component for MSCC-BG bridge class and diaphragm abutments	196
Table 6.5: Details of the most vulnerable component for MSCC-BG bridge class and seat abutments	199
Table 6.6: System fragilities for post 1990 designed MSCC-BG bridges with strip and modular joint seat assemblies	204
Table 6.7: Multispan continuous concrete Tee-girder bridge fragilities	207

Table 6.8: List of the most vulnerable component across damage states for the SPS in MSCC-TG bridge class	209
Table 6.9: Percentage reduction in vulnerability of diaphragm abutments with respect to seat abutments in MSCC-TG bridges	215
Table 6.10: Multispan continuous concrete I-girder bridge fragilities	216
Table 6.11: Details of the most vulnerable component for MSCC-IG bridge class	219
Table 6.12: HAZUS damage state definitions	222
Table 6.13: Median values and dispersion for the HAZUS fragilities	223
Table A.1: Soil profiles considered in the stiffness calculations	237
Table A.2: Details of foundation systems	238
Table A.3: Bridge component details for MSCC-BG bridge class and its seismic performance sub-bins	240
Table A.4: Box-girder cell center-to-center spacing and deck slab thickness	241
Table A.5: Number of cells in the box-girder and number of columns per bent as a function of deck width for MSCC-BG bridges	242
Table A.6: Bridge component details for MSCC-SL bridge class	243
Table A.7: Bridge component details for MSCC-TG bridge class and the respective seismic performance sub-bins	246
Table A.8: Number of superstructure girders and number of columns per bent as a function of deck width for MSCC-TG bridges	247
Table A.9: Bridge component details for MSCC-IG bridge class and the respective seismic performance sub-bins	248
Table A.10: Number of superstructure girders and number of columns per bent as a function of deck width for MSCC-IG bridges	249
Table B.1: PSDMs for multispan continuous concrete box-girder bridge class and the respective seismic performance sub-bins	251
Table B.2: PSDMs for multispan continuous concrete slab bridge class and the respective seismic performance sub-bins	253
Table B.3: PSDMs for multispan continuous concrete Tee-girder bridge class and the respective seismic performance sub-bins	254

Table B.4: PSDMs for multispan continuous concrete I-girder bridge class and the respective seismic performance sub-bins	256
Table B.5: Correlation Coefficients of the component demands of multispan continuous concrete box-girder bridge class and the respective seismic performance sub-bins	258
Table B.6: Correlation Coefficients of the component demands of multispan continuous concrete slab bridge class and the respective seismic performance sub-bins	262
Table B.7: Correlation Coefficients of the component demands of multispan continuous concrete Tee-girder bridge class and the respective seismic performance sub-bins	263
Table B.8: Correlation Coefficients of the component demands of multispan continuous concrete I-girder bridge class and the respective seismic performance sub-bins	266
Table C.1: Investigation of efficiency, proficiency, practicality and sufficiency properties to investigate optimality of intensity measures	271
Table D.1: Component level fragility relationships for multispan continuous concrete box-girder bridge class and the respective seismic performance sub-bins	278
Table D.2: Component level fragility relationships for multispan continuous concrete slab bridge class and the respective seismic performance sub-bins	282
Table D.3: Component level fragility relationships for multispan continuous concrete Tee-girder bridge class and the respective seismic performance sub-bins	283
Table D.4: Component level fragility relationships for multispan continuous concrete I-girder bridge class and the respective seismic performance sub-bins	287
Table E.1: Percentage change in the median values and dispersions of the bridge class fragilities with respect to HAZUS fragilities	293

LIST OF FIGURES

	Page
Figure 2.1: Schematic representation of seismic risk assessment	10
Figure 2.2: Existing fragility curves for multispan continuous concrete box-girder bridges a) seismically designed, b) non-seismically designed	13
Figure 2.3: Schematic representation of the NLTHA procedure used to develop PSDMs	17
Figure 2.4: Schematic representation of the IDA procedure used to develop PSDMs	19
Figure 3.1: Empirical cumulative distribution functions for the chosen bridge classes for a) maximum span length, b) deck width, and c) minimum vertical underclearance	37
Figure 3.2: Probability mass function for number of spans for a) MSC-SBG, b) MSCSL, c) MSCG-T and MSCG-I bridge classes	39
Figure 3.3: Superstructure and substructure classification for different bridge classes	46
Figure 3.4: a) Large relative displacements between deck and the abutment backwall during Northridge earthquake, b) span unseating in the Cypress Street Viaduct during the Loma Prieta earthquake, c) deck collapse in the Interstate 5 overpass during the Northridge earthquake, d) deck damage in the Bolu viaduct during the 1999 Duzce earthquake, and e) pounding damage in Santa Clara River bridge between the deck and abutment backwall during the Northridge earthquake	48
Figure 3.5: Shear failure in bridge columns a) at the intersection of Interstate 5 and 210, and b) of Foothills Freeway Overpass, during the San Fernando earthquake	50
Figure 3.6: Column pull out failures during the San Fernando earthquake	51
Figure 3.7: Shear failure in the a) and c) plastic hinge region of column, and b) flared column, during the Northridge earthquake	52
Figure 3.8: Lateral force deformation curves for typical bridge columns through the design eras	53
Figure 3.9: Schematic of superstructure to substructure connectivity types	55

Figure 3.10: Joint damage to the Embarcadero viaduct during the Loma Prieta earthquake	57
Figure 3.11: Typical joint details from a) Pre 1971 design era in MSCC-SBG, b) Post 1990 MSC-SBG, c) MSCSL, and d) MSCG-I girder bridge class	57
Figure 3.12: Schematic of abutment configurations	59
Figure 3.13: Standard details for diaphragm abutments a) without footing, and b) with footing	60
Figure 3.14: Abutment pile damage during the 1991 Costa Rica earthquake	61
Figure 3.15: Standard details for seat type abutments	62
Figure 3.16: a) Damage to external shear keys, b) span unseating during the Northridge earthquake	63
Figure 3.17: Bridge foundation types	65
Figure 3.18: Pile supported footing retrofit	66
Figure 3.19: a) Type A and Type B joint seals, b) strip seal joint assembly and c) modular joint assembly	69
Figure 3.20: Precast girder and cap beam restrainer	70
Figure 3.21: Schematic showing restrainer layout at a typical seat type abutment	71
Figure 3.22: Damage to abutment shear keys during the Loma Prieta earthquake	72
Figure 4.1: Finite element discretization of the bent	77
Figure 4.2: Concrete stress strain curves with varying transverse reinforcement confinement ratios	78
Figure 4.3: Fiber based discretization of a circular reinforced concrete column and bent beam	80
Figure 4.4: Force displacement response of the abutment backfill	83
Figure 4.5: Force displacement response of the pile	85
Figure 4.6: Effective width of the superstructure	86
Figure 4.7: Force displacement response of an elastomeric bearing pad	87
Figure 4.8: Force displacement model for the shear key	89

Figure 4.9: Load displacement curves from the experimental testing of abutment shear keys	89
Figure 4.10: Stress strain curve for $\frac{3}{4}$ in restrainer cable	91
Figure 4.11: Force deformation response of the restrainer cable	92
Figure 4.12: Analytical model for pounding between deck and abutment backwall	93
Figure 4.13: Fault normal and fault parallel components of ground motion used in deterministic analyses	95
Figure 4.14: General layout of MSCC-BG bridges	98
Figure 4.15: Fundamental mode shapes for Post 1990 MSCC-BG bridges with SCBs and MCBs	101
Figure 4.16: Displacement response of the deck for a MSCC-BG bridge with four columns in the 1971-1990 design era	102
Figure 4.17: Moment curvature response of columns	103
Figure 4.18: Comparison of column moment curvature responses	105
Figure 4.19: Variation of curvature over the height of a column	106
Figure 4.20: Response of abutment backfill - pile systems in MSCC-BG bridges designed in the 1971-1990 design era	108
Figure 4.21: Influence of abutment backfill soil type on the response of bridge components	109
Figure 4.22: Response of a) elastomeric bearing pads, and b) restrainer cables in the longitudinal direction	110
Figure 4.23: General layout of MSCC-SL bridge	112
Figure 4.24: Mode shapes for MSCC-SL bridges with diaphragm and seat abutments	114
Figure 4.25: Longitudinal and transverse displacement of the individual spans in a MSCC-SL bridge with diaphragm and seat abutments	116
Figure 4.26: Response of MSCC-SL bridge columns in longitudinal and transverse direction	117
Figure 4.27: Moment curvature responses for different pile classes and pile types	117

Figure 4.28: Variation of curvature over the height of the column for an MSCC-SL bridge with seat abutments	119
Figure 4.29: Response of abutment soil-pile system in MSCC-SL bridge with diaphragm and seat abutments	120
Figure 4.30: Response of elastomeric bearing pads in MSCC-SL bridge with seat abutments in the a) longitudinal, and b) transverse direction	121
Figure 4.31: Typical layout of MSCC-TG bridges	123
Figure 4.32: First and second mode shapes for MSCC-TG bridges	126
Figure 4.33: Response of components in MSCC-TG bridges with integral pile columns and circular multi column bents	127
Figure 4.34: Typical layout of MSCC-IG bridges	131
Figure 4.35: First and second mode shapes for MSCC-IG bridges with diaphragm and seat abutments	133
Figure 4.36: Variation of curvature over the height of the columns in MSCC-IG bridges with diaphragm abutments	134
Figure 4.37: Abutment backfill soil-pile responses in longitudinal and transverse directions for MSCC-IG bridges with diaphragm abutments	136
Figure 4.38: Longitudinal response of elastomeric bearing pads and transverse response of shear keys in MSCC-IG with seat abutments	138
Figure 5.1: Schematic of the fragility framework	143
Figure 5.2: Distribution of magnitude, distance and PGA in the Baker suite of 160 ground motions	146
Figure 5.3: Response spectra for the scaled and unscaled ground motions in the Baker suite	147
Figure 5.4: Schematic representation of the NLTHA procedure to derive peak component demands	157
Figure 5.5: Illustration of a typical PSDM	159
Figure 5.6: PSDMs for a) column curvature ductility, and b) abutment seat displacement in post 1990 designed MSCC-BG-M bridges	164
Figure 5.7: Plots showing the linear regression of the residuals for column curvature ductility in 1971-1990 designed MSCC-IG-M bridges with respect to a) magnitude, b) distance, and c) epsilon	167

Figure 5.8: Depiction of CDTs for pre 1971 designed brittle columns	175
Figure 5.9: Depiction of CDTs for 1971-1990 era designed strength degrading column	176
Figure 5.10: Depiction of CDTs for a post 1990 designed ductile column	176
Figure 6.1: Plot of median values for MSCC-SL bridges across all damage states	191
Figure 6.2: Illustration of change in median values and relative vulnerability	191
Figure 6.3: System and component level fragility curves for MSCC-SL bridges with seat type abutments and seat width class S1 and S3	193
Figure 6.4: Fragility curves for MSCC-BG bridges with diaphragm abutments across design eras having a) single column bents, and b) multi column bents	196
Figure 6.5: Plot of median values for MSCC-BG bridges with seat abutments across design eras for a) single column bents, b) multi column bents	197
Figure 6.6: Plot of median values of system fragility for a) pre 1971, b) 1971-1990, and c) post 1990 design era	201
Figure 6.7: Comparison of median values for bridge fragility curves for post 1990 MSCC-BG bridges with small and large gaps installed with different joint seal units	204
Figure 6.8: System and component level fragility curves for post 1990 MSCC-BG bridges with SCB and MCB equipped with modular joint seal assembly systems	206
Figure 6.9: Comparison of median values of system fragility for MSCC-TG bridge class	208
Figure 6.10: Plot of median values of system fragility across damage states for MSCC-TG bridges designed a) pre 1971, b) 1971-1990, and c) post 1990	214
Figure 6.11: System and component fragility curves for a) MSCC-TG-M-E2-S4, and b) MSCC-TG-M-E1-S4	215
Figure 6.12: Plot of median fragilities for MSCC-IG with diaphragm abutments consisting of a) single column bents, b) multi column bents, across design eras	217
Figure 6.13: Plot of median fragilities for MSCC-IG with seat type abutments consisting of a) single column bents, b) multi column bents, across design eras	218
Figure 6.14: Plot of median fragilities for MSCC-IG bridges designed in the a) pre 1971, b) 1971-1990, and c) post 1990 era	220

Figure 6.15: Comparison of median values of system fragility for MSCC-BG-S-E3 based on the present study and HAZUS	223
Figure A.1: Typical abutment pile spacing	238
Figure A.2: Typical bridge layout to determine support type	239
Figure A.3: Deck slab thickness for MSCC-SL bridges as a function of span length	244
Figure A.4: Bent cap details in MSCC-SL bridges as a function of span length	245
Figure A.5: Standard I-girders used in the California MSCC-IG bridges	249

SUMMARY

Quantitative and qualitative assessment of the seismic risk to highway bridges is crucial in pre-earthquake planning, and post-earthquake response of transportation systems. Such assessments provide valuable knowledge about a number of principal effects of earthquakes such as traffic disruption of the overall highway system, impact on the regions' economy and post-earthquake response and recovery, and more recently serve as measures to quantify resilience. Unlike previous work, this study captures unique bridge design attributes specific to California bridge classes along with their evolution over three significant design eras, separated by the historic 1971 San Fernando and 1989 Loma Prieta earthquakes (these events affected changes in bridge seismic design philosophy). This research developed next-generation fragility curves for four multispan concrete bridge classes by synthesizing new knowledge and emerging modeling capabilities, and by closely coordinating new and ongoing national research initiatives with expertise from bridge designers.

A multi-phase framework was developed for generating fragility curves, which provides decision makers with essential tools for emergency response, design, planning, policy support, and maximizing investments in bridge retrofit. This framework encompasses generational changes in bridge design and construction details. Parameterized high-fidelity three-dimensional nonlinear analytical models are developed for the portfolios of bridge classes within different design eras. These models incorporate a wide range of geometric and material uncertainties, and their responses are characterized under seismic loadings. Fragility curves were then developed considering

the vulnerability of multiple components and thereby help to quantify the performance of highway bridge networks and to study the impact of seismic design principles on the performance within a bridge class. This not only leads to the development of fragility relations that are unique and better suited for bridges in California, but also leads to the creation of better bridge classes and sub-bins that have more consistent performance characteristics than those currently provided by the National Bridge Inventory. Another important feature of this research is associated with the development of damage state definitions and grouping of bridge components in a way that they have similar consequences in terms of repair and traffic implications following a seismic event. These definitions are in alignment with the California Department of Transportation's design and operational experience, thereby enabling better performance assessment, emergency response, and management in the aftermath of a seismic event. The fragility curves developed as a part of this research will be employed in ShakeCast, a web-based post-earthquake situational awareness application that automatically retrieves earthquake shaking data and generates potential damage assessment notifications for emergency managers and responders.

CHAPTER 1

INTRODUCTION

1.1 Problem Description and Motivation

Quantitative and qualitative assessment of the seismic risk to highway bridges is crucial in pre-earthquake planning, and post-earthquake response of transportation systems. Assessing the consequences of natural hazards such as earthquakes on highway infrastructure systems has typically focused on economic losses and closure time (Basoz and Kiremidjian, 1997; Mackie and Stojadinovic, 2005; Liao and Yen, 2010; Padgett et al., 2010; Zhou et al., 2010; Luna et al., 2008). Such assessments provide valuable knowledge about a number of principal effects of earthquakes such as traffic disruption of the overall highway system, impact on the regions' economy and post earthquake response and recovery, and more recently serve as measures to quantify resilience (Bruneau et al. 2003). According to the Bureau of Transportation Statistics (BTS), U.S. Department of Transportation (US DOT), the nation's freight transported by all modes steadily increased between 1980 and 2009, rising at an average annual growth rate of about 1.4 percent per year (FHWA, 2010). Based on the composite estimates of commercial freight activity in the United States for 2009, trucks account for 9.8 trillion dollars of shipment thereby holding 91% of the relative share among all the other transportation modes and 97% of tonnage. Further, the estimates resulting from a combined BTS and Federal Highway Administration Authority (FHWA) effort to geocode bridges from the National Bridge Inventory (NBI) suggest that the state of California accounts for 28.3% of 159,859 structurally deficient and functionally obsolete bridges in the continental United States. Bridges are considered structurally deficient if significant load-carrying elements are found to be in a poor or worse condition due to

deterioration and/or damage, while functional obsolescence is a function of geometrics of the bridge in relation to those required based on current design standards (FHWA, 2006) and inability to meet traffic demands. The latter is directly related to the age of the bridge and the varied design, detailing and construction practices followed across decades adds to their functional obsolescence. Due to the major dependence of the nations' freight economy on highway infrastructure systems that have a large proportion of deficient bridges, coupled with the increased awareness of the seismic hazard in the region, a proper understanding of their seismic response and vulnerability is important for risk assessment.

Fragility curves, which are conditional probability statements that give the likelihood that a structure will meet or exceed a specified level of damage for a given ground motion intensity measure, have found widespread use in probabilistic seismic risk assessment of highway bridges. The conditioning parameter is typically a single intensity measure such as peak ground acceleration (PGA) or spectral acceleration at the geometric mean of the longitudinal and transverse periods. Fragility curves are a fundamental building block used in multiple (current and potential future) applications including:

- Emergency Response:
 - Optimize initial bridge inspection priorities (through ShakeCast near-real-time alerting system);
 - Rapid initial estimate of loss (for support of emergency declarations).
- Design Support - Performance-Based Earthquake Engineering:
 - Bridge-Specific: Develop bridge-specific fragility curves to serve as a design check and support design strategy decisions.
 - Bridge Classes: Evaluate classes of bridge systems to optimize design guidelines for safety, cost, and functionality.
- Planning Support:
 - Traffic impacts from scenario earthquakes (e.g. Golden Guardian);
 - Performance of specific transportation corridors (e.g. lifeline routes);

- Cost-effectiveness of alternate bridge retrofit strategies;
- Screening for additional seismic retrofit needs.
- Policy Support - Risk Nomenclature
 - Capacity for issuing scientifically-defensible (internal, interagency, or public) statements regarding anticipated transportation system performance that accounts for unavoidable uncertainties in earthquake shaking and variable bridge design/construction/age.

The intent of the present research is to develop fragility curves for predominant concrete bridge classes in California based on unique bridge inventory information which will enable the identification of significant features and creation of seismic performance sub-bins capturing the temporal evolution of design and detailing standards of bridges. The sub-bin fragilities can be used in a variety of current and future applications, mentioned previously, and more importantly emergency response and management in the context of the present study.

Most of the fragility curves developed for California bridges are structure specific (Mackie and Stojadinovic, 2005; Zhang and Huo, 2009). Structure specific fragility curves do not capture the uncertainty associated with the geometric parameters that describe a bridge class and other uncertainties associated with them. On the other hand, Nielson and DesRoches (2007), Padgett and DesRoches (2008), Ramanathan et al. (2010, 2012) developed fragility curves for as-built (seismically and non-seismically designed bridges) and retrofit bridge classes in central and south eastern United States (CSUS). These are not applicable for vulnerability assessment in California due to discrepancies in the composition of bridge classes and design details. Further, there is a significant evolution in the seismic design philosophy for bridges in California over the last few decades which is absent in the case of CSUS bridges, thereby preventing the adoption of CSUS bridge class fragilities for their California counterparts. Added discrepancies in the definition of damage states to support regional risk assessment and

decision-making needs, further add to the incompatibility between CSUS and California bridge class fragilities.

The only fragility curves that are remotely applicable to bridge classes in California were the ones developed by Mander and Basoz (1999) which are employed in HAZUS (HAZUS-MH, 2011) and ShakeCast (Lin and Wald, 2008). ShakeCast is an application developed by the United States Geological Survey (USGS) for automating ShakeMap delivery to critical users such as lifeline utilities. Critical users can receive automatic notifications within minutes of an earthquake indicating the level of shaking and the likelihood of impact to their own facilities. The HAZUS fragility relationships were developed for bridge classes based on a limited number of parameters available in the NBI, damage states based on limited sets of field damage observations and simplified two dimensional analysis techniques. Further details about the limitations of HAZUS fragilities and the need to move beyond them are discussed in the next chapter. Another significant drawback in the field of bridge seismic risk assessments is the mismatch between the damage state definitions used in fragility analysis and overall bridge functionality post a seismic event. This hampers the decision making needs by agencies like the California Department of Transportation (Caltrans) with regards to emergency response and management.

A gap currently exists in the literature and fragility models used in practice to support risk assessment of bridge classes representative of the California bridge inventory that align with decision making needs expressed by Caltrans. Exacerbating this situation is the lack of systematic organization of bridge design, retrofit, and maintenance data (beyond NBI parameters) required to make substantial improvements. Common California bridge classes have a broad range of differences and temporal variations in their geometric and design attributes and quantifying their vulnerability by not accounting for these features, as in the case of the existing HAZUS fragilities, could lead to serious errors in their vulnerability estimates. This necessitates the development of a

binning structure based on the design and detailing attributes and unique fragility functions associated with them.

1.2 Research Objectives

The limitations in the HAZUS fragilities and previous studies on fragilities of bridge classes in CSUS in general were identified in the preceding section. The main objective of this research is to make substantial improvements in fragility relationships for bridges typical of California by leveraging new knowledge and emerging modeling capabilities, and by closely coordinating new and ongoing national research initiatives with Caltrans design and user expertise. Specific endeavors which hold high potential for improving fragility relations include:

1. Identify the most common concrete bridge types in California and perform a detailed analysis to statistically describe their major geometric parameters using the NBI database.
2. Capture and understand the unique design and detailing aspects associated with the evolution of column design philosophy, seat widths, abutment types, superstructure to substructure connectivity, foundation types, to mention a few, based on extensive review of bridge plans and literature search. These details are gathered over three significant design eras, separated by the historic San Fernando (1971) and Loma Prieta (1989) earthquakes (these events affected changes in bridge seismic design philosophy).
3. Supplement the NBI information available about bridges with the aforementioned details and bridge design, retrofit and maintenance data made available through Caltrans in-house databases and expertise to extend and subdivide existing bridge classes into seismic performance sub-bins, primarily separated by the three significant design eras, to better account for the California bridge inventory.

4. Generate three dimensional non-linear finite element models of the chosen bridge classes using the advances in component modeling strategies. This also involves the identification and probabilistic modeling of potentially uncertain modeling parameters.
5. Refinement and development of the component and system level damage states and their mapping in such a way that they align with the design and operational experience of bridge owners to be effectively used in seismic risk assessment. In this way, the fragility curves developed in this study will have direct implications in terms of repair and operational consequences in the aftermath of an earthquake and will be tailored to the decision-making needs at the regional level.
6. Generate a refined set of component and system level fragility curves for the bridge classes along with their seismic performance sub-bins. This will help provide insight into the relative vulnerability of bridge classes and their seismic performance sub-bins, assess the effectiveness of seismic design philosophy currently adopted for the design of bridges, and guide future data collection that is presently absent in the NBI and the state databases.

1.3 Dissertation Outline

The dissertation is organized into seven chapters with the following contents:

Chapter 2 summarizes existing research in the area of seismic risk assessment and seismic bridge fragility curves.

Chapter 3 provides a detailed analysis of the California bridge inventory including statistical distributions for bridge geometric parameters. The general design details and potential vulnerabilities of bridges designed prior to 1971, those designed between 1971 and 1990 and post 1990 are identified based on an extensive review of bridge plans to supplement the information provided by the NBI. Detailed information pertinent to bridge components: superstructure, columns, foundations, abutments are gathered across

the design eras to aid in the development of stochastic finite element models for fragility analysis.

Chapter 4 provides extensive details about the modeling strategies for bridge components: superstructure, single and multi column bents, foundation systems, abutments including backfill soil and piles, restrainers and shear keys. Three dimensional analytical bridge models are developed and deterministic responses are presented to provide insight into the response of bridge components.

Chapter 5 outlines the framework that will be adopted in the development of analytical fragility curves for the bridge classes considered in this study. Details are provided regarding the different aspects of the multi-phase framework: ground motion suite, range of uncertainties considered including distributions, formulation of probabilistic seismic demand models and definition of capacity models.

Chapter 6 presents the results of component and system level fragility curves for the chosen multispan bridge classes and their seismic performance sub-bins. Insights are provided on the relative performance of bridge classes and their seismic performance sub-bins, the importance of sub-binning by design era and the influence of different design details on the vulnerability along with guiding future data collection currently absent in the NBI. Finally, comparisons between the results of the present study and the fragility curves presented in the risk assessment package, HAZUS are also presented.

Chapter 7 presents the conclusions from the present research, along with providing impacts of the work and suggestions for future research.

CHAPTER 2

EXISTING RESEARCH ON HIGHWAY BRIDGE FRAGILITY – A STATE OF THE ART SUMMARY

Probabilistic seismic risk assessment approaches, such as the Probabilistic Performance-based Earthquake Engineering (PBEE) framework (Cornell and Krawinkler, 2000; Mackie and Stojadinovic, 2001), have evolved to become central to risk mitigation decision making for structures and infrastructure systems. Such approaches aim to better understand the risk to engineered systems and apply this knowledge to design structures to achieve goals of life safety, reduced economic loss, or minimized recovery downtime in the aftermath of a seismic event. The central focus of numerous projects such as HAZUS (2011), REDARS (Werner et al., 2003), ShakeCast (Lin and Wald, 2008), and the Pacific Earthquake Engineering Research (PEER) Center highway demonstration project (Moore, 2000) has been on large-scale simulations of transportation networks to provide economic impact analyses in the aftermath of an earthquake. Bridges form a critical link in a highway network and are vulnerable to earthquake hazard, often with severe consequences in terms of economic loss and its effect on the regional economy.

With the advancement of the PBEE framework, the central focus is on metrics such as damage probability functions or fragility curves for describing the performance and vulnerability of highway bridges under seismic input. Fragility curves are conditional probability statements that give the likelihood that a structure will sustain or exceed a specified level of damage for a given ground motion intensity measure. These are expressions of performance at different levels of seismic input intensity unlike the description of performance as “safe” or “unsafe” which is typical of the deterministic design criteria. This is of particular relevance considering the inherent uncertainty in not

only the seismic hazard but also in the structural capacity and various other attributes associated with highway bridge networks. Probabilistic methods facilitate the definition of acceptable performance criteria under hazard levels and therefore have tremendous potential for a wide range of applications as stated in the previous chapter.

The most widely adopted probabilistic seismic risk assessment (PSRA) framework is the one presented by the Pacific Earthquake Engineering Research Center (PEER). The typical strategy employed in the PEER framework is to deconvolve the uncertainty in different parts of the seismic risk assessment problem such as the seismic hazard, structural performance (response and damage) and consequences (financial loss, interruption time) using the theorem of total probability, in an effort to achieve a consistent reliability-based approach for decision making (Cornell and Krawinkler, 2000; Mackie and Stojadinovic, 2005). Each of these assessment modules are essentially independent and are linked together by pinch point variables (Kaplan and Garrick, 1981), such as the intensity measure (*IM*), engineering demand parameter (*EDP*), and the damage measure (*DM*). The mean annual frequency, λ_{DV} , of a decision variable (*DV*) exceeding a limiting value (*dv*), is expressed in equation (2.1).

$$\lambda_{DV}(dv) = \int \int \int_{dm \cdot edp \cdot im} G(dv | dm) \cdot |dG(dm | edp)| \cdot |dG(edp | im)| \cdot |d\lambda(im)| \quad (2.1)$$

In equation (2.1), $G(DV|DM)$ represents the loss model describing the cumulative distribution function (CDF) of a decision variable conditioned on a damage measure such as repair cost or downtime, $G(DM|EDP)$ is the damage, capacity or the limit state model describing the CDF of a *DM* conditioned on a *EDP*, $G(EDP|IM)$ is the demand model describing the CDF of an *EDP* such as curvature ductility, abutment displacement etc., conditioned on an *IM*, and $\lambda(IM)$ is the seismic hazard model describing the mean annual frequency of exceeding an *IM*. It must be noted that the convolution of $G(DM|EDP)$ and $G(EDP|IM)$ yields fragility curves.

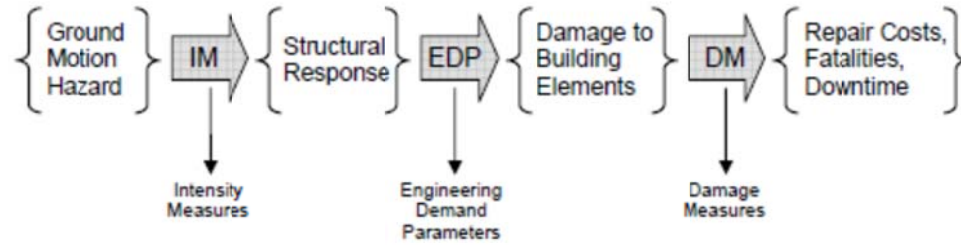


Figure 2.1: Schematic representation of seismic risk assessment (Baker et al, 2005)

2.1 Evolution in the Development of Fragility Curves

Fragility curves have found widespread use in risk assessment of bridges and highway systems and are the fundamental building block in multiple applications including emergency response, design, planning support, and policy recommendations. Over the years, fragility curves have evolved.

The earliest attempt to formalize seismic risk assessment procedures is found in the seminal work by Whitman et al. (1975). Since then several attempts have been made to quantify the risk to highway infrastructure systems. The Applied Technology Council (ATC, 1985) took the first step in performing seismic risk assessment of infrastructure for the state of California using damage probability matrices and restoration functions. Subsequently, several committees constituted by ATC have been solely devoted to the risk assessment of lifelines. The ATC 25 report (ATC, 1991) introduced the concept of continuous fragility functions for lifeline systems including bridges by performing regression on the discrete values of damage probability matrices. Further attempts to push forward the seismic risk assessment methods were made by the Federal Emergency Management Agency (FEMA) by the constitution of a committee of experts and introduction of a Geographic Information Systems (GIS) based risk assessment software, Hazards United States (HAZUS, 1997) in 1997. Since that time HAZUS has undergone several improvements and revisions and now includes models for estimating potential losses from a variety of natural disasters like earthquakes, floods, and hurricanes.

Over the years, structural fragilities have been determined in a variety of ways. The ATC 13 Report (ATC, 1985) documents risk assessment of the infrastructure stock in California essentially based on expert opinion. A panel of 42 experts was assembled to

develop damage probability matrices for bridge infrastructure based on their expertise. This technique has several major drawbacks since the procedure is totally subjective and depends on the number of experts queried and therefore is based on expertise and experience of the individuals with little correlation to actually observed earthquake damage. The 1989 Loma Prieta, 1994 Northridge and 1995 Kobe earthquakes were watersheds for fragility research. Several researchers (Basoz and Kiremidjian, 1997; Yamazaki et al., 1999; Der Kiureghian, 2002; Shinozuka et al., 2000, 2003; Elnashai et al., 2004) developed empirical fragility curves based on actual damage data observed in these earthquakes. Although the adopted procedure differed slightly among the researchers, the general essence was the same. Basoz and Kiremidjian (1997) assembled damage frequency matrices and performed a logistic regression analysis to develop fragility curves while Shinozuka et al. (2003) used the Maximum Likelihood Method to estimate the parameters of a lognormal probability distribution describing the fragility curves. Der Kiureghian (2002) employed a Bayesian approach in order to develop fragility curves. However, lack of sufficient damage data, discrepancies in the damage assessments in the aftermath of a seismic event, variation in the ground motion intensities at the damage sites depending on the earthquake source are some of the limitations of this technique for developing fragility curves.

Advances in modeling capabilities coupled with a lack of sufficient earthquake damage data motivated the development of fragility curves using analytical and simulation based methods. Several researchers have employed analysis techniques with different levels of sophistication to develop analytical fragility curves for bridges. Yu et al. (1991) used simple single-degree-of-freedom models and Elastic Response Spectrum Analysis (RSA) to develop fragility curves for highway bridges in Kentucky while Hwang et al. (2000) furthered this approach by quantifying uncertainties in seismic demand and capacity assessments. This was one of the earliest studies that looked at fragility curves for a class of highway bridges. Nonlinear static procedures (NSP) that use the force-deformation characteristics of structures stemming from pushover analyses started gaining wide acceptance and application. The Capacity Spectrum Method (CSM),

Coefficient Method (CM) and the N2 Method are all different types of nonlinear static procedures. CSM was first proposed by the ATC (1996) while CM was proposed by FEMA-273 (1997). Dutta (1999), Basoz and Mander (1999), Banerjee and Shinozuka (2007), Jeong and Elnashai (2007) used the CSM to develop fragilities for highway bridges in the United States. Currently, the fragilities proposed by Mander and Basoz (1999) are employed in HAZUS-MH for seismic risk assessment of highway infrastructure systems. Further details about the fundamental assumptions and limitations of the HAZUS fragilities are discussed in the next section. Fajfar (2000) proposed the N2 method as a special form of CSM in which pushover analysis of a multi-degree-of-freedom (MDoF) model is combined with the inelastic response spectrum analysis of an equivalent single-degree-of-freedom (SDoF) system in the acceleration-displacement format. Gardoni et al. (2003) and Zhong et al. (2008) proposed a modification to the N2 method to aid in the development of probabilistic seismic demand models (PSDMs) for reinforced concrete bridges with single and two column bents, respectively. Most of the studies employing CSM to develop fragility relationships were restricted to two dimensional analytical bridge models.

Several researchers resorted to more reliable yet computationally expensive techniques such as Nonlinear Time History Analysis (NLTHA) and Incremental Dynamic Analysis (IDA) to develop fragility curves. Kim and Shinozuka (2004) used NLTHA on two dimensional bridge models to study the effect of steel jacketed column retrofits on the performance of bridges. Mackie and Stojadinovic (2005) employed NLTHA and IDA to develop fragility curves. These formed the basis of a rational methodology to evaluate damage potential and to assess probable highway bridge losses for critical decision making regarding post earthquake safety and repairs to highway networks. Mander et al. (2007) used IDA in a performance-based earthquake engineering context to investigate the expected seismic damage and the associated financial loss from highway bridges. Zhang and Huo (2009) developed fragility curves for conventionally designed and base

isolated bridges using NLTHA and IDA to aid in assessing the effectiveness and optimum design parameters of isolation devices. Huang et al. (2010) used NLTHA coupled with a Bayesian updating procedure to develop PSDMs for typical California reinforced concrete bridges with single column bents considering the effect of near-field ground motions and effects from soil characteristics. Nielson et al. (2007), Padgett et al. (2008), Ramanathan et al. (2010, 2012) employed NLTHA to develop fragility curves for common bridges in Central and Southeastern United States (CSUS) in their as-built and retrofitted conditions, accounting for multiple component vulnerability, while Pan et al. (2010) developed fragility curves for as-built and retrofitted multispan simply supported steel girder bridges in New York state using NLTHA. Figure 2.2 summarizes the existing bridge fragilities for multi-span continuous concrete box-girder bridges with and without the consideration of seismic design principles. These curves were developed by various researchers by employing different techniques. Clearly, there is a well pronounced variability in the curves even for consistent damage states which deserves attention.

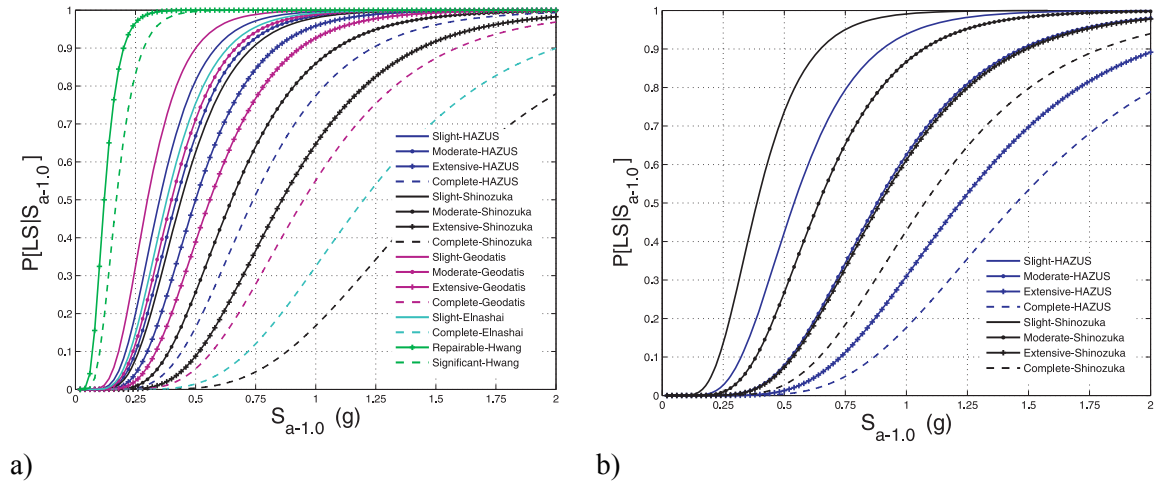


Figure 2.2: Existing fragility curves for multispan continuous concrete box-girder bridges a) seismically designed, b) non-seismically designed

Fragility analysis techniques often differ based on two major aspects: mechanical analysis methods adopted to determine structural response and the reliability assessment

method. The former deals with the approach to simulate seismic loading, assess structural response, and consider geometric effects, while the latter is central to predictive response modeling, uncertainty treatment and system component analysis and combinations, which is discussed subsequently in this section. The mechanical analysis techniques considered in the past account for linear or nonlinear material responses, static, dynamic or spectral responses and the inclusion of geometric effects such as P- Δ or full nonlinear or large deformations. In the context of seismic performance evaluation of bridges, the distinction between analysis techniques can be made in terms of seismic load input to the structure. Therefore, the demand analysis tends to be the primary distinction in the methods. This section presents the details of the RSA, CSM, NLTHA and IDA techniques in an effort to categorize them based on the method formulation, fundamental assumptions and possible implications for their extension to three dimensional fragility analyses of highway bridges. The viability, scope, and application of the various analytical tools are also discussed.

2.1.1 Response Spectrum Analysis (RSA)

The elastic response spectrum analysis method (RSA) is one of the simplest and most efficient techniques used for demand analysis in the development of fragility curves (Yu et al., 1991; Hwang et al., 2000). This simplicity has resulted in the frequent use of RSA in the design field to serve as a quick reference calculation while designing critical components such as columns in a bridge. Typically, the response spectrum of the ground motion or design spectrum is used to obtain the maximum response quantities. The analytical models used are linear elastic models based on effective stiffness properties and assumed equivalent viscous damping ratios. This technique is most applicable for bridges that are expected to perform in the linear elastic range based on cracked section properties. It could also be used for determining inelastic response of bridges with equivalent linearization based on initial stiffness and appropriate modifications based on

energy principles or equal displacement principles. However, the method suffers from a few drawbacks. Where significant nonlinearity occurs, the method under-predicts the displacement demand and significantly over predicts the force. This technique only estimates the maximum modal responses which do not necessarily happen at the same time during earthquake excitation. The estimation of maximum modal responses is facilitated by the use of modal combination rules such as absolute sum (ABS) (Chopra, 2007), square-root-of-sum-of-squares (SRSS) (Rosenblueth, 1951), and complete quadratic combination (CQC) (Der Kiureghian, 1981). These methods are used based on the principle of superposition which is valid as long as the inelastic deformations are small. Typically, in the inelastic range, which is often of interest in fragility modeling, the displacements exceed the elastic range by many fold thereby undermining the validity of typical modal combination rules adopted in RSA.

2.1.2 Nonlinear Static Procedure (NSP) or Capacity Spectrum Method (CSM)

Capacity spectrum method is a simplified procedure for seismic response evaluation of structures. The capacity of the structure is evaluated by performing a nonlinear static pushover analysis of the structure with material as well as geometric nonlinearity included under load patterns which correspond to the dominant mode shapes of the structure. On the other hand, the demand on the structure is evaluated using a scaled down response spectrum derived for individual ground motions. The intersection of the demand and capacity spectrum indicates the estimated maximum response of the structure under the specified seismic ground motion. In order to construct the load pattern for pushover analysis for seismic capacity evaluation of the bridge, an eigenvalue analysis is performed and modal properties of the bridge are realized. Using the orthogonality property of the modes and extending it as an assumption to the realm of the nonlinear structure response, the overall maximum seismic response of the bridge can be estimated by evaluating the maximum response of the structure in two orthogonal

directions separately and combining the results using modal combination rules. The load pattern in pushover analysis for each horizontal direction corresponds to the associated fundamental mode shape.

A fundamental dilemma exists in the application of this method for bridges since the recommendations in ATC 40 (1996) are pertinent to building structures. Although researchers (Dutta, 1999; Basoz and Mander, 1999; Banerjee and Shinozuka, 2007; Jeong and Elnashai, 2007) have used the technique in the past, very little/no guidance is available for the choice of the bridge structural behavior type and the associated damping modification factor. Further, the fragility curves are sensitive to the damping modification factor and therefore the choice of a structure type plays a crucial role in determining the performance under seismic excitation.

2.1.3 Nonlinear Time History Analysis (NLTHA)

NLTHA technique has been exploited by several researchers (Mackie and Stojadinovic, 2001, 2005; Kim and Shinozuka, 2004; Zhang and Huo, 2009; Nielson, 2005; Padgett, 2007; Ramanathan et al., 2010, 2012) and has proven to give reliable estimates of system performance and seismic fragility relationships. It serves as the foundation for even more computationally intensive techniques such as IDA, which is discussed in the next section. NLTHA offers the flexibility to consider analytical models with linear or nonlinear cyclic material characteristics and geometric nonlinearities such as P- Δ or full nonlinear or large deformations. The distinguishing feature of NLTHA when compared to CSM or RSA is the ability to consider a temporal dimension in addition to two or three spatial dimensions defined by the geometry. This approach is the most rigorous, and often the response can be very sensitive to the characteristics of the individual ground motion used as seismic input. Therefore, several analyses are required using different ground motion records to achieve a reliable estimation of the probabilistic distribution of structural response. Since the properties of the seismic response depend on

the intensity, or severity, of the seismic shaking and characteristics of the record, a comprehensive assessment requires numerous NLTHA at various levels of intensity to represent different possible earthquake scenarios. This is typical of the “cloud” approach (Baker and Cornell, 2006) and is also commonly referred to as probabilistic seismic demand analysis (PSDA). This technique involves making an apriori assumption about the probabilistic distribution of seismic demand which tends to be a drawback. Yet another drawback of the technique is associated with the complexity of the approach in general, which limits its usage to a great extent.

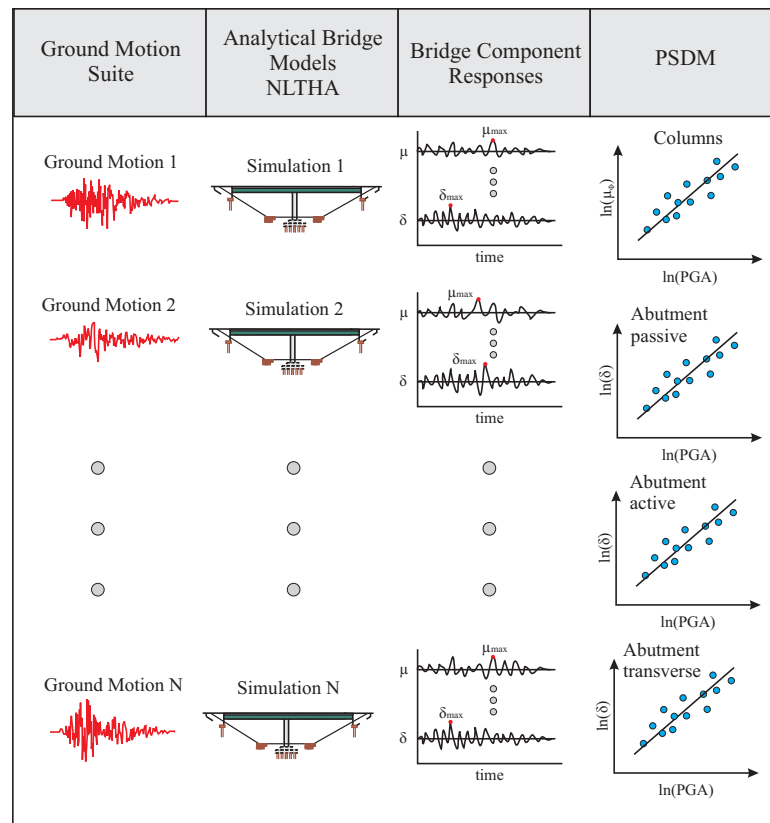


Figure 2.3: Schematic representation of the NLTHA procedure used to develop PSDMs

A schematic of the procedure for NLTHA is shown in Figure 2.3. Statistically significant yet nominally identical 3D analytical bridge models are typically created by sampling on the probability distributions for uncertain parameters. These are then

randomly paired with ground motions and in each case a NLTHA is performed to record peak component demands that are deemed to contribute to the vulnerability of the bridge system. Probabilistic seismic demand models (PSDMs) are developed and convolved with capacity models to obtain fragility curves. This study employs this method for generating fragility curves and extensive details are presented in Chapter 5.

2.1.4 Incremental Dynamic Analysis (IDA)

IDA is a special type of nonlinear dynamic analysis which facilitates seismic structural demand and capacity comparisons through a series of NLTHA for ground motions that are scaled successively until significant strength reduction (collapse) of the primary load bearing elements in the structural system. Unlike the previous technique, IDA may be classified as a “scaling” or “stripe” type technique (Baker and Cornell, 2006) where ground motions are incrementally scaled and analysis is performed at different hazard levels. This enables the structure to transition from linear elastic behavior to final global dynamic instability which marks the conclusion of the analysis and ground motion scaling. The method is analogous to the transition from a single static analysis to an incremental static pushover analysis. IDA was established as a state-of-the-art method to determine the global collapse capacity by the FEMA guidelines (FEMA-350, 2000; FEMA-351, 2000). The overall formulation of the technique was proposed by Vamvatsikos and Cornell (2002) although it has been used in several forms in the work of many researchers (Bazzurro and Cornell, 1994; Luco and Cornell, 2000). IDA provides a thorough understanding of the changes in structural response with increasing ground motion intensities along with providing accurate and reliable estimates of the global collapse capacity of the structure. However, IDA does suffer similar drawbacks as NLTHA with respect to the computational difficulties involved in the approach. Another major drawback associated with the technique is that the process involves scaling the intensity without altering the frequency content of the ground motions. This could lead to

unrealistic time histories which might not be representative of the seismic hazard of the bridge site under consideration. Since the IDA technique is computationally expensive and involves scaling a single earthquake time history to increasing levels of intensity, a smaller subset of ground motions are typically selected to perform analyses.

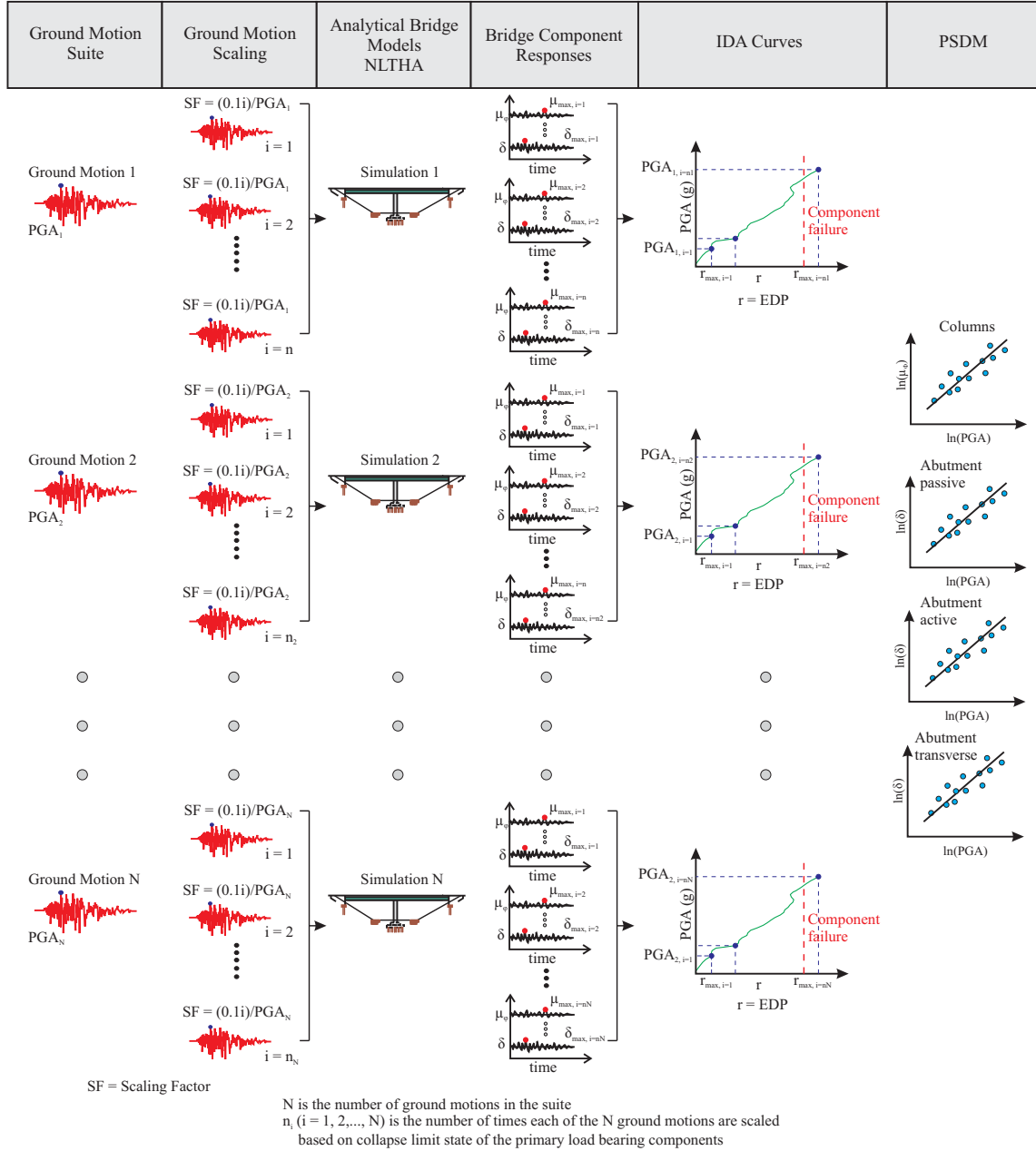


Figure 2.4: Schematic representation of the IDA procedure used to develop PSDMs

IDA curves describing the relation between peak *EDPs* and *IM* are then developed for every bridge-ground motion pair. For every scaling iteration of a ground motion, the component responses are obtained by performing NLTHA and are compared to the respective damage state prescriptive measures. The ground motion scaling is stopped when the prescriptive value associated with the complete damage state is exceeded by any one of the components considered in this study. As mentioned previously, some analysts directly derive fragility curves from IDA data either by deriving point estimates of the damage state exceedance probability at each ground motion level or by estimating the probability density function of the PGA for ground motions in which the damage state thresholds are exceeded. However, this approach requires a large sample size and subsequent number of simulations which is a common limitation of the approach. Alternatively PSDMs are derived for use in the fragility analysis using the same formulation presented for the other methods. Typically, the majority of the applications of IDA assess collapse level fragilities based on the excessive global strength or stiffness reductions revealed by the incremental analyses, which is the actual benefit of the method.

2.2 Structural Reliability Assessment Techniques for Bridges

The previous section described the different mechanical analysis procedure used in the estimation of bridge responses to imposed seismic demand. Likewise, researchers have adopted different techniques to probabilistically model the structural response, propagate and deal with uncertainty and develop fragility curves by the convolution of demand and capacity models. The derivation of component based fragility curves is straight forward and is a closed-form solution (equation (2.1)) basing that the demand and capacity (or resistance) are assumed to be lognormal (Mackie and Stojadinovic, 2001; Cornell et al., 2002; Bazzurro and Cornell, 2002; Ellingwood and Wen, 2005; Nielson and DesRoches, 2007; Padgett et al., 2008; Celik and Ellingwood, 2010). In equation

(2.1), D and C denote demand and capacity, S_D and S_C denote the median values of demand and capacity and $\beta_{D|IM}$ and β_C denote the dispersions (logarithmic standard deviation) of the demand and capacity, respectively. It must be noted that S_C and β_C are defined based on the limit state under consideration.

$$P[D > C | IM] = \Phi \left(\frac{\ln \left(\frac{S_D}{S_C} \right)}{\sqrt{\beta_{D|IM}^2 + \beta_C^2}} \right) \quad (2.1)$$

Estimates of system reliability considering the vulnerability of multiple components can be obtained by convolving the individual PSDMs to develop a joint probabilistic seismic demand model (JPSDM) and then integrating it over all possible failure domains (prescribed limit states) to obtain the probability of failure at a particular IM. The process can be repeated at several IM levels to develop system level fragility curves. However, in situations where the system vulnerability is characterized by the vulnerability of multiple components, as will be in the current research, closed form integration over all possible failure domains tends to be extremely challenging and mathematically intense in formulation.

Several researchers have proposed techniques to develop fragility curves for the bridge as a system. Hwang and Huo (1998) used a logistic model to characterize the response and determine the system reliability of multispan simply supported bridges in Memphis, Tennessee. The parameters of the logistic model were determined from a logistic regression of a vector of Bernoulli random variables (zeros and ones), depending on whether the bridge sustains a particular damage state or not. Shinozuka et al. (2003) used the maximum likelihood estimators to determine parameters of the lognormal distribution (median and dispersion) describing the system fragility curves. As in the case of Hwang and Huo (1998), the event of the system exceeding user defined damage states were simulated using a Bernoulli random variable and the mean and dispersion of the

fragility curves were determined using a standard optimization algorithm. Mander and Basoz (1999) developed fragility curves using the CSM described in section 2.1.2 directly and assumed a value of the dispersion arbitrarily. Hwang et al. (2000a) proposed a simplified method to develop system fragility curves, where the median value of demand was expressed as a function of a ground motion intensity measure using a linear regression analysis, although the value of dispersion was arbitrarily assumed.

Mackie and Stojadinovic (2005) used a mean value, first order, second-moment analysis for each of the limit state functions describing the components that contribute to the system vulnerability. Having determined the mean and standard deviation for each of the response quantities (columns, abutments etc.), parametric first order reliability method (FORM) analysis was used to determine the probability of failure for each of the response measures. The series system assumption was then used to determine the system level fragility curves. Choi et al. (2004) developed first order bounds for system reliability assuming series systems, as one of the earliest attempts to account for some level of correlation among bridge components. Nielson and DesRoches (2007), Padgett and DesRoches (2008) and Ramanathan et al. (2010, 2012) used the joint probabilistic seismic demand model (JPSDM) and Monte Carlo Simulation to develop bridge system fragility curves. The JPSDM is first developed from the individual marginal PSDMs for the response measures realizing that the demands on various components have some level of correlation. A Monte Carlo simulation is then used to compare realizations of the demand (using the JPSDM defined by a conditional joint normal distribution in the transformed space) and component capacities to calculate the probability of system failure for a particular IM value, based on the assumption of a series system. The procedure is repeated for increasing values of the IM. Regression analysis is used to estimate the lognormal parameters, median and dispersion, which characterize the bridge system fragility.

Zhang and Huo (2009) adopted a weighting scheme of bridge component failures to preferentially establish bridge system level failure based on the components that contribute the most to the load carrying capacity or post event functionality criterion. Although the approach realizes that not all components contribute equally to system level damage states, the establishment of weights is particularly subjective and difficult as the number of components characterizing the system vulnerability increases. Kim et al. (2006), Lupoi et al. (2006), Zhang and Huo (2009) used other approaches to define system reliability such as parallel system, combination of series and parallel components, or adaptive systems that add components as damage accumulates.

Closed form solutions are recently emerging and these provide means to evaluate the system failure probability regardless of the system abstraction. Song and Kang (2009) used the matrix-based system reliability method to develop system level fragility curves by considering a wide range of component level failure events also accounting for bridge component correlations. Duenas-Ororio and Padgett (2011) proposed a closed form combinatorial method to develop system fragility curves by explicitly evaluating all possible ways in which bridge components can fail within and across limit states.

Singhal and Kiremidjian (1996), Der Kiureghian (2002), Gardoni et al. (2002, 2003), Koutsourelakis (2010) used a Bayesian framework to formulate system fragility relationships. While Der Kiureghian (2002) used the maximum likelihood method in conjunction with the Bayesian approach, Koutsourelakis (2002) used Markov Chain Monte Carlo techniques along with the Bayesian approach to develop multi dimensional fragility surfaces as a function of multiple ground motion characteristics. The fundamental advantage of the Bayesian formulation is the ability to yield a distribution of possible fragility curves which denote the epistemic uncertainty around them, which are also referred to as confidence bounds.

Statistical learning techniques, also known as surrogate models or metamodels have also been used to generate system level fragility relationships. Metamodels typically

help in replacing computationally expensive finite element models used in simulations for reliability assessment process. Response surface metamodels are the most commonly used due to its transparency and relative ease and have found wide spread use in the performance assessment of civil engineering structures (Bucher and Bourgund, 1990; Rajashekhar and Ellingwood, 1993; Guan and Melchers, 2001). Having developed the metamodels, a logistic regression is used to develop component and system level fragility relationships. Ghosh et al. (2012) extended the approach for the reliability assessment of highway bridges along with the application of several other surrogate models such as multiple adaptive regression splines, radial basis functions and artificial neural networks.

2.3 Fragilities for Bridge Classes, HAZUS and the Necessity to go Beyond HAZUS

The previous section detailed different techniques and mechanical analysis procedures to determine structural fragilities along with their limitations. It must be noted that researchers in the field must continue to investigate improvements in these methods. The aim is to develop more reliable fragility curves that can be used in a variety of ways ranging from damage assessments, retrofit prioritizations, risk assessments and more importantly emergency response in the context of the present study. The intent of the present research is to develop fragility curves for predominant bridge classes in California based on unique California bridge inventory information. Most of the fragility curves developed for California bridges are structure specific (Mackie and Stojadinovic, 2001, 2005; Zhang and Huo, 2009). Structure specific fragility curves are advantageous and useful for risk assessment of the specific bridge structure, but the approach is prohibitive for the performance assessment of regional bridge inventories. Hence, the trend towards performance and vulnerability assessment of bridge classes or portfolios that represent bridges with variable parameters require fragility curves that are generated by varying these parameters, which are not captured in the structure specific scenarios. These parameters can be broadly classified under two categories – geometrical and

material. Attributes such as span length, deck width, column height, number of spans, superstructure type, design details that are unique to a bridge class, fall under the category of geometrical parameters, while concrete compressive strength, reinforcing steel yield strength, stiffness of the bearing pads, soil stiffness fall under the purview of material parameters. Nielson and DesRoches (2007), Padgett and DesRoches (2008), Ramanathan et al. (2010, 2012) developed fragility curves for bridge classes in CSUS considering as-built and retrofit strategies. These fragility relationships cannot be applied for the vulnerability assessment elsewhere due to discrepancies in the bridge class compositions and design details. There has further been a significant evolution in the bridge design philosophy in California, which is detailed in section 2.4.1, which is absent in the CSUS bridges, thereby preventing the adoption of CSUS bridge class fragilities for their California counterparts. Added discrepancies in the definition of damage states to support regional risk assessment and decision-making needs, further add to the incompatibility between CSUS and California bridge class fragilities.

The only fragility curves that are applicable to bridge classes in California were the ones developed by Basoz and Mander (1999) and are employed in HAZUS-MH (2011) and ShakeCast (Lin and Wald, 2008). ShakeCast is an application developed by the United States Geological Survey (USGS) for automating ShakeMap delivery to critical users such as lifeline utilities. Critical users can receive automatic notifications within minutes of an earthquake indicating the level of shaking and the likelihood of impact to their own facilities.

The HAZUS fragilities suffer a few major limitations and these are described henceforth. These fragility relationships were developed for bridge classes based on a limited number of parameters available in the NBI, damage states based on limited sets of field damage observations and simplified two dimensional analysis techniques such as the CSM. Bridge classes, defined beyond the parameters listed in NBI, were extended taking into account seismic design, number of spans (single versus multiple), span

continuity (continuous versus simply supported), and bent type (single versus multi). Particularly, separate fragilities are assigned based on seismic design and this is taken into account in terms of a spectrum modification factor, strength reduction factor due to cyclic motion, drift limits and the longitudinal reinforcement ratio (HAZUS, 2011). California bridges have a significant evolution of the seismic design philosophies, which is described in section 2.3.1, and not accounting for their factors in the stochastic modeling procedure for generating fragility curves can lead to significant errors in the vulnerability assessment. In any case, the stochastic analyses used in the generation of HAZUS fragilities did not consider the variability of the bridge class geometrical attributes such as the variation of number of spans, span length, deck width, column height, at the least. These fragilities included limited uncertainty characterized by material properties such as concrete compressive strength and reinforcing steel yield strength. Additional and specific information for bridges pertinent to a region might be difficult to obtain and hence the curves were developed with the intention that the information out of NBI is all that is required for seismic evaluation of bridge classes.

Another significant drawback of the NBI based fragility relationships employed in HAZUS and ShakeCast is that these curves were derived assuming that the vulnerability of the bridge is characterized by the vulnerability of the columns alone. However, the unseating potential of the bridge deck at the seat abutments or the bents, tearing of the elastomeric bearing pads, collapse of the shear keys etc. adds to the vulnerability of the bridge system and will need significant repairs in the aftermath of an earthquake, and these components are not accounted for in the formulation of the HAZUS fragilities. Further, there is a mismatch between the damage state definitions used in fragility analysis and overall bridge functionality post a seismic event. This hampers the decision making needs by agencies like the California Department of Transportation (Caltrans) with regards to emergency response and management. Attempts have subsequently been made to account for some differences in California bridge design

by incorporating design specific parameters such as span length, span-to-column height ratio, column-to-superstructure dimension ratio, reinforcement nominal yield strength, concrete nominal strength, longitudinal and transverse reinforcement ratio, deck thickness, foundation soil dry unit weight and angle of internal friction (Mackie and Stojadinovic, 2005). These attempts, however, were mainly focused on deriving structure specific fragility relationships or fragility curves applicable for a smaller subset of bridges such as single frame multispan continuous box-girder bridges with a single column bent (Mackie and Stojadinovic, 2005). This research aims to address all of the drawbacks associated with the HAZUS fragilities along with a refinement of the bridge classes by the inclusion of seismic performance sub-bins (SPS) characterized by seismic design philosophy of bridge components and several unique attributes, details of which are provided extensively in Chapter 3.

2.3.1 Emergence of Seismic Design Provisions for Bridges in California

Early seismic design provisions in the United States were developed following the historic 1906 San Francisco earthquake (FEMA, 2006). However, the first design provisions for bridges were not incorporated until 1940. Early seismic design provisions were based on wind loads and static lateral force concepts rather than dynamic analyses principles. The 1940 design provisions involved design for a lateral seismic force equal to a certain percentage of the dead load determined by a design engineer, placed at the center of mass of the bridge. Specifications were made slightly more specific in 1941, where the dead load percentage was specified to be between 2% and 6% based on the foundation type, and subsequently found a place in the American Association of State Highway and Transportation Officials (AASHTO) specifications. Unique structural characteristics such as energy absorption capacity of the structure and natural period were incorporated into the design specifications in 1965 (Moehle et al., 1995). The minimum lateral force of 2% of the dead load of the structure was still retained and engineers were

instructed to pay special attention to bridge structures founded on soft soils and bridges with massive piers.

The 1971 San Fernando earthquake paved the way for a major change in the seismic design philosophy. The lateral design forces were increased by a factor of 2 or 2.5 and the designs had to take into account factors such as fault proximity, site conditions, dynamic structural response, ductile design philosophy and energy dissipation capabilities. All of these aspects were included in the 1971 Caltrans Seismic Design Code (Sahs et al., 2008). The prime focus was to drive damage to the columns while the remainder of the bridge structure remained elastic (Moehle et al., 1995). Despite the modifications in design, the 1989 Loma Prieta earthquake caused spectacular damage to bridge structures. This drove Caltrans to solicit the Applied Technology Council (ATC) to conduct a detailed study and provide design and detailing recommendations, which, however, were not incorporated until after the 1994 Northridge earthquake. The modern day Caltrans Seismic Design Criteria (SDC, 2010) incorporates all the recommendations of the ATC-32 report since its very first inception in 1996. Modern day design follows the capacity design philosophy which ensures flexural failure mode in the bridge columns (Sahs et al., 2008).

California has close to 29,000 bridges which vary in age based on their time of construction. As detailed previously, the seismic design incorporated and the performance depends on the era in which the bridge is constructed. In short, the 1971 San Fernando and 1989 Loma Prieta earthquakes provoked significant changes in the seismic bridge design philosophy. In order to obtain reliable estimates of the risk associated with the bridge classes, it is crucial to capture the design attributes and unique vulnerabilities associated with the bridges based on their time of construction, which is the intent of the present study. Significant details about the characteristics of the design eras, potential vulnerabilities and design attributes are presented in Chapter 3.

2.4 Closure

This chapter provided a detailed description of the seismic risk assessment framework including the different assessment modules that are essentially decoupled in their evaluation. Fragility curves, which form an integral part in the risk assessment framework, help in translating seismic demand (characterized by an intensity measure) into a performance metric (probabilities of exceeding user defined performance thresholds), which would help stakeholders and decision makers in a wide variety of ways, primarily risk mitigation and management. A detailed evolution along the fragility timeline was presented in terms of mechanical analysis approaches, such as response spectrum analysis, capacity spectrum method, incremental dynamic and nonlinear time history analyses (NLTHA), and the reliability assessment frameworks used in their generation and the drawbacks associated with them. Lack of empirical bridge damage data from past earthquakes and advances in computational tools have paved the way for sophisticated and reliable techniques such as NLTHA to be widely used. NLTHA with high fidelity three dimensional analytical models will be used in the current research to develop fragility curves for highway bridge classes.

Transportation risk assessment typically focuses on the performance and anticipated damage to highway bridge clusters in a potential future earthquake. A wide majority of the existing bridge fragilities are site specific and cannot be used to replicate the performance of bridge classes with variable attributes in geometry and material characteristics. The only fragilities that are applicable to bridge classes in California are the ones that are developed by Basoz and Mander (1999) and these are adopted in HAZUS (2011). The potential limitations of the HAZUS fragilities are identified and a case is made for improvement in these probabilistic relationships, which is the focus of the present study. Further, the California bridge inventory has a wide array of bridges varying in age, designed and constructed using unique design specifications and detailing aspects prevalent at that point in time. Therefore, analytical models capturing these

design philosophies and their evolution are needed in order to obtain sufficiently accurate estimates of the vulnerabilities and risk associated with the bridge classes.

CHAPTER 3

CALIFORNIA BRIDGE DESIGN ATTRIBUTES

Understanding and characterizing the highway bridge inventory in California is a critical aspect of seismic vulnerability assessment of highway bridge classes in the state. This chapter presents an in-depth study of the California bridge inventory utilizing the National Bridge Inventory (NBI) database (NBI, 2010). Furthermore, an in-depth review of bridge plans and use of in-house databases such as BIRIS obtained from the California Department of Transportation (Caltrans) is used to supplement the NBI data to capture design details such as column dimensions and reinforcement details, bent cap details, common superstructure and abutment configurations, pile classes, and seat widths, which are absent in the NBI data. This helps to create sub-bins within a bridge class and leads to better bridge classes that have more consistent performance, design and detailing characteristics. The initial sections in this chapter present results from a detailed analyses of the California bridge inventory made available through the NBI database. Subsequent sections are devoted to the issue of sub-binning bridge classes and characterizing bridge geometric information pertinent to these sub-bins utilizing Caltrans in-house databases and an extensive review of bridge plans.

3.1 Bridge Classification Based on National Bridge Inventory and HAZUS

The National Bridge Inventory (NBI, 2010) is a database compiled by the Federal Highway Administration with the purpose of having a unified database for bridges, including identification information, bridge types and specifications, operational conditions, geometric data and functional description, and inspection data. The data available through the NBI database includes state and local county bridges and was

developed primarily for maintenance purposes and not necessarily seismic risk assessment. Every bridge is identified by a unique code consisting of 116 fields and detailed descriptions of the fields are found in the *Recording and Coding Guide for the Structure Inventory and Appraisal of the Nation's Bridges* (NBI Coding Guide, 1995). Although the code does not provide a complete description of the bridge, it provides information sufficient for a broad and general classification of highway bridge classes. Field 43 (A and B) aids in a broad classification of highway bridge classes. Field 43 is composed of two subfields: 43A and 43B, associated with the material type and/or design and type of design and/or construction of the superstructure, as detailed in Table 3.1 and 3.2, respectively.

Table 3.1: Kind of material and/or design listed in NBI (NBI, 1995)

Field 43A	Kind of material and/or design
1	Concrete
2	Concrete continuous
3	Steel
4	Steel continuous
5	Prestressed and post-tensioned concrete
6	Prestressed and post-tensioned concrete continuous
7	Wood or timber
8	Masonry
9	Aluminum, wrought iron, or cast iron
0	Other

HAZUS (2011) provides yet another classification scheme for highway bridge classes. Bridges are classified into 28 classes (HWB1 through HWB28) with similar performance characteristics when compared to NBI in an attempt to obtain better fragility curves when data becomes available. Bridges are classified based on seismic design, number of spans and span continuity in addition to the material and type of construction that is provided by NBI. Complete description of the HAZUS bridge classes is documented in Table 7.2 of the HAZUS Technical Manual (HAZUS-MH, 2011).

Table 3.2: Type of design and/or construction listed in NBI (NBI, 1995)

Field 43B	Type of design and/or construction
01	Slab
02	Stringer/multi-beam or girder
03	Girder and floor beam systems
04	Tee beam
05	Box beam or girders – multiple
06	Box beam or girders – single or spread
07	Frame (except frame culverts)
08	Orthotropic
09	Truss – deck
10	Truss – thru
11	Arch – deck
12	Arch – thru
13	Suspension
14	Stayed girder
15	Movable – lift
16	Movable – Bascule
17	Movable – swing
18	Tunnel
19	Culvert (includes frame culverts)
20	Mixed types
21	Segmental box girder
22	Channel beam
00	Other

Bridge classes in California are classified under thirteen main types and their description based on NBI is listed in Table 3.3. Their equivalent HAZUS classifications are also noted to facilitate comparison later on. Upon examination of the results in Table 3.3, it is seen that the bridge classes indicated in bold account for about 65% of the concrete bridge inventory in the state and these are considered for fragility modeling in the present study. The single span concrete girder bridge class is not considered in this study as these historically tend to be resilient under seismic loading (Nielson, 2007) due to the absence of columns which tend to be the most vulnerable component in many other bridge classes.

As noted in Table 3.3, MSCBG bridges account for the bulk of the overall (state and local) inventory and this class of bridges is comprised of single and multiple frame bridges. Based on the analysis of an in-house database of state bridges assembled by Caltrans engineers, it was seen that MSCBG bridges account for about 37% of the state

bridge inventory and is the predominant bridge type. These consist of single and multiple frame bridges. Fifteen percent of the box-girder bridges have at least one in-span hinge and these are typically referred to as multiple frame (MSC-MBG) bridges. Further, multiple frame bridges were seen to be characterized with five spans or more and this was used as the cut-off number of spans to distinguish them from single frame (MSC-SBG) bridges in the present study.

Table 3.3: Bridge classes in California and their proportion in the overall inventory

Bridge class	Nomenclature	Classification			Number of bridges	
		NBI		HAZUS	Count	%
		43A	43B			
Multispan continuous concrete box-girder	MSCBG	2, 6	05	HWB8, 9, 20, 21	5314	20.89
Single span concrete girder	SSC girder	1, 2, 5, 6	01, 02, 03, 04, 05, 22	HWB3, 4	4582	18.02
Multispan continuous slab	MSCSL	2, 6	01	HWB10, 11, 22, 23	4004	15.74
Multispan continuous concrete girder	MSCG	2, 6	02, 03, 04, 22	HWB10, 11, 22, 23	2164	8.51
Multispan simply supported steel girder	MSSSSG	3	02, 03, 04, 22	HWB13, 14, 25	1085	4.27
Single span steel girder	SSSG	3, 4	01, 02, 03, 04, 05, 22	HWB3, 4	936	3.68
Multispan simply supported concrete girder	MSSSCG	1, 5	02, 03, 04, 22	HWB6, 7, 18, 19	900	3.54
Multispan simply supported concrete box-girder	MSSSCBG	1, 5	05	HWB6, 7, 18, 19	398	1.56
Multispan simply supported slab	MSSSSL	1, 5	01	HWB6, 7, 18, 19	391	1.54
Multispan continuous steel girder	MSCSG	4	02, 03, 04, 22	HWB15, 16, 26, 27	322	1.27
Multispan continuous concrete frame	MSCCF	2, 6	07	HWB10, 11, 22, 23	8	0.03
Multispan simply supported concrete frame	MSSSCF	1, 5	07	HWB6, 7, 18, 19	4	0.02
Other†	Other				5326	20.94
					25434	100

†Other bridge types include concrete and steel culverts, concrete tunnels, concrete and steel bridges with other structural systems, wood/timber, masonry, aluminum, cast/wrought iron bridges.

Bold face entries in the table are the bridge classes considered in this study.

MSCC slab bridges account for about 12% of the state inventory while the MSCC girder bridges account for roughly 11% of the state inventory. The proportion of slab and girder bridges in the state inventory is consistent with their proportions in the overall inventory. MSCG bridges can be further classified into two types depending on the type of girder in the superstructure and the ability to transfer moments from the superstructure to the substructure. MSCG bridges with Tee girders in the superstructure are generally cast monolithic with the deck slab and the bent and thereby transfer moment to the substructure while girder bridges with Standard I and Bulb Tee girders rest on bearing pads at the bent. These are non-integral with the bent and do not transfer any moment to the substructure. Further details are provided in the latter part of this chapter. It was seen that about 45% of the MSCC girder bridges have non-integral (MSCG-I) I- and Bulb-tee girders while 55% of them have integral (MSCG-T) tee girders in their superstructure. The bridge classes considered for fragility modeling in this research are listed in Table 3.4 and account for about 45% of the bridge inventory in the state.

Table 3.4: Bridge classes considered for fragility modeling

Bridge class	Nomenclature
Multispan continuous concrete single frame box girder bridges	MSC-SBG
Multispan continuous concrete slab bridges	MSCSL
Multispan continuous concrete Integral Tee girder bridges	MSCG-T
Multispan continuous concrete Non-integral I- and Bulb-tee girder bridges	MSCFG-I

3.2 Bridge Class Statistics

In addition to facilitating a broad classification of bridges, NBI provides information on several other geometrical parameters associated with bridges. Fields 45, 48, 52 and 54 provide information regarding number of spans, maximum span length, deck width, and minimum vertical underclearance, respectively. It must be noted that NBI does not list the individual span lengths in the case of multispan bridges and only provides information about the maximum span length. Field 34 provides information

regarding skew in the bridge superstructure, measured as the angle between the centerline of a pier and a line normal to the roadway centerline. A value of 99 corresponding to this field indicates variable skew in the bridge.

Parameter estimation and distribution testing (Ang and Tang, 1975) is a common technique adopted to capture the spread of parameters with smaller data sets. However, in the present scenario, with the abundance of data made available by NBI, more reliable techniques such as fitting empirical cumulative distribution functions (CDFs) to the geometric data is chosen. In this technique, the data set containing N data points is rank ordered, generally in ascending order, $x_1 \leq x_2 \leq x_3 \leq \dots \leq x_N$. The probability of the i^{th} observation (or the CDF value) is then calculated by using the rank mean plotting position, given in equation (3.1), which is an unbiased estimator.

$$F_x(x_i) = \frac{i}{N+1} \quad (3.1)$$

Figure 3.1 shows empirical CDFs for maximum span length, deck width and minimum vertical underclearance for the bridge classes chosen in this study. Inspection of the span length distribution (Figure 3.1a) reveals that a majority of the MSCSL bridges have span lengths ranging from 16 ft to 50 ft, while the MSC-SBG have much longer span lengths up to 180 ft. In the case of MSCG-T girders, the range is between 30 and 80 ft, while the MSCG-I girders have span lengths ranging between 30 and 150 ft. These ranges are consistent with suitable span lengths for which these types of construction are generally chosen (BDA, 1988, 1989, 1995, 2004, 2009). Figure 3.1b shows the empirical CDF for deck width across all bridge classes chosen in this study. There is relatively small difference in the overall distribution of deck widths across bridge classes. It is intuitive since deck width is a function of number of traffic lanes on the bridge.

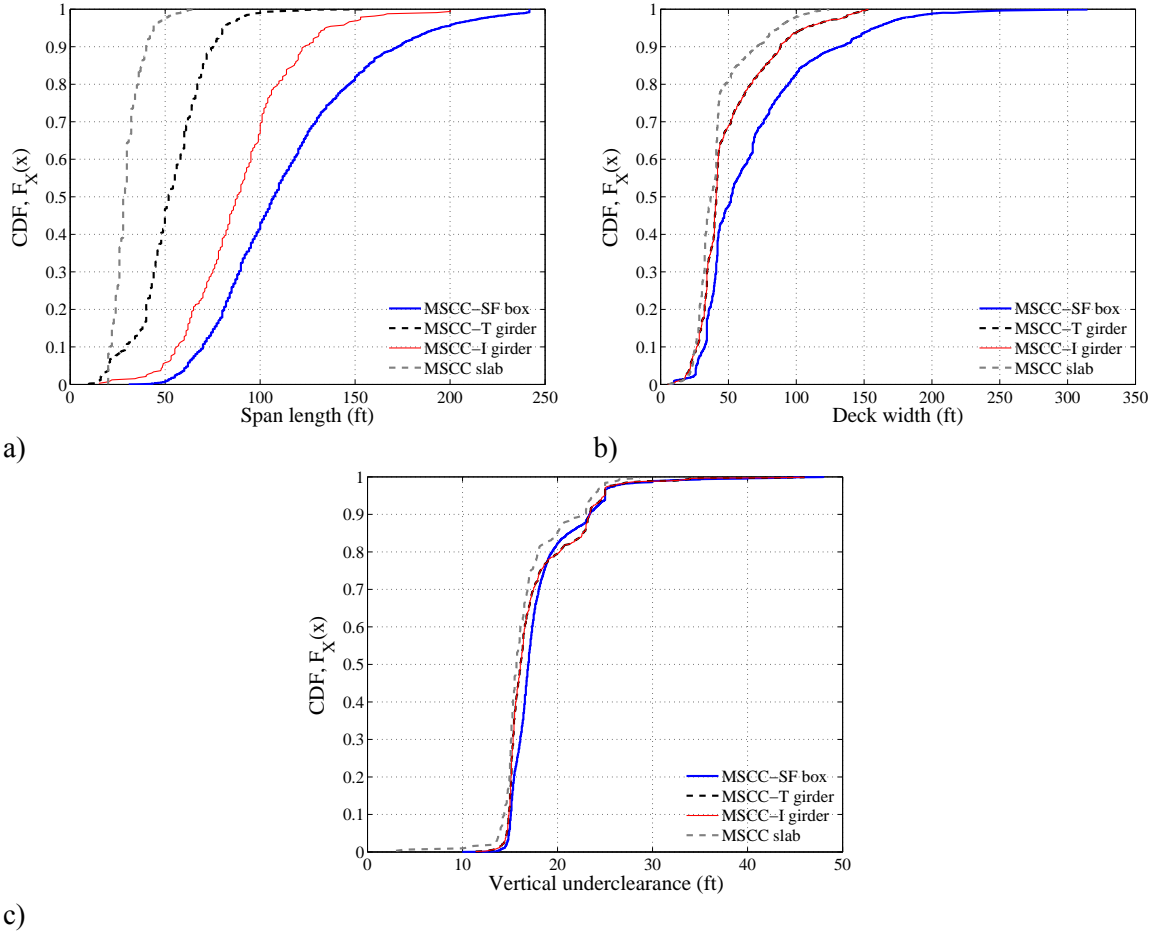


Figure 3.1: Empirical cumulative distribution functions for the chosen bridge classes for a) maximum span length, b) deck width, and c) minimum vertical underclearance

NBI does not explicitly record the height of bridge columns. In this study, column heights are inferred based on the vertical underclearance field in NBI, measured as the height between the underside of the bridge deck and the roadway surface. Based on permissible span-to-depth ratios, column height is obtained by deducting the superstructure depth (excluding the slab thickness) from the vertical underclearance. Empirical CDF for vertical underclearance across bridge classes is shown in Figure 3.1c. Similar to deck widths, the distribution for vertical underclearance is consistent across bridge classes chosen, with a range between 15 and 30 ft. Some basic statistics for these geometric features are provided in Table 3.5 to give an idea of the central tendency and

dispersion. The empirical CDFs completely describe the distributions and will be used in generating parameterized bridge models for fragility analyses.

Table 3.5: General statistics for bridge class geometrical parameters

Geometric parameter	Bridge class	Mean (ft)	Median (ft)	Std. Dev. (ft)
Span length	MSC-SBG	114.8	106.9	40.5
	MSCSL	30.1	27.9	7.61
	MSCG-T	53.1	51.8	17.9
	MSCG-I	89.5	87.9	27.9
Deck width	MSC-SBG	67.2	51.8	42.2
	MSCSL	41.9	37.1	19.1
	MSCG-T	53.0	41.0	33.5
	MSCG-I	53.0	41.0	33.5
Vertical underclearance	MSC-SBG	18.0	16.9	3.7
	MSCSL	16.7	15.7	3.2
	MSCG-T	17.7	16.1	4.2
	MSCG-I	17.7	16.1	4.2

Unlike the geometric parameters described previously, number of spans takes on discrete values and hence non-parametric probability mass functions (PMF) are generated for this parameter. The frequency of this data at each span number is determined and the count divided by the total number of bridges in a particular bridge class is defined as the respective probability of having that number of spans. Figure 3.2 shows PMFs for number of spans across bridge classes. Upon examination of the PMFs in Figure 3.2, it is seen that the most likely number of spans for MSCSL, MSCG-T and MSCG-I bridges is three while it is two for MSC-SBG bridges. This mode statistic for number of spans is used in generating parameterized bridge models for fragility analysis.

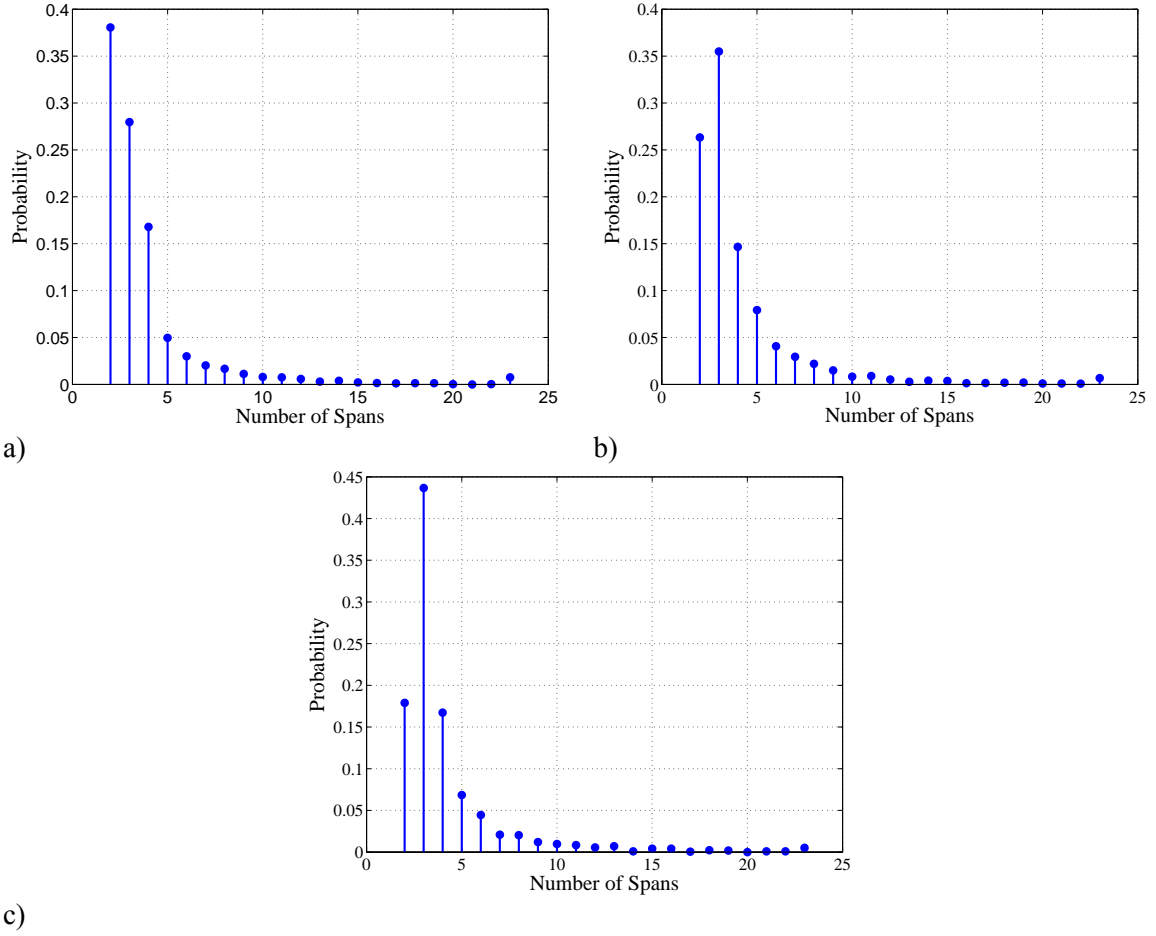


Figure 3.2: Probability mass function for number of spans for a) MSC-SBG, b) MSCSL, c) MSCG-T and MSCG-I bridge classes

As stated previously, NBI records skew in the bridge superstructure. Upon analysis of this parameter, it was seen that the average skew was 14.5° , 13° , and 14.4° for MSC-SBG, MSCSL, and MSCG-T and MSCG-I bridges, respectively and the mode statistic being zero in all cases. Since the majority of the bridges considered in this study have either zero skew or a value less than 15° , it is justified to neglect the effect of skew in this initial study. Further studies will determine the effect of skew on the vulnerability of bridges. At this point, it is recommended to use the modification factors for capturing the effect of number of spans and skew suggested in HAZUS-MH (2011), until more appropriate factors are determined.

3.3 Need for Sub-binning Beyond NBI

Seismic bridge design provisions in California have evolved significantly over the last few decades in response to the deficiencies exposed after significant seismic events (ATC, 1981, 1996; BDS, 1990; SDC, 1999, 2010). In order to develop reliable metrics such as fragility curves to quantify the seismic performance of bridges classes, it is imperative to understand the vulnerability associated with them as these design standards evolve. Geometric attributes captured in the NBI do not furnish any credible information regarding the potential vulnerabilities associated with the bridge classes. Bridge design details and physical characteristics help to capture the vulnerabilities associated with various components. Therefore, there is a need to sub-bin the bridge classes based on design eras with Caltrans bridge design, retrofit and maintenance data in addition to the information provided by NBI.

3.4 Bridge Design Eras and Typical Design Details

This section and the subsequent ones are devoted to identifying unique bridge design attributes and their evolution over three significant design eras, separated by the historic 1971 San Fernando and the 1989 Loma Prieta earthquakes. This is achieved by an in-depth review of bridge plans pertinent to the design eras for the chosen bridge classes, use of Caltrans in-house databases such as BIRIS and extensive input from design engineers and maintenance staff. Caltrans maintains a complete image archive of all bridge as-built plans, bridge inspection reports, photos, and other significant correspondence in the BIRIS database. It also contains completed maintenance activities, and minor and major rehabilitation projects.

The MSCC slab bridge class typically employs columns which are pile extensions above the ground. As will be demonstrated in this section and the subsequent ones, the major change in design philosophies across design eras is the details used in bridge

columns. Since, slab bridges are comprised of pile bents, there is not a major change in its design and performance across design eras (BDA, 1989, 1995, 2004, 2009).

3.4.1 Pre 1971 Design Era

Early Californian bridge seismic design codes dealt with the philosophy that seismic forces were proportional to the dead weight of the structure. Bridges were designed for a lateral seismic force equal to 6% of the structural dead weight until 1965, at which point structural period and amplification factors were considered (Duan and Li, 2003). The concept of ductility was absent and the detailing of reinforcement to achieve ductility by current standards was very poor.

3.4.1.1 Typical design details

The column shear reinforcement consisted of #4 transverse stirrups spaced at 12 in on center regardless of the column size or the size of the longitudinal reinforcing bars. Very short seat widths in the range of 6 to 8 in. were typical at the expansion joints. There was inadequate lap splice lengths of the column longitudinal bars near the footing and inadequate development of the column longitudinal bars into the footing without any standard hooks. Lap splicing of the column stirrups in the cover was also very common.

3.4.1.2 Vulnerabilities

The 1971 San Fernando earthquake revealed several vulnerabilities associated with bridges designed prior to that date. Column shear failure and pull-out of the longitudinal reinforcement was predominant due to the lack of ductility. Provision of short seat widths at the bents and the abutments increased the unseating potential. These were seen during the San Fernando, Loma Prieta and Northridge earthquakes (Yashinsky, 1995; Yashinsky and Karshenas, 2003; Caltrans, 2007; Priestley et al., 1996).

3.4.2 1971-1990 Design Era

The 1971 San Fernando earthquake emphasized the importance of detailing and ductility in the response of bridge structures with the introduction of capacity design principles in their design standards. The lateral load carrying capacity of the bridges was increased by a factor of 2 or 2.5 and the aspects of fault proximity, site conditions, dynamic structural response and ductile details (Yashinsky and Karshenas, 2003). These factors featured in the Caltrans design specifications in 1973. The Applied Technology Council (ATC) developed guidelines which were documented in the ATC-6 report (1981). These formed the basis for design of Caltrans bridges and primarily remained unchanged until the 1989 Loma Prieta earthquake. The standard practice was to design for plastic shear in the columns with the intention of failing the column in flexure while all the other components of the bridge remained elastic.

3.4.2.1 Typical design details

Some of the typical design details of this intermediate era are summarized below:

- The spacing of the transverse reinforcement in the columns was reduced with a typical spacing of 4 to 6 in. However, the confinement of the plastic hinge region was still absent
- Increase in the negative moment reinforcement in footing and pile caps without any shear reinforcement
- Splicing of column longitudinal bars was not permitted at locations of maximum moment
- Seat widths were slightly increased from 6-8 in in the Pre 1971 design era to about 12 in
- Prior to the occurrence of the Loma Prieta and 1994 Northridge earthquake, there seemed to be a common notion that column flares were typically non-structural components and would probably spall during an earthquake. However, it was seen

that the presence of a flare reduced the length of the column and increased the plastic shear demand. This design era was characterized with poor flare details which was improved in the following era

- Joint reinforcement between column and the bent cap and column and the footing was absent

3.4.2.2 Vulnerabilities

Column shear failure in the plastic hinge regions was typical due to the lack of confinement in this zone. Due to the poor flare details as explained in the previous subsection, shear failure was seen in columns with flares. Unseating potential at the bents, abutments and in-span hinge locations continued to be high due to the provision of short seat widths.

3.4.2.3 Retrofit strategies

Caltrans began the Phase-I bridge seismic retrofit program after the 1971 San Fernando earthquake (Yashinsky, 1995). The main objective of this program was to prevent unseating of bridge decks by the inclusion of longitudinal restrainers and transverse shear keys at the bents, abutments and in-span hinge locations. Failure of longitudinal restrainers and shear keys was reported during the 1989 Loma Prieta earthquake (Yashinsky and Karshenas, 2003).

3.4.3 Post 1990 Design Era

With the occurrence of the Loma Prieta earthquake, Caltrans solicited the ATC to provide recommendations for design standards, performance criteria, and practices (Duan and Li, 2003) and concurrently, extensive research focused on the seismic design and retrofitting of bridges in the United States (Priestly et al., 1996). All the recommendations from the ATC described in ATC-32 (1996) were incorporated into the Caltrans Bridge Design Specifications (BDS, 1990), and several internal design manuals (MTD 20-4,

1995; BDA, 1995; MTD 20-1, 1999; SDC, 1999). The fundamental emphasis was on displacement-based or capacity design approach which ensures a ductile failure mode in the columns while the remainder of the bridge remained elastic. The 1994 Northridge earthquake stood testimony to the superior performance of the retrofit program, and is discussed in the later part of this section.

3.4.3.1 Typical design details

- In a general sense, bridges in this era had fewer number of expansion joints and more continuity in the superstructure, larger skews were avoided, and usage of column flares was very minimal
- Tight confinement reinforcement was provided in the column plastic hinge zones with spacing of less than 6 times the longitudinal bar diameter
- Large seat widths on the order of 24 in were provided
- Improvised flare details were provided by isolating the flare from the superstructure by the introduction of a 2 in to 4 in gap
- No lap splices were provided in the plastic hinge zones
- Shear reinforcement was provided in the footing and pile caps
- Joint reinforcement was provided between column and the bent cap and column and the footing

3.4.3.2 Retrofit strategies

With the occurrence of the Loma Prieta earthquake, Caltrans began a Phase-II bridge seismic retrofit program to address a wider range of problems associated with the Pre 1971 design era bridges and adopted a more sophisticated approach (Yashinsky, 1995). The fundamental focus was on the non-ductile Pre 1971 columns by retrofitting them with steel or fiber jackets. As mentioned previously, failure of a number of short hinge restrainers provided during the Phase-I retrofit program was observed during the

Loma Prieta earthquake. These were replaced by longer restrainers and further pipe seat extenders were provided to prevent unseating in the event of failure of the restrainers (Yashinsky and Karshenas, 2003). Footings were strengthened by increasing the height of the cap and providing additional piles. This would minimize the potential for the column longitudinal bars to pull out due to the availability of a greater length in the footing for their development.

3.5 Bridge Components and Typical Details

Having discussed the progression of seismic bridge design specifications and the potential vulnerabilities at the bridge system level over three significant design eras, this section provides details about individual bridge components for the bridge classes considered in this study. The details provided here are based on an extensive review of bridge plans pertinent to the chosen bridge classes in the three design eras.

3.5.1 Bridge Superstructure

Bridges are composed of two parts – superstructure and the substructure, as illustrated in Figure 3.3. Clearly, different bridge types have different load transfer mechanisms in the longitudinal and transverse directions. MSC-SBG and MSCG-T bridges are generally cast-in-place (CIP) and the deck and girders are monolithic over the bents (i.e. have integral bent caps). Longitudinal reinforcing bars or the post-tensioning (if applicable) ensures frame action in the superstructure. MSCSL bridges also fall under the same category where the deck slab is monolithic over the bents. Therefore, during an earthquake, the integral bent cap connection ensures that the columns move along with the superstructure and force transfer occurs by a combination of flexure and shear. On the other hand, the MSCG-I bridges are typically pre-cast (PC) or pre-manufactured at a factory location off-site and assembled at the bridge site. The girders are placed on top of dropped bent caps and are stabilized by the inclusion of end and intermediate

diaphragms. These form a critical part of the load path in transferring the dead loads and seismic forces from the deck and girder system down to the bearings and the bent cap. It must be noted that the presence of bearings allows for a relative rotation between the girders and the bent cap.

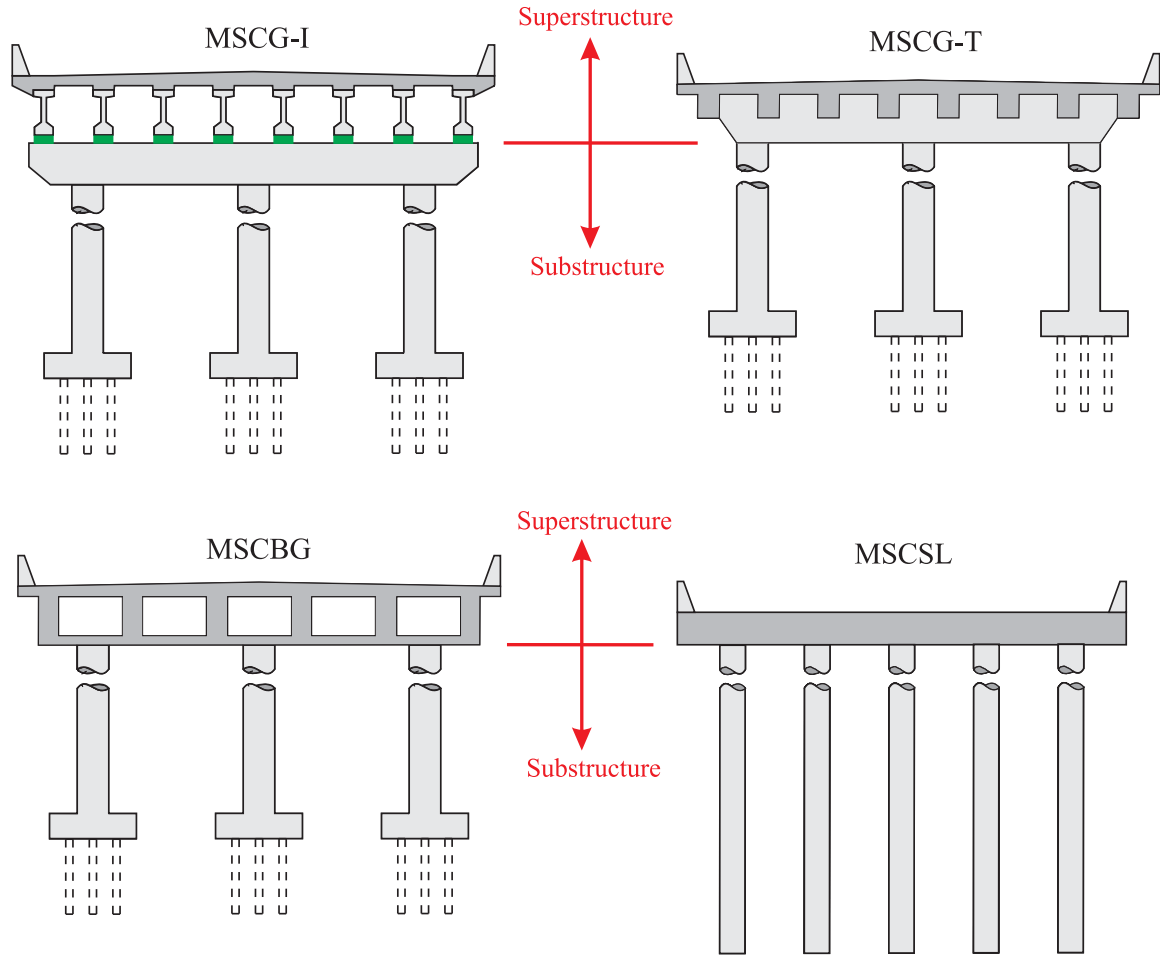


Figure 3.3: Superstructure and substructure classification for different bridge classes

Bridge superstructures have generally performed well during past earthquakes. This is typically because they tend to remain essentially elastic with very little or no non-linear effects. The general vulnerabilities associated with the superstructure are unseating at the seat abutments when large relative displacements between the deck and the abutment backwall exceeds the seat length. Figure 3.4a shows a depiction of excessive displacement between the deck and the abutment backwall during the 1994 Northridge

earthquake. Figures 3.4b and 3.4c shows total collapse of the Cypress Street Viaduct and the Interstate 5 Overpass during the Loma Prieta and Northridge earthquakes, respectively. Local spalling of concrete may also take place due to impact between the deck and the abutment backwall. Figure 3.4e shows pounding damage to a bridge in-span hinge during the 1994 Northridge earthquake.

MSCC-I girder bridges in the pre 1971 and 1971-1990 design eras have been made continuous over the bent for live load i.e., by making the deck continuous over the bents and the inclusion of diaphragm over the piers. This reduces the potential for collapse and typically leads to the girders falling the height of the bearings and then sliding on the bent cap. Figure 3.4d shows deck damage in the Bolu viaduct consisting of precast I girders, during the 1999 Duzce earthquake. In the case of CIP bridges, the columns might experience larger forces in comparison to PC bridges, due to the rigid connection between the superstructure and the substructure in the former case. In either case, the superstructures could develop large lateral forces causing failure of bearings and the connection to the substructure. Extensive details about superstructure configuration for the chosen bridge classes across design eras are documented in Appendix A.



Figure 3.1: a) Large relative displacements between deck and the abutment backwall during Northridge earthquake, b) span unseating in the Cypress Street Viaduct during the Loma Prieta earthquake, c) deck collapse in the Interstate 5 overpass during the Northridge earthquake, d) deck damage in the Bolu viaduct during the 1999 Duzce earthquake, and e) pounding damage in Santa Clara River bridge between the deck and abutment backwall during the Northridge earthquake

3.5.2 Columns

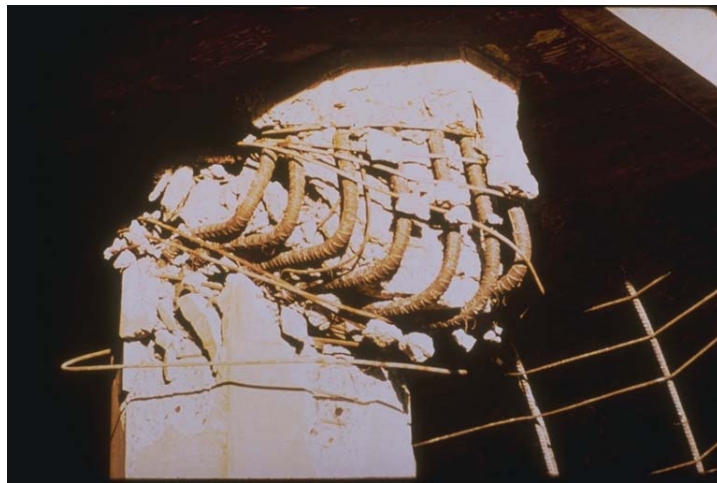
A majority of bridge seismic failures in the past are attributed to column failures. The failure mode (flexure versus shear) depends, in part, on the era in which the column

was designed. The flexural response of reinforced concrete (RC) bridge columns depends on a number of factors such as the longitudinal and transverse reinforcement ratios, reinforcement detailing, aspect ratio as well as the axial load ratio (Wight and MacGregor, 2011). The major contribution rests with the design details which vary based on the design era. The flexural failure mode is typically ductile in nature and is characterized by horizontal cracks and is the preferred mode of failure. On the other hand, the shear response of RC bridge columns is governed by four independent mechanisms: shear friction in compression zone, aggregate interlock, truss mechanism of the transverse reinforcement, and dowel action of the longitudinal reinforcement (Wight and MacGregor, 2011). Dowel action is typically minimal and can therefore be neglected in most cases. The relative contribution of the other three mechanisms to the shear response depends on the era in which the column is designed. Unlike the flexural failure mode, the shear failure mode is brittle in nature and is characterized by diagonal cracks.

3.5.2.1 Pre 1971 Columns

Columns designed prior to 1971 are predominantly characterized by shear response and as a result cannot fully develop their flexural capacity. A typical column in this era has transverse reinforcement consisting of #4 stirrups at 12 in on center irrespective of the column dimensions or the longitudinal reinforcement. The column relies on shear friction and aggregate interlock predominantly for strength and cracking is exacerbated since the aggregate interlock component declines rapidly leading to a brittle failure. However, even if the column yield moment is attained, the strength of the column degrades rapidly thereafter due to the poor confinement provided by the transverse reinforcement. The aforementioned behaviors are undesirable and typically results in total collapse of the bridge structure. Figures 3.5a and 3.5b show cases of shear failure in bridge columns during the San Fernando earthquake.

Another distinct detail associated with this design era was the embedment of the column longitudinal bars into the footing and bent cap without 90 degree hooks. Further, it was common practice to lap splice the column longitudinal bars just above the footing. In either case, the embedment or the lap splice length was too short (less than 20 longitudinal bar diameters) to develop the yield stress of the reinforcement. This caused pull out failures of columns from the footing during the San Fernando earthquake, as shown in Figure 3.6.



a)



b)

Figure 3.5: Shear failure in bridge columns a) at the intersection of Interstate 5 and 210, and b) of Foothills Freeway Overpass, during the San Fernando earthquake



Figure 3.6: Column pull out failures during the San Fernando earthquake

3.5.2.2 1971-1990 Columns

Columns in this design era were designed based on the capacity design process. Sufficient reinforcement was provided to develop the yield moment in the cross-section. However, the importance of cyclic degradation of shear strength and longitudinal bar buckling was not realized. Therefore, even if the yield moment of the cross-section was attained, the capacity degraded fairly quickly due to inadequate confinement of the plastic hinge region. This leads to fracture of the transverse reinforcement and buckling of the longitudinal reinforcement. Figure 3.7 depicts the aforementioned failures in bridge columns during the Northridge earthquake.

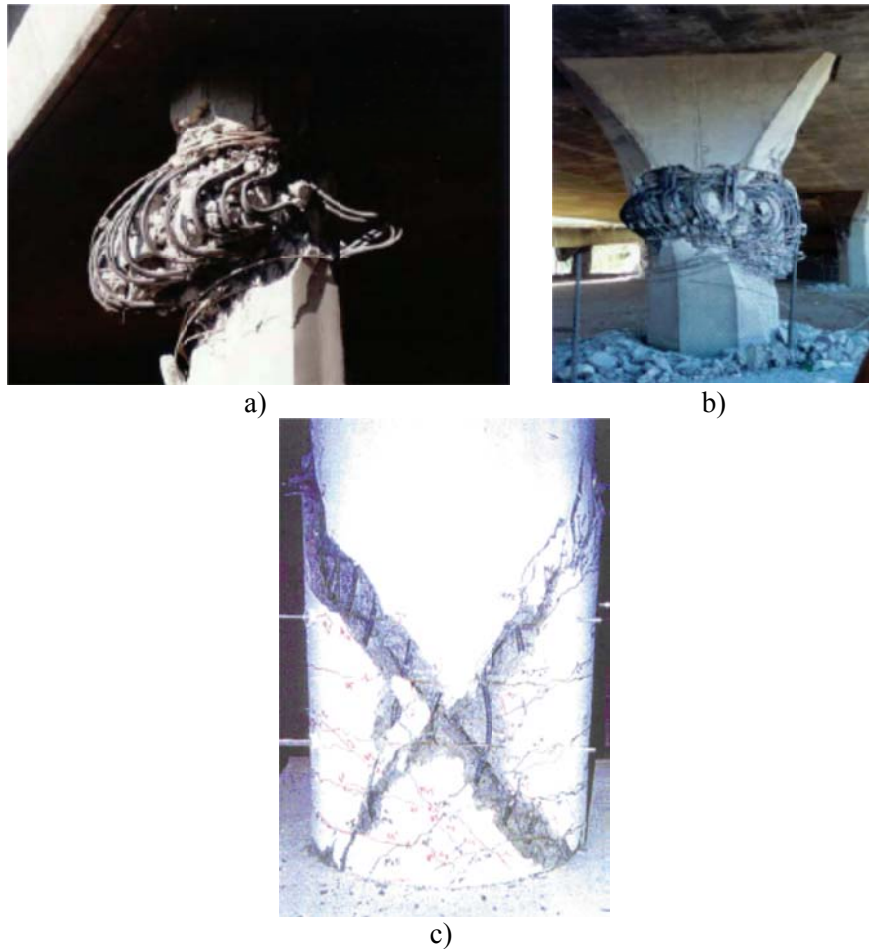


Figure 3.7: Shear failure in the a) and c) plastic hinge region of column, and b) flared column, during the Northridge earthquake

3.5.2.3 Post 1990 Columns

The columns in the modern era are designed by giving complete consideration to the shortcomings of the previous eras. These are characterized by superior confinement of the plastic hinge region thereby preventing longitudinal bar buckling and shear failure. The columns have significant ductility and energy dissipation capacity. Therefore, in the event of an earthquake, they might experience significant nonlinearities, but manage to maintain the gravity load carrying capacity and thereby ensure collapse prevention. The capacity design process adopted in the modern era forces a flexural failure mode in columns prior to shear failure. If this does not occur, then the columns would experience a ductile shear failure primarily due to the truss mechanism of shear strength exhibited by

the transverse reinforcement. In such cases, yielding and eventual fracture of the transverse stirrups or hoops is likely.

Figure 3.8 shows the difference in performance of the columns based on their evolution across the design eras discussed in this section. Details about the column dimensions, longitudinal and transverse reinforcement ratio for the bridge classes is obtained by an extensive review of bridge plans and the details are presented in Appendix A. As stated previously, MSCSL bridges employ columns which are pile extensions and a major change in the pile cross-sections or details were not observed across the design eras considered in this study. Details about the pile cross-sections and the reinforcement layout are also documented in Appendix A.

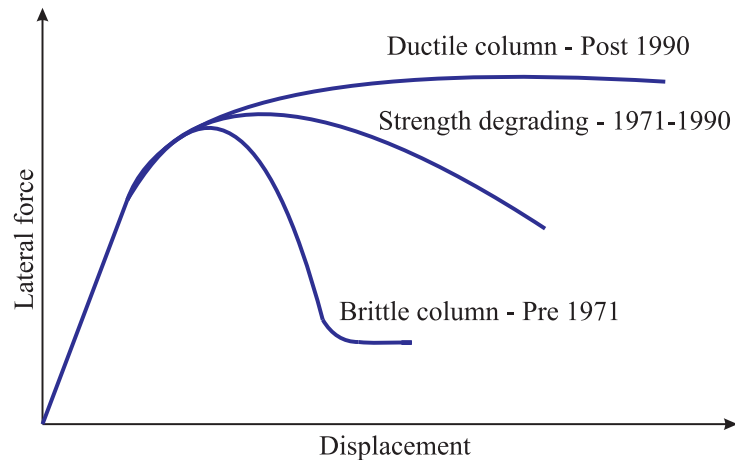


Figure 3.8: Lateral force deformation curves for typical bridge columns through the design eras

3.5.3 Superstructure to Substructure Connectivity

In the past, connections between the column and the superstructure and column and the foundations have proven to be vulnerable. This is particularly relevant in the case of MSC-SBG, MSCSL and MSCG-T bridge classes which have an integral bent cap and the column reinforcement frames into the superstructure. Connections should have the capability of resisting large shear forces, bending moments and axial forces. Often the connections have little room to develop reinforcement and provide confinement. Figure

3.9 shows a schematic of the possible connectivity types based on the bridge class and type. The connectivity types are referred to as Moment Frame Action (MFA) types drawing reference to their ability to transfer moments and shears. These further reinforce the continuity with respect to earthquake forces, more so with the moment frame kind of behavior rather than the continuity with regards to live load as in the case of NBI.

- MFA-0 depicts the case when the reinforcement over the bents is not continuous. The girders are essentially simply supported and the continuity is enforced by the presence of a continuous deck slab across the bent. There is no moment transfer from the superstructure to the substructure. MSCG-I bridges in the Pre 1971 and 1971-1990 design eras fall under this category.
- MFA-1 depicts the case when the girders and the deck slab are continuous across the bent. However, in this case there is also no moment transfer between the superstructure and the substructure. Both MFA-0 and MFA-1 are characterized typically by the presence of bearings. MSCG-I bridges in the Post 1990 design era fall under this category.
- MFA-2 is a moment resisting connection where there is a negative moment transfer between the superstructure and the substructure. This is enabled by the presence of continuous top reinforcement in the superstructure across the bents. However, the bottom reinforcement in the superstructure is terminated just before the bent. MSC-SBG, MSCSL and MSCG-T girder bridge classes in the Pre 1971 and 1971-1990 design era fall under this category.
- MFA-3 is a moment resisting connection where both positive and negative moments are transferred between the superstructure and the substructure. This is the premise of the capacity design process adopted in the modern era bridges. MSC-SBG, MSCSL and MSCG-T bridge classes in the Post 1990 design era fall under this category.

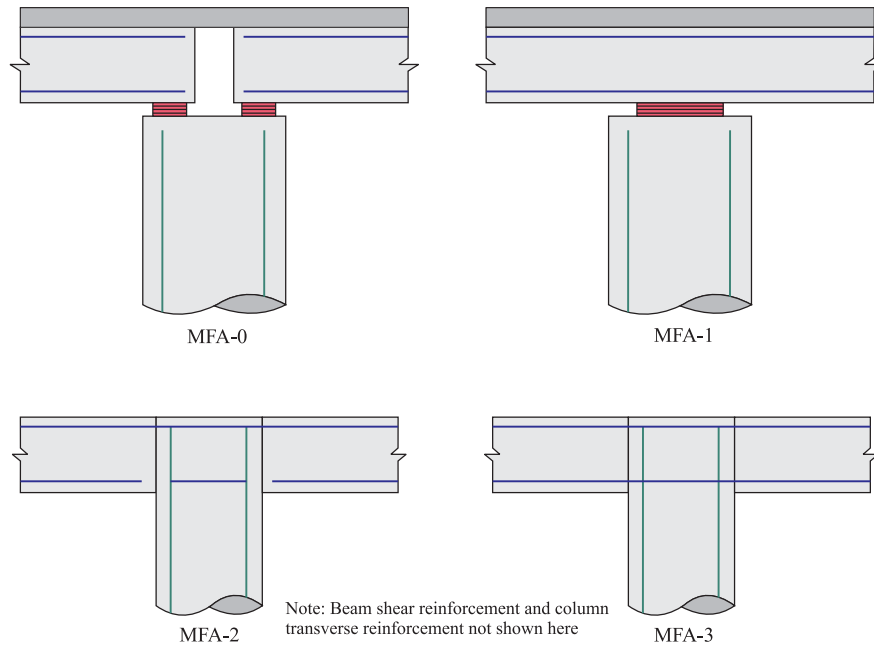


Figure 3.9: Schematic of superstructure to substructure connectivity types

The fundamental advantage of having connectivity types MFA-0 and MFA-1 in a bridge (as in the case of MSCG-I bridge class) is that the superstructure is not subjected to the seismic moments transferred by the column. This helps in achieving longer continuous spans in the superstructure (Priestley et al., 1996). For bridges with single column bents with a moment resisting connection at the base (this is typically the case), the column behaves like a vertical cantilever in both longitudinal and transverse directions and hence the response is independent of the direction. This provides for the design and usage of simple column circular cross-sections. However, the presence of MFA-0 and MFA-1 connectivities prohibits the use of pin connections at the column base in multi column bents.

On the other hand, bridges with connectivities MFA-2 and MFA-3 create the potential for additional redundancies in the seismic load path. Moment resisting connection between the superstructure and substructure provides a potential location of a plastic hinge at the column top thereby increasing the energy dissipation capacity. This

could be particularly beneficial in single column bents, where there is an additional location for energy dissipation complementing the plastic hinge at the column base. This connection type facilitates the provision of pinned connection at the base of multi column bents. However, if moment resisting connections are provided at the base of multi column bents similar to their connection with the superstructure, then it paves the way for adopting simple circular column cross-sections since the stiffnesses are equal in either directions and independent of the response (Priestley et al., 1996).

A main disadvantage associated with the connection of type MFA-2 or MFA-3 is the vulnerability associated with them based on when they were designed. Bridges with type MFA-2 were predominant in the Pre 1971 and 1971-1990 design era and these had inadequate longitudinal reinforcement at the top and no bottom reinforcement (as depicted in Figure 3.9). Seismic forces typically cause the joint to crack and in such cases stability is provided by the longitudinal reinforcement going through the crack and the crack is held intact by the transverse reinforcement. Failure of joints was reported during the Loma Prieta earthquake and is shown in Figure 3.10. Figure 3.11a shows a poorly detailed joint in a Pre 1971 MSC-SBG bridge. Integral connections of this type further might create a critical design condition where seismic moments will add to or subtract from the gravity load moments at the column face. Longitudinal reinforcement on the bottom face will have to be provided in order to carry the positive moment. As mentioned previously, the absence of bottom longitudinal reinforcement at the joint might lead to an increased vulnerability in the case of bridges with connectivity type MFA-2. This problem was however overcome in the Post 1990 era bridges where bottom reinforcement was provided at the joint and the top reinforcement was increased. Figure 3.11b shows a modern MFA-3 type joint that is well detailed and is the preferred type for MSC-SBG and MSCG-T bridge class. Figure 3.11c shows a MFA-3 type joint for MSCSL bridge class. Also shown in Figure 3.11d is connectivity type MFA-0 in an MSCG-I bridge.



Figure 3.10: Joint damage to the Embarcadero viaduct during the Loma Prieta earthquake

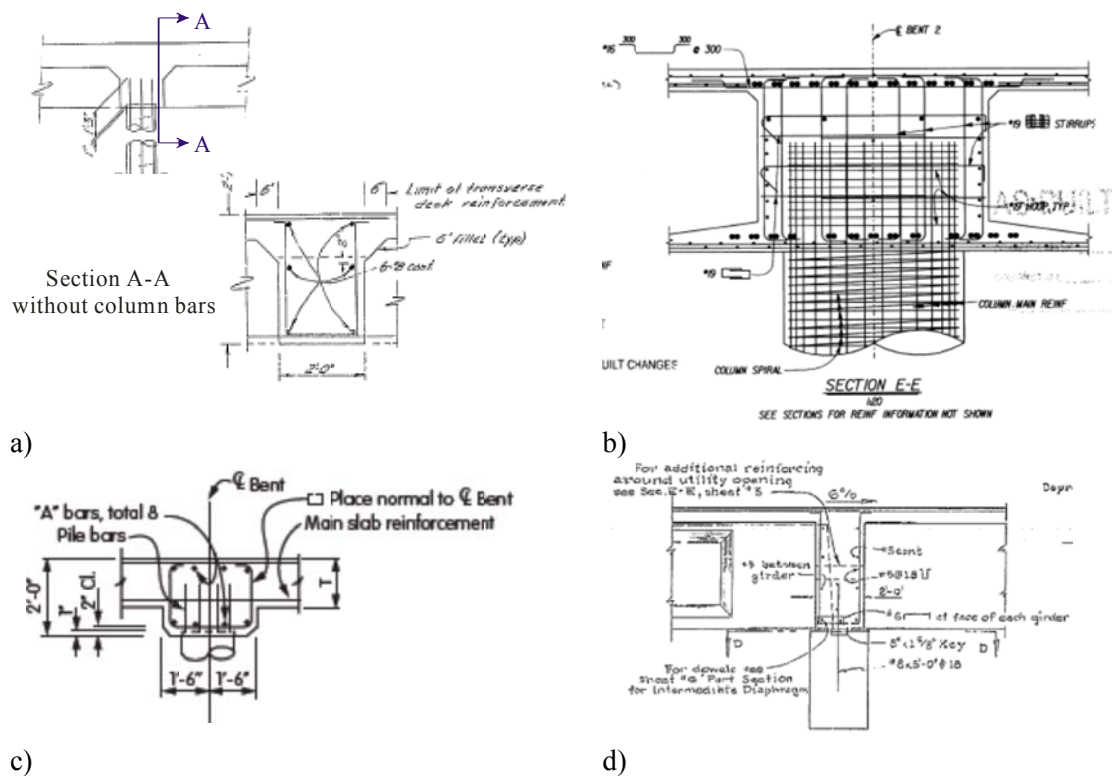


Figure 3.11: Typical joint details from a) Pre 1971 design era in MSCC-SBG, b) Post 1990 MSC-SBG, c) MSCSL, and d) MSCG-I girder bridge class

3.5.4 Abutments

Abutments can be classified into two basic types: open end and closed end. Diaphragm and seat type abutments fall under the category of open end abutments. These abutments are typically placed at the top of the approach embankment and have evolved from the desire to present an open appearance to traffic beneath the structure. The fundamental difference between the seat type and diaphragm abutments is that the former allows superstructure movement independent of the abutment while the latter does not. Closed end abutments present a closed appearance to approaching traffic by placing the structure support adjacent to traffic and are classified as below. Figure 3.12 shows a schematic of the different abutment types. Closed end abutments are used infrequently and better suited for bridge widenings and constrained urban locations. Abutments can be classified as follows:

- a) Backfilled
 - i. Cantilever abutment
 - ii. Strutted abutment
 - iii. Rigid frame
- b) Cellular
 - i. Bin
 - ii. Closure wall

Open end abutments are more economical, adaptable and attractive when compared to the closed end abutments (BDA, 1989). These typically have lower height walls when compared to closed end abutments and therefore have a smaller settlement of the approach slab in bridges. Only open end abutments are considered as a part of this research.

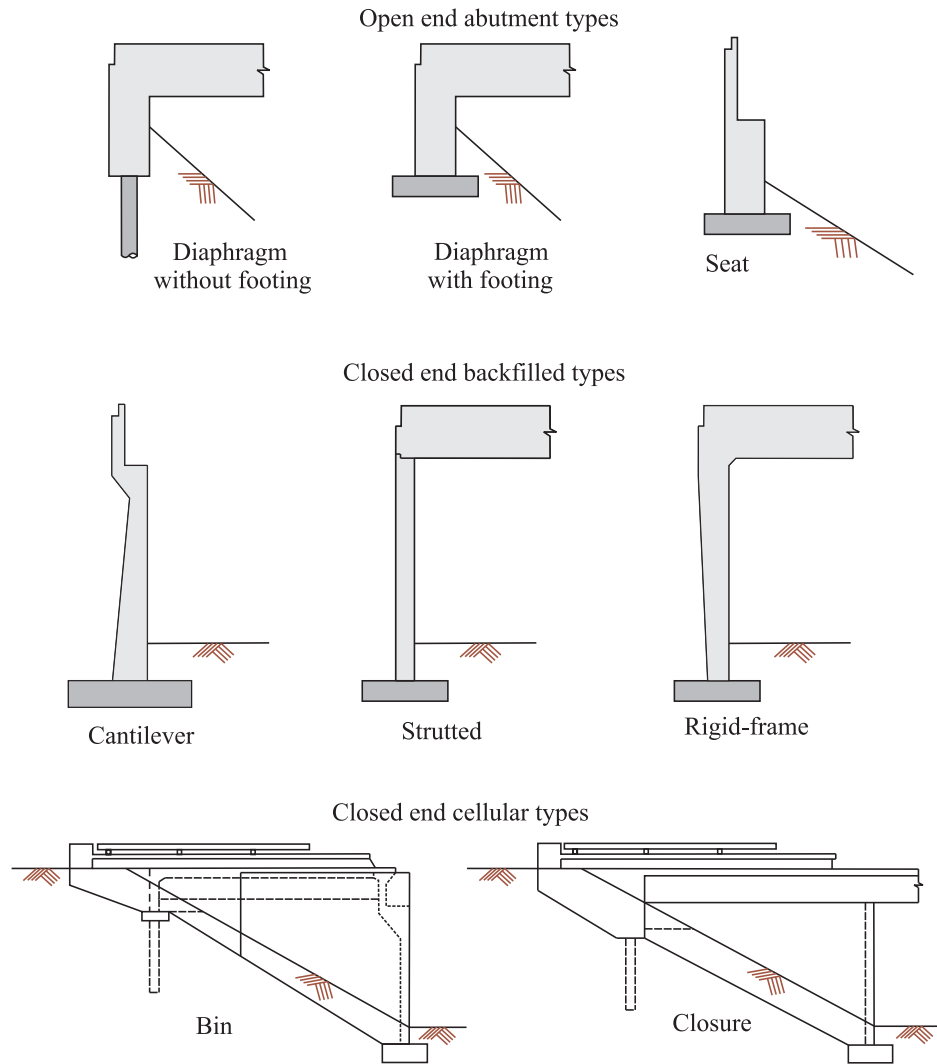


Figure 3.12: Schematic of abutment configurations

3.5.4.1 Diaphragm abutments

Diaphragm abutments are cast monolithic with the superstructure and readily engage the backfill soil and therefore provide a great source for seismic energy dissipation. This configuration is attractive because it reduces the likelihood of span unseating. The gravity loads are typically carried by the piles and the longitudinal resistance to seismic forces is provided jointly by the passive pressure in the backfill soil and the piles. Bridges with diaphragm abutments tend to be stiff and the abutments in particular are stiffer than the adjacent bents thereby attracting a larger proportion of the

imposed seismic force (Priestley et al., 1996). The longitudinal resistance provided by the backfill is based in mobilizing the backfill equal to the depth of the superstructure (SDC, 2010). Figures 3.13a and 3.13b show standard details for diaphragm abutments without and with foundations across bridge classes for all design eras (BDA, 2009). Details about the pile spacing are provided in Appendix A. The design recommendations and guidelines for these abutments are provided such that flexural failure of the backwall precedes shear failure. Typically, the large levels of resistance provided by the passive pressure of the backfill soil in the longitudinal direction is absent in the transverse direction, and the resistance is based on the piles and shear capacity of a wing wall (Priestley et al., 1996). Wing walls typically act as external shear keys and the ultimate force is restricted to 75% of the shear capacity of the adjacent bent (MTD 5-1, 1992).

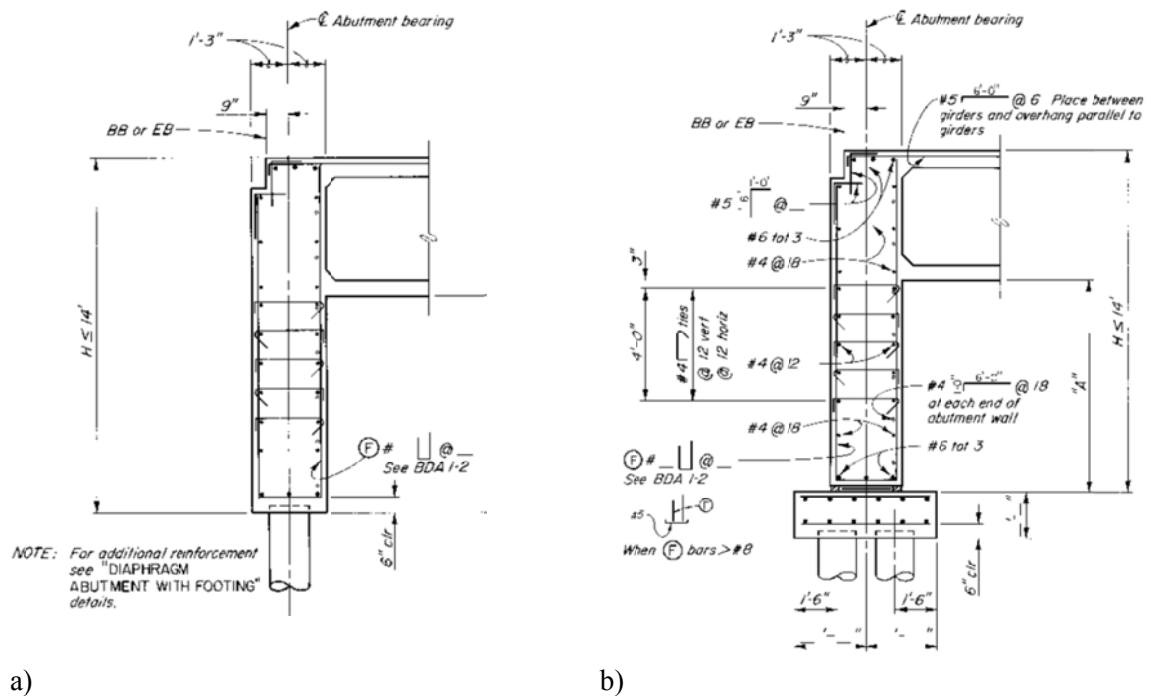


Figure 3.13: Standard details for diaphragm abutments a) without footing, and b) with footing (Source: BDA, 2009)

Past experiences have shown that damage to the abutment during a major earthquake does not lead to the possibility of collapse in the superstructure in the case of diaphragm abutments (MTD 5-1, 1992). However, since the active response of the abutments is solely based on the piles, damage to the piles can take place when the superstructure displaces away from the abutment in the longitudinal direction. Figure 3.14 shows damage to abutment piles during the 1991 Costa Rica earthquake.



Figure 3.14: Abutment pile damage during the 1991 Costa Rica earthquake (Source: Moehle and Eberhard, 2003)

3.5.4.2 Seat type abutments

Seat type abutments provide a bearing support to the superstructure which is restrained longitudinally by the abutment backwall and transversely by the shear keys. The presence of gap between the end of the deck and the backwall increases the potential for unseating. High resistance and stiffness is provided when the initial gap is closed under longitudinal seismic response. However, when the superstructure moves away from the abutment, the resistance depends primarily on the bearing pads. The backwall in a seat type abutment is typically designed to fail under impact and passive response, before damaging forces are transmitted to the lower portion of the abutment (MTD 5-1, 1992).

As in the case of diaphragm abutments, the transverse resistance is provided by the piles and the shear keys. The shear keys are designed to resist shear forces equal to 75% of the shear capacity of the adjacent bent. Figure 3.15 shows standard details for a seat type abutment adopted in the bridge classes across design eras.

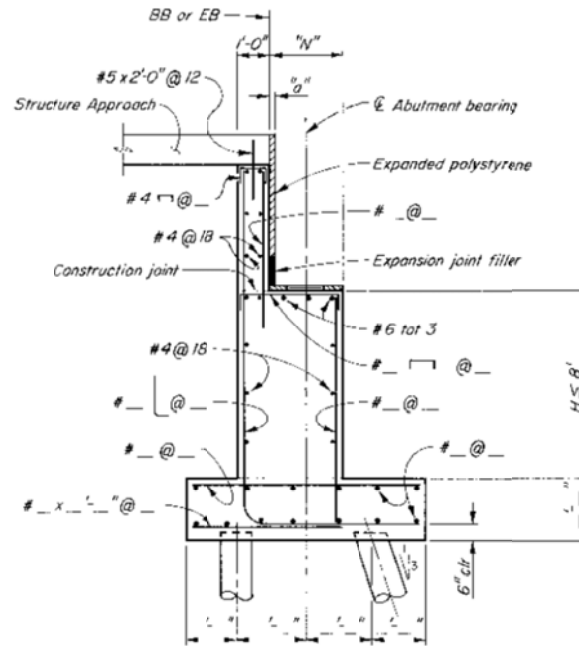


Figure 3.15: Standard details for seat type abutments (BDA, 1988)

The potential vulnerabilities associated with seat type abutments are superstructure span unseating and damage to the shear keys. Figure 3.16a shows damage to external shear key shear key in a seat type abutment during the Northridge earthquake while Figure 3.16b shows span unseating at the abutment. Details about the abutment configuration and pile spacing are provided in Appendix A.

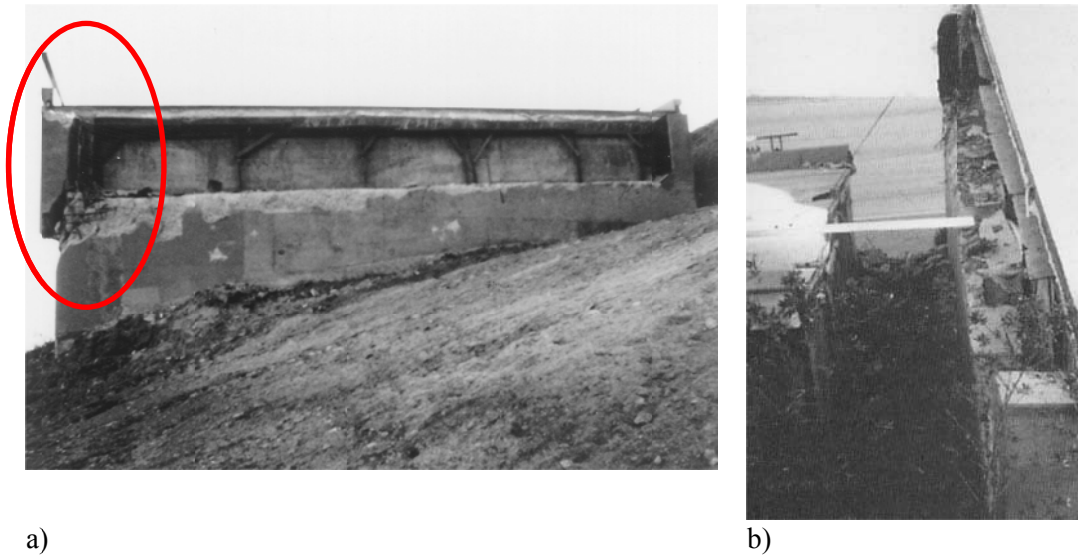


Figure 3.16: a) Damage to external shear keys (Source: Moehle and Eberhard, 2003), b) span unseating (Source: Caltrans, 2007) during the Northridge earthquake

3.5.5 Foundation Systems

Foundations provide a means whereby service and ultimate loads are transmitted from the structure to the underlying soil. Bridge foundations have a number of alternatives such as spread footings, integral pile-shaft or columns and pile supported footings. The appropriateness of the different types are governed by the loading requirements, site specific soil conditions, overhead clearance, existing utilities and proximity of existing facilities such as buildings and railroads (Caltrans, 2008). The fundamental design criterion is to force the plastic hinge to form at the base of the column.

Figure 3.17 shows the possible footing types in bridges. Spread footings (Figure 3.17a) are used in cases where the underlying ground is firm and has rocky conditions. Review of bridge plans for different bridge classes across design eras revealed the prevalence of integral pile shafts and pile supported footings. These two types are considered in the present study. Integral pile shafts are used extensively in MSCG-T and MSC-SBG bridges across all design eras and are cast-in-drilled-hole (CIDH). Review of

bridge plans for MSCSL bridges also revealed the predominant presence of integral pile-columns where columns were pile extensions above the ground without a change in cross-sectional dimensions (shown in Figure 3.17c). These footing types are economical when compared to pile supported footings. In the case of integral pile-columns, the plastic hinge typically forms at a depth close to two pile diameters (Priestley et al., 1996). The length of plastic hinge is typically longer than that in pile supported footings and spalling of concrete is prone to occur with larger hinge rotations and this typically goes undetected in the aftermath of an earthquake unless inspectors focus on excavating sufficient depth underneath the column. Integral pile-column with oversize piles (Figure 3.17d) are common in the case of MSC-SBG bridges where the pile moment capacity is increased above that of the column to force the plastic hinging to occur at the column base. This facilitates easy inspection in the aftermath of an earthquake but the downside being early spalling of the cover concrete due to reduced plastic hinge lengths.

Pile supported footings, shown in Figures 3.17e and 3.17f, typically consist of precast (reinforced or prestressed concrete), driven, or CIDH piles with pile cap footings. In all cases, positive connection is provided between the pile and the pile cap to ensure proper force transfer. As in the case of integral pile shafts, the fundamental philosophy in this case is also to force the plastic hinging at the base of the column.

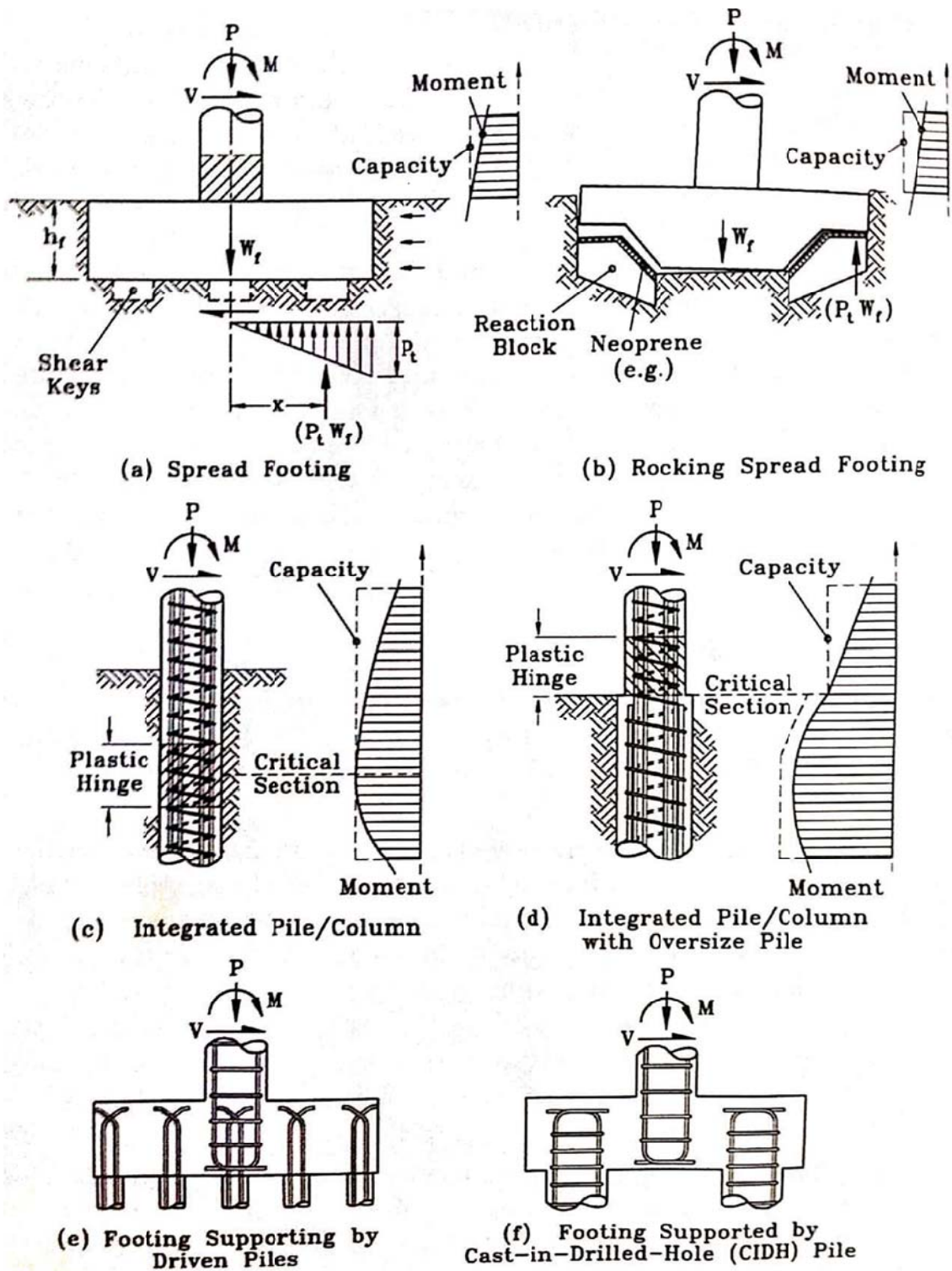


Figure 3.17: Bridge foundation types (Source: Priestley et al., 1996)

Bridge foundations have generally performed well during past earthquakes. Damage to foundations is reported to have taken place after extensive damage to the bridge columns at which point it is redundant. Foundations designed prior to 1971 were smaller in size compared to those designed after 1971 and comprised of positive moment reinforcement alone. This disables them from resisting the negative moment induced by soil overburden or tension piles. Further, the absence of shear reinforcement makes them susceptible to shear failure. Bridge foundations on liquefiable soil may be subjected to vertical settlement and/or lateral movement causing severe damage to them along with damage to the columns and superstructure. Post San Fernando earthquake, several foundations were retrofitted by the provision of negative moment reinforcement. However, post Northridge earthquake, the foundations were further retrofitted by the provision of shear reinforcement and additional piles. Figure 3.18 shows the retrofit strategy in a pile supported footing.

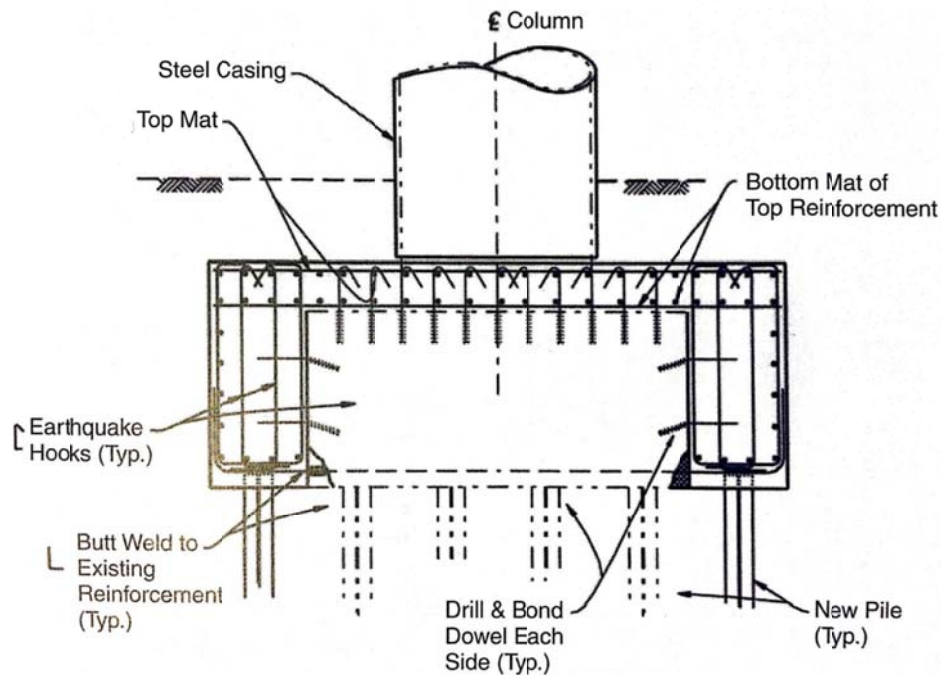


Figure 3.18: Pile supported footing retrofit (Source: Yashinsky and Karshinas, 2003)

Appendix A documents the different foundation systems and soil profiles for the bridge classes considered in this study. Also provided here are details of the pile cross-sections and reinforcement layout. The distributions encompass a wide range of soil profiles from soft soils to stiff clay for different foundation configurations.

3.5.6 Seat, Bearings, Restrainers and Shear Keys

As described in Section 3.4, a major consequence of the San Fernando earthquake was widespread unseating of bridge decks at the abutments, bents and expansion hinges. Majority of the subsequent efforts (Caltrans Phase-I and Phase-II retrofit programs) involved means to prevent unseating by increasing the seat width in new designs, provision of longitudinal restrainers and transverse shear keys to existing bridges. With the failure of a number of short hinge restrainers provided in the Phase-I retrofit program during the Loma Prieta earthquake, longer restrainers and pipe seat extenders were provided. This section presents details about the range of bridge seats, restrainers and shear keys considered across bridge classes and design eras based on the review of bridge plans.

Bridge seat and joint locations vary by the bridge class. Seat type abutments, as the name suggests, consists of a seat at the abutment where the bridge deck rests. A support seat at the bent cap exists for MSCG-I bridges while it is absent in the case of the other bridge classes considered in this study due to the presence of an integral bent cap. Bridge seat widths chronologically increased from the 4 – 12 in (S1) range in the Pre 1971 design era to 12 – 18 in (S2) range in the 1971-1990 design era and 18 – 24 in (S3) and greater than 24 in (S4) range in the Post 1990 design era. The Phase I and II retrofit programs addressed this issue by retrofitting the pre 1971 and 1971-1990 to the post 1990 seat categories by the provision of restrainers and pipe seat extenders. Bridge joints are typically sealed and the type of seal chosen for the purpose depends on the movement rating (MR). MR is the total anticipated movement from widest to narrowest opening of a

joint. This typically equals the total thermal movement plus any anticipated shortening. Typically, joint seals are the first components in a bridge joint to be damaged under a seismic event. The type of seal used generally depends on the movement rating and is tabulated in Table 3.6 (MTD 7-1, 1994). Figure 3.19a through c shows standard details for the joint seal types indicated in Table 3.6.

Table 3.6: Type of seals adopted in bridge joints

Movement rating (MR)	Type of seal
Less than or equal to 0.5 in	Type A (poured sealant)
1 in thru 2 in	Type B (neoprene compression sealant)
2 in thru 4 in	Joint seal assembly (strip seal)
Greater than 4 in	Joint seal assembly (modular unit)

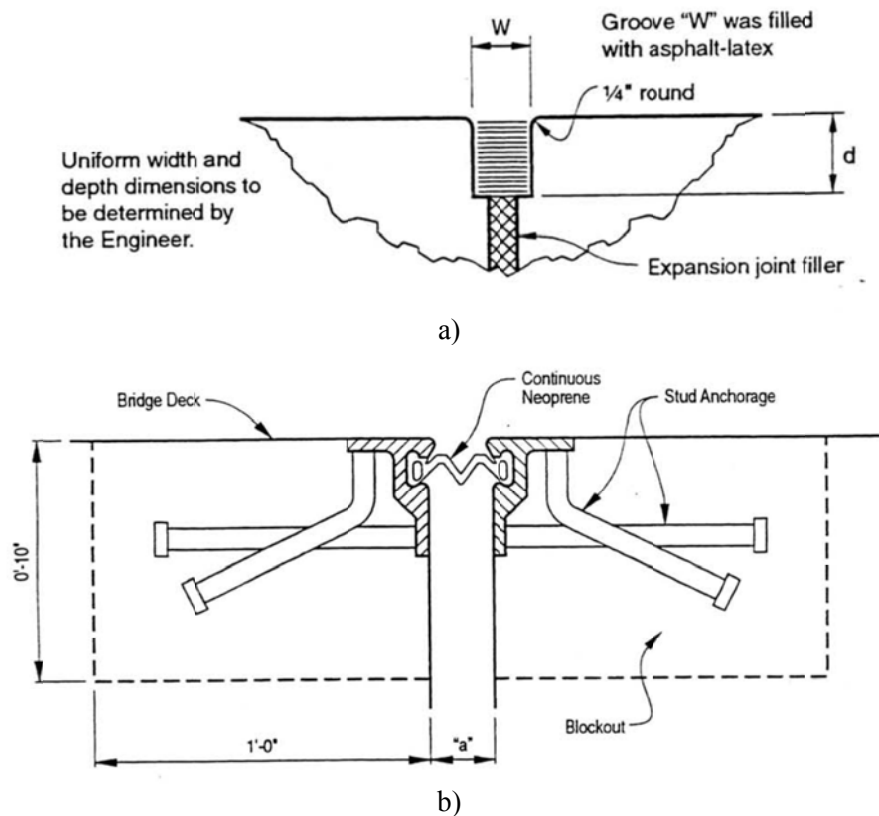




Figure 3.19: a) Type A and Type B joint seals, b) strip seal joint assembly and c) modular joint assembly (Source: MTD 7-1 and D. S. Brown Company)

Utilizing Caltrans's in house databases, MR values at bridge joints (in applicable cases) were catalogued and the statistics of MR values are shown in Table 3.7. Note that the tabulated values in Table 3.7 are pertinent to the entire inventory of state bridges in California. It is assumed that the small gap sizes exist in the case of MSCSL and MSCG-I bridge class joints while both small and large gap sizes exist in the case of MSCG-I and MSC-SBG bridge class joints. Note that the gap here refers to the gap between the bridge deck and the abutment backwall in the case of seat type abutments while it refers to the gap between the deck girders for MSCG-I at the bent. Due to the relatively small proportion of bridges with gaps larger than 6 in, the gaps in this study are restricted to two ranges: 0 to 2 in and 2 to 6 in.

Table 3.7: Distribution of gap sizes in the California state bridge inventory

Gap size	Abutment	Bent cap	In span hinge
0 to 2 in	88%	94%	75%
2 in to 6 in	11%	5%	19%
6 in to 12 in	0.7%	0.4%	5.1%
Greater than 12 in	0.3%	0.2%	0.9%

Restrainers provide yet another means to prevent unseating in bridges and these form an integral part of the as-built design in the 1971-1990 and post 1990 design eras. Large seat widths are the most effective means to prevent unseating and restrainers typically act as the second line of defense in modern day bridges. Restrainers are designed with adequate slack to allow thermal movement of the superstructure while restraining excessive relative movement at the joints. These are adopted in two basic types: cables and rods. The choice typically depends on a few factors such as the structure period, flexibility, strength of the diaphragm, and to some extent the geometry of the superstructure (Keady et al., 2003). Figure 3.20 shows a typical longitudinal restrainer that is used to prevent movement of a precast concrete girder that is continuous over the bent. Figure 3.21 shows a schematic describing the layout of restrainers at the seat type abutments for the bridge classes considered in this study.

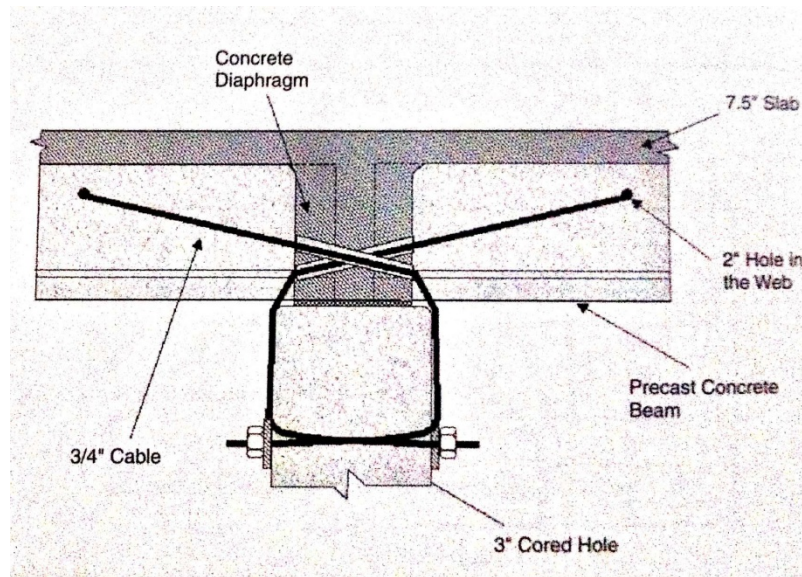


Figure 3.20: Precast girder and cap beam restrainer (Source: Yashinsky and Karshenas, 2003)

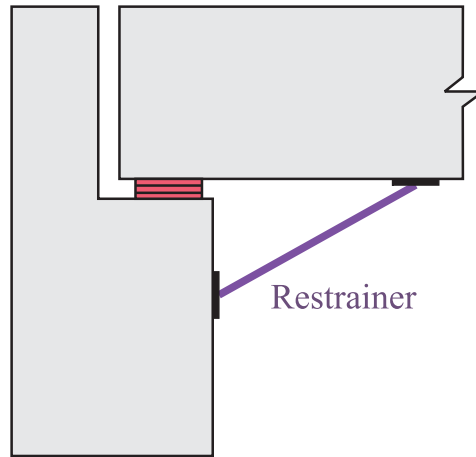


Figure 3.21: Schematic showing restrainer layout at a typical seat type abutment

Shear keys form an integral part of bridges with seat type abutments to facilitate the transfer of shear force between the superstructure and abutment in the transverse direction. These play a crucial role in restraining the transverse movement similar to the restrainers in the longitudinal direction. Shear keys are also located on the bent in the case of MSCG-I bridges to prevent their transverse movement. In the past, shear keys were commonly designed based on the assumption of constrained displacement at the abutments and acceptable failure criterion (Priestley et al., 1996). Damage to shear keys was reported in the past earthquakes and this led to change in their design philosophy. It was realized that the design adopted previously was undesirable and there was a lot of uncertainty in the estimation of maximum shear key forces. Adoption of capacity design principles led to better prediction of the shear key forces (SDC, 1999, 2010). Shear keys in the modern era bridges are expected to remain serviceable during earthquakes. In the present study, shear keys at the abutments are designed to resist 75% of the shear capacity of the bent while those at the bents are designed to resist 120% of the bent shear capacity. The fundamental idea is that significant damage would be inflicted in the columns before the failure of shear keys which is in line with the capacity design process

adopted by Caltrans. Figure 3.22 shows damage to abutment shear keys during the Loma Prieta earthquake.

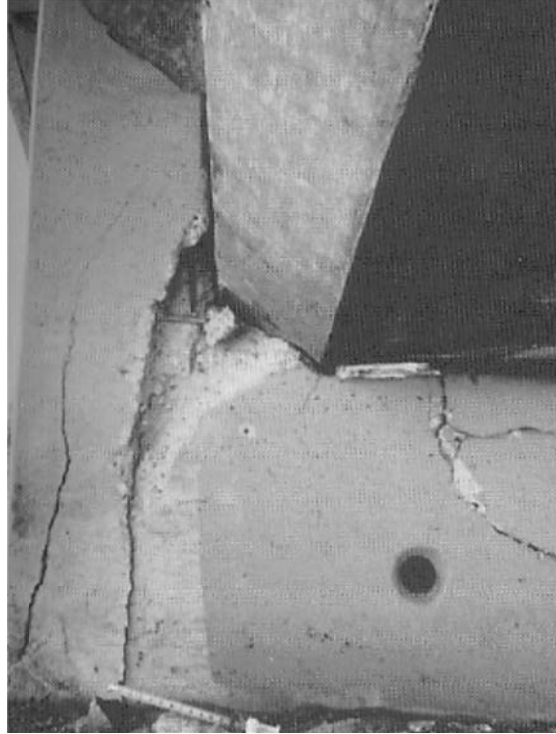


Figure 3.22: Damage to abutment shear keys during the Loma Prieta earthquake

3.6 Conventional Bridge Classes and Seismic Performance Sub-bins

This section details the bridge classes considered in this study along with the seismic performance sub-bins (SPS) separated by the historic 1971 San Fernando and 1989 Loma Prieta earthquakes. As stated in the preceding sections, bridge design and detailing aspects are captured for the bridge classes over the three design eras based on an extensive review of bridge plans, details of which are presented in Appendix A. The nomenclature associated with the bridge classes and the respective SPS are presented in Tables 3.8 and 3.9 and these will be used in the remainder of the thesis document here on. Fragility curves will be developed for each of the SPS in the bridge classes shown in

Table 3.8 as a part of this study. The BC and SPS codes put together completely describe sub-class and the primary bridge class. For example, MSCC-BG-M-E3-S4-L represents Post 1990 multispan continuous concrete box-girder bridge class with multi column bents and seat type abutments with seat width greater than 24 in and a large gap (2 – 6 in) between the girder and the abutment backwall.

Table 3.8: Conventional bridge class codes (BC) adopted in the present study

Spans	Continuity	Material	Superstructure	Bent type	Nomenclature
Multi (MS)	Continuous (C)	Concrete (C)	Box-Girder (BG)	Multi column bent (M)	MSCC-BG-M
				Single column bent (S)	MSCC-BG-S
Multi (MS)	Continuous (C)	Concrete (C)	Slab (SL)	Pile extensions (P)	MSCC-SL-P
Multi (MS)	Continuous (C)	Concrete (C)	T-Girder (TG)	Multi column bent (M)	MSCC-TG-M
				Pile extensions (P)	MSCC-TG-P
Multi (MS)	Continuous (C)	Concrete (C)	I-Girder (IG)	Multi column bent (M)	MSCC-IG-M
				Single column bent (S)	MSCC-IG-S

Table 3.9: Seismic performance sub-bins (SPS) in each bridge class

Design era	Abutment type	Seat width class	Gap size	Nomenclature
Pre 1971 (E1)	Diaphragm Seat	NA (S0)	NA	E1-S0
		4 – 12 in (S1)	Small (S)	E1-S1-S
		12 – 18 in (S2)	Small (S)	E1-S2-S
		18 – 24 in (S3)	Small (S)	E1-S3-S
		> 24 in (S4)	Large (L)	E1-S3-L
			Small (S)	E1-S4-S
			Large (L)	E1-S4-L
1971 – 1990 (E2)	Diaphragm Seat	NA (S0)	NA	E2-S0
		12 – 18 in (S2)	Small (S)	E2-S2-S
		18 – 24 in (S3)	Small (S)	E2-S3-S
		> 24 in (S4)	Large (L)	E2-S3-L
			Small (S)	E2-S4-S
			Large (L)	E2-S4-L
Post 1990 (E3)	Diaphragm Seat	NA (S0)	NA	E3-S0
		18 – 24 in (S3)	Small (S)	E3-S3-S
		> 24 in (S4)	Large (L)	E3-S3-L
			Small (S)	E3-S4-S
			Large (L)	E3-S4-L

3.7 Closure

Four conventional bridge classes are identified for fragility analysis. These four bridge classes account for about 45% of the bridge inventory in California. Detailed review and analysis of the National Bridge Inventory is performed to develop empirical cumulative distribution functions for geometrical parameters such as span length, deck width, column height and number of spans. The conventional bridge classes chosen are divided into sub-bins separated by the 1971 San Fernando and 1989 Loma Prieta earthquakes. The general design details and potential vulnerabilities of bridges designed prior to 1971, those designed between 1971 and 1990 and post 1990 are identified based on an extensive review of bridge plans to supplement the information provided by the NBI. Detailed information pertinent to bridge components: superstructure, columns, foundations, abutments are gathered across the design eras to aid in the development of stochastic finite element models for fragility analysis. By the very nature of the inventory information along with the design details across the three significant eras obtained herein, the resulting fragility curves will be appropriate for suites of bridges across California.

CHAPTER 4

ANALYTICAL MODELING PROCEDURES AND DETERMINISTIC BRIDGE COMPONENT RESPONSES

Advances in modeling capabilities coupled with lack of damage data from past seismic events motivated the development of fragility curves using analytical methods. Fragility curves derived analytically often differ based on the level of detail and sophistication in the analytical models, the approach to simulate seismic loading, assessment of structural response, and considerations of geometric effects in addition to the various reliability assessment techniques (simulation versus closed form) to obtain estimates of component and system vulnerability. High fidelity three dimensional analytical models considering geometric and material nonlinearities are used in this study for fragility curve generation using Nonlinear Time History Analyses (NLTHA). The models are created in the finite element platform OpenSEES (McKenna et al., 2010). The results of NLTHA are used to develop predictive models of demand, and therefore the ability to capture the behavior of various components is dictated by the fidelity and robustness of the model.

This chapter presents a detailed description of the modeling strategies at the component level and their subsequent integration at the bridge system level. Details are provided about the typical layout of representative bridges from four multispan bridge classes with box-girders, slab, Tee and I-girders in the superstructure, across the three significant design eras considered in this study: pre 1971, 1971-1990 and post 1990 eras, drawing on the details provided in the previous chapter. Eigen value analyses and select deterministic component responses are presented and discussed in every case to provide insight into the relative response of various components and to use as a sanity check.

4.1 Bridge Component Modeling Strategies

This section presents details about modeling considerations for various bridge components.

4.1.1 Substructure – Single and Multi Column Concrete Bents

Californian bridges have different pier types such as pier walls, hammerhead piers, single and multi column rigid frame piers or bents. Single (SCB) and multi column bents (MCB) are the most common types based on an in-depth review of bridge plans for the bridge classes chosen in this study. Table 3.8 in Chapter 3 presented details about the bent types considered in the analytical models for various bridge classes across design eras. The bents are modeled using a combination of displacement based beam column elements and rigid links to cause moment and force transfer between the members of the bent. Figure 4.1 presents the finite element discretization of the bents for the bridge classes. Displacement based beam-column elements with fiber defined cross-sections are used to represent the columns and bent beams in the case of MSCC-IG bridge class. In the case of MSCC-BG, MSCC-SL and MSCC-TG bridges with monolithic solid diaphragms, transverse rigid elements are used to represent the diaphragm while displacement beam-column elements with fiber cross-sections are used to represent the columns. In either case, rigid links are used to connect the top of the column to the bent beam or the solid diaphragm. Translation and rotational springs representing the behavior of foundations are located at the base of the column. The details of the concrete and steel material models along with cross-section modeling attributes are presented in the sections that follow.

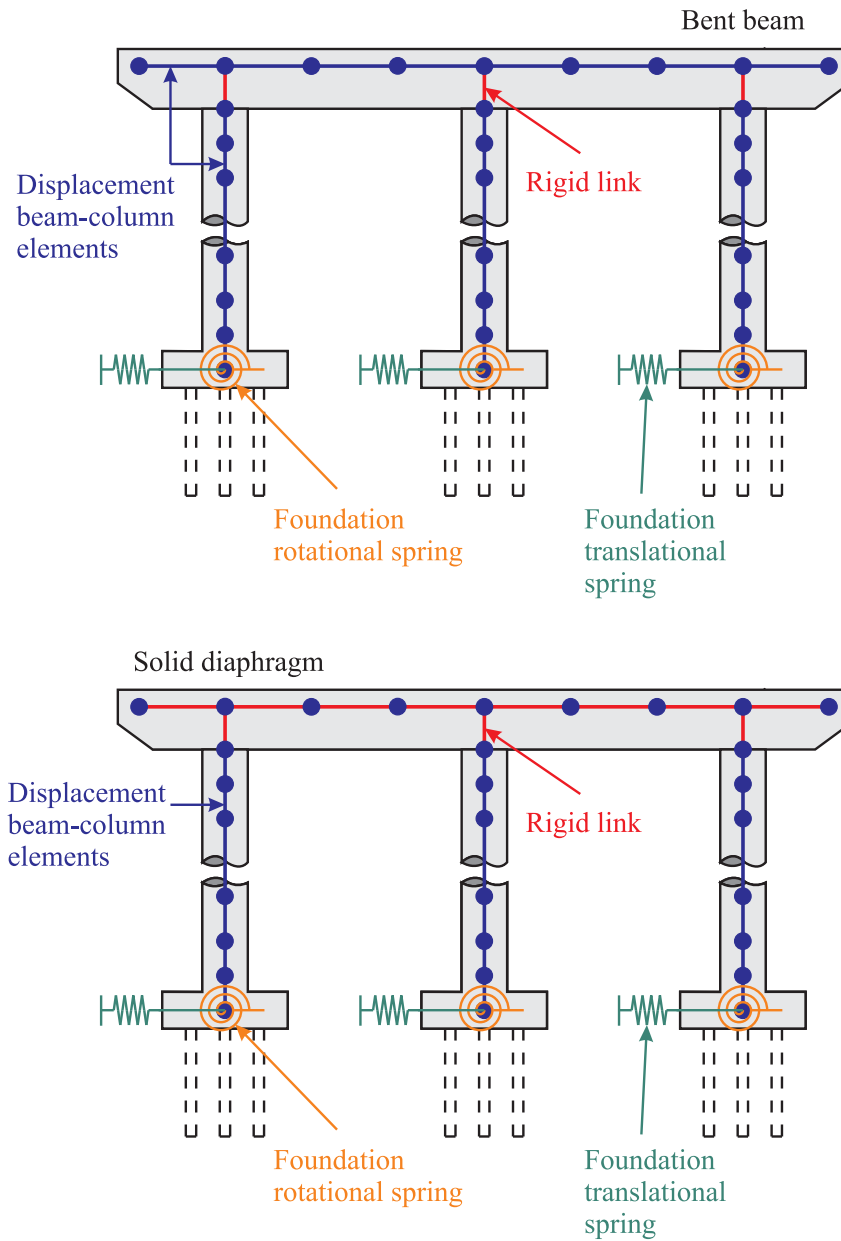


Figure 4.1: Finite element discretization of the bent

4.1.1.1 Concrete, Reinforcing and Prestressing Steel Material Models

Fiber defined cross-sections have the unique advantage of allowing the specification of material properties specific to different locations in a member cross-section. For instance, unconfined concrete properties are assigned to the cover concrete while confined concrete properties are assigned to the core fibers. Further, the precise

location of the longitudinal reinforcing bars and prestressing strands may be specified and material properties assigned to them.

Reinforced concrete behavior is modeled using the *Concrete 07* material provided in OpenSEES. This material used the Chang and Mander's model (1994) to define the monotonic stress strain curves for confined and unconfined concrete. The model was established based on statistical regression analysis on the experimental data from cyclic compression tests performed by a number of researchers. Figure 4.2 shows the stress strain curves for concrete with standard compressive strength, $f'_c = 5000$ psi and reinforcing steel yield strength, $f_y = 60$ ksi with varying degrees of confinement offered by #4 stirrups at 3 in, 6 in and 12 in on center, typical of post 1990, 1971-1990 and pre 1971 bridge columns of 3 ft diameter. It must be noted that the effect of confinement is pronounced on the peak compressive stress and ultimate strain in the confined concrete stress strain relationship as shown in the figure.

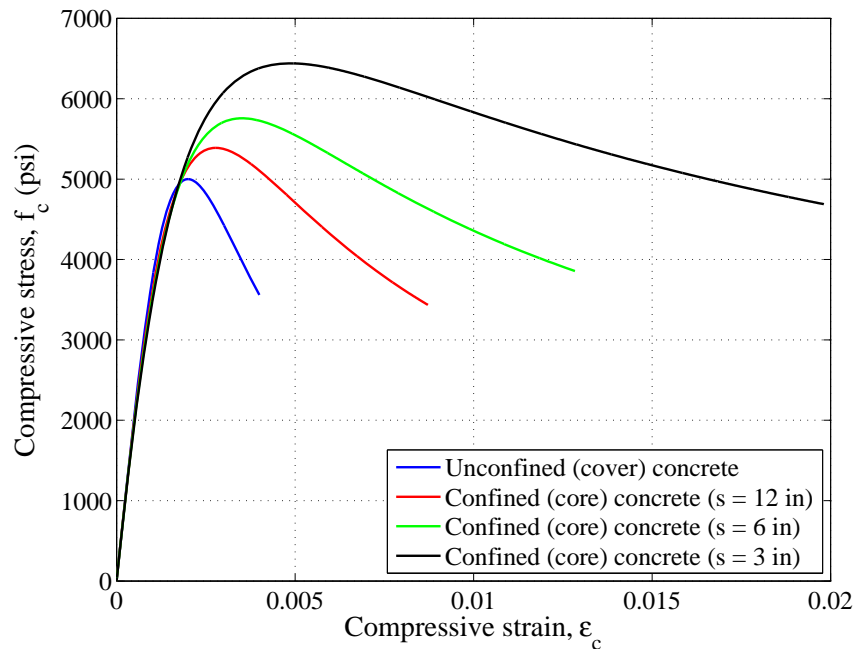


Figure 4.2: Concrete stress strain curves with varying transverse reinforcement confinement ratios

Reinforcing steel is modeled using the *Steel 02* material provided by OpenSEES which uses the Menegotto and Pinto model (1973) later modified by Filippou et al. (1983) to include isotropic strain hardening. The prestressing strands are modeled as an elastic perfectly plastic material. This is used in the case of prestressed and precast prestressed concrete piles which extend as columns above the ground in the case of MSCC-SL bridge class. The material models for reinforcing steel and prestressing strands are shown in Figure 4.3.

4.1.1.2 Fiber Cross-sections – Column and Bent Beam

The bridge columns are modeled using displacement based beam column elements for all the bridge classes across the design eras. The cross-section is modeled using fiber elements and this helps in capturing the spread of plasticity in the column elements. Details such as column diameter, longitudinal and transverse reinforcement ratio vary across bridge classes and further with the design era as presented in Appendix A. Figure 4.3 shows a discretized fiber section for a bridge column which consists of unconfined and confined concrete properties assigned to the fibers along with a precise location of the longitudinal reinforcement and prestressing strands (in the case of pile cross-sections). Also shown in Figure 4.3 is a discretized typical bent beam prevalent in MSCC-SL and MSCC-IG bridges.

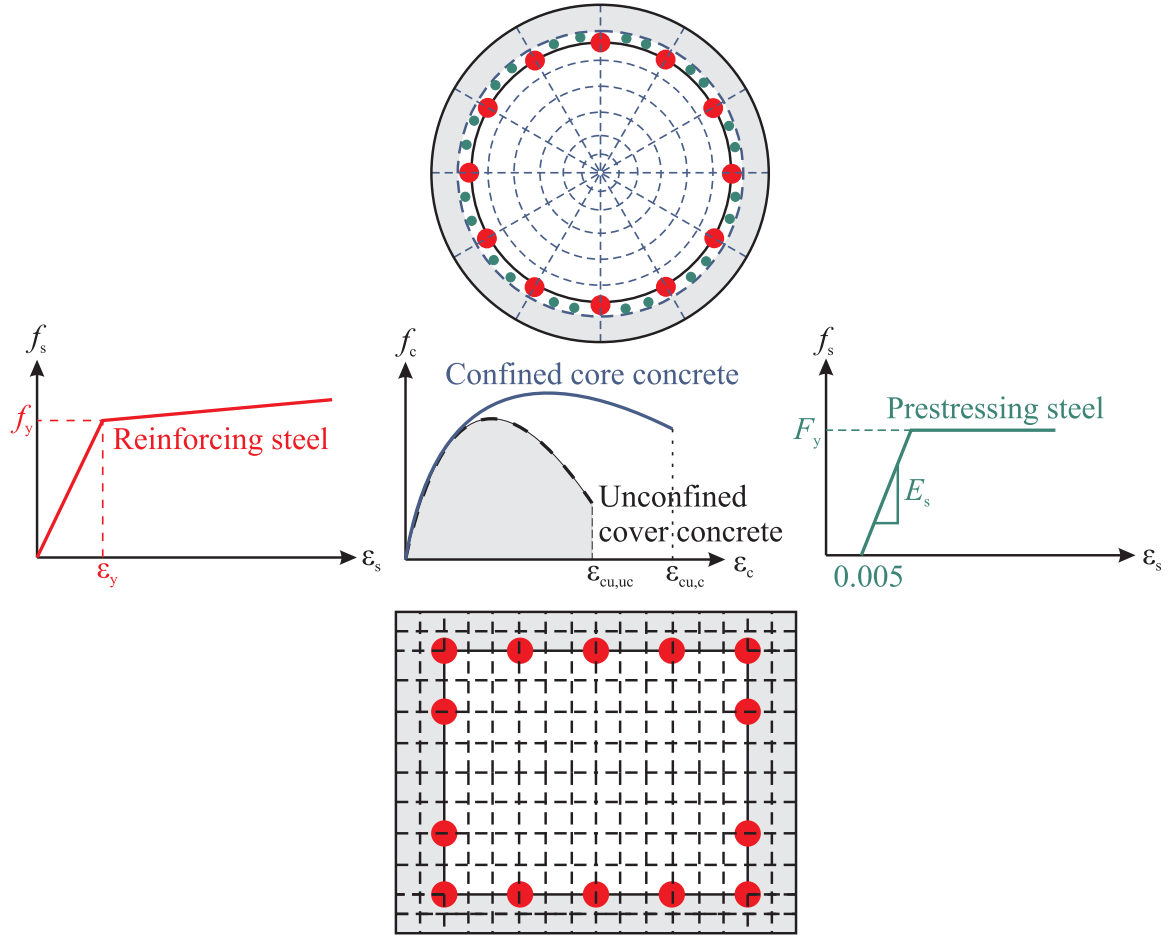


Figure 4.3: Fiber based discretization of a circular reinforced concrete column and bent beam

4.1.1.3 Foundation translation and rotational springs

As stated previously in section 3.5.5, different foundation systems are considered in this study based on the bridge class. These include integral pile shafts and pile supported footings consisting of precast (reinforced or prestressed concrete), driven or CIDH piles. Further, since this study aims at developing fragility curves that are applicable for bridge classes across a wide geographic area, a range of soil profiles from soft to medium and stiff are considered. The foundation systems and the different soil profiles were modeled in LPILE (2012) in order to determine the stiffness of translational and rotational springs that are then located at the base of the columns to represent the

behavior of foundation systems. It should be noted that MCBs founded on pile supported footings are pinned at the base and therefore have no rotational stiffness. On the other hand, MCBs consisting of integral pile columns, as in the case of MSCC-SL and MSCC-TG bridge classes, have translational and rotational stiffness. Further details about the soil profiles and the corresponding stiffness of the translational and rotational springs across bridge classes are provided in Appendix A.

The translational and rotational springs are modeled using simple linear springs and are assigned to zero length elements at the base of the columns as shown in Figure 4.1. In the case of abutment piles, trilinear response stemming from the recommendations of Choi (2002) is used to model their response in the longitudinal and transverse directions. Further details are presented in section 4.1.2.

4.1.2 Abutments

Observations from past earthquakes reveal the potential for great demands on bridge abutments due to seismic forces. Earth pressures on the abutment can result from longitudinal response of the bridge deck and these pressures are further increased due to the pounding of the deck against the abutment backwall in the case of seat abutments. Response of the abutments in the longitudinal direction is different when compared to the transverse direction. Further, the longitudinal response is composed of two types of resistance: passive resistance, which is developed when the abutment wall compresses the backfill soil, and active resistance, when the abutment backwall moves away from the backfill soil. The passive resistance is provided by the backfill soil and the piles while piles alone contribute to the active resistance. Caltrans SDC (2010) states that the effect of wing walls decreases as the width of the abutment increases (beyond 50 ft), and therefore, only piles are considered to contribute to the transverse resistance of the abutments.

Early research typically considered the effect of abutments by the addition of discrete linear springs to the bridge model. Caltrans SDC (1990) provided guidelines for the stiffness of the linear springs based on a passive soil resistance of 20 kip/in/ft for a standard 8 ft backwall. The effect of piles was accounted for by adding a resistance of 40 kips/in/pile in the longitudinal (active and passive) and transverse directions. A limiting value of 55 psi was suggested for the passive backfill soil pressure to limit the load taken by the abutment under cyclic seismic loading. Research conducted at the University of California, Davis (Maroney et al, 1993) on half scale abutment specimens to estimate the longitudinal stiffness concluded that the stiffness proposed by Caltrans SDC (1990) overestimated the passive soil resistance tremendously. Goel and Chopra (1997) developed abutment models and concluded that the transverse abutment modeling considerations suggested by Caltrans SDC (1990) produced good results consistent with experimental tests and field observations. Caltrans SDC (1999) revised its previous deterministic estimate of 20 kip/in/ft of passive soil resistance to fall within a range: 20 kip/in/ft to 50 kip/in/ft. However, in the work performed by Maroney et al. (1994), it was seen that the passive resistance of the abutment decreased as the displacement of the abutment increased and the passive stiffness reduced to zero before the ultimate soil pressure was mobilized. This reinforced the necessity to account for a non-linear soil model to accurately capture the abutment response. This was further reinforced in the work by Martin and Yan (1995) where the ultimate soil pressure was seen to be mobilized with displacements of 6 to 10% of the backwall height based on the type of backfill soil: cohesive vs. cohesionless.

The hyperbolic soil model proposed by Shamsabadi and Yan (2008) is used in the present study to capture the response of the abutment backwall soil in passive response. The model is based on experimental testing of bridge abutments with 5.5 ft. high backwalls and typical cohesionless and cohesive backfill soils conducted at the University of California Los Angeles (Shamsabadi and Yan, 2008). The test results were

then extended to develop closed form solutions for the abutment backfill soil response for a range of backwall heights based on a series of analyses using the limit-equilibrium method that implements mobilized logarithmic-spiral failure surfaces coupled with a modified hyperbolic soil stress strain behavior. Figure 4.4 shows a typical abutment force displacement backbone curve, where F_{ult} is the maximum abutment force developed at maximum displacement, y_{max} . y_{ave} is the displacement corresponding to half the maximum abutment force and K is the average soil stiffness.

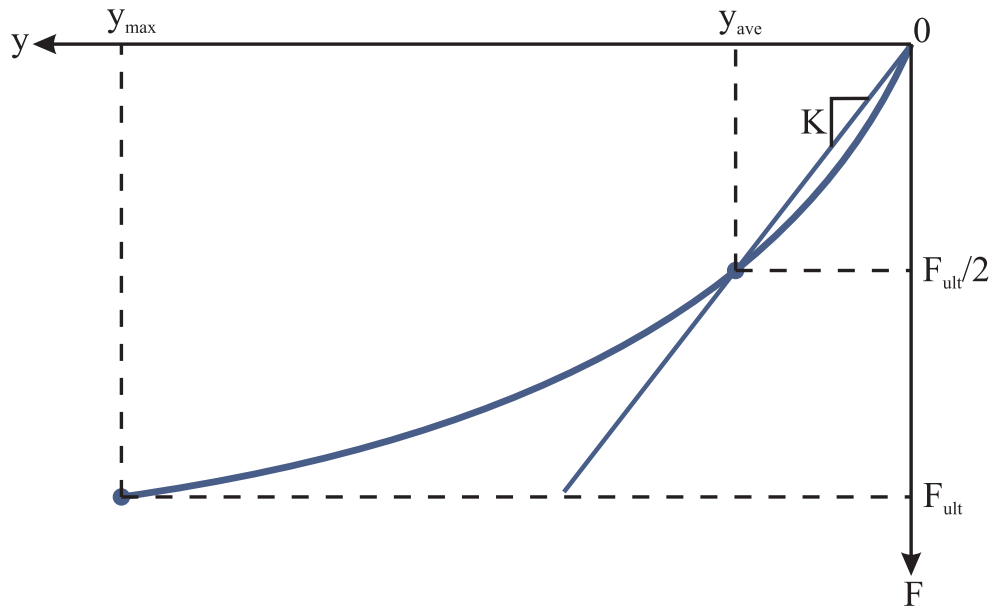


Figure 4.4: Force displacement response of the abutment backfill

Equation (4.1) presents the closed form solution for the force displacement response of the backfill soil, where F is the force expressed in kip/ft width of the backwall, y is the displacement expressed in inches, and H is the height of the backwall expressed in feet.

$$\begin{aligned}
 F(y) &= \frac{8y}{1+3y} H^{1.5} && \text{Granular backfills} \\
 &= \frac{8y}{1+1.3y} H && \text{Cohesive backfills}
 \end{aligned} \tag{4.1}$$

Shamsabadi and Yan (2008) noted that the maximum displacement of the backwall is $0.05H$ and $0.1H$ (expressed in inches) for granular (sandy soils) and cohesive (clayey soils) backfills, respectively, and substitution of these values in equation (4.1) yields the ultimate force in the abutment. According to MTD 5-1 (1992), the longitudinal stiffness assumed for seismic analyses should be based on mobilizing the soil equal to the depth of the backwall. Zero length springs characterized by nonlinear soil behavior are used to capture the response of the abutment soil. The *HyperbolicGapMaterial* provided by OpenSEES is used to model the response of the backfill soil, which is based on the model proposed by Shamsabadi and Yan (2008). It must be noted that in the case of diaphragm abutments, the gap between the deck and abutment backwall is zero while a gap exists in the case of seat type abutments. The abutment dimensions: width and height of the backwall, and backfill soil type (sand vs. clay) are considered as random variables in this study and typical ranges of the values will be presented in the next chapter.

As stated previously, piles are considered to provide longitudinal and transverse stiffness to the abutments. For the passive longitudinal response, piles act in parallel with the backfill soil, while piles alone account for the active resistance. The transverse resistance just like the active resistance is also provided solely by the piles. Trilinear response stemming from the recommendations of Choi (2002) is used to model the response of the piles. The model assumes that piles become plastic at a deformation of 1 in and first yielding occurs at a displacement equal to 30% of the ultimate deformation. The initial stiffness is assumed to degrade with soil surface yielding. The force deformation response of the pile along with the model parameters are presented in Figure 4.5. The stiffness of the abutment pile depends on the type: CIDH, driven steel H section, driven steel pile, drilled shafts and is considered a random variable and these take on a range of values across all simulations, as detailed in Chapter 5 of this thesis.

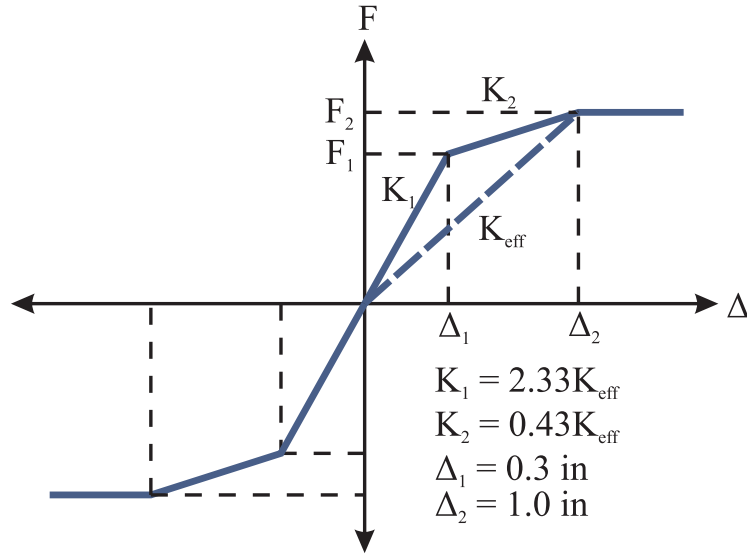


Figure 4.5: Force displacement response of the pile

4.1.3 Deck Elements

The deck elements are modeled using elastic beam column elements since the superstructure generally remains elastic during seismic events. The properties of the deck elements are calculated based on composite section properties wherever applicable (MSCC-BG, MSCC-IG, MSCC-TG). Effective width of the superstructure is considered in order to calculate cross-section properties that are assigned to the longitudinal deck elements. In the case of open soffit superstructures with I- and T-girders as in the case of MSCC-IG and MSCC-TG bridge classes, the girders offer less resistance to the torsional resistance of the bent cap and the effective width is reduced accordingly (SDC, 2010). In either case, the width of the superstructure is reduced for one-quarter span length on either side of the bent to calculate the cross-section properties to be assigned to the deck elements. The calculation of the effective deck width is illustrated in Figure 4.6. As will be demonstrated in the next chapter, the width of the bridge is a random variable and derivation of empirical CDFs for the same was demonstrated in Chapter 3. Other geometric parameters such as deck slab thickness, girder dimensions (in the case of MSCC-IG, MSCC-TG, MSCC-BG) are considered to vary across simulations.

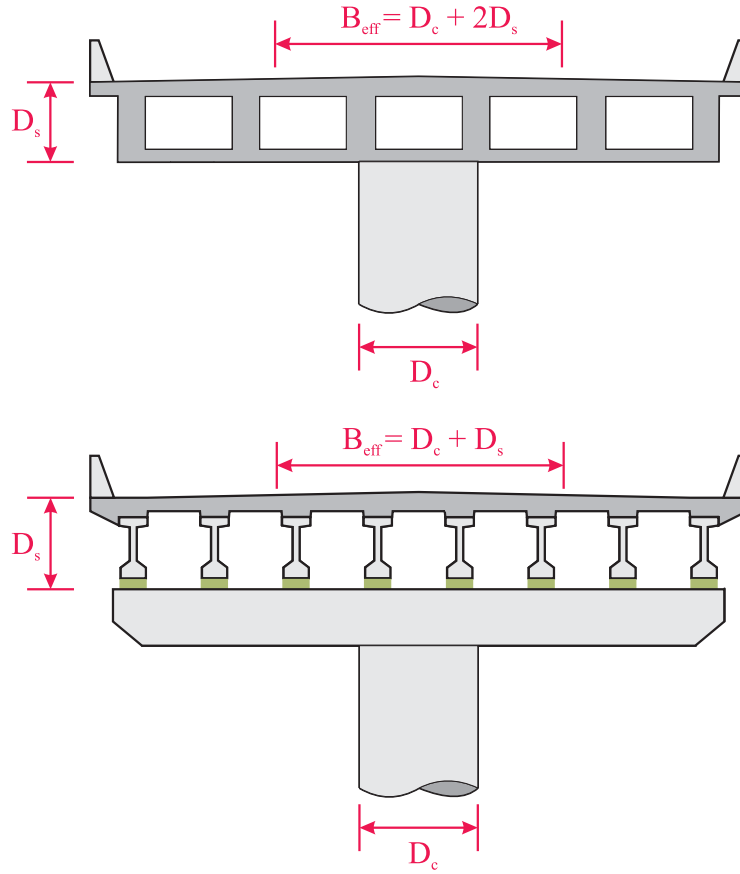


Figure 4.6: Effective width of the superstructure

4.1.4 Elastomeric Bearing Pads

Elastomeric bearings are the most commonly adopted bearing types in concrete bridges. These bearings typically transfer horizontal forces by friction and their behavior is characterized by sliding which in turn depends on the initial stiffness. Once the coefficient of friction is exceeded, the stiffness of the rubber pads drops to zero and therefore, their response can be characterized by elastic perfectly-plastic material. The initial stiffness, k_{pad} , of the bearing pad is calculated using equation (4.2), where, G is the shear modulus, A is the cross-sectional area, and h is the thickness of the bearing pad.

$$k_{pad} = \frac{GA}{h} \quad (4.2)$$

Figure 4.7 shows the force deformation response of the elastomeric bearing pad. The yield force, F_y , is calculated by multiplying the normal force, N , acting on the bearing with the coefficient of friction, μ , of the pad. Scharge (1981) presented an expression for the coefficient of friction, specific to elastomer on concrete, based on experimental tests and is a function of the normal stress, σ_n , as presented in equation (4.3). The response of the bearing pad is captured using the *Steel01* material provided by OpenSEES and is applied to a zero length element to capture its force deformation response.

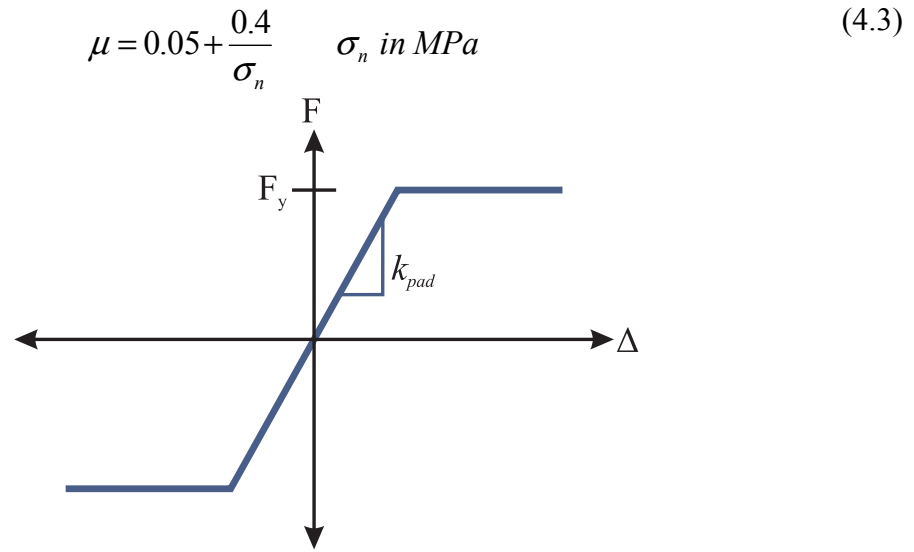


Figure 4.7: Force deformation response of an elastomeric bearing pad

As will be demonstrated in the next chapter, the dimensions of the bearing pad, coefficient of friction, and shear modulus are considered random variables and take on a range of values.

4.1.5 Shear Keys

Shear keys play an important role in constraining the relative transverse movement between the deck and the abutments in the case of continuous bridge

superstructures. Typically shear keys have the potential to fail through one of the four different mechanisms: shear friction, flexure, shear and bearing (Megally et al, 2002). Shear keys are located at the abutments and at the bents in the case of MSCC-IG bridges with seat type abutments, while they are located at the abutments alone for all the other bridge classes considered in this study with seat type abutments. No shear keys are used in bridges with integral bents and diaphragm abutments. MTD 5-1 (1992) indicates that transverse shear keys at the abutments should be designed to resist 75% of the adjacent bent capacity to prevent significant damage to the underlying piles. Based on personal communication with Caltrans design engineers (Caltrans, 2010-2012), the shear keys at the bents are designed to resist 120% of the bent shear capacity. These are inherently very strong components and provide complete transverse coupling of the bent beyond the point of formation of plastic hinge in the underlying columns.

Figure 4.8 shows the nonlinear force deformation response of the shear key that is adopted in the present study. P_{cap} denotes the capacity of the shear key and is calculated based on the expressions in equation (4.4).

$$P_{cap} = factor \times V_{bent} \quad (4.4)$$

where, $factor = 0.75$ at bents, 1.2 at abutments, and V_{bent} is the shear capacity of the bent, calculated as in equation (4.5). The bent shear capacity is determined by adding the shear strength of concrete and that of steel reinforcement (ACI, 2008).

$$V_{bent} = n \left(3.5 \sqrt{f'_c} (0.8D)^2 \right) \sqrt{1 + \frac{N_u}{500A_g} + \frac{A_v f_y (0.8D)}{s}} \quad (4.5)$$

where, n is the number of columns per bent, f'_c is the concrete compressive strength (psi), D is the column diameter (in), N_u is the column axial load (lbs), A_g is the gross cross-sectional area (in²), A_v is the area of transverse reinforcement (in²), f_y is the steel yield strength (psi), and, s is the transverse reinforcement spacing (in).

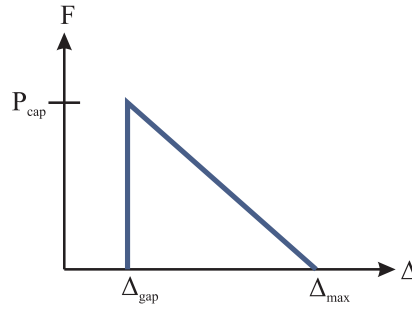


Figure 4.8: Force displacement model for the shear key

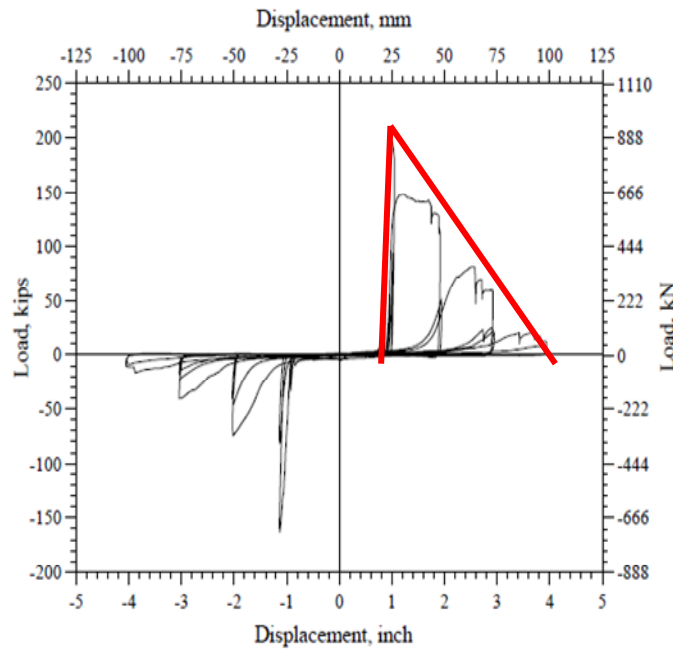


Figure 4.9: Load displacement curves from the experimental testing of abutment shear keys (Megally et al., 2002)

The model chosen in this study is based on the research by Megally et al. (2002) based on a series of experiments on external shear keys in bridge abutments. They found that shear keys undergo a maximum displacement of 3.5 in before their capacity reduces to zero. Figure 4.9 shows the load deformation response from the experiments conducted on abutment shear keys at the University of California San Diego (Megally et al., 2002). Zero length elements characterized by this nonlinear force deformation response are used to capture the response of shear keys.

4.1.6 Restrainers

Restrainers serve to limit relative longitudinal displacement between the spans and prevent unseating. These are often employed in bridges with insufficient seat widths which is typical in the pre San Fernando era. As mentioned previously, several bridges constructed prior to the San Fernando and Loma Prieta earthquakes have been retrofit with restrainer cables as a part of the Caltrans Phase I and II retrofit programs. Cable restrainers are considered in this study although it is realized that restrainers come in several forms including plates and rods. Restrainer cables, $\frac{3}{4}$ in in diameter (0.222 in² cross sectional area) are considered across design eras for MSCC-BG and MSCC-IG with seat type abutments.

Parameters associated with the restrainers are also considered variable in the simulations. Although $\frac{3}{4}$ in diameter restrainers are adopted, the length of the cables is assumed to vary across simulations and so is the initial slack in the cables, since these have shown to significantly affect the response of the bridge (Saiidi et al, 1996). Further details about the range of these parameters are provided in the next chapter. BDA 14-1A (2009) gives information about the restrainer properties and based on testing by Caltrans, the yield force, F_y , for $\frac{3}{4}$ in cables is reported as 46 kips and the specified modulus of elasticity, E , is 14,000 ksi. Figure 4.10 shows the typical stress strain curve for a $\frac{3}{4}$ in restrainer cable (BDA, 2009).

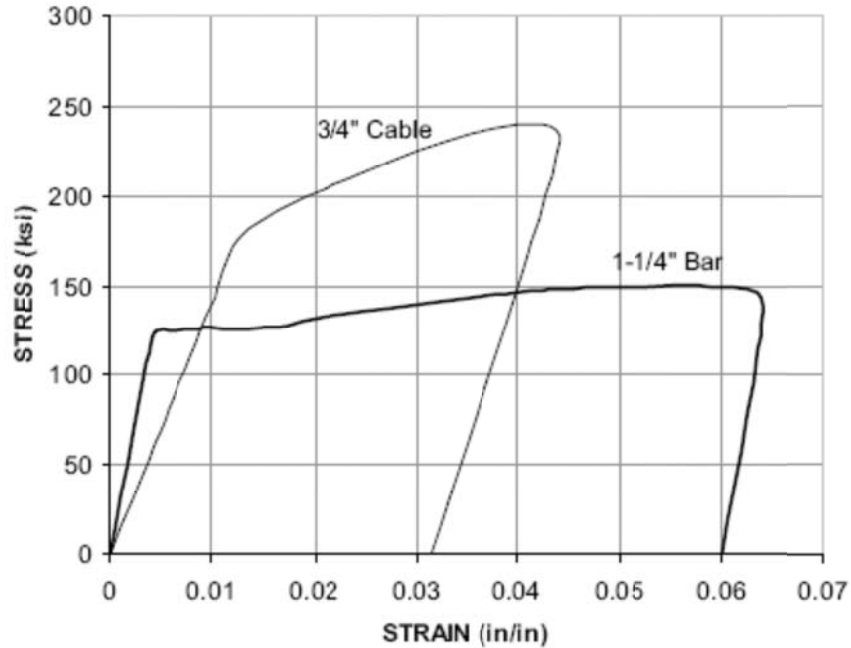


Figure 4.10: Stress strain curve for $\frac{3}{4}$ in restrainer cable (BDA, 2009)

The fundamental restrainer design philosophy is to limit the longitudinal movement of the bridge superstructure and to keep them tied together during an earthquake without yielding. Several restrainer design procedures are available, such as the one adopted by Caltrans, American Association of State Highway and Transportation Officials (AASHTO), W/2 method, equivalent linear static design for restrainers and modified Caltrans method, all with varying levels of complexity (Saiidi et al., 2001). In this study, the W/2 method is adopted for designing the restrainers which assumes that the bridge superstructure unseats during an earthquake and is supported by the restrainers alone. Therefore, the restrainers on each side of the span are designed to resist one-half of the weight of the span. The W/2 method was reported to perform well in most bridges (Saiidi et al, 2001).

Figure 4.11 shows the stress strain curve adopted for the restrainer cable in the present study. For a certain length, the yield displacement is calculated using equation (4.6). The number of restrainers are then determined using equation (4.7). A post yield

stiffness of 1% is used as shown in Figure 4.11, consistent with the observations in tests on restrainer cables. Zero length elements characterized by this force deformation response are used to capture the response of restrainer cables.

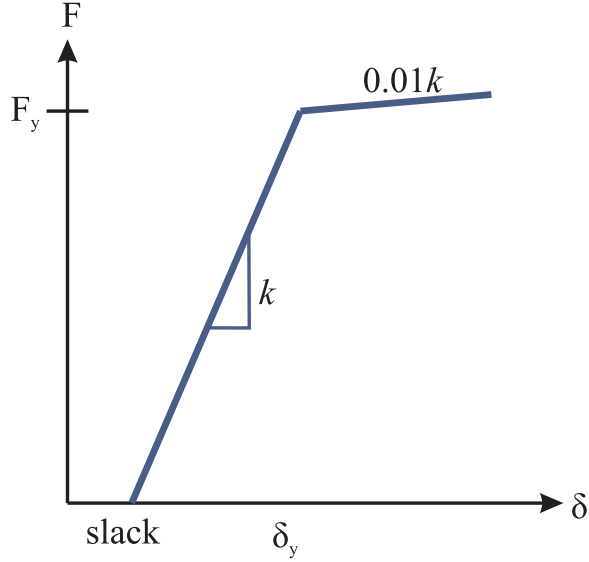


Figure 4.11: Force deformation response of the restrainer cable

$$\delta_y = \frac{F_y L}{A_s E} \quad (4.6)$$

$$n = \frac{\left(\frac{W/2}{F_y} \right)}{A_s} \quad (4.7)$$

4.1.7 Impact or Pounding Elements

The contact element approach proposed by Muthukumar (2003) is used in this study for modeling the impact between the deck and abutment backwall. A bilinear model that captures impact and energy dissipation is used and is shown in Figure 4.12. The stiffness parameters, K_{t1} , K_{t2} , yield displacement, δ_y , and maximum deformation, δ_m , are shown in the figure and are consistent with those presented in Nielson (2005).

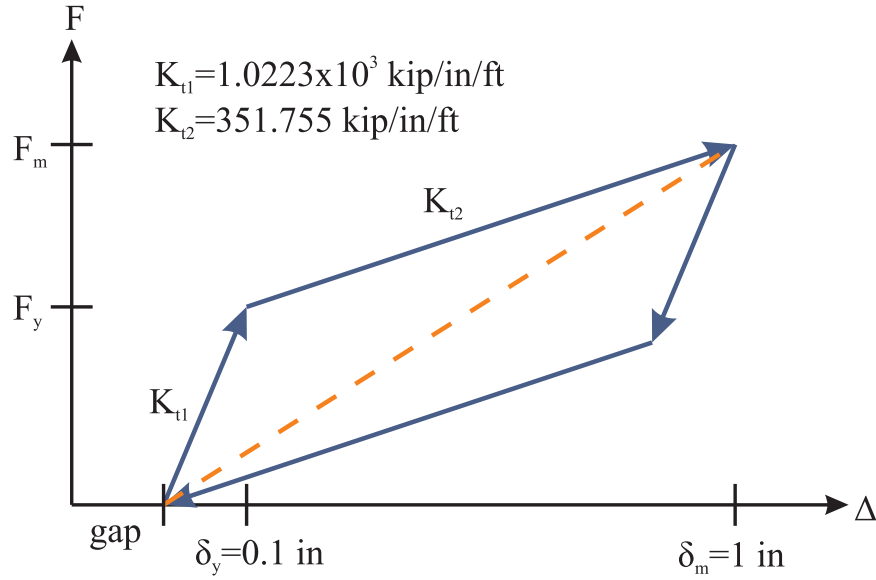


Figure 4.12: Analytical model for pounding between deck and abutment backwall (Muthukumar, 2003)

4.2 Global Bridge Finite Element Models

The preceding section provided extensive component modeling strategies adopted in the present study. This section presents the integration of various component level models to generate a global analytical model of the bridge to be used in fragility analyses. Elastic beam column elements with lumped mass representing the longitudinal deck elements are connected to rigid elements in the transverse direction. Displacement based nonlinear beam column elements with fiber defined cross sections are used to model the columns. Translational and rotational springs at the base of the columns are used to replicate the behavior of column footings. Zero length elements capturing the response of the abutment backfill soil and piles are connected in parallel and are connected to the transverse deck elements in the case of diaphragm abutments. In the case of seat type abutments, zero length elements describing the response of elastomeric bearing pads, restrainers and pounding between the deck and abutment backwall are connected in

parallel and are connected to the transverse rigid deck elements. These are then connected in series with the soil-pile springs to capture the response of the abutment system.

In the case of MSCC-BG, MSCC-SL and MSCC-TG bridges, where the superstructure is integral with the bent, rigid links are used to connect the column tops to the transverse rigid deck elements. These help in transferring all of the forces and moments and are typical of an MFA-3 type connection. In the case of an MFA-2 type connection, where only the negative moments are transferred between the superstructure and substructure, rigid links are used to transfer all forces and moments except the longitudinal moment. A tension only rigid link is used to transfer the longitudinal moment from the deck to the bent.

In the case of MSCC-IG bridge class with bearing supported superstructure, the column nodes are connected using rigid links to the bent beam. Nonlinear displacement based beam column elements with fiber defined cross-sections are used to model the bent beam. Zero length elements characterized by the force displacement response of elastomeric bearings are used to connect the bent beam with the transverse rigid deck elements. These are joined in parallel with the restrainer elements at the bent similar to the case at the seat type abutments.

4.3 Analytical Bridge Models and Deterministic Responses

In this section, select component responses from the chosen bridge classes are presented to provide insight into their response and criticality using NLTHA on deterministic bridge models. In all cases, the deterministic responses are illustrated using a single ground motion from the suite of ground motions developed for the PEER Transportation Systems Research Program (Baker et al., 2011). Further details about the ground motion suite are provided in Chapter 5. The chosen ground motion pertains to a rock site with an average shear wave velocity of 2180 ft/sec and is characterized by a moment magnitude of 7.62 and hypocentral distance of 16.27 km. The ground motion

time histories for the fault normal and fault parallel components are shown in Figure 4.13. Also shown as an inset in the figure is the response spectrum corresponding to the two orthogonal components.

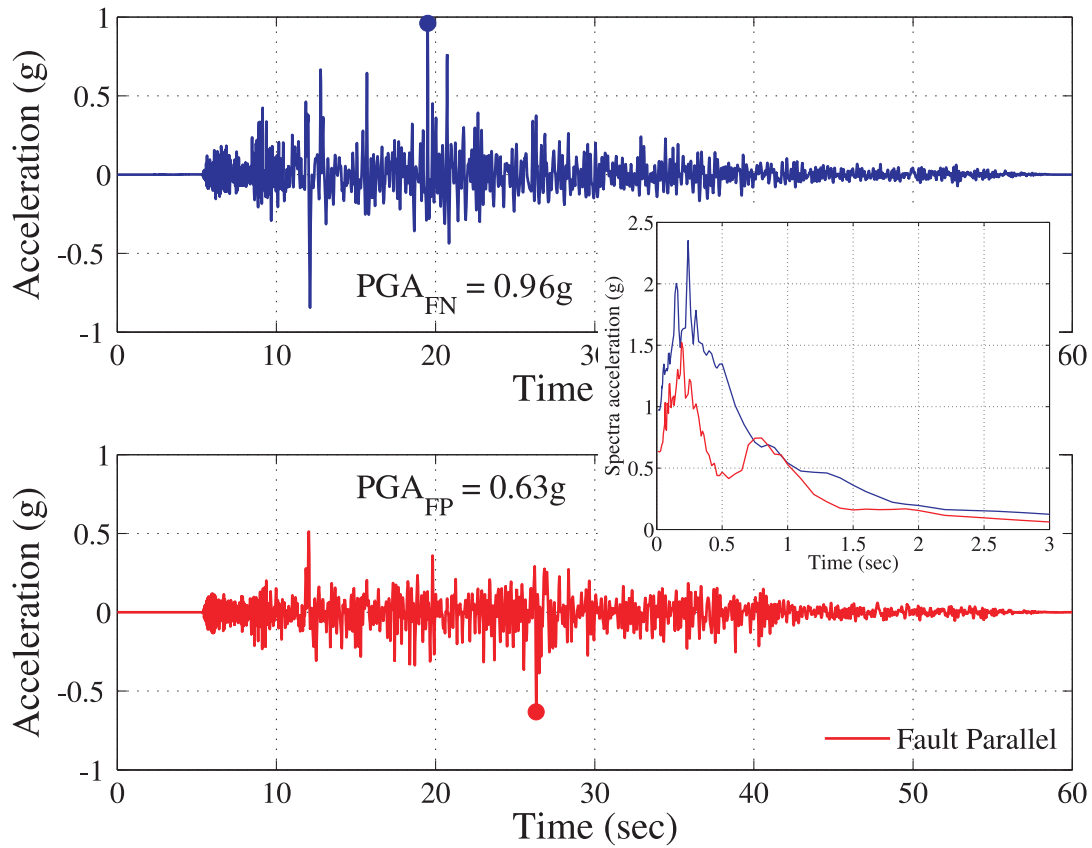


Figure 4.13: Fault normal and fault parallel components of ground motion used in deterministic analyses

The forthcoming sections present details and insight into the performance of bridges and their components. Bridge models with median values of geometric and material properties are developed and time history analyses is performed in each case. The following cases are considered:

- MSCC-BG bridges with single (MSCC-BG-S) and multi column (MSCC-BG-M) bents and seat and diaphragm abutments across all design eras (E1, E2, E3). Since this bridge class forms the bulk of the bridge inventory in the state of California,

an effort is made to contrast and compare the performance through deterministic analyses

- MSCC-SL with integral pile columns or pile extensions (MSCC-SL-P)
- MSCC-TG with multi column bents consisting of pile extensions (MSCC-TG-P) and circular columns (MSCC-TG-M) with seat and diaphragm abutments in the post 1990 design era (E3)
- MSCC-IG with single (MSCC-IG-S) and multi column (MSCC-IG-M) bents with seat and diaphragm abutments in the 1971-1990 design era (E2)

4.3.1 Multispan Continuous Concrete Single Frame Box Girder Bridges

4.3.1.1. General Layout

MSCC-BG bridges are typically used for longer spans and this class constitutes the bulk of the highway bridge inventory in California. Figure 4.14 shows the typical configuration of a two span continuous concrete box-girder bridge. Two span analytical finite element models are developed for this bridge class across design eras, consistent with the mode statistic for the number of spans, as discussed in section 3.2. The geometric parameters describing the bridge models used for deterministic analyses across design eras are documented in Table 4.1. It must be noted that all of the parameters reported in Table 4.1 are median values of the respective distributions that will be used in the generation of fragility curves. The number of columns per bent and the number of cells in the box-girder are a function of the width of the bridge. Further details about the geometric attributes obtained from the review of bridge plans are presented in Appendix A. Box-girder bridges are integral at the bent and this section typically is a solid diaphragm. As described in Chapter 3, the superstructure to substructure connectivity is type 2 in the case of Pre 1971 era bridges while it is type 3 in the other two design eras. Also shown in Table 4.1 are the box-girder dimensions, column size and reinforcement

details. MSCC-BG bridges employ circular columns and their diameter and reinforcement depends on the number of columns per bent, determined in this study based on an extensive review of bridge plans. Based on the design era and the associated longitudinal and transverse reinforcement ratio, the number of #11 longitudinal reinforcing bars and spacing of #4 stirrups are calculated and employed in the finite element models. The girders are typically proportioned based on acceptable depth-to-span ratios which are 0.055 and 0.04 for cast-in-place (CIP) reinforced concrete and CIP prestressed concrete boxes, respectively. The latter is considered to present results from the deterministic analyses. Both SCBs and MCBs are supported on a pile cap with a group of piles underneath it, as shown in Figure 4.14. SCBs are prevalent in all design eras, while the maximum number of columns in a MCB differ based on the design era and so is the individual column diameter. MCBs are pinned to the pile cap while SCBs have a moment transfer connection. The stiffness of the translational and rotational springs at the base of the column are also reported in Table 4.1. Both abutment types have a 6 ft tall backwall with Class 70 CIDH piles spaced at 7 ft on center. Concrete compressive strength of 4860 psi and reinforcing steel yield strength of 67.4 ksi are adopted.

The superstructure box-girder frames into the diaphragm abutment thereby transferring all forces and moments. In the case of seat type abutments, the box-girders rest on 14 in x 14 in x 2.5 in elastomeric bearing pads at the abutment seat. Two cases of seat type abutments are modeled: one where a small gap of 0.75 in exists between the deck and the abutment backwall and another where a larger gap of 3.75 in is considered between the deck and the backwall. 14 ft long, $\frac{3}{4}$ in diameter restrainer cables are considered at the seat type abutments with 0.625 in slack. The number of restrainers is determined based on the W/2 method discussed in the preceding section and the number of restrainers is indicated in Table 4.1. The mass of the deck is increased by 35% to account for any additional mass on the bridge such as railing, electrical poles etc.

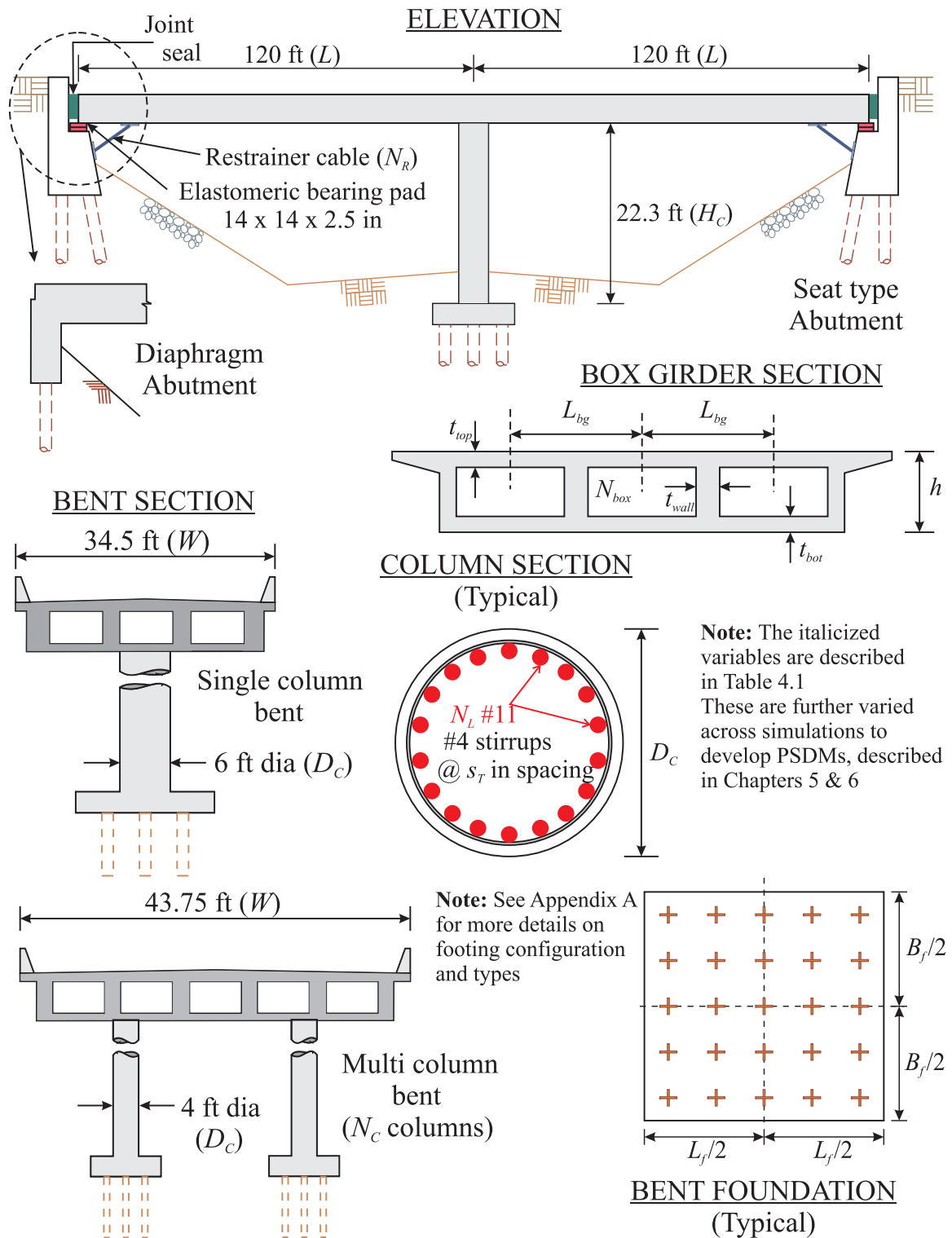


Figure 4.14: General layout of MSCC-BG bridges

Table 4.1: Deterministic bridge model attributes for MSCC single frame box-girder bridges

Attributes	Pre 1971		1971-1990				Post 1990				
	SCB	MCB	SCB	MCB			SCB	MCB			
Column details											
Number per bent (N_C)	1	2	1	2	3	4	1	2	3	4	5
Column height (ft) (H_C)	22.3	22.3	22.3	22.3	22.3	22.3	22.3	22.3	22.3	22.3	22.3
Diameter (ft) (D_C)	6	4	6	5	5	5	6	5	5	5	4
Longitudinal reinforcement (#11 bars) (N_L)	50	22	62	44	44	44	58	42	42	42	26
Transverse reinforcement spacing (in) (#4 stirrups) (s_T)	12.0	12.0	3.0	3.0	3.0	3.0	3.0	3.0	3.0	3.0	3.0
Superstructure details											
Span length (ft) (L)	120.0	120.0	120.0	120.0	120.0	120.0	120.0	120.0	120.0	120.0	120.0
Deck width (ft) (W)	34.5	43.75	35.25	43.75	90.0	110.0	35.25	43.75	70.0	90.0	127.5
Box-girder details											
Number of boxes (N_{box})	3	5	3	5	9	11	3	5	7	9	15
Total superstructure depth (in)* (h)	57.6	57.6	57.6	57.6	57.6	57.6	57.6	57.6	57.6	57.6	57.6
Top flange depth (in) (t_{top})	8.875	7.875	8.875	7.875	8.375	8.375	8.875	7.875	8.375	8.375	8.375
Bottom flange depth (in) (t_{bot})	6.0	6.0	6.5	6.5	6.5	6.5	7.0	7.0	7.0	7.0	7.0
Wall thickness (in) (t_{wall})	12.0	12.0	12.0	12.0	12.0	12.0	12.0	12.0	12.0	12.0	12.0
Cell center-to-center spacing (ft) (L_{bg})	11.5	8.75	11.75	8.75	10.0	10.0	11.75	8.75	10.0	10.0	8.5
Number of restrainers (N_R)	10	12	10	12	20	32	10	12	20	26	34
Column footing details – Spring stiffnesses											
Translational (kip/in)	1700	800	1400	1200	1200	1200	1400	1200	1200	1200	800
Rotational (kip-in/rad)	4.1×10^7	0	6.5×10^7	0	0	0	6.5×10^7	0	0	0	0

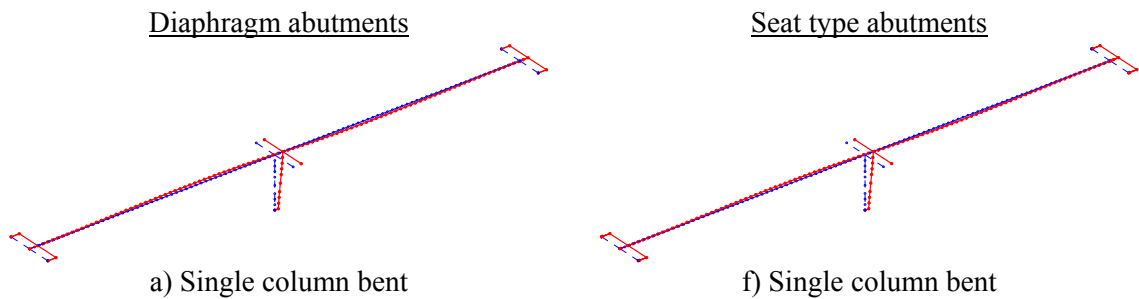
*Proportioned based on permissible depth-to-span ratio: 0.055 for CIP reinforced concrete and 0.04 for CIP prestressed concrete

4.3.1.2. Eigen Value and Time History Analysis

Eigen value analysis of the bridge models are performed in OpenSEES and the fundamental and second mode time periods are listed in Table 4.2. The fundamental mode shapes for different configurations of the post 1990 bridges with diaphragm and seat abutments is shown in Figure 4.15. In the case of seat type abutments, the fundamental mode is in the longitudinal direction. However, in the case of diaphragm abutments, the fundamental mode could either be longitudinal or transverse, as shown in Figure 4.15. In most of the cases, the second and higher modes invoke transverse and torsional responses of the bridges.

Table 4.2: First and second mode time periods for MSCC-BG bridges considered for deterministic analysis

Design era	No. of columns	Diaphragm abutments		Seat type abutments	
		First mode (sec)	Second mode (sec)	First mode (sec)	Second mode (sec)
Pre 1971	1	0.63	0.57	0.73	0.64
	2	0.77	0.63	1.23	1.07
1971-1990	1	0.57	0.53	0.78	0.73
	2	0.72	0.51	0.96	0.79
	3	0.77	0.38	0.99	0.83
	4	0.82	0.76	1.12	1.02
Post 1990	1	0.57	0.54	0.74	0.68
	2	0.64	0.37	1.01	0.91
	3	0.81	0.78	0.99	0.83
	4	0.71	0.38	1.02	0.93
	5	1.11	1.09	1.58	1.43



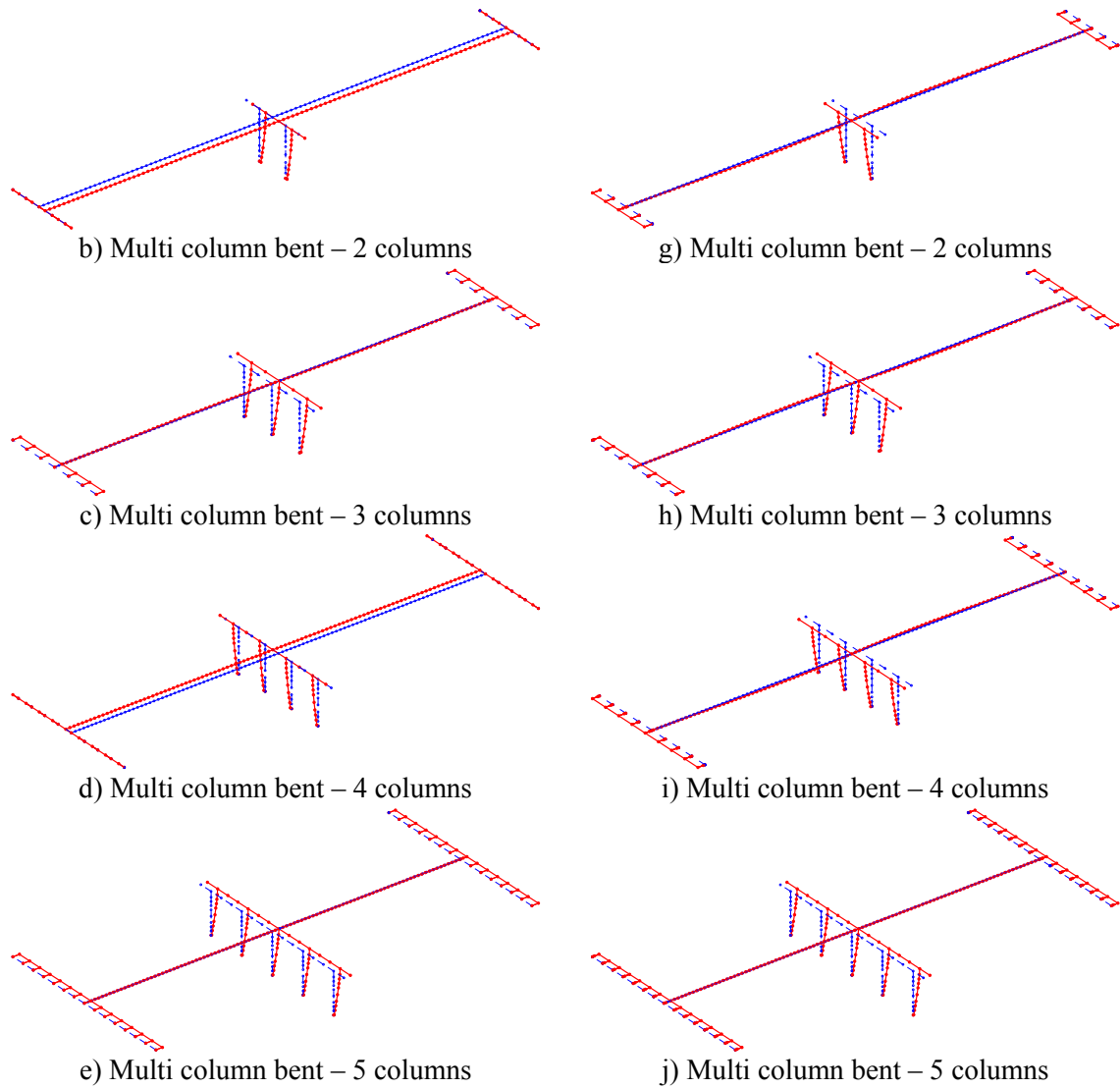


Figure 4.15: Fundamental mode shapes for Post 1990 MSCC-BG bridges with SCBs and MCBs

4.5% Rayleigh damping is used in the time history analysis performed on the bridge model. Subjection to a pair of ground motions records show in Figure 4.13. The ground motion records with a PGA of 0.96g is applied along the longitudinal axis of the bridge while the record with a PGA of 0.63g is applied in the transverse direction. Only the response of a few bridge components is presented below due to the large number of components and responses in each of the bridge models with different number of columns and abutment type.

Figure 4.16 shows the displacement response of the deck nodes in either spans in the longitudinal and transverse directions for a bridge with four columns designed in the 1971-1990 era with diaphragm and seat abutments. It can be seen that the response of both the spans match perfectly which is expected when the superstructure is continuous. It can be seen that the deck undergoes a longitudinal displacement of about 4 in for both the abutment types. The transverse displacement is slightly different based on the abutment type. Bridges with diaphragm abutments undergo a larger transverse displacement since in this case a monolithic connection exists between the deck and the abutments a larger mass is excited.

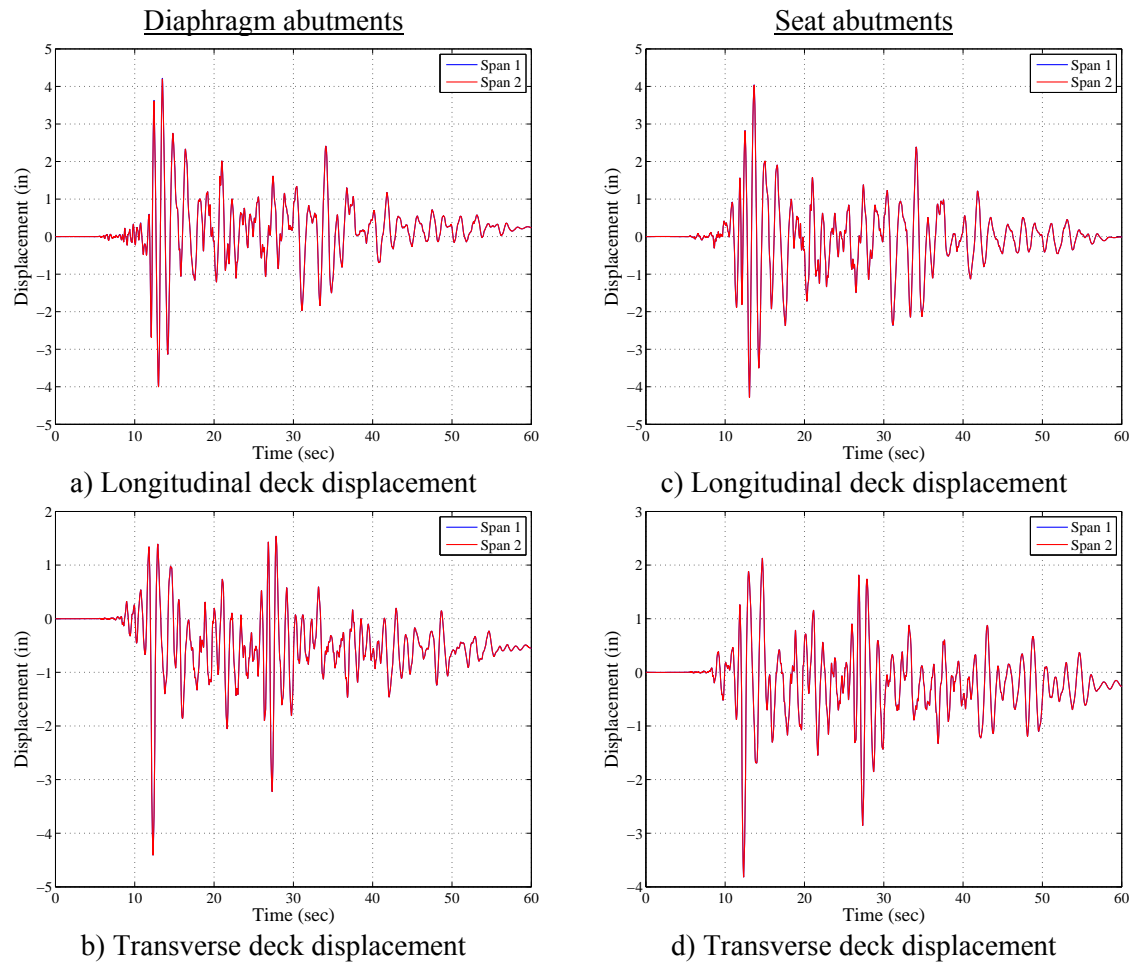


Figure 4.16: Displacement response of the deck for a MSCC-BG bridge with four columns in the 1971-1990 design era

In all the cases considered, moment curvature response of the column is monitored and a few of them are shown in Figure 4.17. Figures 4.17(a) and (b) show the seismic moment curvature response of a column in the longitudinal and transverse direction belonging to a pre 1971 designed MSCC-BG bridge with SCB and diaphragm abutments. It is seen that the columns are subjected to a larger longitudinal moment and curvature. Figure 4.17(c) shows the response of the column in transverse direction for a pre 1971 designed bridge with seat abutments and MCB, while Figure 4.17(d) shows the longitudinal response of a SCB of the same design era and seat abutments.

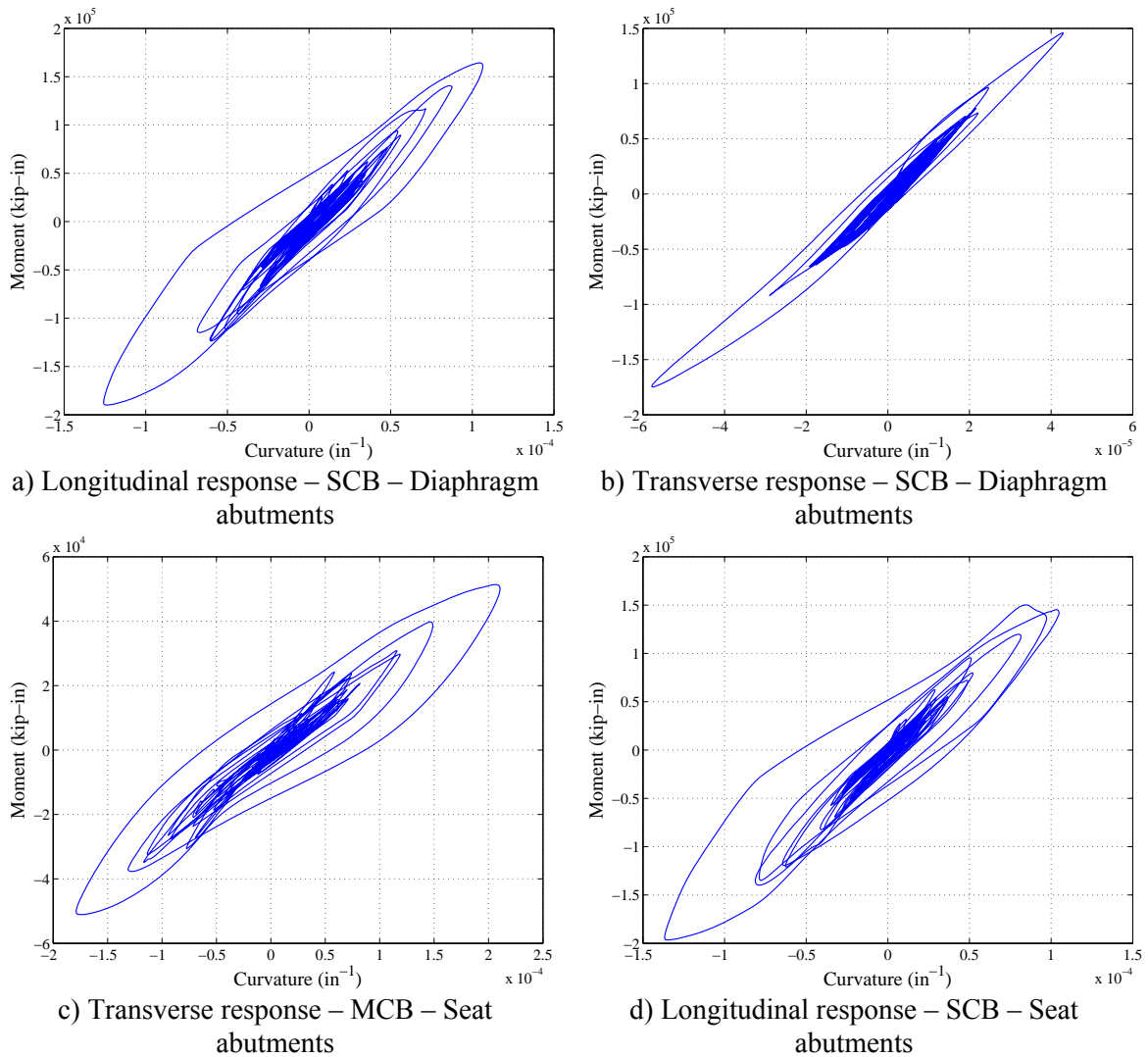
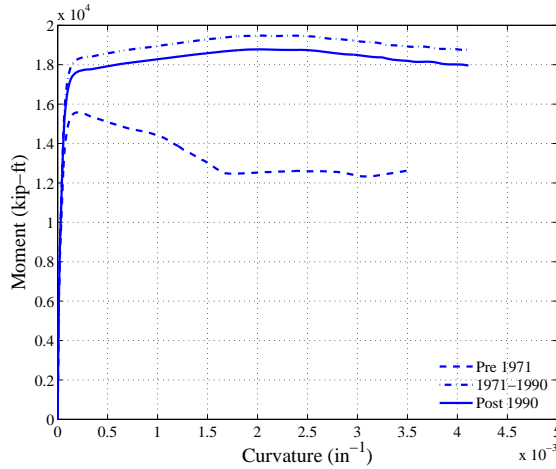


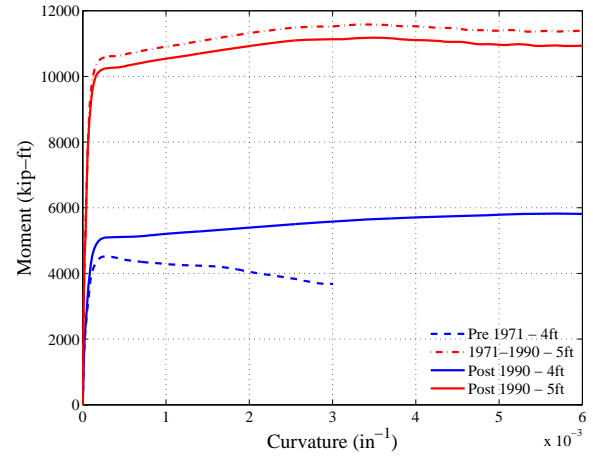
Figure 4.17: Moment curvature response of columns

Curvature ductility, μ_ϕ , is a common way of interpreting the response of columns and is defined as the ratio of ultimate curvature and yield curvature. Moment curvature analysis of the section is used to determine the yield curvature by fitting a bilinear response to the original data. Figure 4.18 shows the moment curvature response across design eras for columns in SCBs and MCBs. Clearly, the evolution of column design philosophy is visible in Figures 4.18(a) and (b) as seen in the strength degradation and limited ductility in the case of Pre 1971 columns. These characteristics are enhanced in the columns in the other two design eras and this is consistent with the trends observed based on the review of bridge plans, as described in the previous chapter. Figure 4.18(c) shows the bilinear approximation to the moment curvature response of a column cross-section. The curvature at transition of the two linear segments is reported as the yield curvature signifying the curvature at the onset of the first yield of the outermost reinforcing bar.

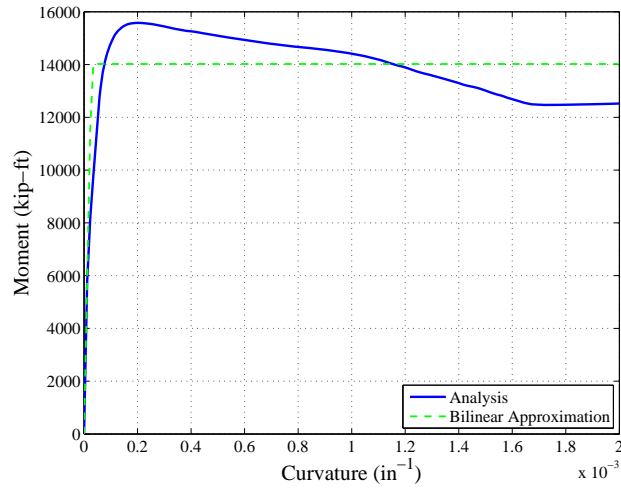
As mentioned previously, SCBs have a connection at the column bases close to fixity while MCBs are pinned at the base. The plot of curvature over the height of the column is shown in Figure 4.19 for bridges designed post 1990. It is seen that the columns become significantly nonlinear during the ground motions excited. This further demonstrates the significant ductility capacity of modern columns in comparison to the ones designed prior to 1971. In the case of SCBs, it is seen that the regions of the column close to the superstructure have higher curvature ductility when compared to the regions close to the pile cap. This is mainly because of the heavy moment and shear transfer from the superstructure. Further, the heavy superstructure mass excites the sections of the column close to the superstructure (like a lumped mass) thereby causing significant yielding in the column sections in this region. Similar behavior is seen in the case of multi column bents which are in any case free to rotate at the base.



a) Columns in single column bent



b) Columns in multi column bent



c) Bilinear approximation to determine yield curvature

Figure 4.18: Comparison of column moment curvature responses

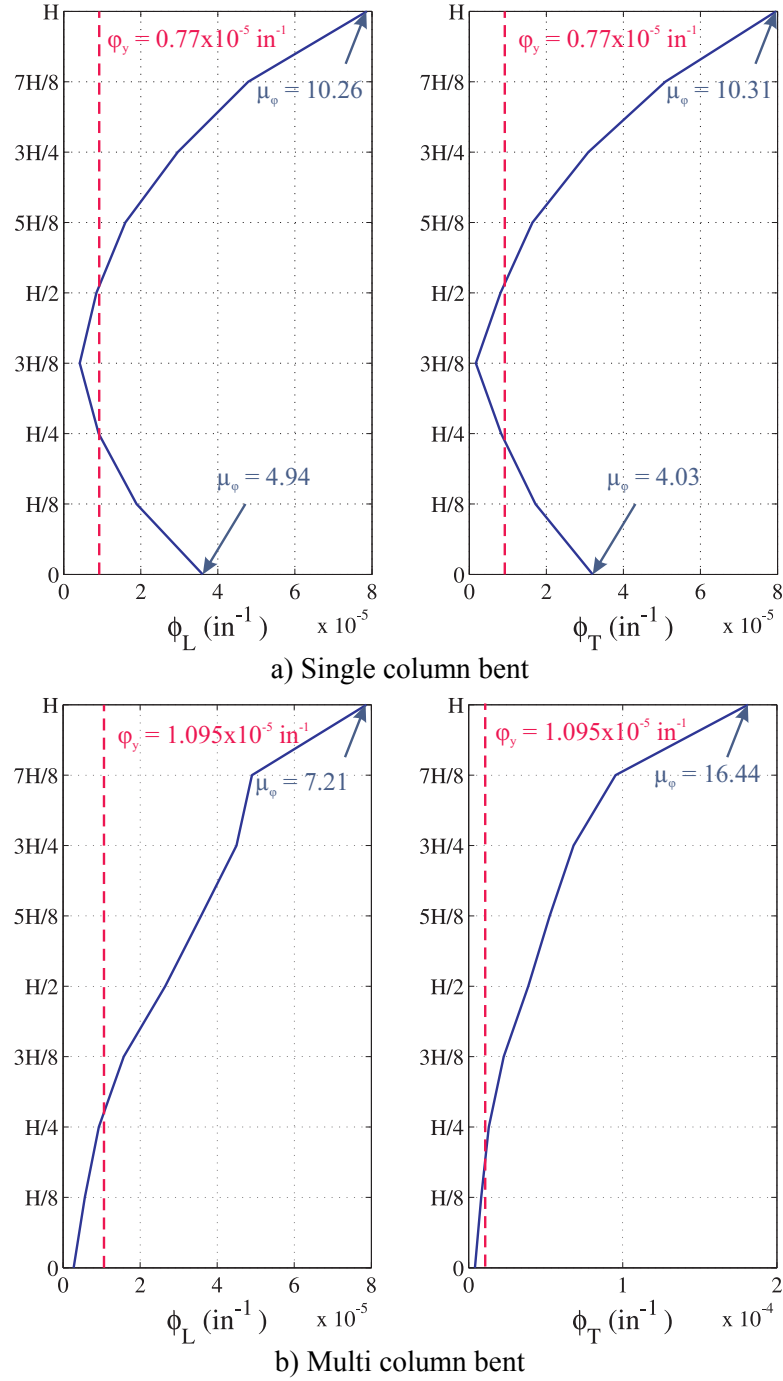
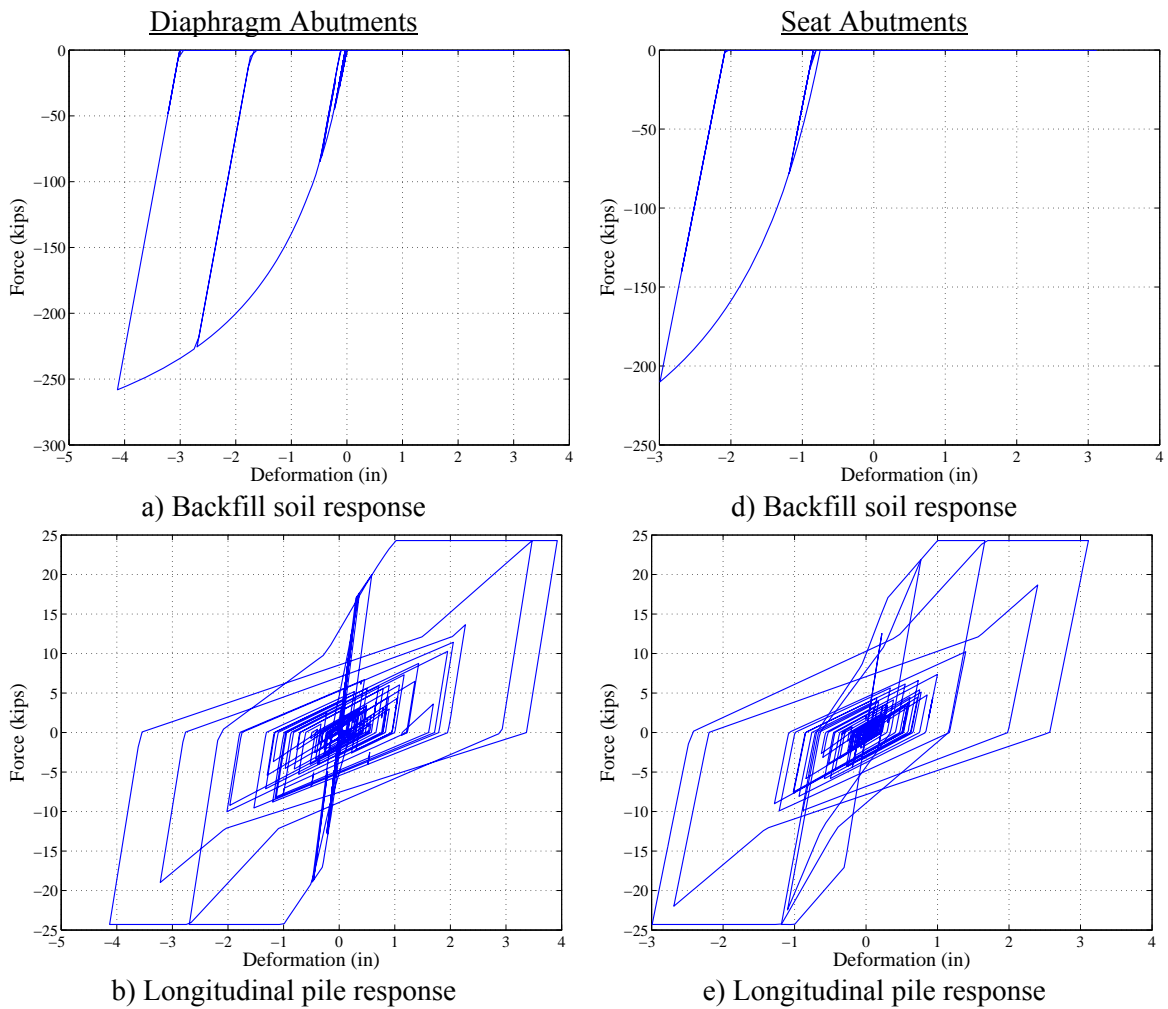


Figure 4.19: Variation of curvature over the height of a column

Figure 4.20 shows the response of the abutment soil-pile system for diaphragm versus seat abutment in a MSCC-BG bridge with SCB designed in the 1971-1990 design era. The longitudinal response of the abutments is characterized by the contribution of

backfill soil and piles in the passive action and solely by the piles in active action. Piles alone account for the transverse response of the abutments. Note that in both the cases, the backfill soil is clay. In the case of diaphragm abutments, the abutments act monolithically with the superstructure while in the case of seat type abutments, the abutment engages when the gap between the deck and the backwall closes which is 0.75 in in this case. This is depicted in the response of the backfill soil shown in Figures 4.20(a) and (d). For the same reasons, the backfill soil experiences greater nonlinearity in the case of diaphragm abutments when compared to their seat type counterparts.



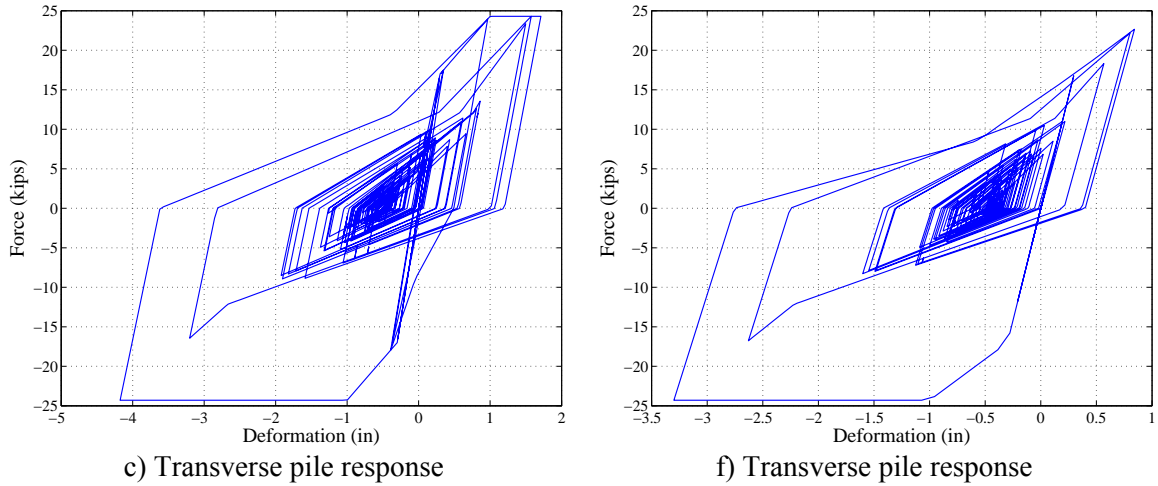


Figure 4.20: Response of abutment backfill - pile systems in MSCC-BG bridges designed in the 1971-1990 design era

Similar to the case of backfill soils, the extent of nonlinearity in piles is greater in the case of diaphragm abutments when compared to seat type abutments in both longitudinal and transverse directions. The reduction in the case of seat type abutments may be attributed to the load being resisted by restrainers and bearings in the longitudinal directions and the bearings and shear keys in the transverse direction.

The next logical question that arises would be the impact of backfill soil type on the response of bridges. Figure 4.21 shows the response of a MSCC-BG bridge with a SCB and diaphragm abutments designed in the 1971-1990 design era: one with a clayey backfill and the other with a sandy backfill. Abutment backwalls with sandy backfills are stiffer than clayey backfills and thereby attract more force, as seen in Figure 4.21(a). The displacement of the backwall and piles are smaller for sandy backfills when compared to clayey backfills, as seen in Figures 4.21(b) and (c). It can be concluded that the backfill soil type affects the bridge dynamic characteristics. This is further substantiated by the column response shown in Figure 4.21(d). Unlike the lower displacement response of the abutment soil-pile system, the columns in a bridge with sandy backfills experience larger curvatures and moments when compared to their counterparts with clayey backfills. In

any case, the mode shapes are identical and there is a small change in the modal periods: 0.61 sec for clayey backfill versus 0.57 sec for sandy backfills.

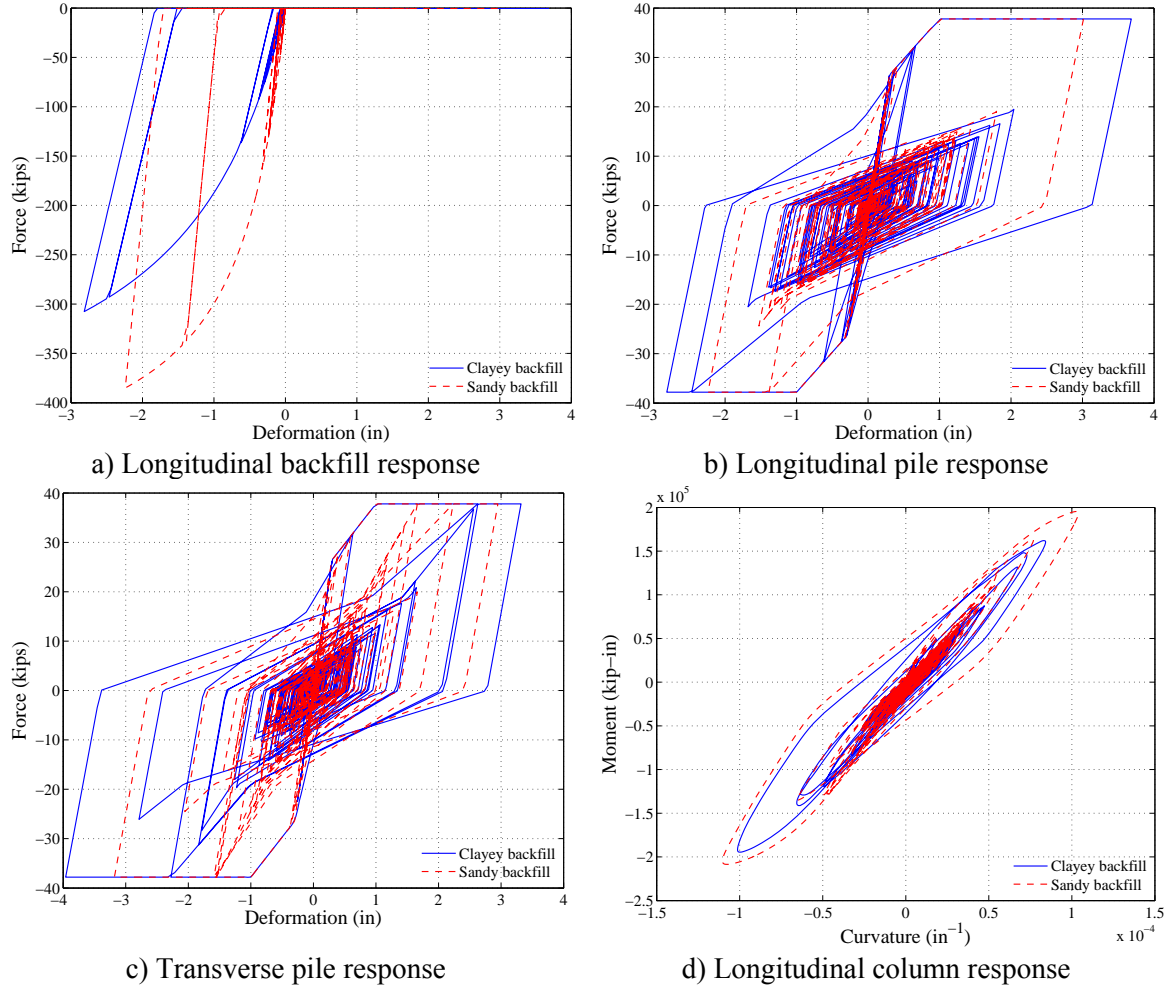


Figure 4.21: Influence of abutment backfill soil type on the response of bridge components

Figure 4.22 shows the response of restrainers and elastomeric bearing pads in a MSCC-BG bridge with seat type abutments designed in the post 1990 design era. As the superstructure moves towards and away from the abutment backwall, the elastomeric bearing pads and restrainer cables share the load transferred by the superstructure in proportion to their stiffness. When the bearing pads yield, restrainers pick up the additional forces transferred from the superstructure until the gap between the deck and

abutment backwall closes, at which point, the abutment soil-pile system engages in resisting the superstructure forces.

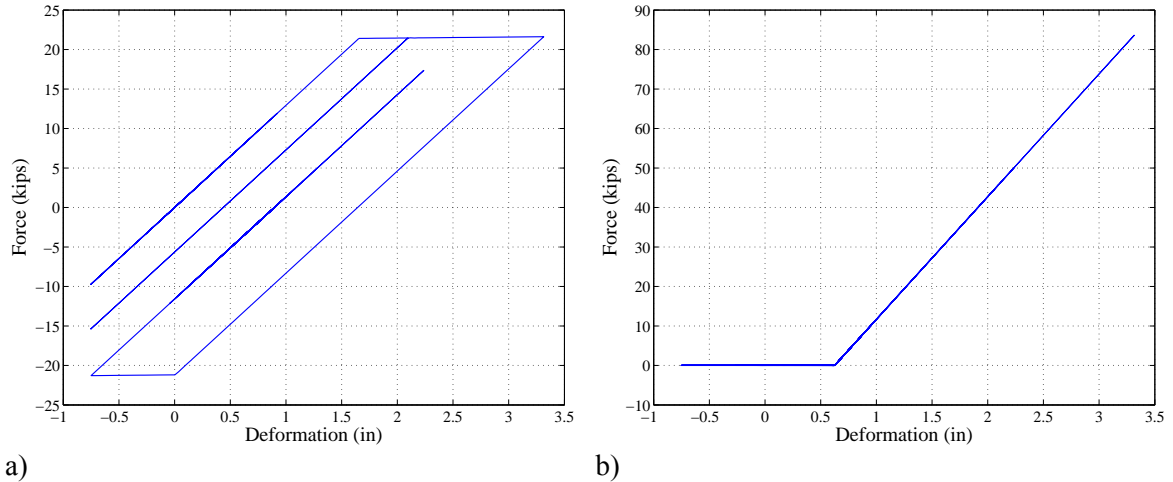


Figure 4.22: Response of a) elastomeric bearing pads, and b) restrainer cables in the longitudinal direction

4.3.2 Multispan Continuous Concrete Slab Bridges

4.3.2.1. General Layout

Slab bridges typically employ standard piles as columns (or integral pile columns) and unlike the case of columns in MSCC-BG bridges described in the previous section, there is no evolution in the pile cross-section and reinforcement patterns across the three significant design eras considered in this study. Slab bridge construction is generally employed over shorter span lengths and the overall configuration is similar to that of the box-girder bridges. The general layout of MSCC-SL bridges is shown in Figure 4.23.

Three span slab bridges are most prevalent in the inventory and based on the review of bridge plans it was seen that the ratio of the maximum span length to the length of the approach spans is typically 1.2. As shown in Figure 4.23, for the sake of deterministic analyses, three span finite element models are developed with the center span considered as the longest measuring 28 ft and the two approach spans measuring 23

ft each. The deck measures 37 ft in width and the bridge consists of two multi column bents with 15 ft tall columns. Both diaphragm and seat type abutments with clayey and sandy backfills are considered and the height of the backwall is 6 ft in both the cases. A 0.75 in gap is considered between the deck and the abutment backwall in the case of seat type abutments. These parameters are median values of their respective ranges. A typical value of the depth-to-span ratio for slab bridges with continuous spans is 0.05 and therefore a 22 in thick deck slab is considered in model used to present deterministic analyses results.

Since slab bridges have shorter spans, the substructure for this class of bridges is smaller when compared to all the other bridge classes and hence these typically employ smaller integral pile columns. These typically measure 16 in in diameter and are of two fundamental types: precast concrete (PC) piles and precast prestressed concrete (PPC) piles. The details of the pile cross-sections are also shown in Figure 4.23. Based on a review of bridge plans and Caltrans standard drawings over the last four decades, it was seen that MSCC-SL used only 45 ton (90 kips) and 70 ton (140 kips) piles. These are generally referred to as Class 45 and Class 70 piles, where the class number denotes the design load or one-half the ultimate load in tons. This yields ultimate loads of 180 kips and 280 kips for Class 45 and Class 70 piles, respectively. As shown in Figure 4.23, the details of Class 45 and 70 PC and PPC piles are summarized below:

- Class 45 precast concrete piles: These measure 15 in in diameter and the longitudinal reinforcement consists of 8 #6 bars and transverse reinforcement comprised of #5 gauge wire spirals at 3 in on center
- Class 45 precast prestressed concrete piles: These measure 15 in in diameter and consist of 16- ϕ 7/16 prestressing strands. 4 #6 reinforcing bars are present in the top 3.5 ft of the column and these frame into the superstructure. The transverse reinforcement consists of #5 gauge wire spirals at 3 in on center

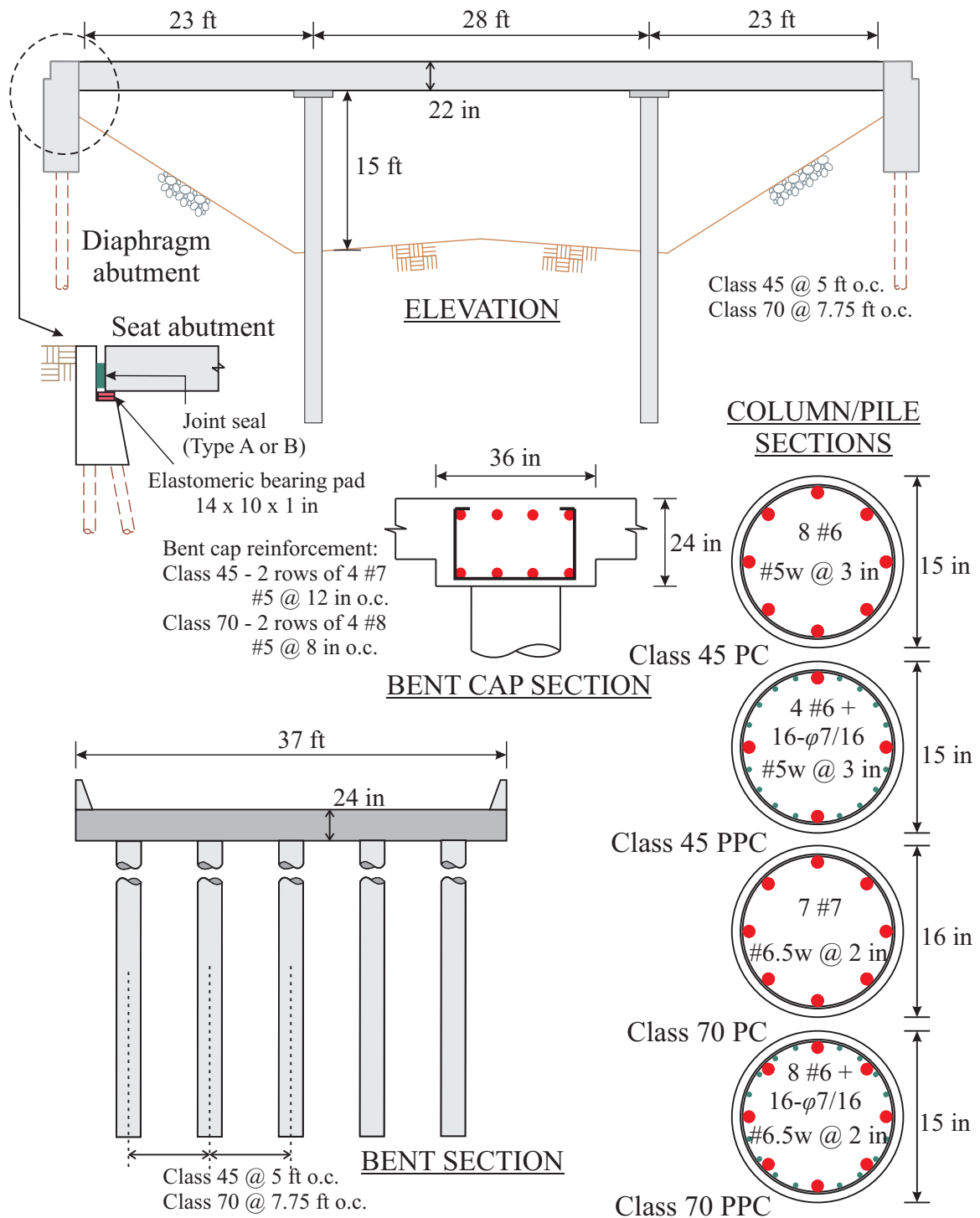


Figure 4.23: General layout of MSCC-SL bridge

- Class 70 precast concrete and cast-in-driven hole (CIDH) piles: These measure 16 in in diameter and the longitudinal reinforcement consists of 7 #7 bars. The transverse reinforcement is comprised of #6.5 gauge wire spirals at 2 in on center
- Class 70 precast prestressed concrete piles: These measure 15 in in diameter and consist of 16- ϕ 7/16 prestressing strands. 8 #6 reinforcing bars are present in the top 3.5 ft of the column and these frame into the superstructure. The transverse reinforcement consists of #6.5 gauge wire spirals at 2 in on center

Akin to MSCC-BG bridges, MSCC-SL bridges are integral at the bent. As mentioned in Chapter 3, slab bridges have MCBs alone. However, it must be noted that the MCBs in this case are not pinned at the base since the columns extend below the ground surface as piles. The stiffness of the translational and rotational springs at the base of the column is 30 kip/in and 80,000 kip-in/rad, respectively. The center to center spacing of the integral pile columns at the bent and the spacing of abutment piles depends on the span length and the pile class. In the present case, the center-to-center spacing of the columns at the bent is 5 ft in the case of Class 45 piles and 7.75 ft in the case of Class 70 piles. The same applies to the spacing of abutment piles. The presence of a bent cap depends on the span length and detailed information regarding the dimensions and reinforcement layout is given in Appendix A in the form of design charts. In this case, the bridge has a 36 in \times 24 in bent beam. The reinforcement consists of two rows of 4 #7 bars each at the top and bottom and #5 stirrups at 12 in on center in the case of Class 45 piles, and two rows of 4 #8 bars each at the top and bottom and #5 stirrups at 8 in on center in the case of Class 70 piles. The superstructure slab frames into the diaphragm abutment thereby creating a monolithic connection. However, in the case of seat type abutments, the deck slab rests on elastomeric bearing pads. In all cases, 14 in \times 10 in \times 1 in elastomeric bearing pads are used. The survey of bridge plans did not reveal the presence of restrainer cables and shear keys at the abutments and henceforth these are not considered in the analytical models for this bridge class.

4.3.2.2. Eigen Value and Time History Analysis

MSCC-SL bridges have shorter periods when compared to MSCC-BG bridges due to their relative stiff nature. Table 4.3 lists the first two modal periods for MSCC-SL bridges with diaphragm and seat abutments and the pile class. It must be noted that the pile class dictates the center-to-center spacing of the integral columns at the bent. This in turn drives the number of columns in a bent and therefore, the pile class can affect the period of the structure, as seen in Table 4.3. For both abutment types, the fundamental mode is in the longitudinal direction and the second mode is in the transverse direction. Higher modes are vertical and torsional. The first two mode shapes for slab bridges with both abutment types is shown in Figure 4.24.

Table 4.3: Modal time periods for MSCC-SL bridges

Abutment	Pile class	First mode (sec)	Second mode (sec)
Diaphragm	Class 45	0.47	0.44
	Class 70	0.57	0.54
Seat	Class 45	0.64	0.61
	Class 70	0.76	0.74

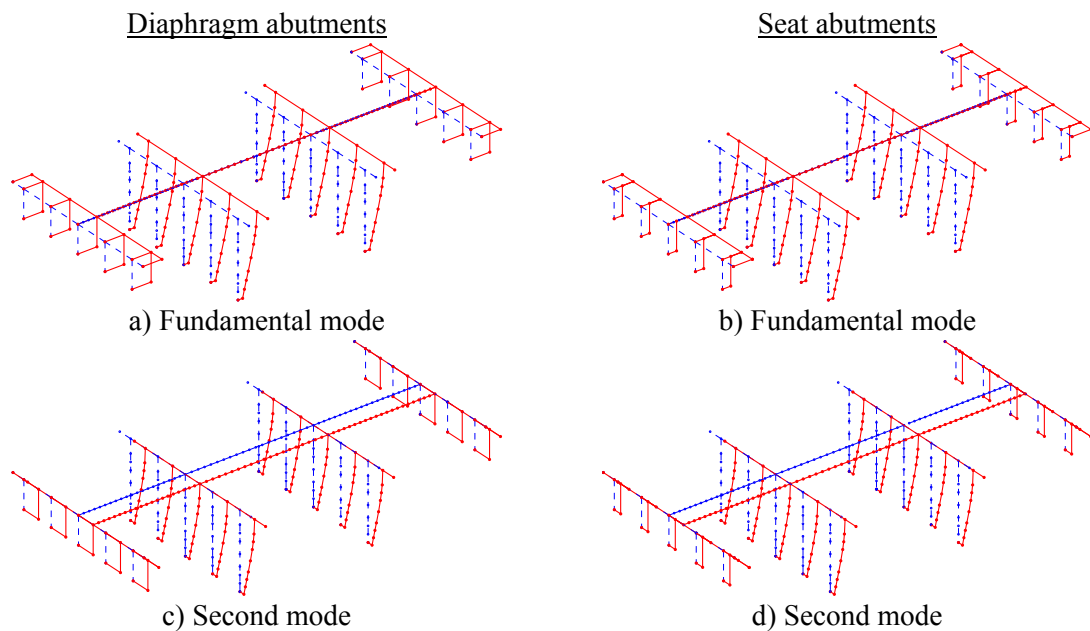


Figure 4.24: Mode shapes for MSCC-SL bridges with diaphragm and seat abutments

Time history analyses are conducted using the orthogonal pair of ground motions shown in Figure 4.13 and the response of deck, columns, abutment soil-pile system, and elastomeric bearings is recorded. Figure 4.25 shows the longitudinal and transverse displacement response of the mid span sections. The displacements of the three spans are equal owing to the continuity of the superstructure across the bents. The maximum longitudinal and transverse displacements are 2.4 in and 1.55 in, respectively for diaphragm abutments, while these values are 4.15 in and 3.95 in for seat type abutments. Bridges with seat type abutments are relatively flexible when compared to those with diaphragm abutments and the presence of the gap between the deck and backwall leads to an increased deck displacement, as seen in Figures 4.25(c) and (d). Further the absence of shear keys leads to an increased displacement in the transverse direction.

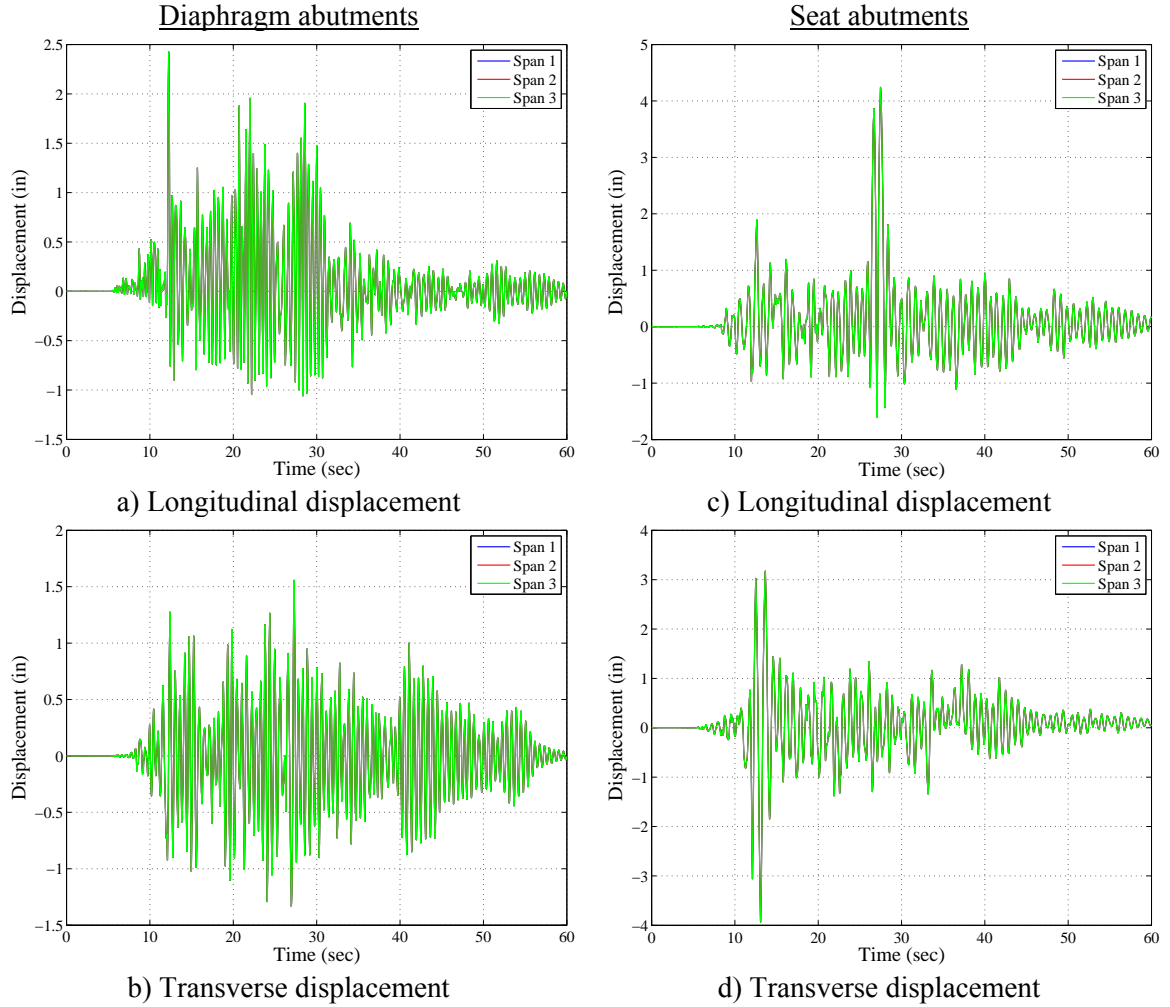


Figure 4.25: Longitudinal and transverse displacement of the individual spans in a MSCC-SL bridge with diaphragm and seat abutments

The response of the columns in the longitudinal and transverse directions for MSCC-SL bridges employing Class 70 PPC piles with diaphragm and seat abutments is shown in Figure 4.26. Figure 4.27 shows the moment curvature response of Class 45 and 70, PC and PPC pile cross-sections and the respective yield curvatures determined using a bilinear approximation, as described in the previous section. It is seen that the columns behave in their elastic range in both cases. This may be attributed to the fact that slab bridges have larger number of integral pile columns across the bent thereby offering more ways for the superstructure forces and moments to be distributed.

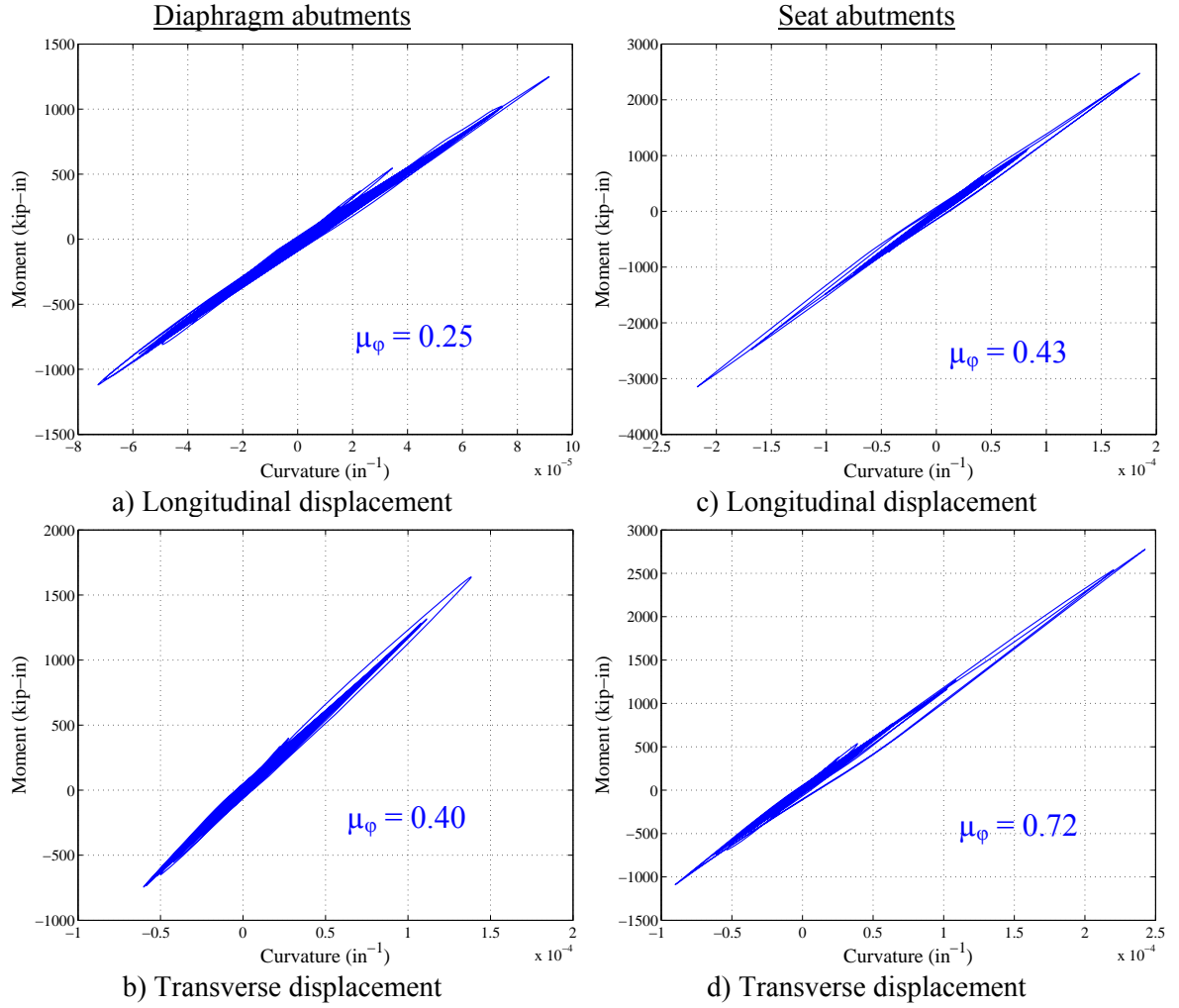


Figure 4.26: Response of MSCC-SL bridge columns in longitudinal and transverse direction

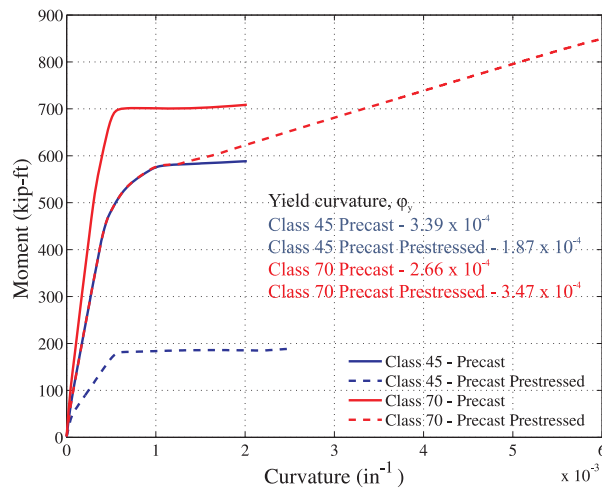


Figure 4.27: Moment curvature responses for different pile classes and pile types

From Figure 27, it is seen that PC piles have a higher moment and lower ductility capacity when compared to PPC piles. This may be attributed to the presence of larger amounts of primary longitudinal reinforcing bar in PC piles when compared to PPC piles. However, the enhanced ductility in the case of PPC piles is due to the presence of prestressing strands and improved confinement.

The curvature ductility of columns in bridges with seat abutments is higher than their diaphragm counterparts. This is because in the case of diaphragm abutments, the abutment system is completely engaged with the superstructure thereby reducing the demand on the columns. While in the case of seat abutments, majority of the superstructure forces go into the columns until the gap between the deck and the abutment backwall is closed, at which point abutments begin to engage and share forces and moments. The variation of curvature over the height of the column for a MSCC-SL bridge with Class 45 PC piles and seat abutments is shown in Figure 4.28. Only the portion of the column close to the superstructure yields in the transverse direction while the other sections remain elastic. Further, the curvature profile indicates the potential for the integral pile columns to undergo a double curvature bending.

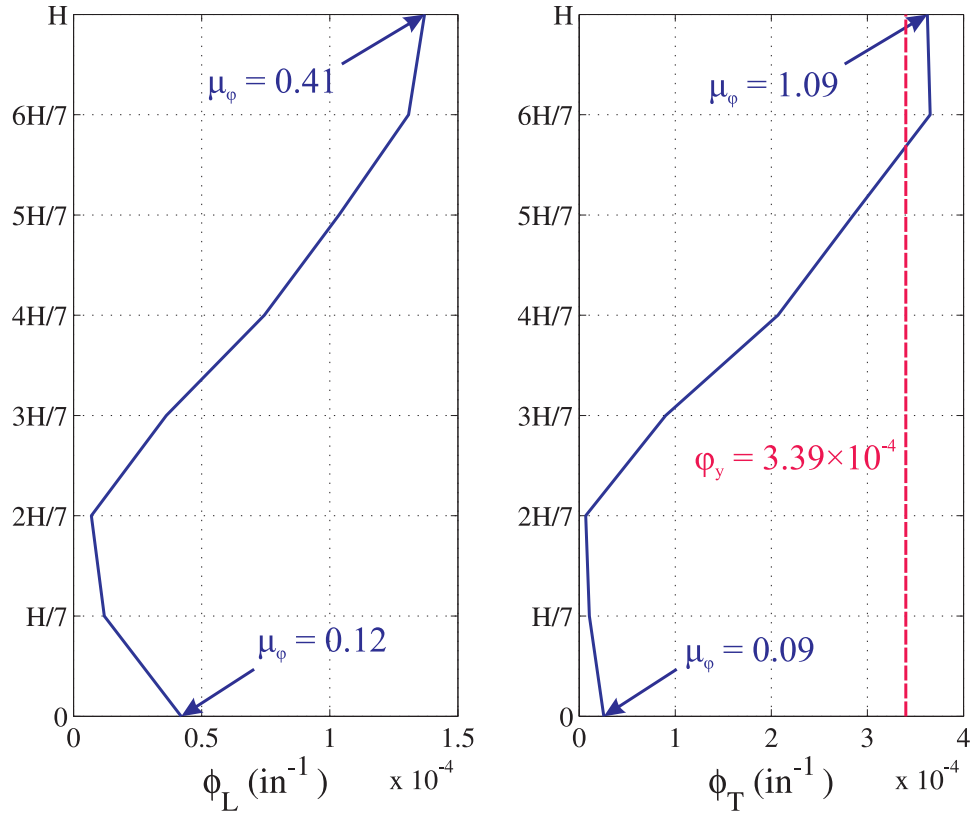


Figure 4.28: Variation of curvature over the height of the column for an MSCC-SL bridge with seat abutments

The response of the abutment backfill soil and piles in the longitudinal and transverse directions is shown in Figure 4.29. Class 45 PC piles are used in the simulations. The backfill soil responds only in passive action and it is seen that the passive displacement of the soil in seat abutments is greater than that of diaphragm abutments. On the other hand, the active displacement of piles in seat abutments is higher than the passive displacement and the trend is reverse in the case of diaphragm abutments. Further, it is seen that the transverse displacement of piles in diaphragm abutments is higher than that in the case of seat abutments. This is expected since the entire bridge structure frames into diaphragm abutments and behaves like a vertical cantilever in the transverse direction leading to greater displacements. It must be noted that piles alone contribute to the transverse resistance of the abutments.

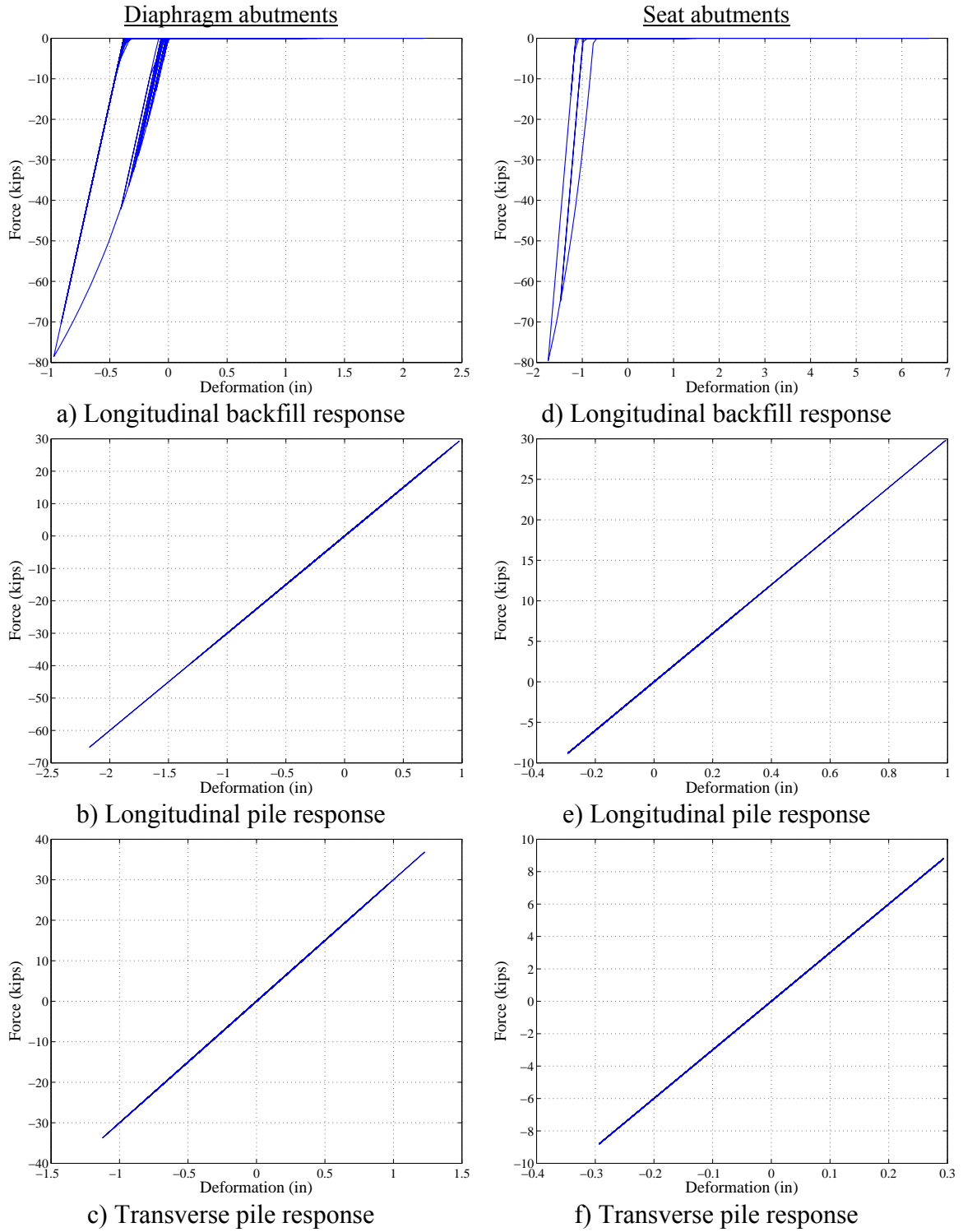


Figure 4.29: Response of abutment soil-pile system in MSCC-SL bridge with diaphragm and seat abutments

Unlike the case of the MSCC-BG bridges where the elastomeric bearing pads did not undergo significant deformations and nonlinearity, the elastomeric bearing pads in the case of MSCC-SL and seat abutments undergo significant deformations. This is due to the absence of restrainer cables and shear keys in this bridge class to share a proportion of the forces. Figure 4.30 shows the response of elastomeric bearing pads in slab bridges in longitudinal and transverse directions.

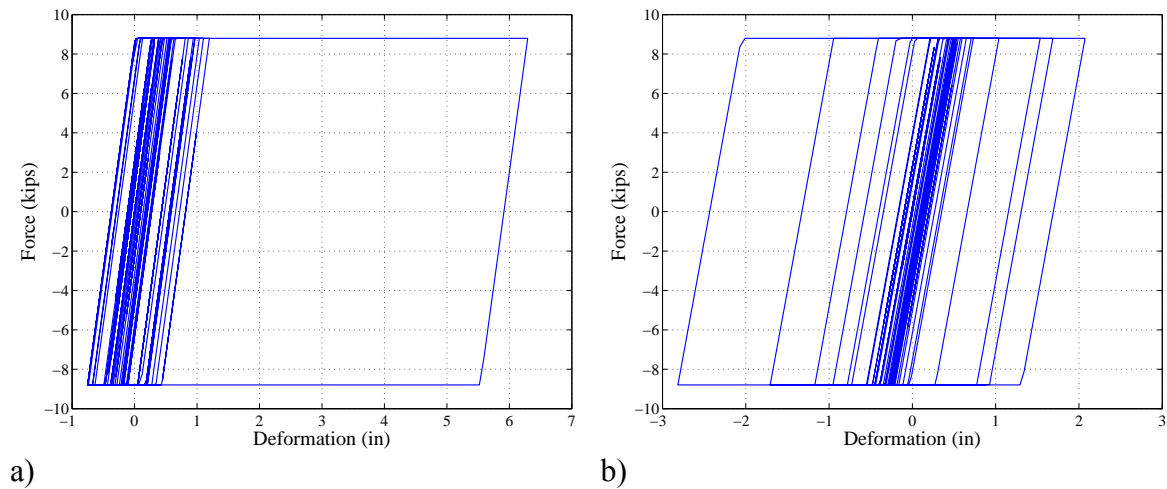


Figure 4.30: Response of elastomeric bearing pads in MSCC-SL bridge with seat abutments in the a) longitudinal, and b) transverse direction

4.3.3 Multispan Continuous Concrete Tee Girder Bridges

4.3.3.1. General Layout

Multispan Tee girder bridges are normally adopted over span range of 30 ft to 80 ft and have typical depth to span ratios of 0.05. Their behavior is similar to MSCC-SL bridges described in the previous section. Tee girder bridges are integral at the bent and the superstructure consists of girders cast monolithically with the deck slab. As in the case of MSCC-SL bridges, MSCC-TG bridges have multi column bents (MCB) alone consisting of either integral pile columns (MSCC-TG-P) or circular columns founded on pile footings (MSCC-TG-M). Unlike, integral pile columns which did not undergo any

change across the design eras, circular columns underwent a major shift in response characteristics being described as brittle in the pre 1971 design era to ductile in the modern day bridges.

Deterministic responses from Tee girder bridges designed in the post 1990 design era are presented in this section. Three spans bridges are the most likely configurations for this bridge class. Three span analytical models are developed with the center span measuring 60 ft and the two adjacent spans measuring 50 ft for the sake of deterministic analysis and a typical layout is shown in Figure 4.31. The bridge is 50 ft wide and the superstructure deck is supported over 5 girders and consists of MCBs with 22 ft tall columns. The models employ both integral pile columns and MCB with circular columns for comparison purposes. As in the case of MSCC-SL bridges, Class 45 and 70, PC and PPC piles are employed for MCB with integral pile columns. The bridge bent has 10 columns per bent if Class 45 integral pile columns are adopted while they have 9 columns in the bent if Class 70 integral pile columns are adopted. In the case of MCB with circular columns, 3 ft diameter columns with 24 #11 longitudinal reinforcing bars and #4 stirrups at 3 in on center are employed. The bent has two columns if circular columns are adopted. Further details correlating the width of the bridge, number of column per bent and column center-to-center spacing is provided in Appendix A. The integral pile columns have translational and rotational springs at the base of the column to replicate the behavior of the portion of the pile extending beneath the surface of the ground. The stiffness of the translational and rotational springs is 30 kip/in and 80,000 kip-in/rad, respectively. On the other hand, MCB with circular columns are pinned at the base, and therefore only a translational spring of stiffness 800 kip/in is provided.

connection. In the case of seat abutments, the deck slab-girder group rests on elastomeric bearing pads, (16 in \times 12 in \times 1.5 in) in dimension on the abutment seat. The gap between the superstructure and abutment backwall is 0.75 in. The abutment backfill soil and piles engage with the superstructure when this gap closes. As in the case of MSCC-SL bridges, review of bridge plans for MSCC-TG bridges did not reveal the presence of restrainer cables and shear keys and hence these are not considered in the bridge analytical models.

4.3.3.2. Eigen Value and Time History Analysis

Table 4.4 lists the first two modal periods for MSCC-TB bridges with diaphragm and seat abutments and MCB with circular columns. The modal periods for MSCC-TG bridges with integral pile columns is shown in Table 4.5. It is seen that bridges with integral pile columns are flexible when compared to bridges with circular columns. Further the modal periods for either pile class and pile type are very similar. Also it is seen that the fundamental periods for bridges with integral pile columns are similar for diaphragm and seat abutments, although, the second mode period differs depending on the abutment type. Further, the MSCC-SL bridges are stiffer when compared to MSCC-TG bridges (see Tables 4.3, 4.4, and 4.5).

Figure 4.32 shows the first two mode shapes for MSCC-TG with integral pile columns and MCB with circular columns having diaphragm and seat abutments. In all cases the first mode is a combination of transverse and torsional response and so is the second mode. The third mode is a longitudinal mode and the higher order modes invoke vertical and torsional response.

Table 1.4: Modal periods for MSCC-TG bridges with circular columns

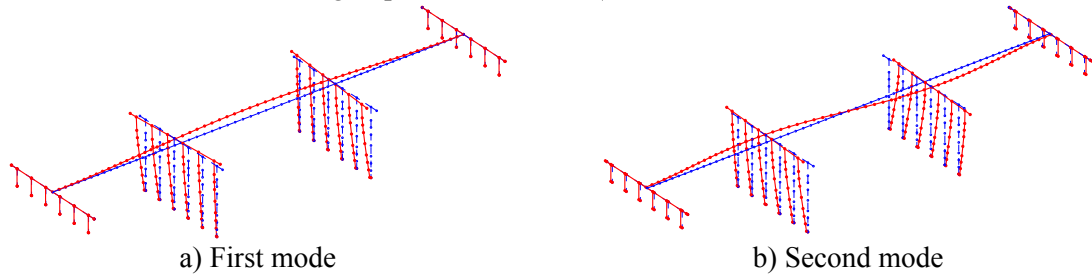
Abutment type	First mode (sec)	Second mode (sec)
Diaphragm	0.55	0.31
Seat	0.61	0.58

Table 4.5: Modal periods for MSCC-TG bridges with integral pile columns

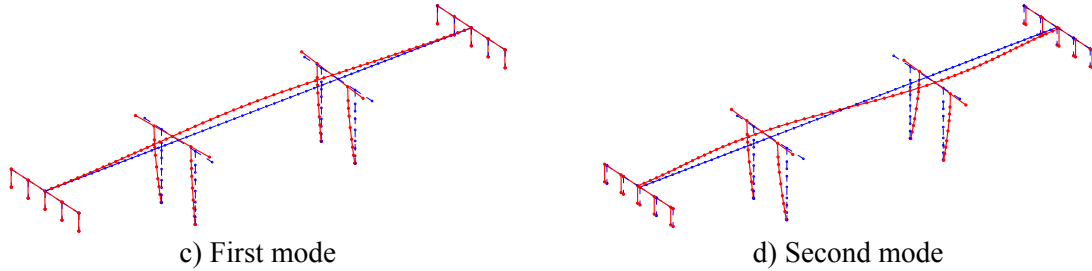
Abutment type	Pile class	Pile type	First mode (sec)	Second mode (sec)
Diaphragm	Class 45	Precast concrete	0.76	0.35
	Class 45	Precast prestressed concrete	0.75	0.35
	Class 70	Precast concrete	0.72	0.36
	Class 70	Precast prestressed concrete	0.71	0.35
Seat	Class 45	Precast concrete	0.79	0.62
	Class 45	Precast prestressed concrete	0.73	0.58
	Class 70	Precast concrete	0.78	0.63
	Class 70	Precast prestressed concrete	0.78	0.63

The typical response of circular columns and integral pile columns is similar to those shown in the previous sections. Although not shown here, it was seen that the curvature ductility of the integral pile columns was higher than that of MCB with circular columns. It should be noted that this can cause significant damage to the bridges with integral pile columns since they are brittle in nature. Further, as stated before, there has been no improvement in the pile details across the years which could render bridges with these column types more vulnerable than ductile circular columns belonging to this design era. Figure 4.33 shows a comparison between the response of typical bridge components in MSCC-TG bridges with integral pile columns and MCB with circular columns for both the abutment types.

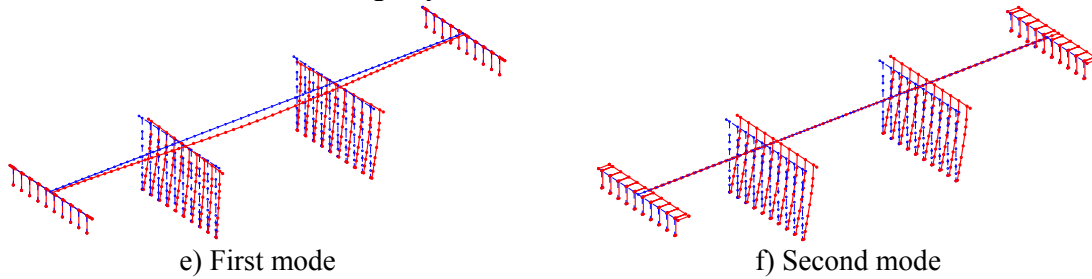
Integral pile columns - Diaphragm abutments



MCB with circular columns – Diaphragm abutments



Integral pile columns - Seat abutments



MCB with circular columns – Seat abutments

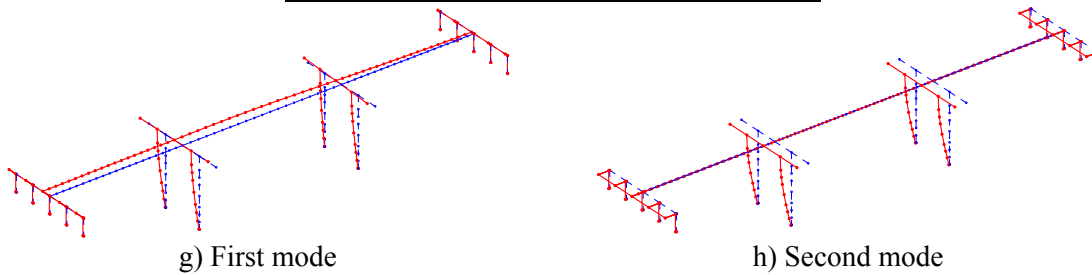


Figure 4.32: First and second mode shapes for MSCC-TG bridges

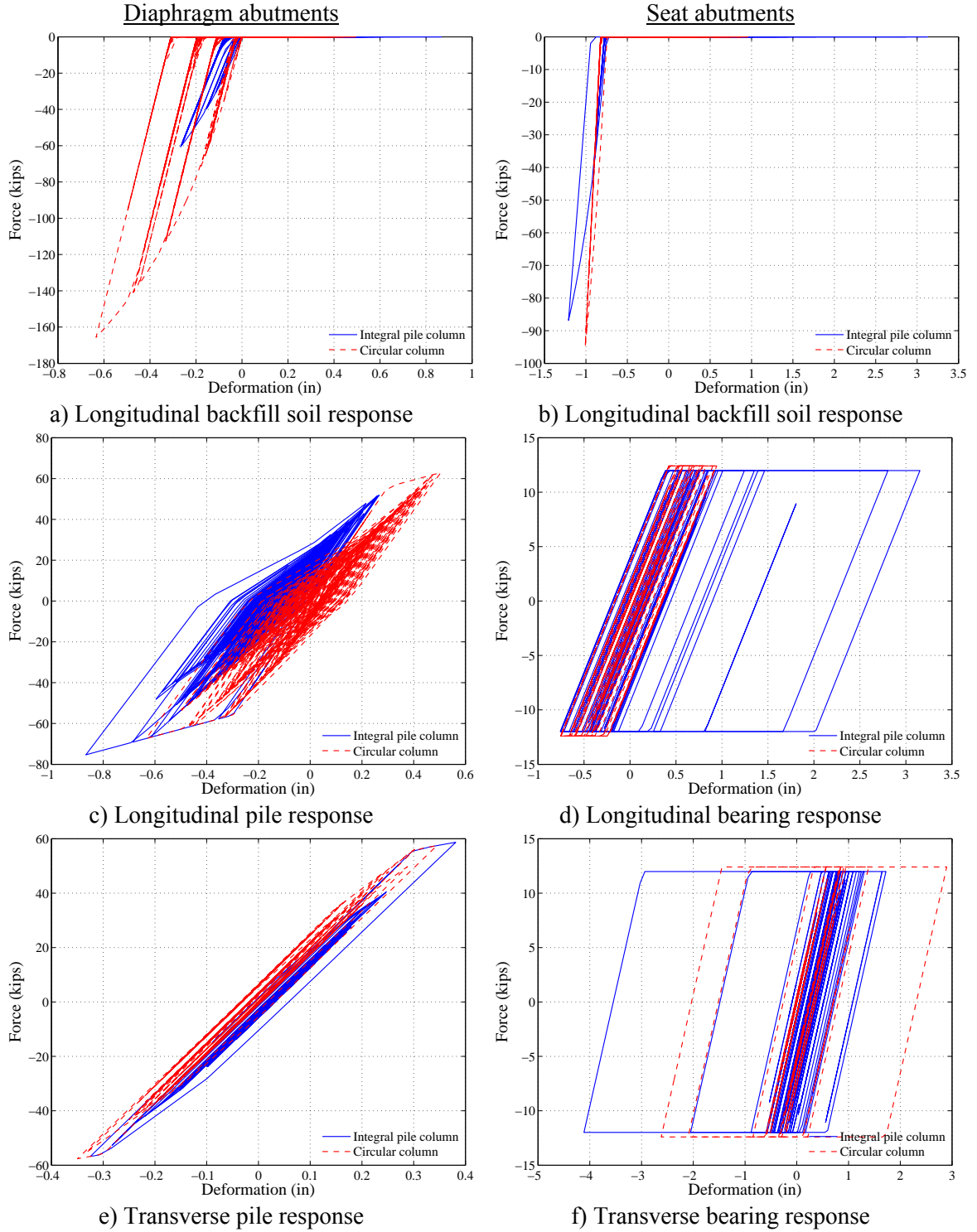


Figure 4.33: Response of components in MSCC-TG bridges with integral pile columns and circular multi column bents

The passive force and deformation response of the backfill soil in diaphragm abutments is higher for MCB with circular columns when compared to integral pile columns (Figure 4.33(a)). On the other hand, the backfill soil response is comparable for both column types in case of seat abutments as shown in Figure 4.33(b). Also, backfill soils experience greater nonlinearity and hence cause more energy dissipation in case of diaphragm abutments when compared to seat abutments. This may be attributed to the greater engagement of the superstructure and backwall in the case of diaphragm abutments when compared to seat abutments. With respect to the response of piles in the longitudinal direction in diaphragm abutments, it is seen that the active response of piles in bridges with MCB and circular columns dominates over the active response of piles in bridges with integral pile columns. However, the passive response of piles in diaphragm abutment bridges with integral pile columns is greater than that of MCB and circular columns. This is because the passive response of piles in bridges with integral pile columns takes a major share of the compressive force (Figure 4.33(c)) in contrast to the backfill soil in the case of bridges with circular MCB (Figure 4.33(a)). The behavior of piles in longitudinal direction is the opposite in the case of seat abutments. The response of piles in transverse direction is similar for both column types irrespective of the abutment type. Although the piles undergo inelasticity in the case of diaphragm abutments, they behave linearly in the case of seat abutments. The latter is expected since significant yielding of the elastomeric bearing pads is noticed in bridges with seat abutments, as shown in Figure 4.33(d) and 4.33(f).

With respect to bearings, it is seen that larger demands are imposed on the bearings in integral pile columns. This is consistent with the greater curvature ductility exhibited by the columns in these bridges which directly translates to an increased bearing displacement in the longitudinal direction (Figure 4.33(e)). In the transverse direction (Figure 4.33(f)), the bearing response is symmetric about the bridge centerline in the case of circular MCB while the bearings undergo increased nonlinearity in one

direction in bridges with integral pile columns. In other words, there is an apparent shift in the equilibrium position. This reflects the fact that significant residual displacements exist in these bridges due to the imposed ground motion.

4.3.4 Multispan Continuous Concrete I-Girder Bridges

4.3.4.1. General Layout

MSCC-IG bridges differ in response and performance when compared to MSCC-TG bridges although both bridge classes have the superstructure deck resting on girders. The fundamental differences in configuration and flow of forces were detailed in the previous sections. MSCC-IG are typically used for spans ranging between 30 ft and 150 ft and employ standard “I” and “Bulb-Tee” girders in the superstructure (see Appendix A for details). As in the case of slab and Tee girder bridges, three spans are the most likely number of spans in this case and hence three spans are considered for analytical modeling.

Figure 4.34 shows the general layout of MSCC-IG bridges. For the sake of deterministic analysis, a bridge with median value of the parameters designed in the 1971-1990 design era is considered. The center span measuring 60 ft is considered the longest and the two approach spans on either side measure 44 ft, such that the ratio of the maximum span to the approach span was found to be 1.4 based on the review of bridge plans. In general the choice and dimensions of the girder is dictated based on permissible depth-to-span ratio which is 0.05 for standard I-girders and 0.045 for Bulb-Tee girders. The deck slab is 7.5 in thick and details about Standard I- or Bulb-Tee girders can be found in Appendix A. The Standard I-girder has a flange width of 19 in and overall depth of 36 in with weight per unit run of 450 lb/ft. If Bulb-Tee girders were selected, the girder adopted would have a flange width of 48 in and overall depth of 55 in with weight per unit run of 964 lb/ft. The deterministic responses presented in this section employ

Standard I-girders in the superstructure. It must be noted that the choice of the girder type influences the mass and sectional properties (area and moment of inertia of the cross-section) of the superstructure elastic beam column elements. However, these do not affect the response of bridge components significantly since their variation is limited. The girders rest on (16 in \times 12 in \times 1.5 in) elastomeric bearing pads at the bent and at the seat abutments. As in all the other cases, both diaphragm and seat abutments are considered for deterministic and fragility analyses (in subsequent chapters). Both the abutment types have 6.0 ft high backwalls supported on Class 45 or 70, PC or PPC piles spaced 7 ft on center. A gap of 0.75 in is considered between the superstructure and the backwall in seat type abutments. Survey of bridge plans revealed the presence of longitudinal restrainer cables and transverse shear keys at the bent and seat abutments and these are considered in the analytical models. 14 ft long $\frac{3}{4}$ in diameter restrainer cables are considered at the seat type abutments and the bents with 0.625 in slack.

As in the case of MSCC-BG bridges, MSCC-IG bridges have SCBs and MCBs with two, three or four columns per bent. SCBs have the bridge deck slab supported on five girders and 6 ft diameter circular columns with potential plastic hinge zones at the base where the column frames into the pile cap and at the top where it frames into the bent beam. The bridge is 28 ft wide and consists of a single 22 ft tall column and the center-to-center spacing of the I-girders is 5.4 ft. The column cross-section has 72 -#11 longitudinal reinforcing bars and consists of #4 stirrups at 3 in on center. Translational and rotational springs are provided at the base of the column in the longitudinal and transverse directions to replicate the behavior of the underlying pile foundation. The stiffness of the translational and rotational springs is 1400 kip/in and 6.5×10^7 kip-in/rad, respectively.

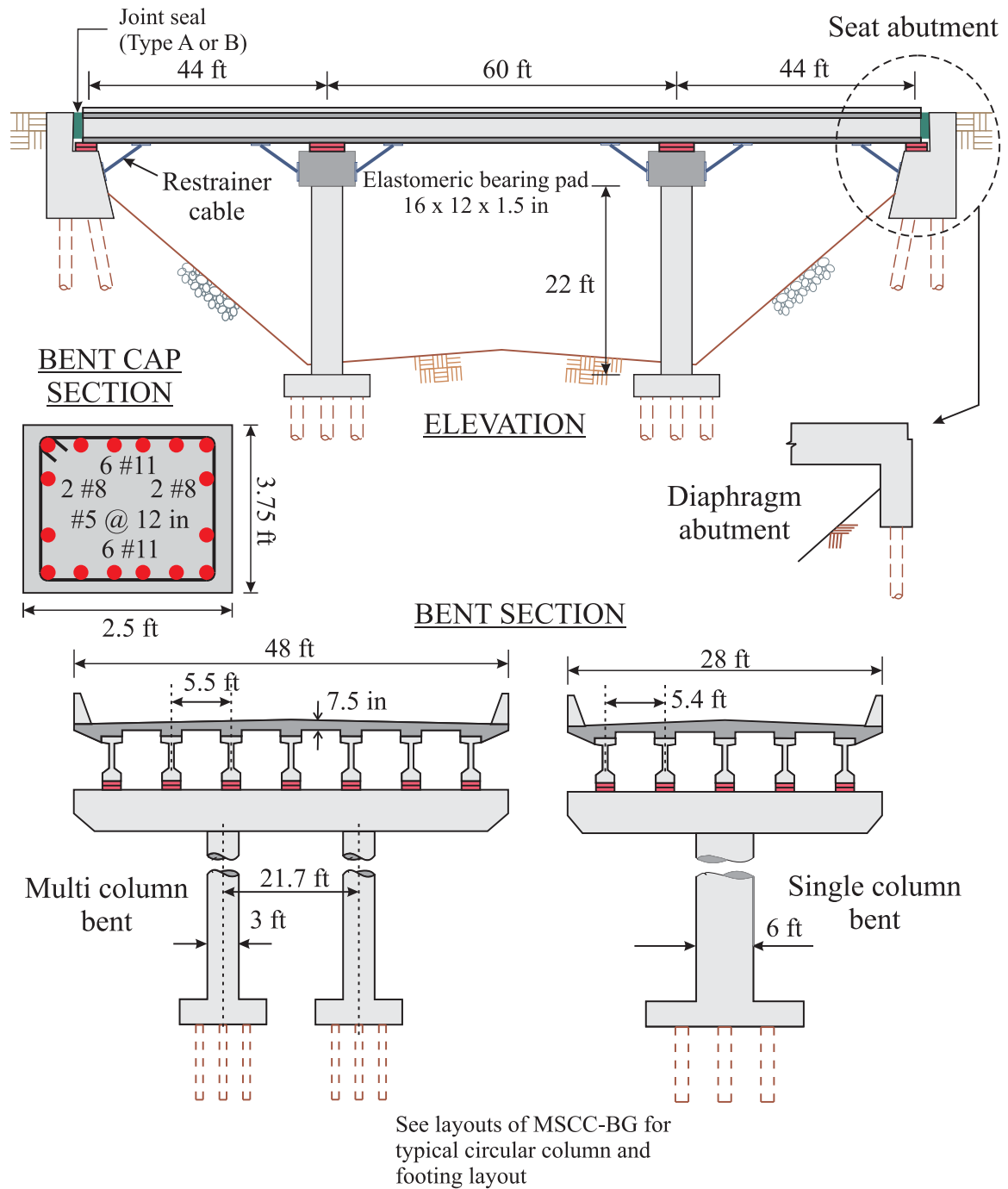


Figure 4.34: Typical layout of MSCC-IG bridges

On the other hand, the bridges with MCBs have bridge deck supported on seven girders and 3 ft diameter circular columns with 36 -#8 longitudinal reinforcing bars and

#4 stirrups at 3.5 in on center. As in the other cases, MCBs in MSCC-IG are not pinned to the base and have two translational and rotational springs of stiffness 800 kip/in and 3×10^7 kip-in/rad, respectively, in the longitudinal and transverse directions. In this section, the bridge has two columns in the bent with a center-to-center spacing of 21.7 ft and the bridge measures 48 ft in width, supported on seven Standard I-girders with 5.5 ft center-to-center spacing.

Unlike the previous cases where the bent is integral with the superstructure, MSCC-IG bridges have bearing supported superstructures and in this case, the columns frame into the bent beam. The bridge has a 2.5 ft \times 3.75 ft rectangular bent beam reinforced with two rows of 6 -#11 bars at the top and bottom and 4 -#8 bars in the middle, as shown in Figure 4.35. The shear reinforcement consists of #5 stirrups at 12 in on center.

4.3.4.2. Eigen Value and Time History Analysis

The fundamental and second mode time periods for MSCC-IG bridges with SCBs and MCBs, diaphragm and seat abutments are indicated in Table 4.6. The results show that MCB are more flexible when compared to SCB and seat abutments are more flexible when compared to diaphragm abutments. The first two mode shapes for the cases mentioned in the Table 4.6 are shown in Figure 4.35. The fundamental mode is in the longitudinal direction for MCB irrespective of the abutment type and the second mode is in the transverse direction. However, SCBs do not have the same mode shapes for either abutment types. For diaphragm abutments, it is seen that the fundamental mode is in the transverse direction while the second mode is in the longitudinal direction. The mode shapes are reversed for SCB in bridges with seat abutments, where the fundamental mode is in the longitudinal direction and the second mode is in the transverse direction. Irrespective of the bent type, bridges with seat abutments are characterized by a longitudinal first mode and transverse second mode, as shown in Figure 4.35.

Table 4.6: Model time periods for MSCC-IG bridges with seat and diaphragm abutments

Abutment type	Number of columns	First mode (sec)	Second mode (sec)
Diaphragm	SCB	0.48	0.37
	MCB	0.57	0.42
Seat	SCB	0.68	0.57
	MCB	1.04	0.72

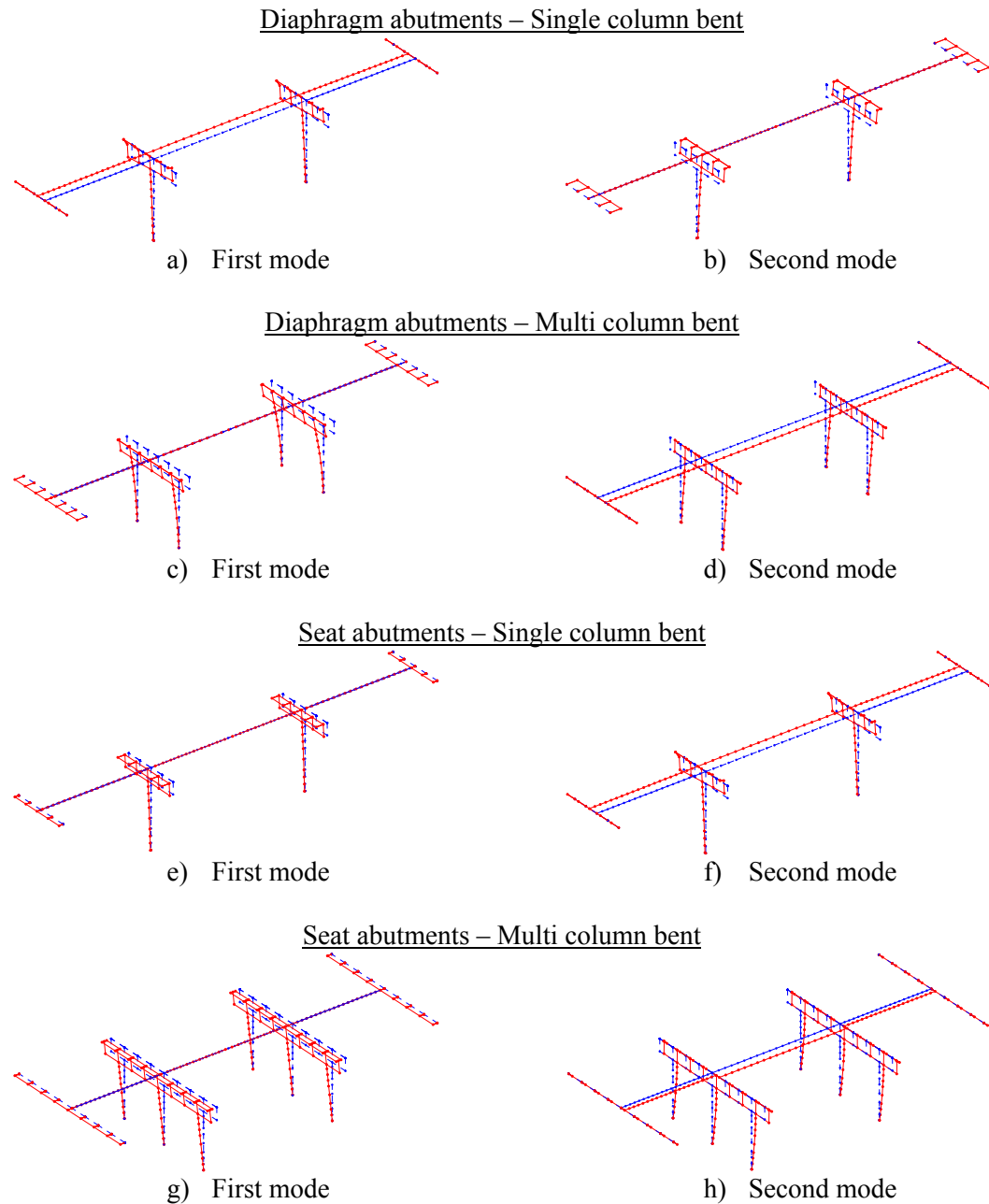


Figure 4.35: First and second mode shapes for MSCC-IG bridges with diaphragm and seat abutments

Figure 4.36 shows the variation of curvature over the height of the column for SCBs and MCBs in MSCC-IG bridges and diaphragm abutments. Clearly, the columns remain elastic under the imposed seismic load. Although not shown here, the same is observed in the case of seat abutments. Based on Figure 4.36, it can be seen that SCB are likely to develop plastic hinges at the base of the column while it is seen that the potential hinge location is at the top of the column close to the bent beam in the case of MCB.

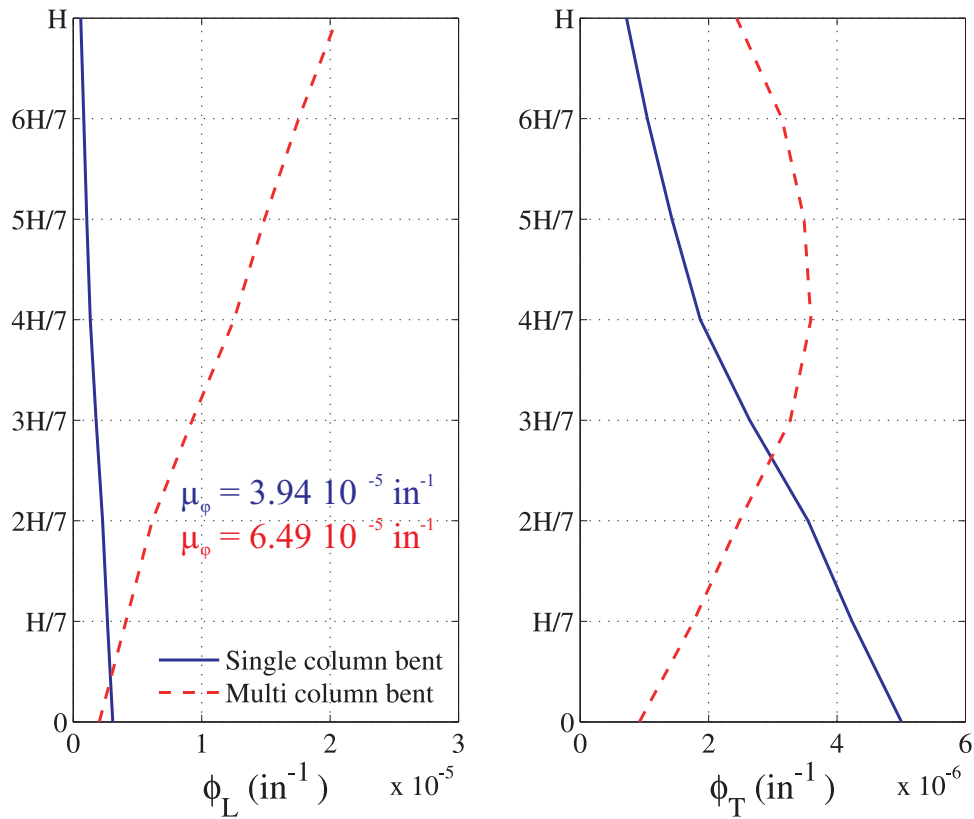
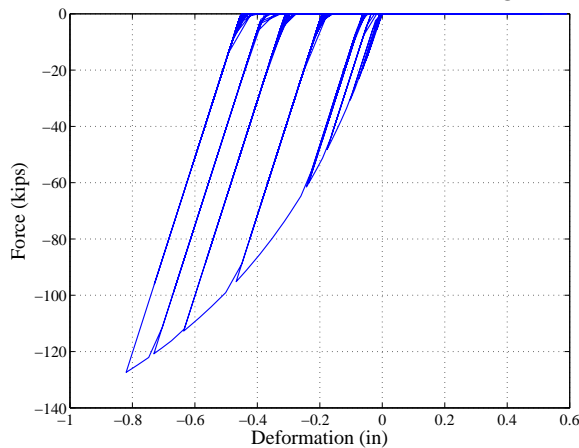


Figure 4.36: Variation of curvature over the height of the columns in MSCC-IG bridges with diaphragm abutments

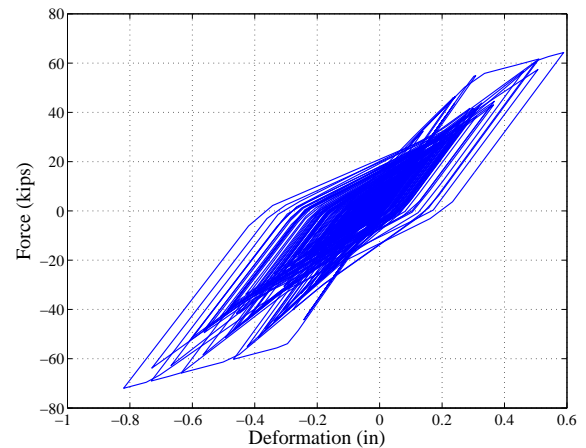
The response of the abutment backfill soil and piles in the longitudinal and transverse directions for MSCC-IG bridges with diaphragm abutments, SCB and MCB bents is shown in Figure 4.37. Although a direct comparison between the responses of SCB and MCB is not possible due to differences in the bridge attributes (deck width,

number of girders etc.), qualitative comparisons are feasible. It is seen that the backfill soil in MCB undergo larger passive deformation when compared to that in the case of SCB. Both the active and passive displacement of piles is greater in the case of MCB in comparison to SCB. In the case of SCB, the piles undergo similar passive and active displacements while in the case of MCB, the passive deformation of piles is almost twice their active deformation. Further, it is seen that in the case of MCB, the piles reach their ultimate capacity in passive action and this might lead to significant damage to them and might require replacement. The transverse displacement of piles is similar in the case of both MCB and SCB and is less than the corresponding active and passive displacements. These responses are very similar in the case of seat abutments.

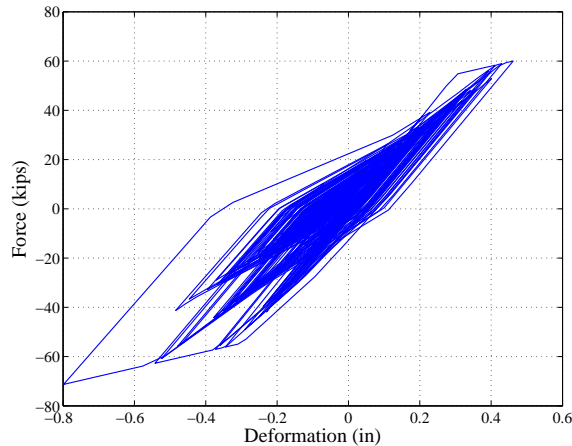
Single column bent



a) Abutment soil – longitudinal response



b) Longitudinal pile response



c) Transverse pile response

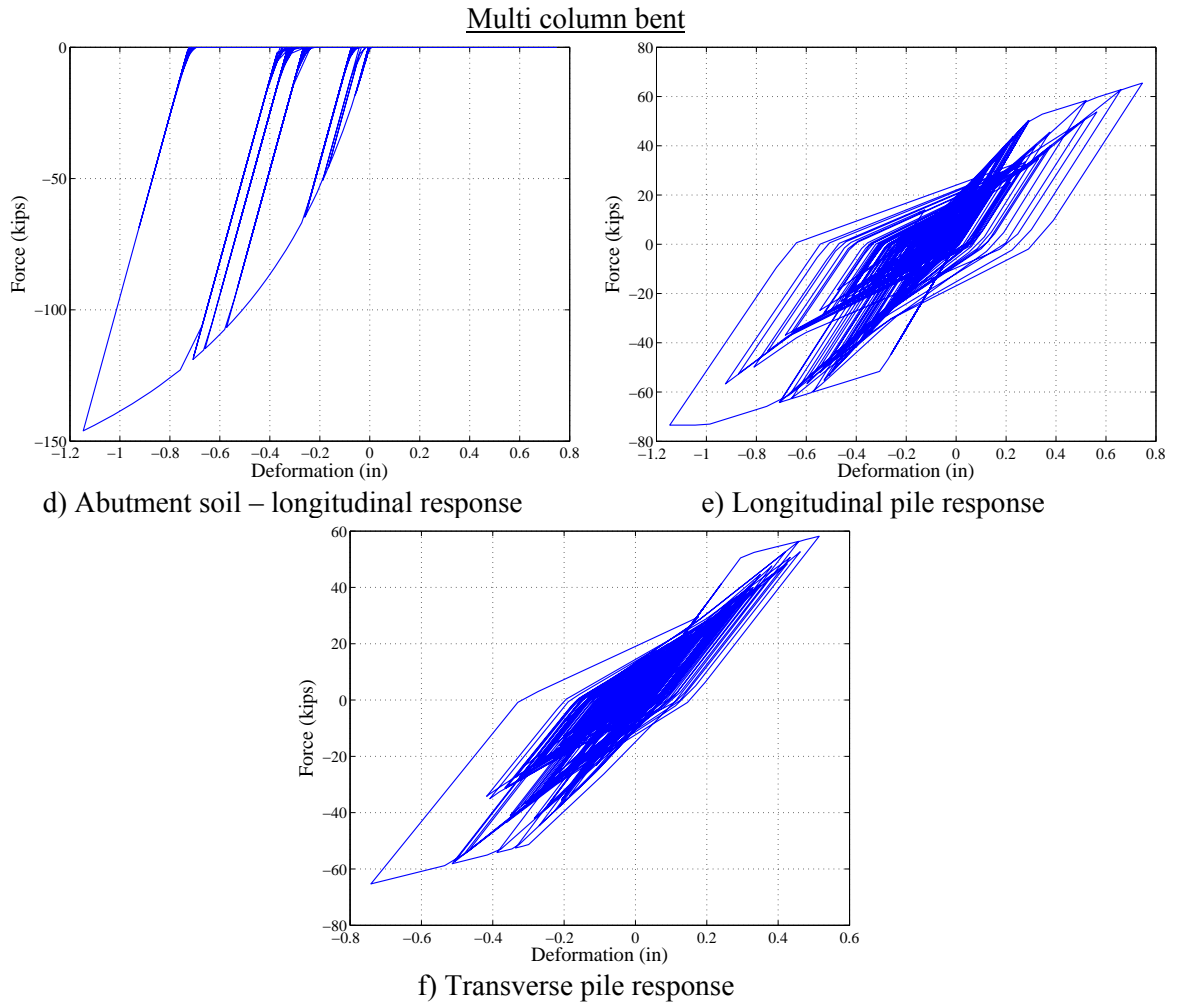


Figure 4.37: Abutment backfill soil-pile responses in longitudinal and transverse directions for MSCC-IG bridges with diaphragm abutments

The response of elastomeric bearing pads in the longitudinal direction and shear keys in the transverse directions for MSCC-IG bridges with SCB and MCB and seat abutments is shown in Figure 4.38. As in the case of abutment backfill soil and piles, elastomeric bearing pads undergo a larger displacement in the case of MCB when compared to SCB in both longitudinal and transverse directions. In the case of both SCB and MCB (Figure 4.38(a), (c)) it is seen that the bearing undergo significant yielding and might need replacement under one such scenario earthquake. Further, the ground motion used in deterministic analysis is seen to cause significant force and deformation demands

on the shear keys in the case of both SCB and MCB. The shear key is seen to be completely damaged in the case of MCB (Figure 4.38(d)). This is also reflected in the transverse response of the elastomeric bearing pad, shown in Figure 4.38(e). Initially the bearing pads are constrained by the presence of the shear keys thereby restricting their displacement to 0.75 in which is the gap present between the girder and the shear key in the transverse direction. The closure of the gap engages the shear keys leading to their eventual collapse. At this point, the bearings undergo significant deformation and the superstructure shifts transversely to a new equilibrium position, as replicated in the response of the bearings (see Figure 4.38(e)). The restrainers remain elastic at the bents and abutments in all cases.

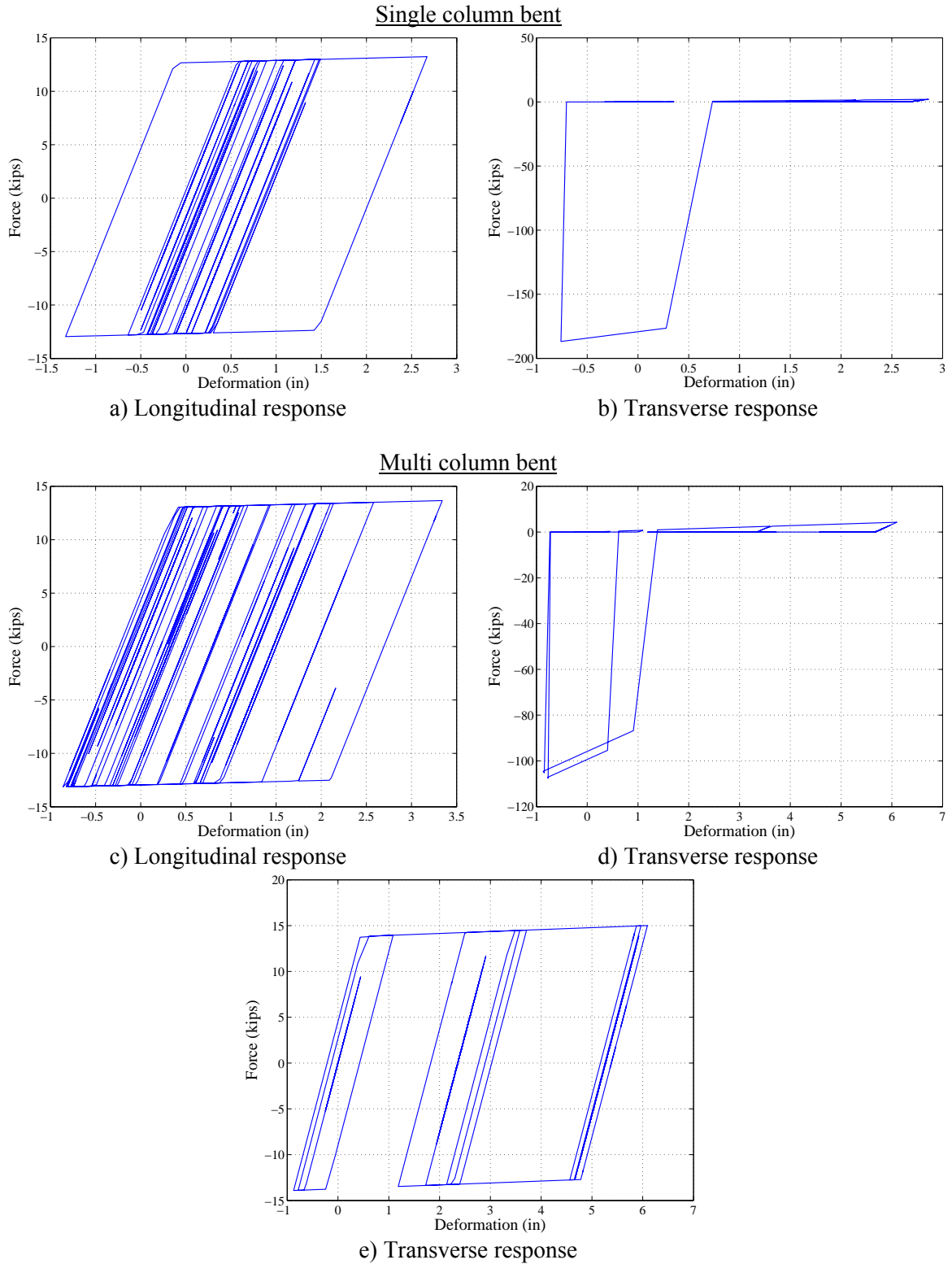


Figure 4.38: Longitudinal response of elastomeric bearing pads and transverse response of shear keys in MSCC-IG with seat abutments

4.4 Closure

In this chapter, extensive details are provided about the modeling strategies for bridge components: superstructure, single and multi column bents including columns and bent beam (wherever applicable), foundation systems, abutments including backfill soil and piles, restrainers and shear keys. These models are developed based on experimental data for the components and experience from their performance during past earthquakes. Detailed nonlinear three dimensional (3-D) analytical bridge models are created in OpenSEES by assembling the individual bridge component models.

Deterministic 3-D analytical models are developed and presented for four multispan concrete bridge classes with box-girders, slab, Tee and I-girders in the superstructure. Details are provided about the typical layout of each of these bridges across the three significant design eras considered in this study: pre 1971, 1971-1990 and post 1990 eras. Using a pair of orthogonal time histories from the PEER Transportation Systems Research Program having a moment magnitude of 7.62, hypocentral distance of 16.27 km, and peak ground accelerations of 0.96g and 0.63g, respectively, the deterministic bridge models are loaded along the two perpendicular bridge axes. The intention with presenting bridge component responses is not to facilitate drawing of conclusions, but rather pave the way for comparing the relative response of various bridge types and their components and to use it as a sanity check. A significant conclusion that can be drawn is that columns are not always the critical components as suggested in previous research in this area. It is seen that in a few bridge classes such as multispan continuous concrete I-girder bridges, columns remain elastic for the imposed seismic loading, while there is significant damage to the elastomeric bearings and shear keys. This suggests the need to consider and include multiple components in determining the vulnerability of the bridge system. The following is a brief summary of insights gained from the deterministic bridge component responses:

- **MSCC-BG bridges:** Evolution of column design philosophy is reflected in the response of bridge columns with post 1990 columns behaving in a ductile fashion when compared to their pre 1971 counterparts. Across all design eras, SCBs experience larger curvature ductility when compared to MCBs. Backfill soils and piles in diaphragm abutments experience greater nonlinearity when compared to seat type abutments. Abutments with sandy backfills exhibit larger forces and lower displacements when compared to abutments with clayey backfills. Columns in bridges with sandy backfills experience larger moments and curvatures when compared to columns in bridges with clayey backfills, thereby depicting the importance of backfill soil type on bridge component dynamic response characteristics.
- **MSCC-SL bridges:** The curvature ductility of columns in bridges with seat abutments is higher than their diaphragm counterparts. The columns in this bridge class show a tendency to undergo double curvature bending. Passive displacement of backfill soil in seat abutments is higher while the active and transverse displacement of piles is higher in the case of diaphragm abutments. The elastomeric bearing pads in seat abutments undergo significant nonlinearity in both longitudinal and transverse directions.
- **MSCC-TG bridges:** Curvature ductility of integral pile columns is higher than traditional MCBs. Passive force-deformation response of backfill soil in bridges with integral pile columns and diaphragm abutments is greater than traditional MCBs and diaphragm abutments. The backfill soil response is comparable for either bent types and seat type abutments. The elastomeric bearing pads in bridges with integral pile columns are subject to a greater demand when compared to traditional MCBs.
- **MSCC-IG bridges:** Plastic hinge tends to form at the base of the column in SCBs while they are likely to form close to the column top in the case of MCBs. The

passive deformation of the backfill soil and response of piles in all directions is higher in the case of MCBs when compared to SCBs. The same is the case with elastomeric bearing pads.

The component and system level responses presented in this chapter are for sample bridges in the bridge classes considered with typical values of the parameters. It is realized that the component responses might change as the values of the bridge modeling parameters change. A complete probabilistic evaluation will allow for the characterization and depiction of uncertainty in geometric and material parameters and will allow for drawing significant conclusions about the relative contribution of the bridge components to the overall system level performance.

CHAPTER 5

FRAGILITY FRAMEWORK

This chapter outlines the framework that will be adopted in the development of analytical fragility curves for the bridge classes considered in this study. Fragility curves provide an effective approach to compare design alternatives, particularly, the impact of evolution in design and detailing aspects by considering the vulnerability of multiple components and uncertainty in performance. The multiphase framework adopted here consists of independent assessment modules linked by pinch point variables such as intensity measures (IM) and engineering demand parameters (EDP) and is consistent with that proposed by Nielson (2005, 2007). Figure 5.1 shows a schematic of the framework and its essential components, which are listed below:

- Ground motion suite
- Stochastic finite element models
- Probabilistic seismic demand models (PSDM)
- Capacity estimates
- Fragility formulation (component and system level)

The first step is to assemble a suite of ground motions that is representative of the seismic hazard in the area of interest. The next step is to develop statistically significant and nominally identical bridge models by sampling on the structural parameters viz., material and geometric, to fully represent a wide range of bridges encompassing the bridge class considered. The stochastic finite element models and ground motions (components in two orthogonal directions) are randomly paired, and nonlinear time history analyses are performed to record the response of components that are deemed to contribute to the vulnerability of the bridge system.

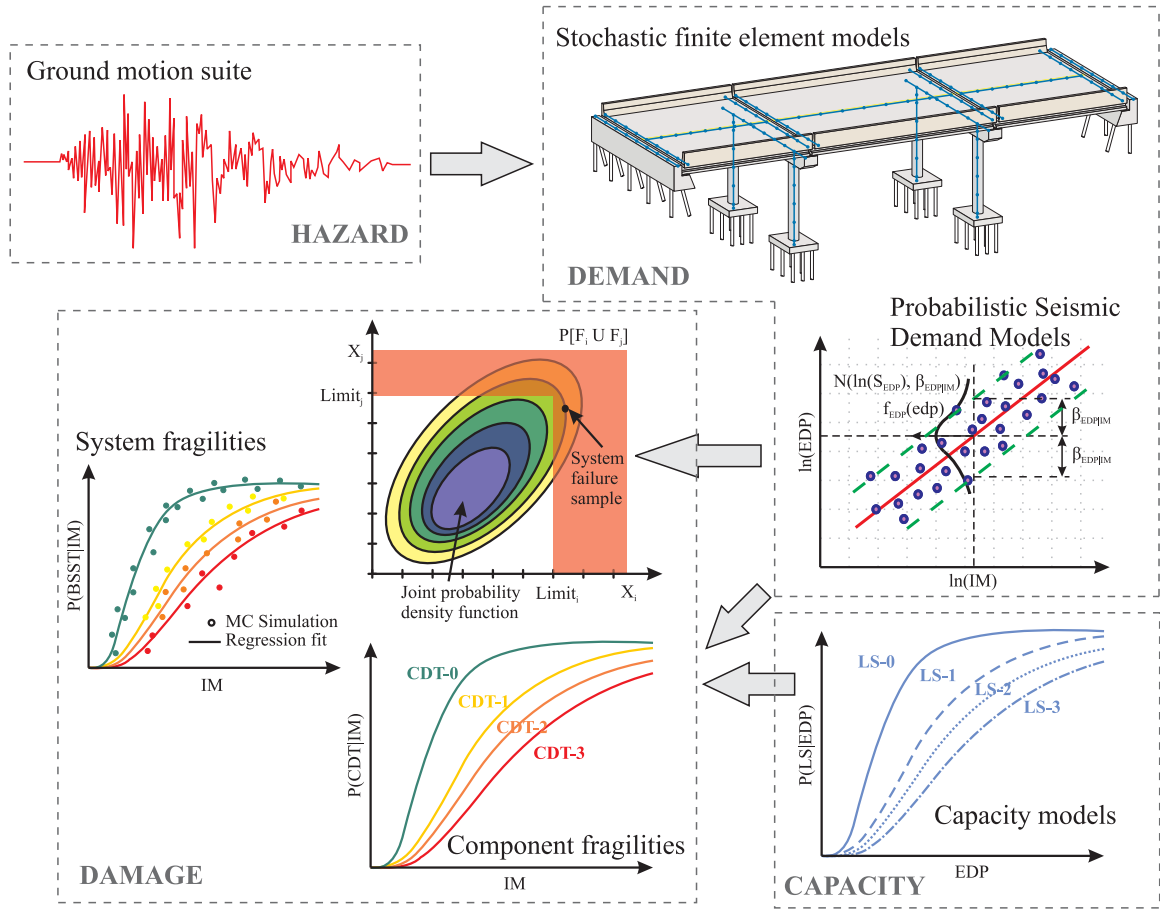


Figure 5.1: Schematic of the fragility framework

Probabilistic seismic demand models (PSDM) are developed for the component responses and this helps in establishing the “demand” side of the problem. The component capacities are determined based on a combination of experimental results and expert opinion involving coordination and one-on-one interaction with Caltrans maintenance and design staff, establishing the “resistance” side of the problem. However, probabilistic risk assessment procedures and performance based engineering, in general, are aimed at determining performance at different levels of structural capacity, each of them typically having an operational consequence or repair requirements. These are typically referred to as limit states or performance states and are quantified by values of engineering demand parameters based on experimental results or expert opinion based on

experience and observed damage during past earthquakes. Both the demand and capacity (or resistance) are assumed to be lognormal (Mackie and Stojadinovic, 2001; Cornell et al., 2002; Bazzurro and Cornell, 2002; Ellingwood and Wen, 2005; Nielson and DesRoches, 2007; Padgett et al., 2008; Celik and Ellingwood, 2010) and the component fragility can be derived using a closed form solution described in equation (5.1), where, D and C denote demand and capacity, S_D and S_C denote the median values of demand and capacity and $\beta_{D|IM}$ and β_C denote the dispersions (logarithmic standard deviation) of the demand and capacity, respectively. It must be noted that S_C and β_C are defined based on the limit state under consideration.

$$P[D > C | IM] = \Phi \left(\frac{\ln \left(\frac{S_D}{S_C} \right)}{\sqrt{\beta_{D|IM}^2 + \beta_C^2}} \right) \quad (5.1)$$

In order to develop system fragility definitions, a joint probabilistic seismic demand model (JPSDM) is developed by combining the individual marginal PSDMs. It must be noted that the individual marginal demand distributions are not independent and a correlation structure is derived based on the analysis data. Realizations of the JPSDM are compared with those from the joint capacity distribution (based on the assumption of statistical independence) using Monte Carlo (MC) simulation to derive system fragility relationships. However, it should be noted that the components are combined in such a way that they have similar consequences in terms of traffic, repair, and closure implications. The subsequent sections in this chapter provide details about each part of the fragility framework. However, further details about the component and system level fragility formulation along with the results are presented in the next chapter.

5.1 Ground Motion Suite

Assembling a suite of ground motions that accurately characterizes the seismic hazard is crucial to developing fragility curves applicable to bridge classes spread over a wide geographic area. The general idea is to have a suite of ground motion time histories that cover a wide range of IMs expected in the area of interest based on seismic hazard analysis and for which the demand models and fragility curves are constructed. Another important aspect is to propagate uncertainty in the realization of other hazard characteristics such as magnitude and epicentral distance. A suite of 160 motions assembled by Baker et al. (2011) for the PEER Transportation Research Program is adopted for the fragility analysis. All of the ground motions in the suite were obtained from the PEER Next Generation Attenuation (NGA) Project ground motion library (Chiou et al., 2008) and these pertain to shallow crustal earthquakes with magnitudes ranging from 4.3 to 7.9. The Baker set consists of two sets of 120 broad-band ground motions having distribution of response spectra associated with moderately large earthquakes at small distances. Further it includes a set of 40 ground motions with strong velocity pulses characteristic of sites experiencing near-fault directivity effects. The details of the suite are as given below:

- Set 1a - Broad-band ground motions for a soil site: This set consists of 40 unscaled ground motions each selected in such a way that their response spectra match the median and logarithmic standard deviations predicted for a magnitude 7 strike slip earthquake at a distance of 10 km.
- Set 1b - Broad-band ground motions for a soil site: This set consists of 40 unscaled ground motions each selected in such a way that their response spectra match the median and logarithmic standard deviations predicted for a magnitude 6 strike slip earthquake at a distance of 25 km.
- Set 2 - Broad-band ground motions for a rock site: This set consists of 40 unscaled ground motions each selected in such a way that their response spectra

match the median and logarithmic standard deviations predicted for a magnitude 7 strike slip earthquake at a distance of 10 km.

- Set 3 – Pulse-like ground motions: This set consists of 40 unscaled ground motions containing strong strike-normal component velocity pulses of varying periods. This set helps in capturing the situations of near fault ruptures.

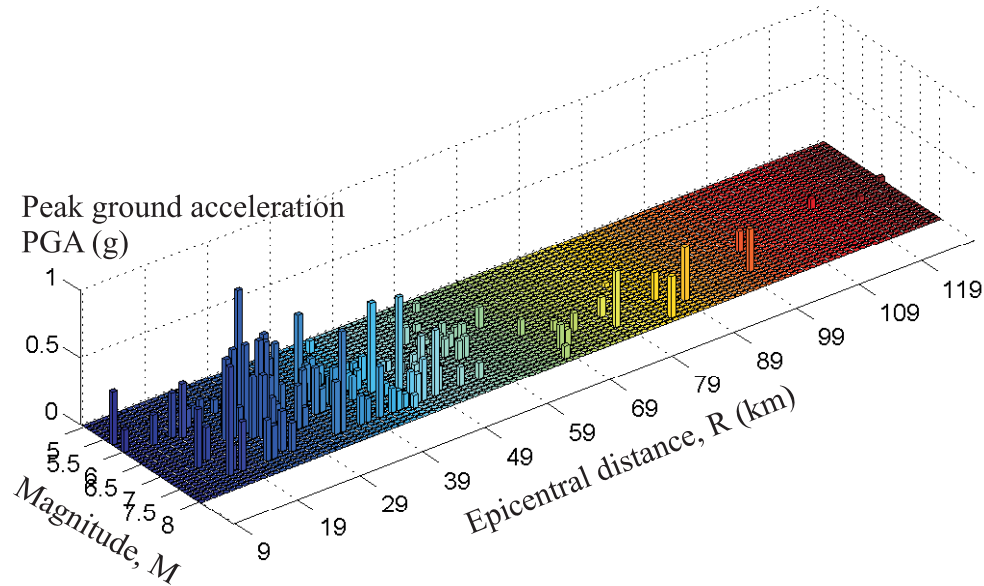


Figure 5.2: Distribution of magnitude, distance and PGA in the Baker suite of 160 ground motions (Baker et al., 2011)

Figure 5.2 shows the distribution of magnitude, distance and peak ground acceleration (PGA) for each of the 160 ground motion records in the suite. It is seen that the selected records cover a broad range of the aforementioned parameters. Based on interaction with the Caltrans design engineers (Caltrans, 2010-2012), it is noted that the highest probabilistic design hazard level in California is that corresponding to a hazard level of 10% probability of exceedance in 100 years and this is greatest for Palmdale. Figure 5.3 shows the response spectra in logarithmic scale for the unscaled records in the Baker set. Also shown is the Palmdale spectrum. The goal in selecting records for time history analyses is that the suite covers a reasonably broad range of intensity measure under consideration along with a range of spectral shapes, durations and pulse properties

that may occur in the area. However, as seen in Figure 5.2, the suite does not have a significant number of time histories in the higher range of IM of interest. Further, in order to have a sufficient number of time histories with IMs higher than the Palmdale spectrum, the entire suite of 160 motions are scaled by a factor of two and an expanded suite of 320 ground motions is used for the fragility analyses in the present study. The response spectra for the scaled ground motions are also shown in Figure 5.3. Summary data for the ground motions in the Baker suite along with significant amount of additional information, including the acceleration time history files are available on the project website: <http://peer.berkeley.edu/transportation/projects/ground-motion-studies-for-transportation-systems>.

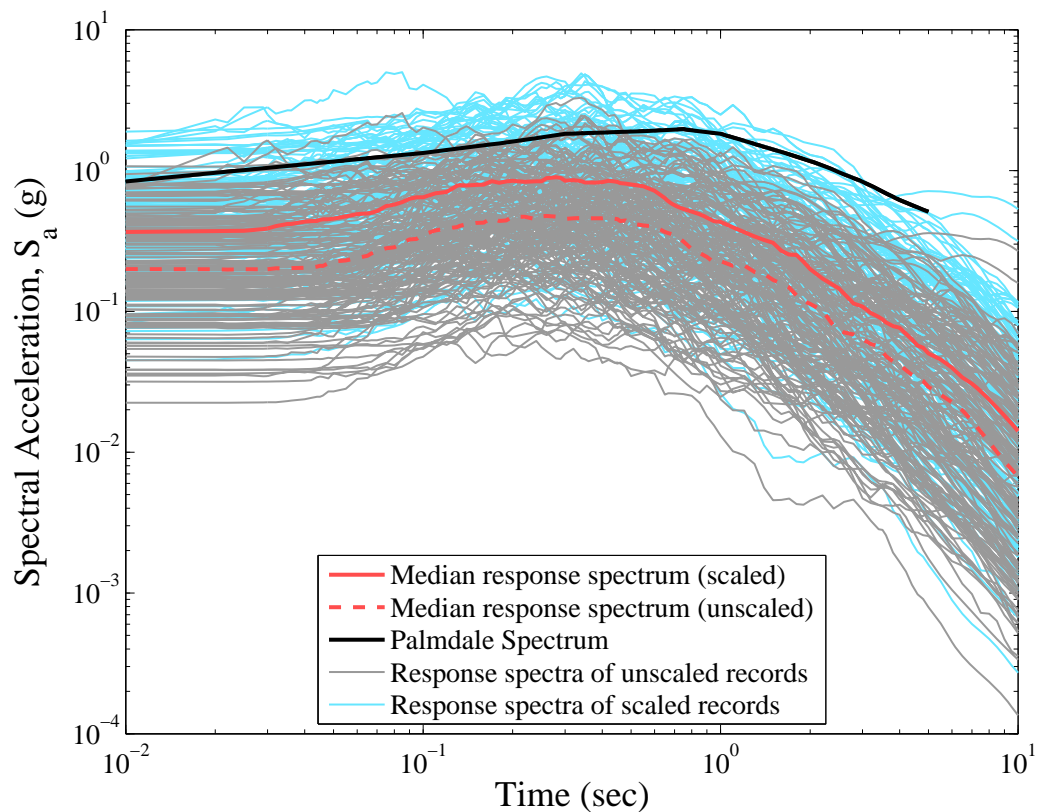


Figure 5.3: Response spectra for the scaled and unscaled ground motions in the Baker suite

5.2 Parameterized Stochastic Finite Element Models and Propagation of Uncertainty

Treatment of uncertainty in seismic reliability and performance assessment has been a subject of research for many years (Melchers, 1999; Ellingwood and Wen, 2005). Uncertainties can be classified under two main types: aleatoric and epistemic. There is inherent randomness in the occurrence of seismic events typically classified as aleatoric uncertainty. The historic data is limited and this leads to statistical error in the estimates of the aleatoric uncertainty. Further, there is uncertainty in the earthquake prediction model itself (due to limited data) and this is typically classified as epistemic uncertainty. These uncertainties do not arise as a result of the applied methodology or techniques; they reside in the historical and physical understanding of the natural processes involved. Epistemic uncertainties are fundamentally associated with the lack of knowledge and assumptions in modeling techniques and can generally be reduced with the acquisition of additional information and understanding (Ellingwood and Wen, 2005). They are present in both deterministic and probabilistic scenarios, although in the case of the former they are typically masked by factors of safety. In the case of probabilistic techniques for design and assessment, a good practice to integrate these two types of uncertainties is to present the final aleatoric frequencies with confidence bounds of epistemic uncertainties (typical of the relative frequency approach) or to integrate both of them in a single probability distribution using Bayesian techniques (Singhal and Kiremidjian, 1998; Ramanathan et al., 2012).

The uncertainty associated with the recorded ground motions in the suite is traditionally considered aleatoric in nature due to the inherent randomness in the seismological mechanisms. Uncertainty in structural geometric and material parameters is considered in this study in addition to the uncertainty from the ground motions and these are elaborated in the next section.

5.2.1 Uncertainty in Material Parameters

5.2.1.1 Concrete Compressive Strength and Reinforcing Steel Yield Strength

The bridge classes considered in this study use concrete as the construction material and the cast-in-place concrete used in bridge construction in California typically has design strength of 5000 psi at 28 days. Following the recommendations of Choi (2002), the compressive strength of concrete is modeled using a normal distribution with mean value, μ_{fc} , of 5000 psi and standard deviation, σ_{fc} , of 627 psi. Ellingwood and Hwang (1985) indicated that the yield strength, f_y , of Gr. 60 ($f_y = 60$ ksi) follows a lognormal distribution with the following parameters: median, $\lambda = 4.21$ ksi, and coefficient of variation, $\zeta = 0.08$. These parameters are adopted in the present study to model the distribution of yield strength of the reinforcing bars.

5.2.1.2 Elastomeric Bearing Pad Attributes

All of the bridge classes considered in this study use elastomeric bearing pads at the seat abutments which consist of rubber pads that transmit forces by friction. In the case of MSCC-IG bridge class, the girders sit on bearing pads at the bents in addition to their presence at seat abutments. Caltrans (MTD 7-1, 1994) recommends the usage of rubber pads with a shear modulus, G , of 169 psi in the design of elastomeric bearing pads. Previous research (Lindley, 1992; Mtenga, 2007) showed variability in the shear modulus of bearing pads and further indicated strong correlation with the hardness of the material. Mtenga (2007) presented a range of G values for the bearing pads as a function of hardness and this range is used in this study. Since sufficient information is not available on the probability distribution of the shear modulus, a uniform distribution is assumed with lower and upper limits set at 80 ksi and 250 ksi, respectively. The shear modulus is used to determine the stiffness of the bearing pads for a given dimension.

The coefficient of friction, μ , is another key parameter that defines the response of the elastomeric bearing pads. An empirical expression (see equation (4.4)) is used for determining μ as a function of the normal stress, and to account for uncertainty in μ , a multiplication factor (MF) is considered. A lognormal distribution is assumed for the MF based on the recommendations of Mander et al. (1996) and Dutta (1999) with a median value, λ , of zero and logarithmic standard deviation, ζ of 0.10.

5.2.2 Uncertainty in Geometric and Structural Parameters

The distributions for geometric and structural parameters are mostly derived from the NBI and are based on review of a significant number of plans pertinent to bridges across design eras for the bridge classes considered in this study.

5.2.2.1 NBI based Bridge Geometric Parameters

Empirical distributions for bridge geometric parameters such as maximum span length, deck width, and column height were presented in Section 3.3 of Chapter 3. Although NBI provides information on the number of spans and probability mass functions were derived and presented in Chapter 3, this study uses the mode statistic for the number of spans due to the complexity involved in parameterizing this variable. The median value modification factor prescribed in HAZUS-MH (2011) is recommended to be used to determine fragilities for bridges with spans not equal to the mode statistic adopted here.

5.2.2.2 Abutment Backwall Height

Most of the structural parameters are attributed to uniform distribution due to a lack of significant data or information that can be used to associate a distribution of any other type. Based on the review of bridge plans, the height of the backwall in the case of diaphragm and seat abutments is assumed to be uniformly distributed between 3.5 ft and 8.5 ft.

5.2.2.3 Column Reinforcement Ratios

The longitudinal and transverse reinforcement ratios in the bridge columns are sampled from uniform distributions with limits established based on the review of bridge plans. Table 5.1 details the parameters of the uniform distribution describing the longitudinal and transverse reinforcement ratios. In the pre 1971 design era, the transverse reinforcement consists of #4 stirrups at 12 in on center, which was a common standard irrespective of the column size or reinforcement. Hence this parameter was not varied in the simulations for the bridges in this design era. Further, MSCC slab bridges employ integral pile columns whose cross-section is standard and hence the reinforcement is not varied in this case.

Table 5.1: Distributions for longitudinal and transverse reinforcement ratios in bridge columns

Bridge class	Design era	Longitudinal reinforcement ratio		Transverse reinforcement ratio	
		u_l^*	u_u^*	u_l^*	u_u^*
MSCC-BG	Pre 1971	1.4	2.4	N.A.	N.A.
	1971-1990	1.0	3.7	0.30	0.90
	Post 1990	1.0	3.5	0.40	1.70
MSCC-IG	Pre 1971	1.08	3.61	N.A.	N.A.
	1971-1990	1.18	5.31	0.31	1.07
	Post 1990	1.49	5.35	0.31	1.61
MSCC-TG	Pre 1971	1.08	3.61	N.A.	N.A.
	1971-1990	1.18	5.31	0.31	1.07
	Post 1990	1.49	5.35	0.31	1.61

* u_l, u_u are the parameters describing a uniform distribution representing lower and upper bounds.

5.2.2.4 Gaps

The gap between the superstructure and abutment backwall is assumed to be uniformly distributed. As mentioned in Section 3.5.6 of Chapter 3, the gap uniformly ranges between 0 and 1.5 in across all bridge classes and design eras. However, in the case of the MSCC-BG bridges, simulations are performed for two ranges of gap sizes: smaller gaps uniformly distributed between 0 and 1.5 in and larger gaps uniformly distributed between 1.5 in and 6.0 in. Further, the transverse gap between the

superstructure and shear keys is assumed to be uniformly distributed between 0 and 1.5 in for the case of MSCC-BG and MSCC-IG bridge classes.

5.2.2.5 Restrainer Attributes

The length and initial slack of the restrainer cables are assumed to be random variables sampled from uniform distributions. The length of the cables is bounded between 8 ft and 20 ft and samples are drawn at 2 ft increments. The initial slack is sampled from a uniform distribution bounded between 0.25 in and 1.0 in.

5.2.2.6 Pile Effective Stiffness

Piles form an integral part of the foundation system beneath the abutments. Translational springs characterizing by the pile stiffness are provided in the longitudinal and transverse directions at the abutments. As stated in previous chapters, piles could be of many different types such as driven steel H section piles, CIDH concrete piles, PC piles or PPC piles. Based on input from the Caltrans design engineers (Caltrans, 2010-2012), the stiffness of the piles is assumed to follow a lognormal distribution with a logarithmic standard deviation, ζ , of 0.3. The median value is taken as 65 kips/in for steel H sections and 80 kips/in for all of the aforementioned concrete piles. It should be noted that the stiffness adopted here is much higher than the 40 kip/in value used in previous studies (Choi, 2002; Nielson, 2005; Padgett, 2007).

5.2.2.7 Foundation Translational and Rotational Spring Stiffnesses

The soil profile changes vastly over a wide geographic area and the stiffness of the foundation translation and rotational springs depends on the soil profile at a particular location. In order to obtain realistic estimates of bridge performance within a class, it is imperative to capture a wide range of soil profiles. Other factors such as the type of foundation system (see section 3.5.5), end conditions of the columns (pinned vs. restrained) and column details (size and reinforcement) affect the stiffness of the

foundation springs. Appendix A documents the different soil profiles considered in this study along with details of the common foundation systems. The different foundation systems and the soil profiles are modeled and analyzed in LPILE (2012) using substantial input from Shantz (2011) and Table 5.2 summarizes the parameters for the truncated normal distribution describing the stiffness of the foundation translation and rotational springs.

5.2.2.8 Other Bridge Structural Attributes

Several other attributes are uniformly distributed between the simulations such as type of backfill soil: sand versus clay; pile class: Class 45 versus Class 70; pile type: PC versus PPC piles. The type of backfill soil affects the hyperbolic force deformation response of the abutment in terms of the initial stiffness, ultimate strength and the deformations. The class and type of pile dictates the pile geometry and reinforcement details (amount and layout) and therefore affects the strength and stiffness characteristics. The type of girder (Standard I- versus Bulb-Tee) is also assumed to be uniformly distributed among the simulations due to their existence in the California bridge inventory. The type of girder affects the deck geometric properties such as cross-sectional area, moment of inertia and the mass.

Table 5.2: Probability distributions for foundation translational and rotational spring stiffnesses

Foundation type	Bridge class	Distribution type	Translational spring stiffness (kip/in)			Rotational spring stiffness (kip-in/rad)		
			μ	σ	μ_L	μ	σ	μ_L
Pile extension 16 in dia integral pile column	MSCC-SL, MSCC-TG	Truncated normal*	30	20	2	8×10^4	3×10^4	2×10^4
Pile shafts								
6ft dia – 1% long. steel – Fixed top	MSCC-BG	Truncated normal	600	350	100	5×10^6	3×10^6	0
6ft dia – 1% long. steel – Free top	MSCC-IG	Truncated normal	250	125	50	7×10^6	2×10^6	3×10^6
6ft dia – 3% long. steel – Fixed top	MSCC-BG	Truncated normal	700	400	200	6×10^6	4×10^6	0
6ft dia – 3% long. steel – Free top	MSCC-IG	Truncated normal	300	150	80	1×10^7	3×10^6	5×10^6
8ft dia – 1% long. steel – Fixed top	MSCC-BG	Truncated normal	900	500	200	6×10^6	4×10^6	0
8ft dia – 1% long. steel – Free top	MSCC-IG	Truncated normal	400	200	80	1.4×10^7	4×10^6	7×10^6
8ft dia – 3% long. steel – Fixed top	MSCC-BG	Truncated normal	1300	600	250	7×10^6	5×10^6	0
8ft dia – 3% long. steel – Free top	MSCC-IG	Truncated normal	500	250	100	2.3×10^7	7×10^6	1×10^7
Pile group – pile cap and piles								
6ft dia column – 1% long. steel	MSCC-IG, MSCC-BG	Truncated normal	1700	800	400	4.1×10^7	1.2×10^7	2.2×10^7
6ft dia column – 3% long. steel	MSCC-IG, MSCC-BG	Truncated normal	1400	600	600	6.5×10^7	1×10^7	5×10^7
3ft dia column – 1.5% long. steel	MSCC-IG, MSCC-BG, MSCC-TG	Truncated normal	800	600	175	0	0	0

* μ and σ represent the mean and standard deviation for the normal distribution and μ_L denotes the truncation limit

5.2.3 Uncertainty in Other Parameters

5.2.3.1 Mass

Mass factor is a parameter used to capture the uncertainty in mass from incidental sources and is applied as a factor to modify the mass of the superstructure. It should be noted that the mass factor does not account for the variations due to changes in bridge geometric parameters such as span length, deck width, column height etc., which are explicitly accounted for in the analytical modeling procedure. Various incidental sources accounting for the mass factor include the presence of parapets and barrier rails, variable deck slab thickness, electric poles and other equipment, re-pavement procedures, variation in the material densities etc. The mass factor is assumed to be uniformly distributed with bounds of 1.1 and 1.4. The bounds are established by estimating the additional mass observed from the review of bridge plans.

5.2.3.2 Damping

The recommendations of Fang et al. (1999) for tall buildings are extended to bridges (Nielson, 2005; Padgett, 2007) and the uncertainty in damping is modeled using a normal distribution. Bavirisetty et al. (2003) estimated the 2nd and 98th percentile of damping ratio in bridges to be 0.02 and 0.07 respectively and using these recommendations, the damping ratio is sampled from a normal distribution with mean, μ , of 0.045 and standard deviation, σ , of 0.0125.

5.2.3.3 Direction Factor

Previous studies (Nielson, 2005; Padgett, 2007; Ramanathan et al., 2010) considered the angle of incidence of the seismic load as a uniform random variable. However, recent studies by Mackie et al. (2011) demonstrated the negligible effect of the angle of incidence on the mean ensemble response of bridge components. Hence, the

incidence angle is not considered as a major source of uncertainty in this study. However, the fault normal and fault parallel components of the ground motion are randomly applied along the longitudinal and transverse axes of the bridge i.e., 50% of the simulations have the fault normal component applied along the longitudinal bridge axis while 50% of the simulations have the fault parallel component applied along the longitudinal axis.

5.2.4 Parameterized Stochastic Bridge Models

The previous sections listed the parameters that are varied to capture uncertainty in the bridge class attributes along with the suite of ground motions across the three significant design eras. Statistically significant yet nominally identical 3-D bridge models are developed by sampling across the range of parameters listed previously using Latin Hypercube Sampling (LHS) (McKay et al., 1979). LHS provides an effective scheme to cover the probability space of the random variables when compared to pure random sampling using naïve Monte Carlo Simulation (Celik and Ellingwood, 2010). Figure 5.4 shows a schematic of the procedure adopted to capture the demands in bridge components due to the imposed seismic hazards. One hundred and sixty analytical bridge models are generated consistent with the number of unscaled ground motions in the Baker suite and these are then paired randomly to create a bridge model-ground motion pair. The same bridge models are used for the suite of ground motions scaled by a factor of two. In each case, NLTHA is performed and the peak component demands are recorded to derive the relationship between the peak demands and the ground motion intensity measure, which is described in the next section.

The study considers the vulnerability of multiple components. The components of interest are columns, abutment seat (seat type abutments), elastomeric bearings, joint seal, restrainer cables, deck displacement, foundations, abutments, and shear keys. The response of the aforementioned components are recorded and the engineering demand parameters (EDP) representing the component responses are indicated in Table 5.3.

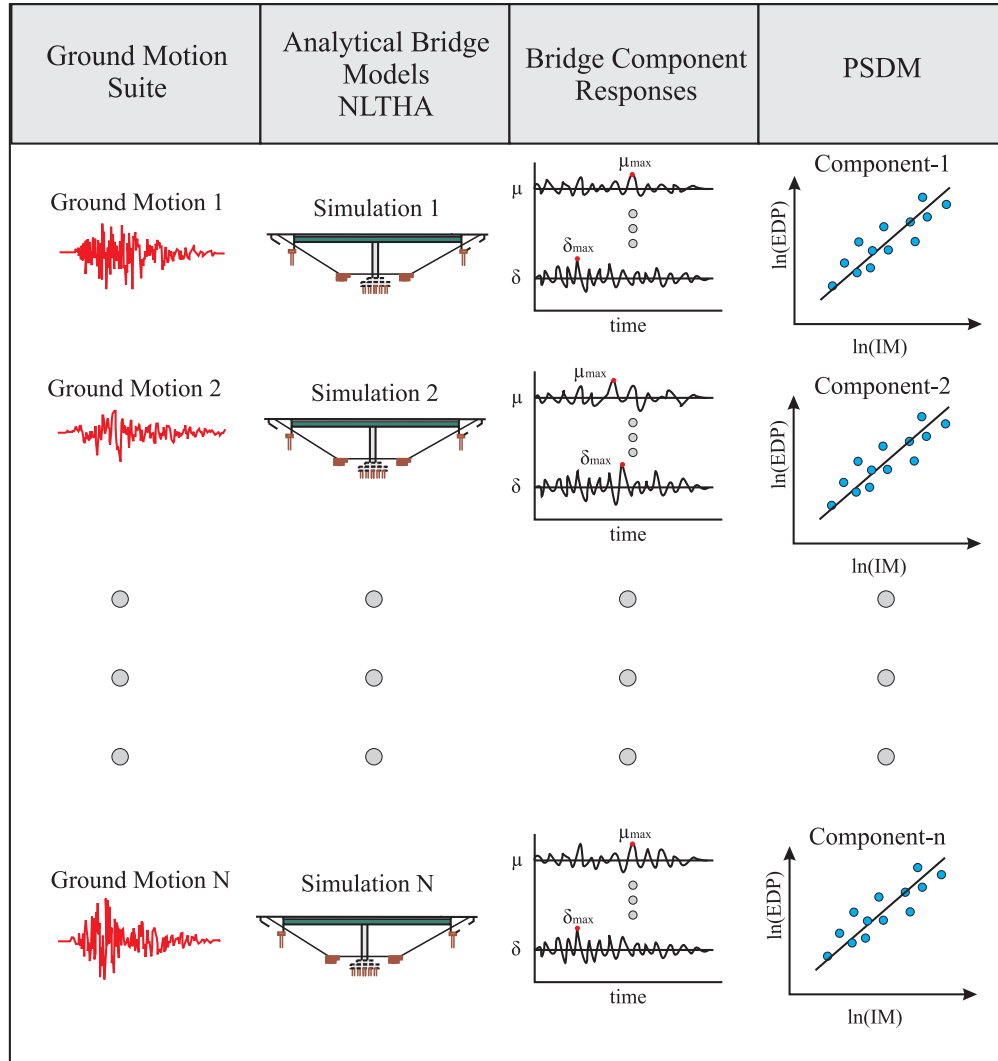


Figure 5.4: Schematic representation of the NLTHA procedure to derive peak component demands

Table 5.3: Engineering demand parameters for bridge components monitored in NLTHA

Component	Engineering demand parameter	Notation	Units
Columns	Curvature	φ	1/inch
Abutment seat	Displacement	δ_{seat}	Inches
Joint seal	Displacement	δ_{seal}	Inches
Elastomeric bearing pads	Displacement	δ_{brng}	Inches
Restrainer cables	Displacement	δ_{rest}	Inches
Deck	Displacement	δ_{deck}	Inches
Foundation translation	Displacement	δ_{fnd}	Inches
Foundation rotation	Rotation	θ_{pile}	Radians
Passive abutment displacement	Displacement	δ_p	Inches
Active abutment displacement	Displacement	δ_a	Inches
Transverse abutment displacement	Displacement	δ_t	Inches
Shear key	Displacement	δ_{key}	Inches

5.3 Probabilistic Seismic Demand Models

Probabilistic seismic analysis of structures involves the construction of seismic demand models, often stated as probabilistic models of structural response conditioned on a seismic intensity measure (IM). Demand models are probability distributions of structural demand conditioned on the IM, known as Probabilistic Seismic Demand Models (PSDMs). The seminal work by Cornell et al. (2002) formulated the conditional seismic demand-IM relationship, referred to as the PSDM, in terms of a two parameter lognormal distribution as in equation (5.2). This form and the one expressed in equation (5.3) have been readily adopted for bridge component probabilistic seismic demand analysis.

$$P[D \geq d | IM] = 1 - \Phi\left(\frac{\ln(d) - \ln(S_D)}{\beta_{D|IM}}\right) \quad (5.2)$$

In equation (5.2), $\Phi(\bullet)$ is the standard normal cumulative distribution function, S_D is the median value of the demand in terms of an IM, and $\beta_{D|IM}$ is the lognormal standard deviation, commonly referred to as the dispersion. The relationship between the median demand and IM was expressed in the power form given in Equation 5.3 as below,

$$S_D = a(IM)^b \quad (5.3)$$

Equation (5.3) can be expressed in the transformed space, shown in equation (5.4), where the model parameter $\ln(a)$ is the vertical intercept and the parameter b is the slope. They can be obtained by performing a linear regression analysis.

$$\ln(S_D) = \ln(a) + b \cdot \ln(IM) \quad (5.4)$$

The development of PSDMs in the case study presented herein involves subjecting a set of 3-D analytical bridge models to a suite of N ground motions and recording the peak demand measures, for instance, column curvature ductility, bearing

and abutment deformations. The median demand, as mentioned previously can be expressed as in equation (5.3) and the dispersion can be estimated based on equation (5.5).

$$\beta_{D|IM} \equiv \sqrt{\frac{\sum (\ln(d_i) - \ln(aIM^b))^2}{N-2}} \quad (5.5)$$

It must be noted that the characterization of median demand using a power-law formulation and constant dispersion are assumptions that are often made but are not necessarily the only possible models to express seismic demand as a function of an IM. However, these representations have been used widely and have been shown to perform very well (Mackie and Stojadinovic, 2001; Cornell et al., 2002; Bazzurro and Cornell, 2002; Ellingwood and Wen, 2005; Nielson and DesRoches, 2007; Padgett et al., 2008; Celik and Ellingwood, 2010; Ramanathan et al., 2012). Figure 5.5 shows a typical PSDM illustrating all the parameters involved in its description. The PSDMs for bridge components for various bridge classes across the design eras are presented in Appendix B.

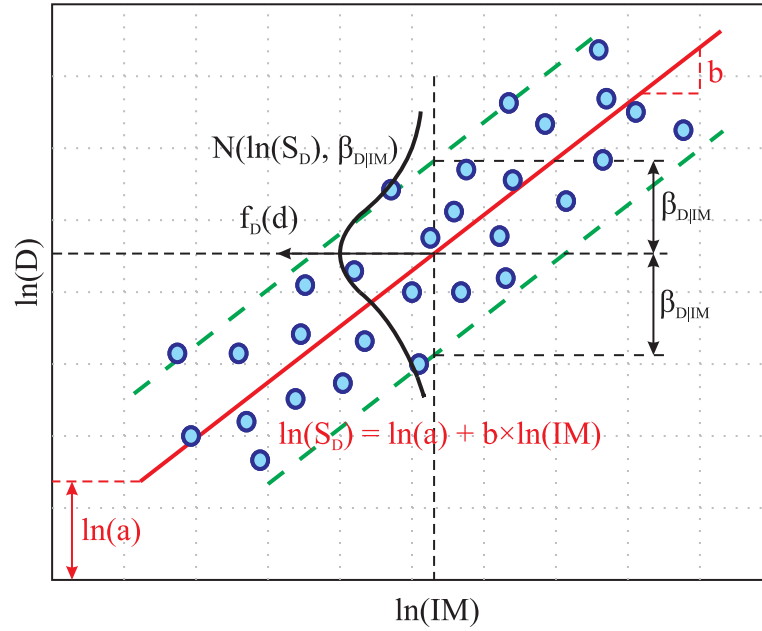


Figure 5.5: Illustration of a typical PSDM

Based on the formulations presented in equations (5.2) through (5.5) it is evident that the selection of an optimal IM can play a predominant role on the accuracy of the model in estimating seismic demand. Their optimal selection is instrumental to obtain reasonable estimates of the vulnerability of various components as the uncertainty associated with the demand is dependent on the variable chosen as an IM to some extent, although this is not the only source of the uncertainty. Spectral acceleration at 1.0 sec, $S_a(1.0)$ is chosen as the IM in this study and the next section illustrates and substantiates the choice of $S_a(1.0)$ as the optimal IM.

5.4 Choice of an Optimal Intensity Measure

5.4.1 Introduction and Characteristics of an Optimal Intensity Measure

Probabilistic seismic demand models provide the first step in developing fragility curves, which are conditional probability statements of the likelihood that the structure will meet or exceed a specified level of damage for a IM. As stated previously, a PSDM is a conditional statement of the probability that a component experiences a demand for a given IM level, illustrating the importance of the IM as a conditional parameter in the probabilistic model. Their optimal selection is instrumental in obtaining reasonable estimates of the vulnerability of various components as the uncertainty associated with the demand model is dependent in part on the variable chosen as an IM.

Several researchers have explored the issue of selection of IMs. The Applied Technology Council report, ATC-13 (1985) uses the Modified Mercalli Scale as the IM while the more recent ATC documents such as ATC-63/FEMA P695 (2008), use S_a at the fundamental period of the structure as their preferred IM. The risk assessment software package, HAZUS-MH (2011) uses peak ground acceleration (PGA), peak ground displacement (PGD) and $S_a(1.0)$. Luco and Cornell (2007) proposed the use of structure specific IMs and showed that S_a at the fundamental period of the structure, T_I , $S_a(T_I)$,

performs very well. An IM that takes into account the second mode frequency content and inelasticity was also proposed and tested and was found to satisfy the essential characteristics of an IM (Luco and Cornell, 2007). Bazzurro and Cornell (2002) and Shome and Cornell (1999) proposed a vector IM comprised of $S_a(T_1)$ and the spectral acceleration ratio, $S_a(T_2)/S_a(T_1)$, where T_2 is the second mode period of the structure. They also considered a scalar IM that combines $S_a(T_2)$ and $S_a(T_1)$. Baker and Cornell (2005) also proposed a vector valued IM comprising of $S_a(T_1)$ and a second parameter which would either be the magnitude, distance or epsilon associated with the ground motion. It was also shown that epsilon has a significant ability to predict structural response. Mackie and Stojadinovic (2001) investigated the use of 24 IMs in their study of PSDMs for typical California bridges and suggested that $S_a(T_1)$ and spectral displacement (S_d) at the fundamental period, T_1 , $S_d(T_1)$ are the ideal IMs as they were found to reduce uncertainty in the demand models. However, all the aforementioned studies are pertinent to deterministic scenarios and did not consider portfolio of structures with variable geometric properties. Padgett et al. (2008) and Shafieezadeh et al. (2011) explored IMs for portfolios of bridges with geometric variation and concluded that PGA is an optimal IM for probabilistic seismic demand analysis of classes of bridges based on metrics of sufficiency, practicality, proficiency, efficiency, and hazard computability.

The formulation of a PSDM was shown in equations (5.2) through (5.5). Based on the formulations presented in these equations, it is evident that the selection of an optimal IM can play a predominant role on the accuracy of the model in estimating seismic demand. Their optimal selection is instrumental to obtain reasonable estimates of the vulnerability of various components as the uncertainty associated with the demand is dependent on the variable chosen as an IM to some extent, although this is not the only source of the uncertainty.

The natural question that arises following this development is “What properties make an IM optimal?” Giovenale et al. (2004) pointed out that *sufficiency*, *efficiency* and

hazard computability are the essential properties of a good IM. In addition, *practicality* (Luco and Cornell, 2007) and *proficiency* (Padgett et al., 2008) are properties that need to be considered, the latter one being a composite measure of efficiency and practicality. The satisfaction of these fore mentioned properties further validates the strength and accuracy of the power law assumption of the PSDM for a given IM, among other conclusions. Shafieezadeh et al. (2011) provides a detailed discussion of each of these characteristics of optimal IMs, including how to quantify and interpret each property. Efficiency is commonly used to establish the superiority of an IM. An efficient IM reduces the amount of variation in the estimated demand for a given IM value and at the same time maintains it constant over the entire range of the chosen IM. A lower value of the logarithmic standard deviation of the seismic demand, commonly referred to as the dispersion, $\beta_{D|IM}$, indicates an efficient IM.

Another property to measure the validity of an IM is sufficiency. An IM needs to be sufficient in order to justify the usage of total probability theorem in PSDA. Sufficiency refers to the property where an IM is independent of ground motion characteristics like magnitude (M), epicentral distance (R), and epsilon (ϵ). This is quantified by the p -value which is a measure of the probability that the randomly distributed points from the analysis would result in a regression line as flat as possible (tending towards zero slope) than that observed actually. Statistically, it is the probability of getting a value of the test statistic as extreme as or more extreme than that observed by chance alone, if the null hypothesis is true. This is achieved by a linear regression of the residuals from the PSDM with respect to M , R and ϵ . Practicality is a measure of the dependence of the demand upon the IM level and the slope, b , is a good indicator of this dependence. When the slope, b , approaches zero, there is negligible dependence of the demand upon the IM, thereby indicating an impractical IM. A higher value of b indicates that the IM is more practical.

Proficiency is a composite measure of efficiency and practicality. This property is derived by rearranging the terms in the formulation presented in equation (5.2) after substitution by equation (5.4). The term in the denominator in the formulation given in equation (5.6) is defined as modified dispersion, ζ , expressed in equation (5.7) and is a measure of proficiency. A lower value of ζ indicates a more proficient IM thereby indicating a lower uncertainty in the demand model by the choice of the IM.

$$P[D \geq d | IM] = \Phi \left(\frac{\ln(IM) - \frac{\ln(d) - \ln(a)}{b}}{\frac{\beta_{D|IM}}{b}} \right) \quad (5.6)$$

$$\zeta = \frac{\beta_{D|IM}}{b} \quad (5.7)$$

These properties will be used to determine the most optimal IM for the bridge classes considered in this study. This study investigates the IMs listed in Table 5.4 to determine the optimality in developing fragility curves for portfolios of highway bridges. Only the results for the primary components are presented here since these directly map into the system level damage states and have more significance in comparison to the secondary components, each of which will be described in detail in the next section.

Table 5.4: Intensity measures investigated for optimality

Intensity measure	Definition
PGA	Peak ground acceleration
$S_a(0.2)$	Spectral acceleration at 0.2 sec
$S_a(0.3)$	Spectral acceleration at 0.3 sec
$S_a(1.0)$	Spectral acceleration at 1.0 sec

5.4.2 Practicality, Efficiency and Proficiency

The results from the tests for practicality, efficiency and proficiency are presented in this section. The dispersion, $\beta_{D|IM}$ is a measure of efficiency while the slope, b of the PSDM is a measure of practicality as previously stated. Proficiency is quantified by the modified dispersion value, ζ . An optimal IM would be characterized by smaller values of

$\beta_{D|IM}$ and ζ and larger values of b and R^2 . Appendix C reports values of these measures for IMs mentioned in Table 5.4 and primary component demands for the bridge classes considered in this study. The controlling values of the aforementioned parameters: b , $\beta_{D|IM}$ and ζ are highlighted in the table and so is the most optimal IM for the particular sub-class under consideration. PGA is the most practical IM followed by $S_a(1.0)$ and $S_a(0.3)$. In terms of efficiency and proficiency, $S_a(1.0)$ is by far the optimal IM across the bridge classes. Figure 5.6 shows a sample PSDM for column curvature ductility and abutment seat displacement in a post 1990 designed MSCC-BG with multi column bents using $S_a(1.0)$ as the IM.

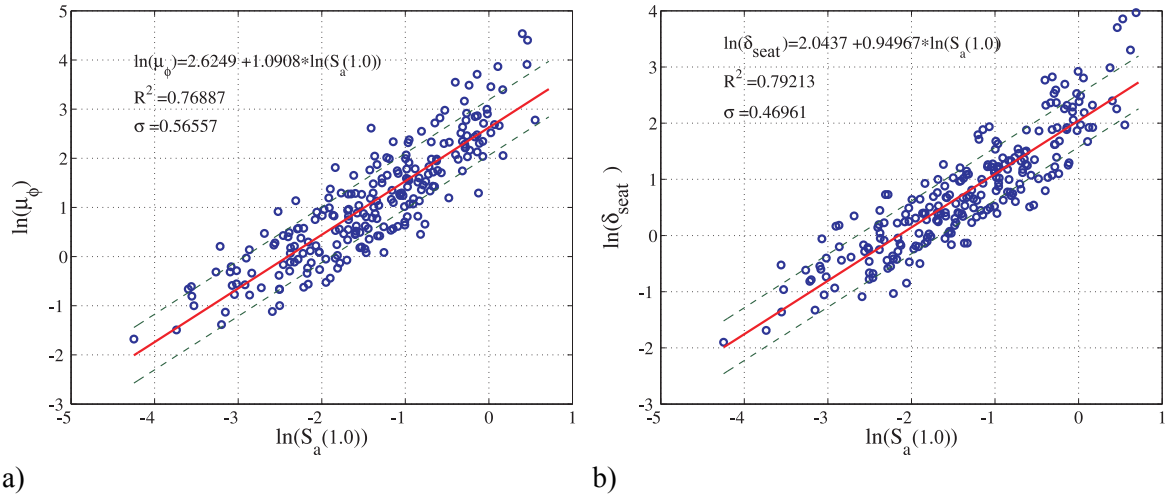


Figure 5.6: PSDMs for a) column curvature ductility, and b) abutment seat displacement in post 1990 designed MSCC-BG-M bridges

5.4.3 Sufficiency

Sufficiency investigates the statistical independence of the IM with respect to ground motion characteristics. A sufficient IM ensures the accuracy of results obtained using the probabilistic structural assessment framework used commonly today (Mackie and Stojadinovic, 2001; Luco and Cornell, 2007):

$$\nu(LS) = \int \int_{DM \ IM} G(LS | DM) dG(DM | IM) d\lambda(IM) \quad (5.8)$$

In equation (5.8), $G(LS|DM)$ denotes the probability of exceeding a limit state (LS) given the value of structural demand measure, $G(DM|IM)$ denotes the probability of exceeding a demand measure given the value of ground motion IM and $\lambda(IM)$ denotes the mean annual frequency of exceeding each value of the IM. Using the theorem of total probability yields the mean annual frequency of exceeding a limit state, $\nu(LS)$, as shown in Equation (5.8). Sufficiency of the IM ensures that the estimate of $G(DM|IM)$ is independent of ground motion parameters (or other hazard parameters), and enables this straightforward application of the theorem of total probability without introducing model bias or the need to consider joint probability density functions of multiple hazard parameters.

Sufficiency of an IM has been traditionally tested using ground motion characteristics like M and R and more recently, the epsilon, ϵ , parameter introduced by Baker and Cornell (2006). ϵ is a measure of the difference between spectral acceleration of a ground motion record and the mean of a corresponding attenuation relationship at a particular period and is evaluated by computing the difference between an individual records' $\ln(S_a(T_I))$ and the mean predicted $\ln(S_a(T_I))$ and then dividing the difference by the standard deviation of the ground motion prediction equation (Baker and Cornell, 2006). The ground motion prediction model developed by Abrahamson and Silva (2008) is used in the present study. As mentioned earlier the sufficiency property is quantified by the p -value which is estimated by performing a linear regression upon the residuals, $\epsilon_d|IM$ from the PSDM with respect to characteristics such as M , R , and ϵ . By definition, p -value is the probability of rejecting the null hypothesis (Hines et al., 2003), which in this case is the independence of IM from ground motion characteristics like M , R , and ϵ . Higher p -value therefore give weaker evidence for rejecting the null hypothesis, meaning lower statistical significance and therefore a sufficient IM. Therefore, it is customary to reject the null hypothesis if the p -value is less than a particular significance level. Popular levels of significance are 0.1% (0.001), 1% (0.01) and 5% (0.05). This study uses a 5%

significance level to determine the sufficiency of the proposed IMs. Table D1 in Appendix C also reports the p -values with respect to M , R , and ε (denoted by p_M , p_R , p_ε , respectively) for the primary component demands for commonly used IMs. Based on the significance level, it is generally observed that all of the candidate IMs are sufficient in a majority of the cases. In general sufficiency typically serves as a prequalification test and the emphasis is placed on efficiency, proficiency, and practicality to choose the optimal IM. Figure 5.7 shows the linear regression on the residuals for column curvature ductility with respect to M , R and ε for a MSCC-IG-M in the 1971-1990 design era. Also shown are the p -values on the respective plots. The plots clearly demonstrate that the regression linear lines are almost horizontal (zero slope) thereby demonstrating the sufficiency property.

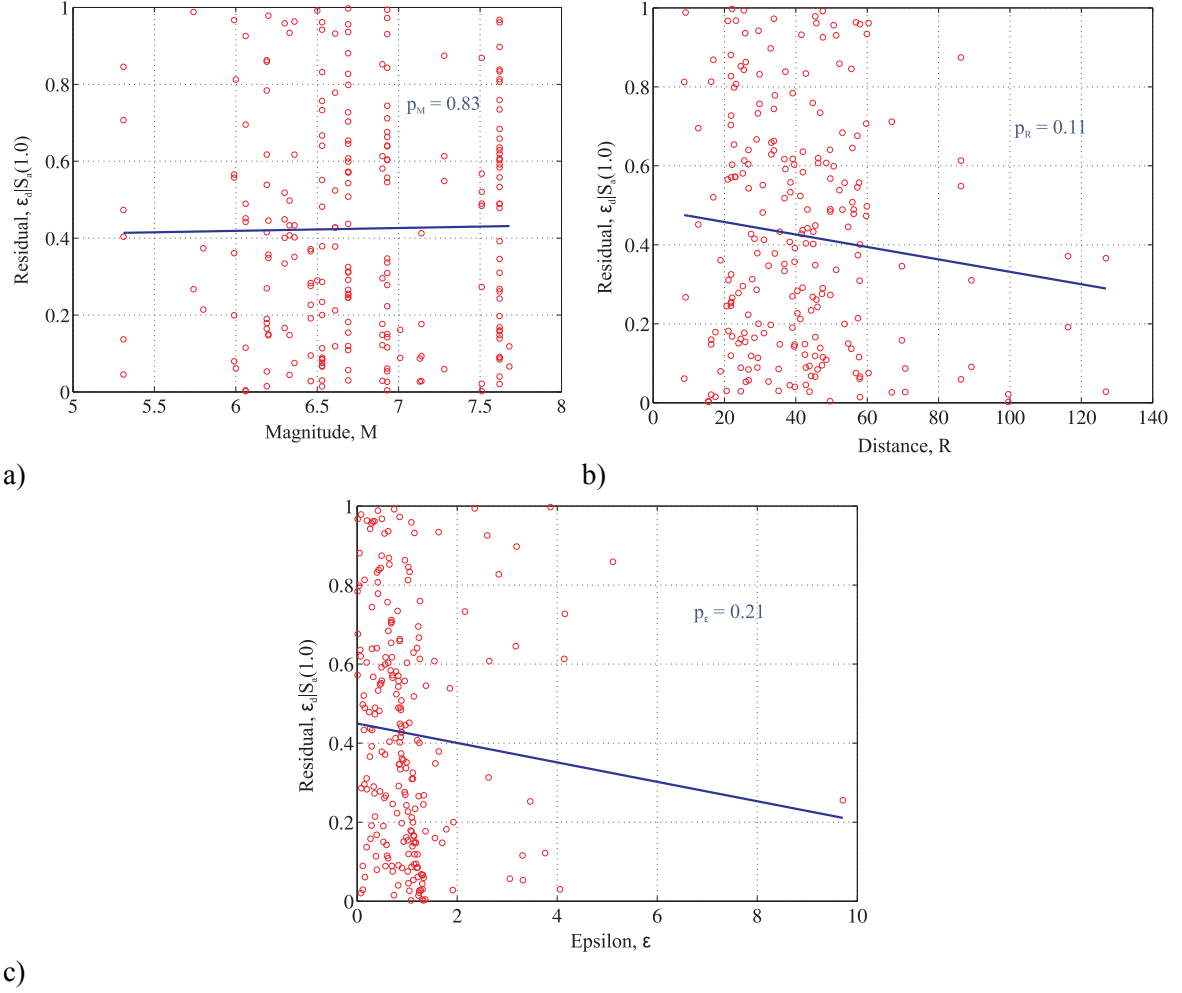


Figure 5.7: Plots showing the linear regression of the residuals for column curvature ductility in 1971-1990 designed MSCC-IG-M bridges with respect to a) magnitude, b) distance, and c) epsilon

5.4.4 Hazard Computability

Hazard computability is an important property for optimal IM selection as it dictates the ease with which probabilistic seismic hazard maps are available or can be developed to facilitate the convolution described in equation (5.8). The candidate IMs considered in this study satisfy this property since hazard curves are typically available in terms of PGA and S_a at specific periods such as 0.2 sec, and 1.0 sec. Many researchers (Luco and Cornell, 2007; Baker and Cornell, 2005; Bazzurro and Cornell, 2002; Shome and Cornell, 1999) demonstrated the superiority of $S_a(T_I)$ as an optimal IM for deterministic scenarios while Padgett et al. (2008) and Shafieezadeh et al. (2011)

highlighted the superiority of PGA as the optimal IM for portfolios of bridge structures. S_a at characteristic fundamental periods are effectively impossible to estimate across portfolios of bridge structures and further their values change across the class. Further, it is literally impossible to define hazard curves for these characteristic periods thereby making them prohibitive from a hazard computability stand point to be adopted as an optimal IM even if other properties determined them to a suitable candidate.

5.4.5 Optimal IMs across Bridge Classes and Seismic Performance Sub-bins

Table 5.5 details the optimal IM across the bridge classes (BC) and seismic performance sub-bins (SPS) considered in this study assessed based on the aforementioned properties. It is clearly seen that $S_a(1.0)$ dominates the selection and is therefore chosen as the preferred IM in this study. PGA is also seen to perform well in many cases and fragility curves will therefore also be presented using PGA as an IM.

Table 5.5: Optimal IM across the bridge classes and the respective SPS considered in this study

BC	SPS	E1-S0	E1-SX	E2-S0	E2-SX	E3-S0	E3-SX
MSCC-BG-S		PGA	$S_a(1.0)$	$S_a(1.0)$	$S_a(1.0)$	$S_a(1.0)$	$S_a(1.0)$
MSCC-BG-M		$S_a(1.0)$	$S_a(1.0)$	$S_a(1.0)$	$S_a(1.0)$	$S_a(1.0)$	$S_a(1.0)$
MSCC-SL-P		$S_a(1.0)$	$S_a(1.0)$	$S_a(1.0)$	$S_a(1.0)$	$S_a(1.0)$	$S_a(1.0)$
MSCC-TG-P		$S_a(1.0)$	$S_a(1.0)$	$S_a(1.0)$	$S_a(1.0)$	$S_a(1.0)$	$S_a(1.0)$
MSCC-TG-M		$S_a(1.0)$	$S_a(1.0)$	PGA	$S_a(1.0)$	$S_a(1.0)$	$S_a(1.0)$
MSCC-IG-S		PGA	$S_a(1.0)$	$S_a(1.0)$	$S_a(1.0)$	PGA	$S_a(1.0)$
MSCC-IG-M		$S_a(1.0)$	$S_a(1.0)$	$S_a(1.0)$	$S_a(1.0)$	$S_a(1.0)$	$S_a(1.0)$

5.5 Component Capacity or Limit State Models

Seismic fragility involves the convolution of the demand and capacity models. The formulation of the demand models was explained in the previous section. Definition of the component capacities or limit states is not a trivial task and is a crucial step in the fragility formulation. The individual limit states are characterized by representative values for the median, S_C , and dispersion, β_C , (see equation (5.1)) for the component

damage states distributions which are also assumed to be lognormal akin to the PSDMs. Discrete damage states are defined for each component corresponding to significant changes in its response and consequences to its own performance and performance of the bridge at the global or system level. Although the damage state definitions are discrete, the assumption is that a continuous range of damage exists between the discrete states to enable the closed-form computation of the component fragility curves. It is essential that the limit state definitions use the same metric as the EDP for the respective bridge components. Table 5.3 listed the bridge component EDPs that are used to monitor the response of specific components and assess their performance.

A significant contribution in the present study is that the damage state definitions for the components are derived in such a way that they align with the Caltrans design and operational experience. This will facilitate the evaluation of repair-related decision variables, repair cost and repair time, which are the end products in a typical risk assessment procedure. The major challenge lies in being able to group components that have similar consequences at the system level in terms of functionality and repair consequences. A common question that could arise is: “Do the complete collapse of columns have the same effect on bridge functionality as the complete damage to a shear key or tearing of an elastomeric bearing pad?” In order to be able to address the aforementioned concerns, two classes of components are proposed viz., primary and secondary. Primary components are defined as those that affect the vertical stability and load carrying capacity of the bridge. Extensive or complete damage to these components might lead to closure of the bridge. Columns and abutment seat belong to this category with regards to the bridge classes considered in this research. When looking at bridges with in-span hinges, which is out of the scope of the present study, the internal hinge is also considered as a primary components as excessive hinge opening (values exceeding the support seat length) could lead to unseating of the superstructure.

Secondary components may be defined as the ones that do not affect the vertical stability of the bridge. Failure of these components will not force closure of the bridge but might lead to restrictions on the travel speed and traffic conditions on the bridge. Table 5.6 lists the primary and secondary components in the bridge classes considered in this study for both diaphragm and seat abutments.

Table 5.6: List of primary and secondary components in the bridge classes considered in this study

Seat Abutments		Diaphragm Abutments	
<i>Primary components</i>			
Columns		Columns	
Abutment seat			
<i>Secondary Components</i>			
Joint seal		Maximum deck displacement	
Elastomeric bearing pads		Bent foundation translation	
Restrainers		Bent foundation rotation	
Maximum deck displacement		Abutment passive displacement	
Bent foundation translation		Abutment active displacement	
Bent foundation rotation		Abutment transverse displacement	
Abutment passive displacement		Joint seal*	
Abutment active displacement		Elastomeric bearing pads*	
Abutment transverse displacement		Restrainers*	
Shear key displacement		Shear key displacement*	

*These components are only present in the case of MSCC-IG bridges with diaphragm abutments

*These components are only present in the case of MSCC-IG bridges with diaphragm abutments

Tables 5.7 and 5.8 show the general description of the bridge system level damage states (BSST) and the component damage thresholds (CDT) for primary components, respectively. The bridge system level damage state descriptions, BSST-0 through BSST-3 are defined in Table 5.7 and are aimed at operational consequences in the aftermath of an earthquake. The CDT of primary components map directly to the BSSTs since the loss of a primary component affects the load carrying capacity and overall stability of the bridge system. In the case of secondary components, only two broad CDTs are defined, CDT-0 and CDT-1 and these map directly into BSST-0 and BSST-1, respectively. The damage state descriptions for CDT-0 and CDT-1 in the case of secondary components are shown in Table 5.9. The combinations of the Component

Damage Thresholds (CDT) of primary and secondary components, detailed in Table 5.7, are aimed at achieving similar consequences in terms of bridge operations (repair and traffic implications) in the aftermath of an earthquake. As described in Table 5.7, the primary components: columns and abutment seat (the latter only in the case of seat abutments) directly map into the BSSTs and equally contribute to the vulnerability across all damage states. On the other hand, the secondary components (detailed in Table 5.6) map into BSST-0 and BSST-1 since their complete failure will not have a similar consequence as that of the primary components. Both these tables are developed in close collaboration with Caltrans (Caltrans, 2010-2012) to ensure that the component mapping is in alignment with the inspection/maintenance closure decisions and the training guides for post-earthquake inspections (Sahs et al., 2008). The CDTs may be broadly defined as below:

- CDT-0 (Aesthetic damage) is a performance parameter threshold beyond which aesthetic damage of the component occurs. The associated repair is primarily aimed at restoring the aesthetics
- CDT-1 (Repairable minor functional damage) is a performance parameter threshold beyond which significant repairs are required to restore component functionality
- CDT-2 (Repairable major functional damage) is a performance parameter threshold beyond which extensive repairs are required to restore component functionality
- CDT-3 (Component replacement) is a performance parameter threshold beyond which component replacement is likely to be the most cost-effective means to restore component functionality

The CDT values can be described using a prescriptive (physics-based) approach, descriptive (judgmental-based) approach or by incorporating both (Padgett et al., 2007) using Bayesian updating principles. The prescriptive approach is based on the mechanics of the problem where a functional level is associated with component damage such as

spalling of cover concrete in a column, buckling or rupture of the longitudinal column reinforcement etc. The descriptive approach is based on the functionality level of the components post disaster and is usually in terms of repair cost and downtime. In this study a combination of both techniques are used to define the threshold value.

Having broadly defined the CDTs for various components, the threshold values are determined based on experimental studies from the literature and based on extensive input from the Caltrans design and bridge maintenance groups. The subsequent sections provide these median values, S_C , for the CDTs along with visible signs of associated damage and repair strategies. As mentioned before, the capacity distributions are assumed to be lognormal similar to the demand distributions. The uncertainty associated with the median values of the CDTs is prescribed in the form of a logarithmic standard deviation or dispersion, β_C . The assignment of dispersion is done in a subjective manner due to lack of enough information to quantify it and a dispersion value of 0.35 is adopted across the components and the respective damage states. This value is particularly a good estimate for columns and is consistent with the test results documented in the PEER column structural performance database (Berry and Eberhard, 2004).

Table 5.7: General description of bridge system level damage states along with component damage thresholds

Bridge system damage states	BSST-0 MINOR	BSST-1 MODERATE	BSST-2 EXTENSIVE	BSST-3 COMPLETE
ShakeCast Inspection Priority levels	Low	Medium	Medium-High	High
Likely Immediate Post-Event Traffic State	Open to normal public traffic – No Restrictions	Open to limited public traffic – speed/weight/lane restrictions	Emergency vehicles only – speed/weight/lane restrictions	Closed (until shored/braced) – potential for collapse
Traffic Operation Implications				
Is closure/detour needed?	Very unlikely	Unlikely	Likely	Very likely
Are traffic restrictions needed?	Unlikely	Likely	Very Likely	Very Likely - Detour
Emergency Repair Implications				
Is shoring/bracing needed?	Very unlikely	Unlikely	Likely	Very likely
Is roadway leveling needed?	Unlikely	Likely	Very Likely	Very Likely - Detour
Component Damage Threshold mapping				
Primary components	CDT-0 to 1	CDT-1 to 2	CDT-2 to 3	Above CDT-3
Secondary components	CDT-0	CDT-1	NA	NA

NA indicates that these CDTs are not defined for the secondary components

Table 5.8: Component level damage state descriptions – Component Damage Thresholds (CDT) for Primary Components

	CDT-0	CDT-1	CDT-2	CDT-3
Component damage states	No damage	Aesthetic damage	Repairable minor functional damage	Repairable major functional damage
				Component replacement

Table 5.9: Component level damage state descriptions – Component Damage Thresholds (CDT) for Secondary Components

Component damage states	CDT-0		CDT-1	
	No damage	Aesthetic damage/ Repairable minor functional damage	Repairable major functional damage/ Component replacement	

5.5.1 Columns

Curvature ductility, μ_ϕ , is the chosen EDP for columns. The columns in the pre 1971 design era have very poor confinement of the longitudinal reinforcement due to the large spacing between the transverse reinforcement (#4 stirrups at 12 in on center is a commonly adopted standard). It is realized that curvature ductility has its limitations in terms of applicability to non-ductile columns which is characteristic of the pre 1971 design era; it is chosen to maintain consistency, with added conservatism to the threshold values. A lot of information is available on the performance of bridge columns and experimental results pertinent to columns are documented in Veletzos et al. (2006), Berry and Eberhard (2003, 2004), Mackie and Stojadinovic (2005). Four damage states, CDT-0 through 3 are chosen and the median μ_ϕ values characterizing these damage states along with observed damage and typically employed repair strategies are documented in Table 5.10. Pictorial representations of typical column force deformation relationships with expected damage is shown in Figures 5.8 through 5.10.

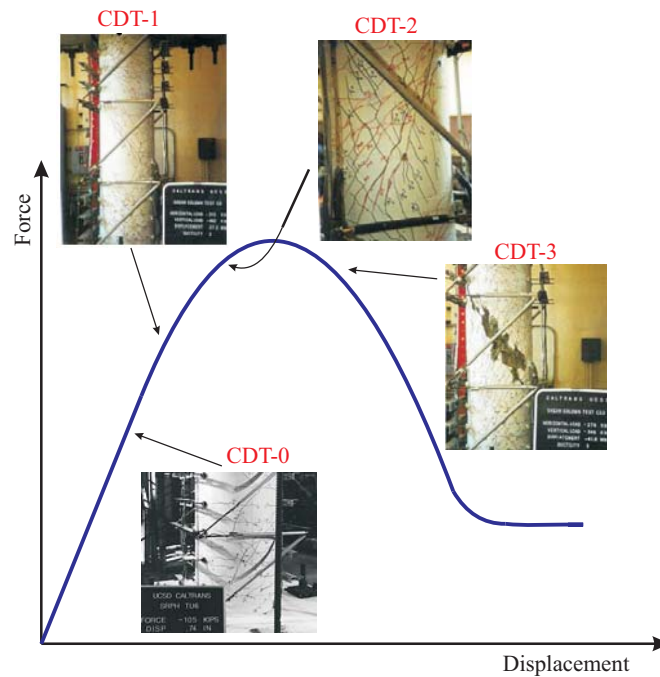


Figure 5.8: Depiction of CDTs for pre 1971 designed brittle columns (Sahs et al, 2008)

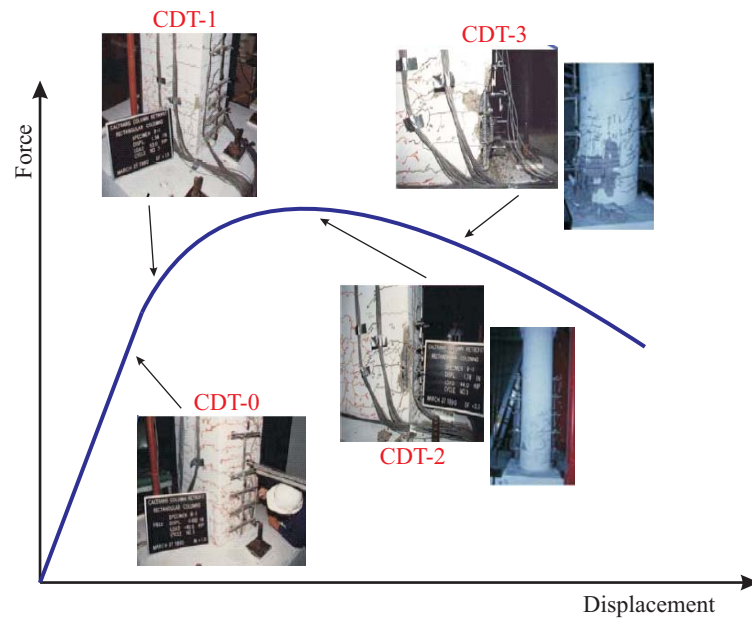


Figure 5.9: Depiction of CDTs for 1971-1990 era designed strength degrading column (Sahs et al, 2008)

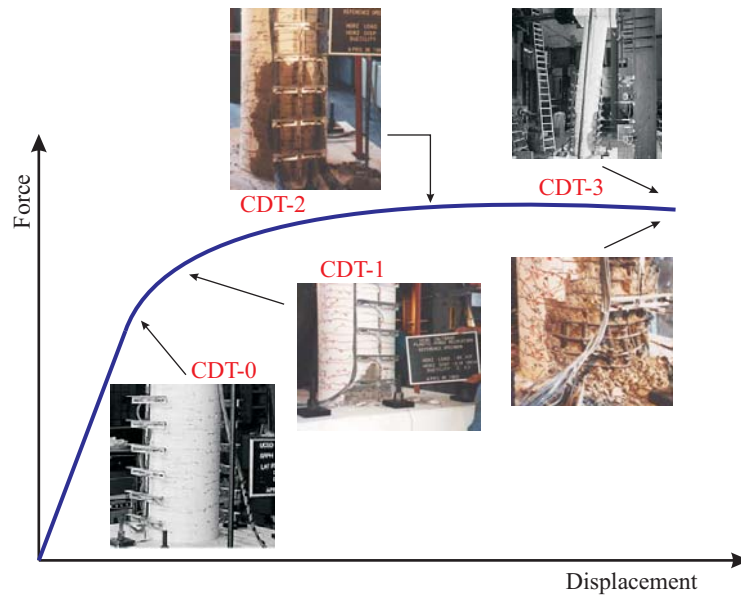


Figure 5.10: Depiction of CDTs for a post 1990 designed ductile column (Sahs et al, 2008)

Table 5.10: Median values of column CDTs along with damage description and likely emergency and permanent repair strategies

Design era	CDT level	μ_ϕ	Damage description	Typical emergency repair	Typical permanent repair
Pre 1971 Brittle column	CDT-0	0.80	Cracking	None	Seal and paint
	CDT-1	0.90	Minor cover spalling anywhere along the column height	None	Epoxy injection; minor concrete removal and patch; seal and paint
	CDT-2	1.00	Large shear cracks; major spalling; exposed core; confinement yield (no rupture)	Shoring very likely	Add Class-F jacket
	CDT-3	1.20	Loss of confinement; longitudinal bar buckling or rupture; core crushing	Closure/detour; shore deck if to re-open	Replace column or bridge
1971- 1990 Strength degrading column	CDT-0	1.00	Cracking	None	Seal and paint
	CDT-1	2.00	Minor cover spalling anywhere along the column height	None	Epoxy injection; minor concrete removal and patch; seal and paint
	CDT-2	3.50	Major spalling; exposed core; confinement yield (no rupture)	Possibly shoring	Major concrete removal and patch; add Class-F jacket
	CDT-3	5.00	Loss of confinement; longitudinal bar buckling or rupture; core crushing; large residual drift	Closure/detour; shore deck if to re-open	Replace column or bridge
Post 1990 Ductile column	CDT-0	1.00	Cracking	None	Seal and paint
	CDT-1	4.00	Minor cover spalling concentrated at the top and bottom of the column	None	Epoxy injection; minor concrete removal and patch; seal and paint
	CDT-2	8.00	Major spalling; exposed core; confinement yield (no rupture)	Possibly shoring	Major concrete removal and patch; add Class-F jacket
	CDT-3	12.0	Loss of confinement; longitudinal bar buckling or rupture; core crushing; large residual drift	Closure/detour; shore deck if to re-open	Replace column or bridge

5.5.2 Abutment Seat and Joint Seal

A detailed description of the available seat width and joint seals assembled in the seats was provided in Section 3.5.6 of Chapter 3. Bridge classes with seat abutments have a potential for unseating at the abutments. Along with columns, the seat is considered a primary component. In addition to the evaluation of unseating potential, damage to the joint seal is also monitored considering the same EDP as the unseating potential. Similar to the unseating potential associated with the abutment seat, damage to joint sealant is commonly observed in bridges after earthquakes. The joints are typically sealed with some kind of a joint sealant and damage to the sealant is considered a secondary component. The different types of joint sealants were also mentioned in Chapter 3. Bridge seat widths chronologically increased from the 4 – 12 in (S1) range in the Pre 1971 design era to 12 – 18 in (S2) range in the 1971-1990 design era and 18 – 24 in (S3) and greater than 24 in (S4) range in the Post 1990 design era. The Phase I and II retrofit programs addressed this issue by retrofitting the pre 1971 and 1971-1990 to the post 1990 seat categories by the provision of restrainers and pipe seat extenders. Therefore, all the four categories of seat widths, S1 through S4 exist in the pre 1971 design era, while categories S2 through S4 exist in the 1971-1990 design era and only the S3 and S4 categories exist in the post 1990 design era bridges. Further, the joint gap is based on the movement rating (MR) of the bridge and a joint seal (Type A or B) is typically used for joints with MR less than 2 in, and a joint seal assembly (strip or modular) is used for joints with MR greater than 2 in. Joint seals are considered in the case of all the bridge classes considered in this study. In the case of MSCC-BG bridges, due to the presence of larger gaps with MR greater than 2 in for a few bridges, the effect of gap size is investigated on the fragility curves. The displacement of the joint and damage to the seal is highly correlated with damage to the abutment backwall in the case of seat type abutments. Table 5.11 gives the median CDT values for the joint seat and the CDT values

for the joint sealant are mentioned in Table 5.12. The joint opening is the EDP used in either case.

Table 5.11: Median values of CDT for abutment seat

Type	Gap size	Notation	Units	CDT-0	CDT-1	CDT-2	CDT-3
S1: 4-12 in seat	Small: MR < 2 in	AS1-S	Inches	0.5	1.0	2.0	3.0
S2: 12-18 in seat	Small: MR < 2 in	AS2-S	Inches	1.0	3.0	6.0	9.0
S3: 18-24 in seat	Small: MR < 2 in	AS3-S	Inches	1.0	3.0	10.0	15.0
S3: 18-24 in seat	Large: MR > 2 in	AS3-L	Inches	2.0	6.0	10.0	15.0
S4: >24 in seat	Small: MR < 2 in	AS4-S	Inches	1.0	3.0	14.0	21.0
S4: >24 in seat	Large: MR > 2 in	AS4-L	Inches	2.0	6.0	14.0	21.0

The CDT values for the abutment joint seat depend on two factors: seat width and the joint gap, which dictate the unseating potential and pounding damage potential, respectively. Seat width governs higher CDT values (CDT-2 and -3) where unseating is possible and joint gap is considered to govern the lower CDT levels (CDT-0 and -1). In all cases, except AS1-S, the CDT-3 threshold is set to a value 3 in less than the minimum seat width. CDT-0 is set to the approximate gap width, thereby corresponding to the initiation of joint pounding damage. The CDT-1 values are set to 300% of the gap width to correspond with significant levels of joint pounding (Caltrans, 2010-2012). In order to obtain an intermediate limit, CDT-2 is set to two-thirds of the CDT-3 threshold value to correspond to movement of more than one half of the minimum seat width, in consultation with Caltrans design engineers (Caltrans, 2010-2012). The CDT values used for the S1 or 4-12 in seat group are governed by the potential for unseating at 4 in.

Table 5.12: Median values of CDT for joint seal

Seat type	Units	CDT-0	CDT-1
Joint seal: Type A poured	Inches	0.75	--
Joint seal: Type B compression	Inches	0.75	--
Seal assembly: Strip	Inches	2.0	5.0
Seal assembly: Modular	Inches	4.0	10.0

The CDT values for joint seal are based on the MR of the bridges where the joints are installed. For Type A and Type B joint seals, only CDT-0 is defined due to lack of

unique higher-level damage model for sealed joints. This intuitively makes sense since once damaged or torn, the seals are expelled and replaced with new ones suggesting the necessity for just one CDT. The CDT-0 values are close to the MR of the system. In the case of Joint seal assemblies (strip and modular), the CDT-1 values are arbitrarily set to 250% of the CDT-0 values to correspond to anticipated damage of the mechanical elements of the assembly beyond damage to the seal component which is captured in CDT-0.

5.5.3 Superstructure Deck

The maximum displacement of the deck is considered to be a secondary component and the link between this EDP and damage to the deck is chosen based on the recommendations of Caltrans design engineers (Caltrans, 2010-2012). The maximum displacement provides an intuitive baseline for overall levels of seismic loading. The CDT values are chosen herein based on observed displacements during past earthquakes and with an intention to trigger an inspection priority accordingly more so with damage anticipated elsewhere in the bridge. The repair strategies typically involve injecting epoxy into the crack typically.

Table 5.13: CDT values for maximum deck displacement

Component	Units	CDT-0	CDT-1
Maximum deck displacement	Inches	4.00	12.00

5.5.4 Abutments - Passive, Active and Transverse Responses

In general the abutment backwalls are designed to shear off. The design considerations ensure that no damage occurs to the stem wall other than the concrete that needs to be chipped out during repairs to the back wall. The CDT-0 value for the passive response is defined corresponding to 0.5% drift ratio measured at the top of the back wall. The CDT-1 value is fixed based on 2% of typical deck thickness (ATC/MCEER,

2002). The CDT values are listed in Table 5.14. The active and transverse response of the abutments is governed by the behavior of piles and the CDT values are specified corresponding to the first yield and ultimate deformation of the underlying piles. The typical repair strategies associated with the abutments involves repairs to the backwalls and in some cases, the replacement of the approach slab. In many cases, this might also involve the replacement of the shear keys (in the case of seat abutments) and this is considered as a separate secondary component in this study.

Table 5.14: CDT values for abutment passive, active and transverse response

Component	Units	CDT-0	CDT-1
Passive abutment response	Inches	3.00	10.0
Active abutment response	Inches	1.50	4.00
Transverse abutment response	Inches	1.00	4.00

5.5.5 Bent Foundation –Translation and Rotational Responses

Damage to the foundations is captured with the help of two EDPs: translation and rotation of the bent foundation. The translational CDT values are consistent with those provided for the abutments. The rotational CDT values are representative of the axial pile movement of ± 0.5 in at the opposite edges of a 20 feet wide pile cap. The translation and rotation CDT values associated with the column foundations are tabulated in Table 5.15. The width of 20 feet was chosen as this was observed to be the largest possible width for pile caps based on the review of bridge plans. The typical repair strategy associated with bent foundations involves enlargement of the pile cap and provision of additional piles surrounding the existing ones. The enlarged pile cap is then tied to the existing pile cap by drilling into the existing cap and inserting dowel bars.

Table 5.15: CDT values for translation and rotational foundation response

Component	Units	CDT-0	CDT-1
Translation	Inches	1.00	4.00
Rotation	Radian	1.50	6.00

5.5.6 Elastomeric Bearing Pads, Restrainers and Shear Keys

The EDP associated with all these components is the displacement. Elastomeric bearing pads are manufactured to undergo large displacements without any significant strength degradation based on Caltrans specifications. The bearing pads remain elastic until about 100% shear strain and experience significant damage and tearing over 300 to 350% shear strain. The typical pads are close to 2 in thick and these dimensions are used to establish the CDT values documented in Table 5.16. The typical repair strategy is to replace the bearing pads when damage is noticed upon inspection.

The restrainer CDT values are based on typical design values for restrained relative displacement between the two ends of the joint (abutment backwall and deck in this case) for various systems that includes both restrainer cable yield displacement and slack (BDA, 2009). The CDT-0 and CDT-1 values are set at 75% and 200% of the yield displacement. The CDT values are listed in Table 5.16.

The presence of external shear keys limits the service-level and excessive transverse displacement and are typically designed to break off or shear similar to the abutment backwall. The bridges considered in this study are assumed to have only exterior shear keys. Internal shear keys are typical in older bridges and most of these were removed and replaced with exterior shear keys during the Caltrans Phase-I and –II retrofit programs. The CDT values of the shear keys documented in Table 5.16 are based on the testing of these components in the University of California San Diego (Megally et al., 2002), as stated previously in Chapter 4. Repairs to shear key involves injecting epoxy into the minor cracks observed at displacements corresponding to CDT-0. However, shear keys are normally replaced when they are broken off at displacements close to CDT-1.

Table 5.16: CDT values for elastomeric bearing pads, restrainers and shear keys

Component	Units	CDT-0	CDT-1
Elastomeric bearing pads	Inches	1.00	4.00
Restrainers	Inches	1.50	4.00
Shear keys	Inches	1.50	5.00

5.5.7 Component Limit States Summary

Table 5.17: Summary of CDT values adopted in this study

Component	EDP	Units	Median values, S_C				β_C
			CDT-0	CDT-1	CDT-2	CDT-3	
<u>Primary Components</u>							
Columns							
Pre 1971	Curvature ductility	NA	0.8	0.9	1.0	1.2	0.35
1971-1990	Curvature ductility	NA	1.0	2.0	3.5	5.0	0.35
Post 1990	Curvature ductility	NA	1.0	4.0	8.0	12.0	0.35
Abutment seat							
AS1-S	Displacement	Inches	0.5	1.0	2.0	3.0	0.35
AS2-S	Displacement	Inches	1.0	3.0	6.0	9.0	0.35
AS3-S	Displacement	Inches	1.0	3.0	10.0	15.0	0.35
AS3-L	Displacement	Inches	2.0	6.0	10.0	15.0	0.35
AS4-S	Displacement	Inches	1.0	3.0	14.0	21.0	0.35
AS4-L	Displacement	Inches	2.0	6.0	14.0	21.0	0.35
<u>Secondary Components</u>							
Joint seal							
Type A	Displacement	Inches	0.5	NA	NA	NA	0.35
Type B	Displacement	Inches	1.0	NA	NA	NA	0.35
Strip	Displacement	Inches	2.0	5.0	NA	NA	0.35
Modular	Displacement	Inches	4.0	10.0	NA	NA	0.35
Bearings							
Restrainers	Displacement	Inches	1.0	4.0	NA	NA	0.35
Shear keys	Displacement	Inches	1.5	5.0	NA	NA	0.35
Deck	Displacement	Inches	4.0	12.0	NA	NA	0.35
Bent foundation							
Translation	Displacement	Inches	1.00	4.00	NA	NA	0.35
Rotation	Rotation	Radian	1.50	6.00	NA	NA	0.35
Abutments							
Passive	Displacement	Inches	3.00	10.0	NA	NA	0.35
Active	Displacement	Inches	1.50	4.00	NA	NA	0.35
Transverse	Displacement	Inches	1.00	4.00	NA	NA	0.35

The previous sections detailed the capacity models component wise along with details about the choice of the respective CDT values and typical repair strategies adopted. As stated previously, the capacity models are assumed to be lognormal characterized by a median value and dispersion. Table 5.17 provides a summary of the CDT values adopted for the bridge components.

5.6 Closure

The multi phase framework used in the development of fragility curves is presented in this chapter. Details are provided regarding the different components of the framework: ground motion suite, stochastic finite element models capturing a wide range of uncertainties, formulation of probabilistic seismic demand models and definition of capacity models. A suite of 160 ground motions developed by Baker et al. (2011) is considered for use in the development of fragility curves and details are presented regarding the composition of the suite. The treatment of uncertainty in the bridge models representing the respective bridge classes and seismic performance sub-bins is achieved through probability distributions of a wide range of material, geometric and other miscellaneous attributes in addition to the empirical geometric distributions generated using the NBI information. These include concrete compressive strength, reinforcing steel yield strength, bearing pad coefficient of friction, mass, damping etc. to mention a few. Having presented the formulation of the probabilistic seismic demand model (PSDM), extensive details are provided about the formulation of capacity models which will then be convolved with the PSDMs to aid in the development of component and system level fragility curves, which will be presented in the next chapter.

The study consider multiple component vulnerability, and classification of bridge components into two categories viz., primary and secondary is proposed based on the individual damage mapping to a system level consequence. Engineering demand parameters are identified to capture the response of components and drawing upon

literature and the expertise of Caltrans design and maintenance professionals, component damage thresholds and repair strategies are identified across the portfolio of bridge components deemed to contribute to the vulnerability of the bridge system.

Another important aspect addressed in this chapter is the selection criteria for an optimal intensity measure. Spectral acceleration at 1.0 sec is identified and proposed to be used as the intensity measure of choice for generating fragility curves based on test metrics such as efficiency, proficiency, practicality, sufficiency and hazard computability.

CHAPTER 6

SYSTEM AND COMPONENT FRAGILITY CURVES

The end goal of seismic risk assessment of highway bridge infrastructure systems is the quantification of the expected damage in terms of metrics such as cost or time in the event of an earthquake. Estimates of vulnerabilities at the system and component level plays a significant role in assessing probable bridge losses to facilitate critical decision making pertinent to post earthquake safety, preparedness, mitigation and management. Fragility curves, which are conditional probability statements that express the probability of meeting or exceeding specific user defined damage states, play a significant role in risk assessment. Component and system level fragility relationships further help in the assignment of inspection priorities and assessing the post-earthquake serviceability condition of bridges and their components.

The previous chapters in addressed the different aspects of the fragility framework arriving at the formulation of probabilistic seismic demand models (PSDMs) and capacity models. Each of these is characterized by median values and dispersions completely describing a lognormal distribution, representing the component responses in the case of PSDMs, and the capacity (or resistance) for defined damage states in the case of the capacity models. The component fragility can be derived using a closed form solution described in equation (6.1), where, D and C denote demand and capacity, S_D and S_C denote the median values of demand and capacity and $\beta_{D|IM}$ and β_C denote the dispersions (logarithmic standard deviation) of the demand and capacity, respectively.

$$P[D > C | IM] = \Phi \left(\frac{\ln \left(\frac{S_D}{S_C} \right)}{\sqrt{\beta_{D|IM}^2 + \beta_C^2}} \right) \quad (6.1)$$

It must be noted that S_C and β_C are defined based on the limit state under consideration. As stated in the previous chapter, the components contributing to the vulnerability of the bridge system are divided into primary and secondary components based on their influence on the stability and operational consequences in the aftermath of an earthquake (see Table 5.6 in Chapter 5). Spectral acceleration at 1.0 sec, $S_a(1.0)$, was established as the optimal intensity measure (IM) in Chapter 5 and fragility curves will be developed and presented using this IM. Substituting the formulation for the median demand, S_D described in the PSDM formulation, and subsequent simplification, as illustrated in equation (6.2), leads to the formulation in (6.3) which is representative of the lognormal distribution describing the component fragilities with median, λ_c and dispersion, ζ_c . Component fragility curves provide valuable information about the most vulnerable component in the bridge system thereby prioritizing inspection and retrofit.

$$P[LS | IM] = \Phi \left(\frac{\ln(a IM^b) - \ln(S_C)}{\sqrt{\beta_{D|IM}^2 + \beta_C^2}} \right) = \Phi \left(\frac{\ln(IM) - \left(\frac{\ln(S_C) - \ln(a)}{b} \right)}{\frac{\sqrt{\beta_{D|IM}^2 + \beta_C^2}}{b}} \right) \quad (6.2)$$

$$P[LS | IM] = \Phi \left(\frac{\ln(IM) - \ln(\lambda_c)}{\zeta_c} \right) \quad (6.3)$$

The logical step following the determination of component fragilities is to integrate these to enable the macroscopic view of the vulnerability of the bridge system. Contrary to some of the previous studies (Nielson, 2005; Padgett, 2007; Ramanathan et al., 2010, 2012), the components in this study are combined in a way such that they have equal consequences in terms of repair and traffic implications in the aftermath of an earthquake. Although the aforementioned studies tried to address the issue of consequence based system level damage states by adjusting the component capacities, the adjusted capacities did not correlate well to description of damage at the component level. On the contrary, in the present study, the component level damage states were

defined in such a way that they were reflective of physical damage and the components were then combined based on the influence of their respective damages on the system level repair and traffic consequences. This was detailed in Table 5.7 of Chapter 5, where the primary components directly mapped to the bridge system level thresholds (BSSTs) while the secondary components at most contributed to BSST-1.

Several techniques to develop system level fragility curves were presented in Chapter 2. In this study, the estimate of system fragility curves is facilitated through the development of joint probabilistic seismic demand model (JPSDM), recognizing that the demands on various components have some level of correlation. If $\underline{X} = (X_1, X_2, \dots, X_n)$ represents the vector of demands, X_i , placed on the n components of the system, then the vector, $\underline{Y} = \ln(\underline{X})$ represents the vector of component demands in the transformed lognormal space. Since the marginal component demands, X_i , are lognormally distributed, the transformed demands, Y_i , are normally distributed in the transformed space. The JPSDM is formulated in this space by assembling the vector of means, $\mu_{\underline{Y}}$ and the covariance matrix, $\sigma_{\underline{Y}}$. It must be noted that the covariance matrix, $\sigma_{\underline{Y}}$, considers the correlation coefficients between $\ln(X_i)$ and not X_i . The correlation coefficients between the component demands are obtained by using the results of the NLTHA and the resulting covariance matrix is then assembled. A Monte Carlo simulation is then used to compare realizations of the demand (using the JPSDM defined by a conditional joint normal distribution in the transformed space) and component capacities to calculate the probability of system failure. It is important to note that correlation across the component capacities is not considered, although, a 100% correlation is assumed across damage states for a given component. Samples (10^6 in this case) are drawn from both the demand and capacity models and the probability of demand exceeding the capacity is evaluated for a particular IM value. The procedure is repeated for increasing values of the IM. Regression analysis is used to estimate the lognormal parameters, median and dispersion, which characterize the bridge system fragility. For a given system level damage state, the

series system assumption is used to generate fragility curves. However, the number of components comprising the series system varies based on the BSST under consideration and is dictated by the mapping of component level damage states defined previously. The mapping ensures the consistency of the series assumption in an attempt to achieve similar consequences in terms of repair and traffic implications at the system level.

The methodology presented in this section is used to develop system and component level fragility curves for the bridge classes and the respective seismic performance sub-bins (SPS) considered in this study. The nomenclature introduced in section 3.6 of Chapter 3 will be used to present the results. Finally, comparisons are also made with the fragilities in HAZUS-MH (2011) and insight is provided into the relative vulnerability of bridge classes and their seismic performance sub-bins, assess the effectiveness of seismic design philosophy currently adopted for the design of bridges, and guide future data collection that is presently absent in the NBI and the state databases.

6.1 Multispan Continuous Concrete Slab Bridges

Fragility curves are developed for MSCC-SL bridges with both seat and diaphragm abutments and the median values and dispersions are documented in Table 6.1. Since slab bridges employ integral pile columns which have seen no modifications in their geometry or reinforcing bar configuration over the decades, the fragilities reported in Table 6.1 are applicable across the design eras considered in this study. Table 6.1 also documents the average dispersion, ζ^* , which could be used as a single value of dispersion characterizing the fragility across all the four damage states. Appendix D documents the median and dispersion values for the component fragility curves for the bridge classes and SPS considered in this study.

Table 6.1: Multispan continuous slab bridge fragilities

Seismic performance sub-bin	BSST-0		BSST-1		BSST-2		BSST-3		ζ^*
	λ	ζ	λ	ζ	λ	ζ	λ	ζ	
MSCC-SL-P-S0	0.175	0.700	0.737	0.628	1.024	0.653	1.277	0.654	0.66
MSCC-SL-P-S1-S	0.090	0.462	0.167	0.477	0.287	0.481	0.394	0.486	0.48
MSCC-SL-P-S2-S	0.120	0.459	0.351	0.495	0.499	0.597	0.627	0.649	0.55
MSCC-SL-P-S3-S	0.120	0.476	0.348	0.499	0.537	0.683	0.652	0.716	0.59
MSCC-SL-P-S4-S	0.121	0.476	0.345	0.499	0.543	0.683	0.654	0.716	0.60

The plot of median values across damage states is shown in Figure 6.1. In the figure, BC stands for the bridge class which is MSCC-SL in the present case and EX denotes the applicability across all the design eras. A simple technique to compare differences in the fragility curves is to evaluate the relative change in the median value of the fragility curves. This facilitates the determination of the effect of certain attributes on the overall vulnerability of the bridge system. A positive change indicates a less vulnerable structure while a negative change indicates a more vulnerable structure. Figure 6.2 illustrates this using fragility curves for MSCC-SL-P-EX-S1 and MSCC-SL-P-EX-S4 for the BSST-3 damage state. The following inferences can be drawn:

- Diaphragm abutments (BC-P-EX-S0) are less vulnerable when compared to seat type abutments (BC-P-EX-SX) across the range of seat widths considered (S1 through S4). The percentage change in median values between diaphragm and seat abutments with largest seat width (S4) is 200%, 143%, 92% and 96% for BSST-0, -1, -2, and -3, respectively.
- The vulnerability of bridges reduces with an increase in the seat width. However, the median and dispersion values for MSCC-SL-P-EX-S2 through -S4 is very similar as seen in Figure 6.1 and documented in Table 6.1. The consistency in fragility parameters is due to the fact that the columns dominate the overall vulnerability across the damage states and as such increased seat width beyond 18 in (S2 category) does not contribute to the reduction in vulnerability. This is

demonstrated in Figure 6.3 which shows a plot of system and component fragilities for MSCC-SL-P-EX-S1 and –S3 across all damage states. Clearly, in the case of MSCC-SL-P-EX-S1, the abutment seat is the most vulnerable component and the vulnerability of these is reduced when the seats are increased (S2 through S4) making columns the most vulnerable component in the latter cases. However, the present study shows relatively little impact on the system fragility if the seat width is increased beyond the 12 – 18 inch range but other components are not improved such as the columns, as suggested by similar values of median and dispersion for the SPS with seats S2 through S4.

- Alternatively, it can be concluded that the most effective technique would be to focus on retrofitting the columns once the seat has been increased to at least the 12 – 18 inch (S2) range. The results suggest that the columns govern the overall vulnerability with seats increased to categories S2 through S4. It is not to be misconstrued that shorter seat widths are just as effective or that seats do not contribute to the vulnerability. Improvement in the performance of columns by retrofitting or replacement of the non-ductile columns with ductile ones, will demonstrate the impact of increasing the seat width potentially.
- This further reinforces the relatively fragile performance of the pile sections which are adopted as columns in the case of slab bridges and recommends for the improvement of the standard pile details to lead to betterment in their performance.
- The difference in vulnerabilities of slab bridges with diaphragm and seat abutments underscores the necessity to capture the type of abutment in a bridge which is not captured in the NBI. However, information about actual seat width is only of secondary interest. Coarse information on seats, such as short versus longer seats is sufficient to inform the system level vulnerability sufficiently accurate.

Table 6.2 provides details about the most vulnerable component across damage states in the SPS considered for this bridge class.

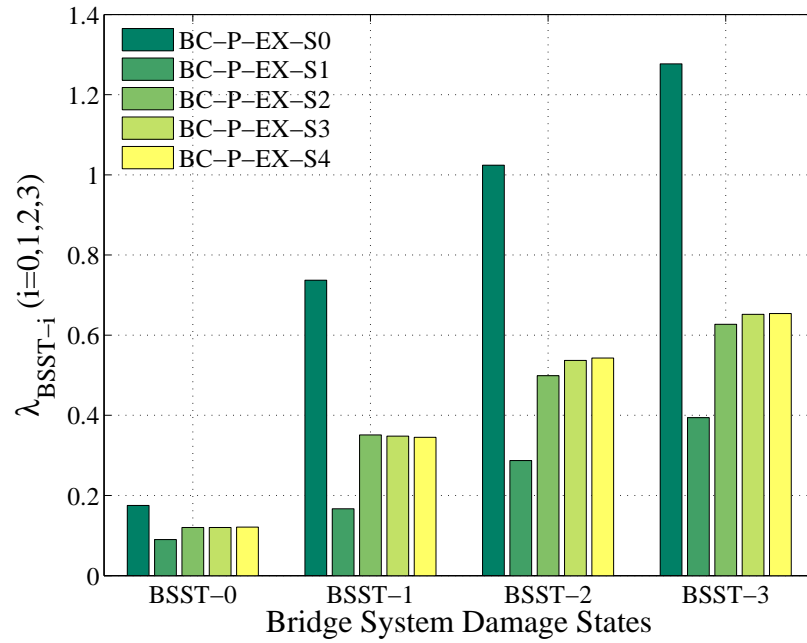


Figure 6.1: Plot of median values for MSCC-SL bridges across all damage states

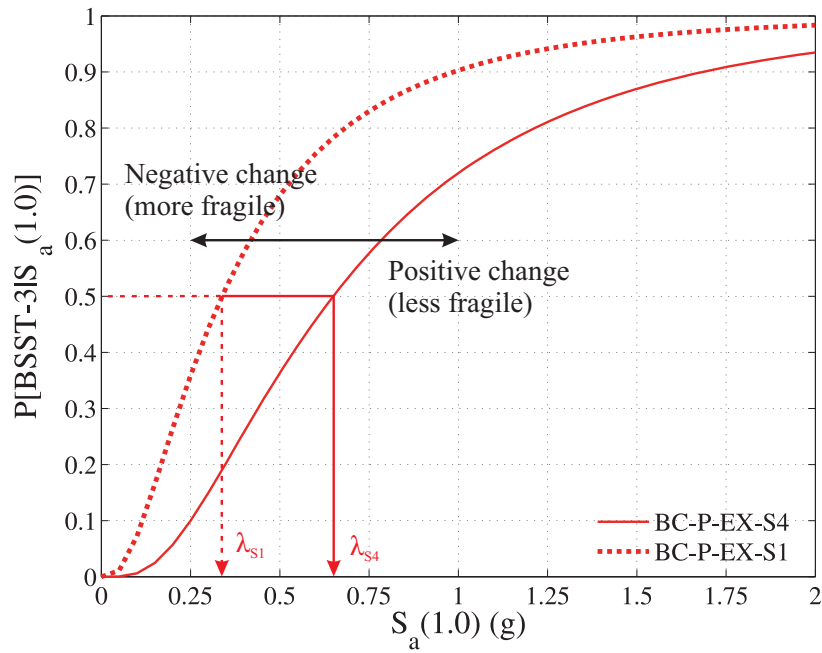
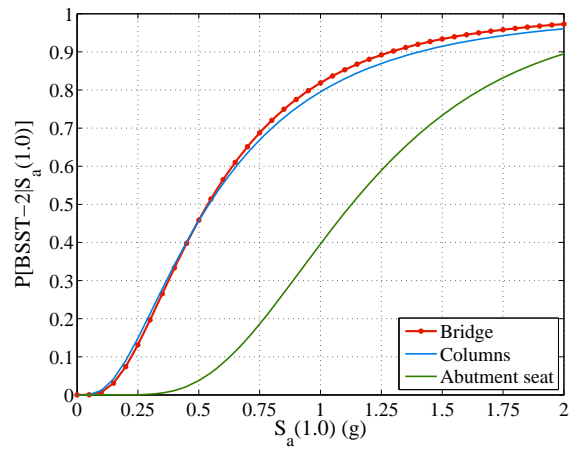
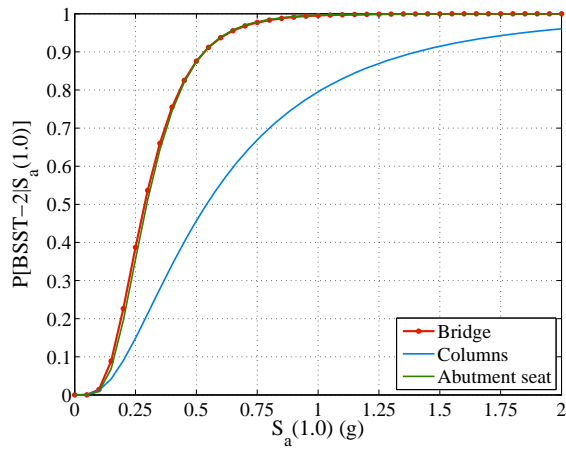
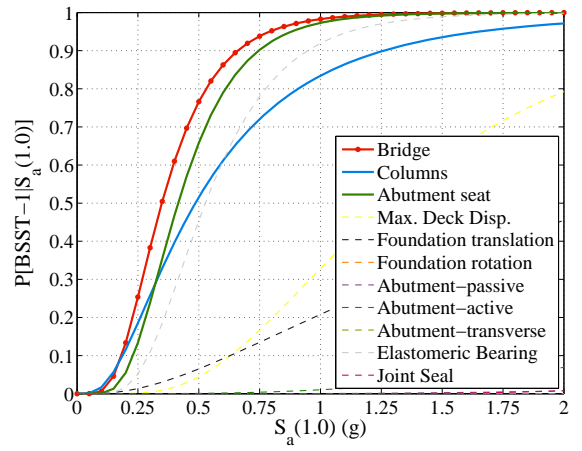
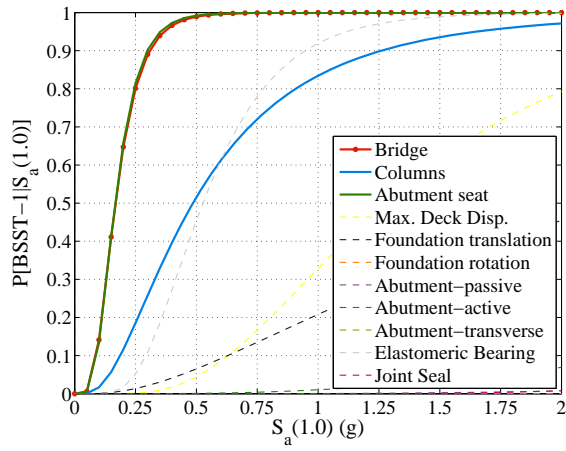
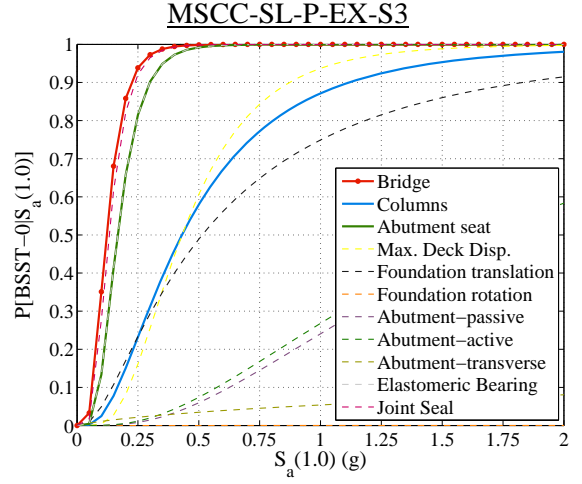
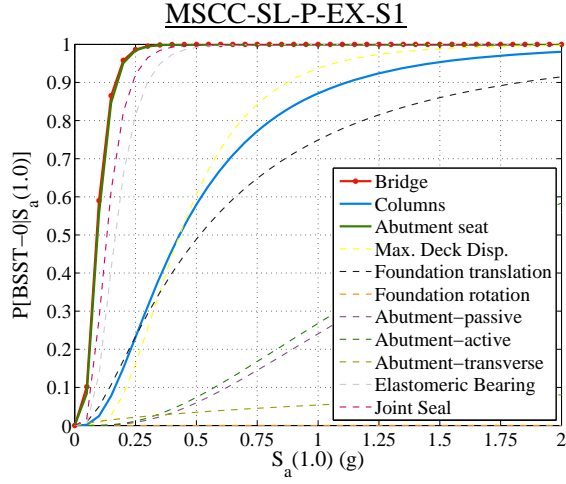


Figure 6.2: Illustration of change in median values and relative vulnerability



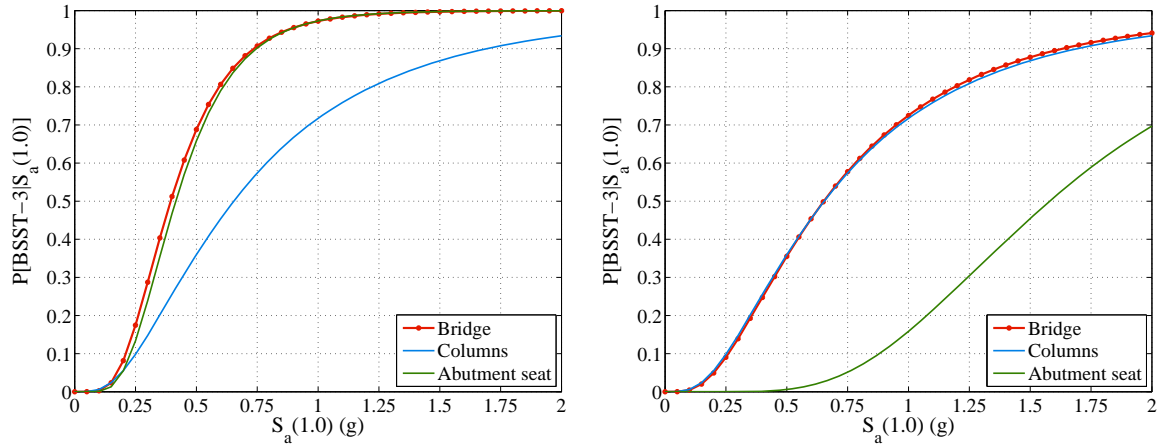


Figure 6.3: System and component level fragility curves for MSCC-SL bridges with seat type abutments and seat width class S1 and S3

Table 6.2: Details of the most vulnerable component across the SPS for MSCC-SL bridge class

Seismic performance sub-bin	BSST-0	BSST-1	BSST-2	BSST-3
MSCC-SL-P-EX-S0	Abut transverse	Columns	Columns	Columns
MSCC-SL-P-EX-S1	Abut seat	Abut seat	Abut seat	Abut seat
MSCC-SL-P-EX-S2	Joint seal	Abut seat	Columns	Columns
MSCC-SL-P-EX-S3	Joint seal	Abut seat	Columns	Columns
MSCC-SL-P-EX-S4	Joint seal	Abut seat	Columns	Columns

6.2 Multispan Continuous Concrete Single Frame Box-girder Bridges

Component and system level fragility curves are developed for MSCC-BG bridges with diaphragm and seat abutments, single and multi column bents across the three significant design eras considered in this study. Table 6.3 lists the median, λ , and dispersion, ζ , values for the SPS considered along with an average dispersion, ζ^* . Figure 6.4 shows a comparison of fragility curves for single (SCB) and multi column bents (MCB) in bridges with diaphragm abutments. A comparison of median fragilities for SCBs and MCBs with seat type abutments is shown in Figure 6.5. Based on these two figures and Table 6.3, inferences can be drawn based on the influence of the type of bent and abutment on the bridge fragility.

Table 6.3: Multispan continuous concrete box-girder bridge fragilities

Seismic performance sub-bin	BSST-0		BSST-1		BSST-2		BSST-3		ζ^*
	λ	ζ	λ	ζ	λ	ζ	λ	ζ	
<u>Pre 1971 design era</u>									
MSCC-BG-S-E1-S0	0.13	0.53	0.17	0.60	0.19	0.61	0.22	0.59	0.58
MSCC-BG-M-E1-S0	0.08	0.51	0.10	0.51	0.11	0.52	0.12	0.52	0.51
MSCC-BG-S-E1-S1	0.02	0.77	0.08	0.62	0.14	0.53	0.17	0.54	0.61
MSCC-BG-S-E1-S2	0.02	0.82	0.09	0.67	0.15	0.54	0.17	0.54	0.64
MSCC-BG-S-E1-S3	0.02	0.79	0.09	0.67	0.14	0.55	0.17	0.54	0.64
MSCC-BG-S-E1-S4	0.02	0.80	0.09	0.66	0.15	0.55	0.17	0.54	0.64
MSCC-BG-M-E1-S1	0.01	0.73	0.06	0.61	0.08	0.59	0.09	0.60	0.63
MSCC-BG-M-E1-S2	0.01	0.80	0.06	0.66	0.08	0.62	0.09	0.62	0.68
MSCC-BG-M-E1-S3	0.01	0.80	0.06	0.64	0.08	0.60	0.09	0.61	0.66
MSCC-BG-M-E1-S4	0.01	0.77	0.06	0.67	0.08	0.61	0.09	0.60	0.66
<u>1971-1990 design era</u>									
MSCC-BG-S-E2-S0	0.15	0.56	0.38	0.61	0.70	0.70	1.00	0.70	0.64
MSCC-BG-M-E2-S0	0.12	0.55	0.24	0.56	0.38	0.57	0.50	0.57	0.56
MSCC-BG-S-E2-S2	0.08	0.61	0.31	0.53	0.47	0.51	0.62	0.52	0.54
MSCC-BG-S-E2-S3	0.08	0.61	0.31	0.53	0.47	0.51	0.62	0.51	0.54
MSCC-BG-S-E2-S4	0.09	0.61	0.31	0.54	0.48	0.51	0.62	0.51	0.54
MSCC-BG-M-E2-S2	0.07	0.52	0.18	0.58	0.27	0.62	0.36	0.63	0.59
MSCC-BG-M-E2-S3	0.07	0.52	0.18	0.59	0.28	0.64	0.36	0.64	0.59
MSCC-BG-M-E2-S4	0.07	0.55	0.18	0.58	0.27	0.64	0.35	0.64	0.60
<u>Post 1990 design era</u>									
MSCC-BG-S-E3-S0	0.16	0.42	0.52	0.39	0.95	0.40	1.26	0.40	0.40
MSCC-BG-M-E3-S0	0.11	0.54	0.32	0.53	0.61	0.56	0.84	0.57	0.55
MSCC-BG-S-E3-S3	0.09	0.55	0.57	0.53	1.44	0.48	2.06	0.49	0.51
MSCC-BG-S-E3-S4	0.09	0.56	0.57	0.53	1.44	0.48	2.06	0.49	0.51
MSCC-BG-M-E3-S3	0.06	0.57	0.26	0.55	0.59	0.59	0.87	0.60	0.58
MSCC-BG-M-E3-S4	0.06	0.58	0.26	0.55	0.61	0.60	0.88	0.61	0.59

6.2.1 Trends based on Diaphragm Abutments

The following inferences can be drawn for SCBs and MCBs in bridges with diaphragm abutments across the three significant design eras considered in this study.

- The vulnerability of both SCBs and MCBs reduces with the evolution of the column design philosophy. Post 1990 era designed bridges with diaphragm

abutments are much less vulnerable when compared to their pre 1971 counterparts irrespective of the type of bent.

- In general, it is seen that SCBs are less vulnerable when compared to the MCBs. MCBs with diaphragm abutments are 46%, 50% and 34% more vulnerable in comparison to their SCB counterparts in the pre 1971, 1971-1990 and post 1990 design eras, respectively. Similar observations are seen in the case of seat abutments with MCBs, which are 47%, 42% and 57% more vulnerable than SCBs in the pre 1971, 1971-1990 and post 1990 design eras, respectively.
- The relative change in median values of post 1990 and 1971-1990 era SCBs with respect to their pre 1971 counterparts is 473% and 355% respectively, while the equivalent quantities in the case of MCBs is 592% and 317%, respectively – at the BSST-3 damage state. This indicates that the evolution of column design has a major impact in the reduction of vulnerability in MCBs when compared to SCBs although the former are more vulnerable when compared to the latter. The reduced vulnerability of SCBs when compared to MCBs may be attributed to a wide variety of reasons including the bridge geometry and dimensions, end conditions of the columns (pinned condition in the case of MCBs versus rotational restraint in the case of SCBs), to mention a few.
- Further the difference in vulnerabilities of SCBs and MCBs underscore the necessity to capture the type of bent in a bridge which is not available through the NBI.

Table 6.4 lists the most vulnerable component in MSCC-BG bridges with diaphragm abutments across the system damage states.

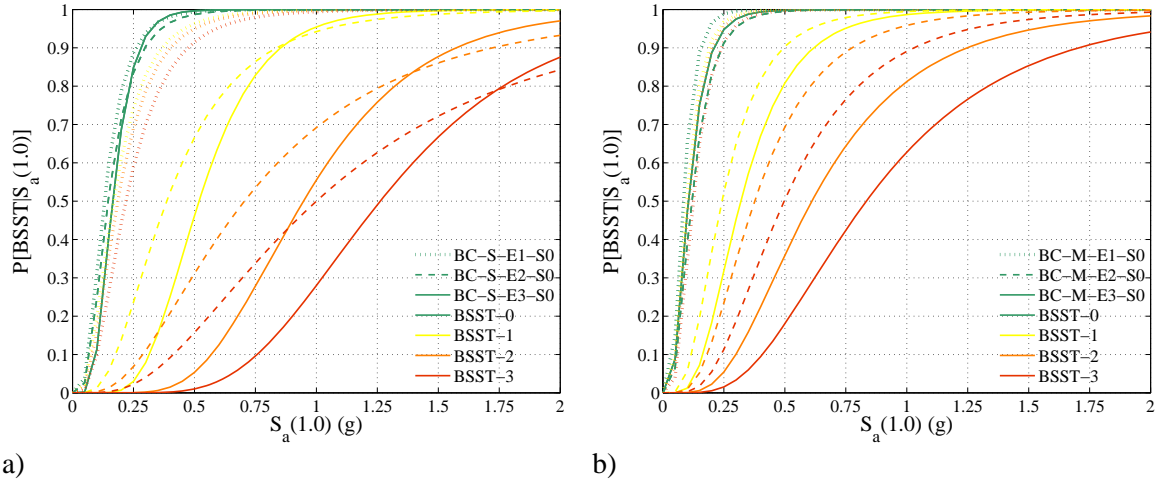


Figure 6.4: Fragility curves for MSCC-BG bridges with diaphragm abutments across design eras having a) single column bents, and b) multi column bents

Table 6.4: Details of the most vulnerable component for MSCC-BG bridge class and diaphragm abutments

Seismic performance sub-bin	BSST-0	BSST-1	BSST-2	BSST-3
MSCC-BG-S-E1-S0	Columns	Columns	Columns	Columns
MSCC-BG-S-E2-S0	Abut transverse	Columns	Columns	Columns
MSCC-BG-S-E3-S0	Abut transverse	Columns	Columns	Columns
MSCC-BG-M-E1-S0	Columns	Columns	Columns	Columns
MSCC-BG-M-E2-S0	Abut transverse	Columns	Columns	Columns
MSCC-BG-M-E3-S0	Abut transverse	Columns	Columns	Columns

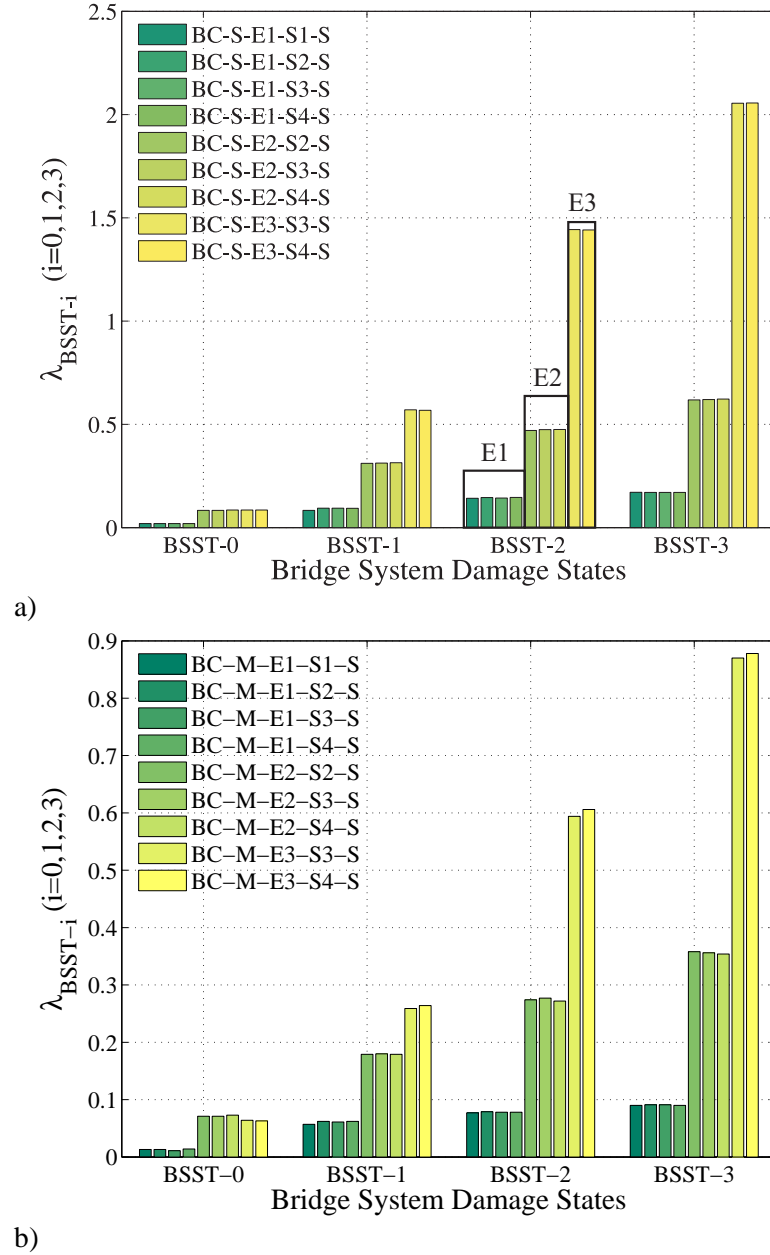


Figure 6.5: Plot of median values for MSCC-BG bridges with seat abutments across design eras for a) single column bents, b) multi column bents

6.2.2 Trends based on Seat Abutments

The following inferences can be drawn for SCBs and MCBs in bridges with seat type abutments across the three significant design eras considered in this study. It must be noted that bridges in the E1 era have all possible ranges of seat widths (S1 through S4),

while those designed in the 1971-1990 design era have only three possible ranges (S2 through S4). Bridges designed post 1990 fall under the S3 and S4 categories and this is depicted in Figure 6.5(a). Additionally, the same trend exists with respect to seat width availability per era in the case of MSCC-TG and MSCC-IG bridge classes which are discussed subsequently in this chapter.

- As in the case of diaphragm abutments, it is seen that the vulnerability of both SCBs (Figure 6.5(a)) and MCBs (Figure 6.5(b)) decreases with an evolution of column design philosophy.
- For a given design era, it is seen that the median fragilities remain consistently similar across the range of seat widths. This is due to the fact that columns govern the vulnerability in most cases and the details of the most vulnerable component are documented in Table 6.5. This serves as an indicator to prioritize the efforts leading to betterment in the performance of columns which will then help realize the true impact of increasing the seat widths.
- In any case, it is seen that there is a tremendous reduction in the vulnerability of post 1990 and 1971-1990 designed bridges with both SCBs and MCBs when compared to their respective pre 1971 counterparts.
- SCBs with seat type abutments are much less vulnerable when compared to MCBs with seat abutments. The median fragilities for post 1990 designed bridges with SCBs is found to be 2.06g in contrast to 0.88g for MCBs therefore making the MCBs 57% more vulnerable when compared to the SCBs. This once again underscores the necessity to capture the type of bent which is not captured by NBI to date.

Table 6.5: Details of the most vulnerable component for MSCC-BG bridge class and seat abutments

Seismic performance sub-bin	BSST-0	BSST-1	BSST-2	BSST-3
MSCC-BG-S-E1-S1	Abut seat	Abut seat	Abut seat	Abut seat
MSCC-BG-S-E1-S2	Joint seal	Abut seat	Columns	Columns
MSCC-BG-S-E1-S3	Joint seal	Abut seat	Columns	Columns
MSCC-BG-S-E1-S4	Joint seal	Abut seat	Columns	Columns
MSCC-BG-M-E1-S1	Joint seal	Abut seat	Abut seat	Abut seat
MSCC-BG-M-E1-S2	Joint seal	Abut seat	Columns	Columns
MSCC-BG-M-E1-S3	Joint seal	Abut seat	Columns	Columns
MSCC-BG-M-E1-S4	Joint seal	Abut seat	Columns	Columns
MSCC-BG-S-E2-S2	Joint seal	Columns	Columns	Columns
MSCC-BG-S-E2-S3	Joint seal	Columns	Columns	Columns
MSCC-BG-S-E2-S4	Joint seal	Columns	Columns	Columns
MSCC-BG-M-E2-S2	Joint seal	Columns	Columns	Columns
MSCC-BG-M-E2-S3	Joint seal	Columns	Columns	Columns
MSCC-BG-M-E2-S4	Joint seal	Columns	Columns	Columns
MSCC-BG-S-E3-S3	Joint seal	Abut seat	Columns	Columns
MSCC-BG-S-E3-S4	Joint seal	Abut seat	Columns	Columns
MSCC-BG-M-E3-S3	Joint seal	Columns	Columns	Columns
MSCC-BG-M-E3-S4	Joint seal	Columns	Columns	Columns

6.2.3 Trends based on the Design Era

Figure 6.6 shows a plot of median values based on design era. The following are some of the inferences that can be drawn:

- In general, irrespective of the type of bent or abutment, pre 1971 era bridges are highly vulnerable when compared to 1971-1990 and post 1990 era bridges.
- Across all the design eras, for a particular abutment type, it is seen that SCBs are much less vulnerable when compared to MCBs. The reduction in vulnerability of SCBs in comparison to MCBs is consistent for both seat and diaphragm abutments. As mentioned previously, this underscores the necessity to capture the type of bent in order to obtain reasonably good estimates of the overall vulnerability of the bridge system.

- Across the first two design eras, diaphragm abutments are much less vulnerable when compared to seat type abutments. The reduction in vulnerability of diaphragm type in comparison to seat type is consistent for both SCBs and MCBs. The lower vulnerability of diaphragm abutments may be attributed to the complete engagement of the superstructure with the abutment and load transfer mechanisms. Further, in the case of seat abutments, the overall system fragility has an added contribution from the abutment seats in addition to the columns which is absent in the case of diaphragm abutments.
- However, in the post 1990 design era, the trend is reversed and seat abutments are seen to be less vulnerable when compared to diaphragm abutments. This may be attributed to the increased demands on the columns of the latter which is found to be the most vulnerable component.
- The differences in fragilities of diaphragm and seat abutments emphasize the necessity to capture the type of abutment in order to get a reasonable estimate of the overall bridge system fragility.

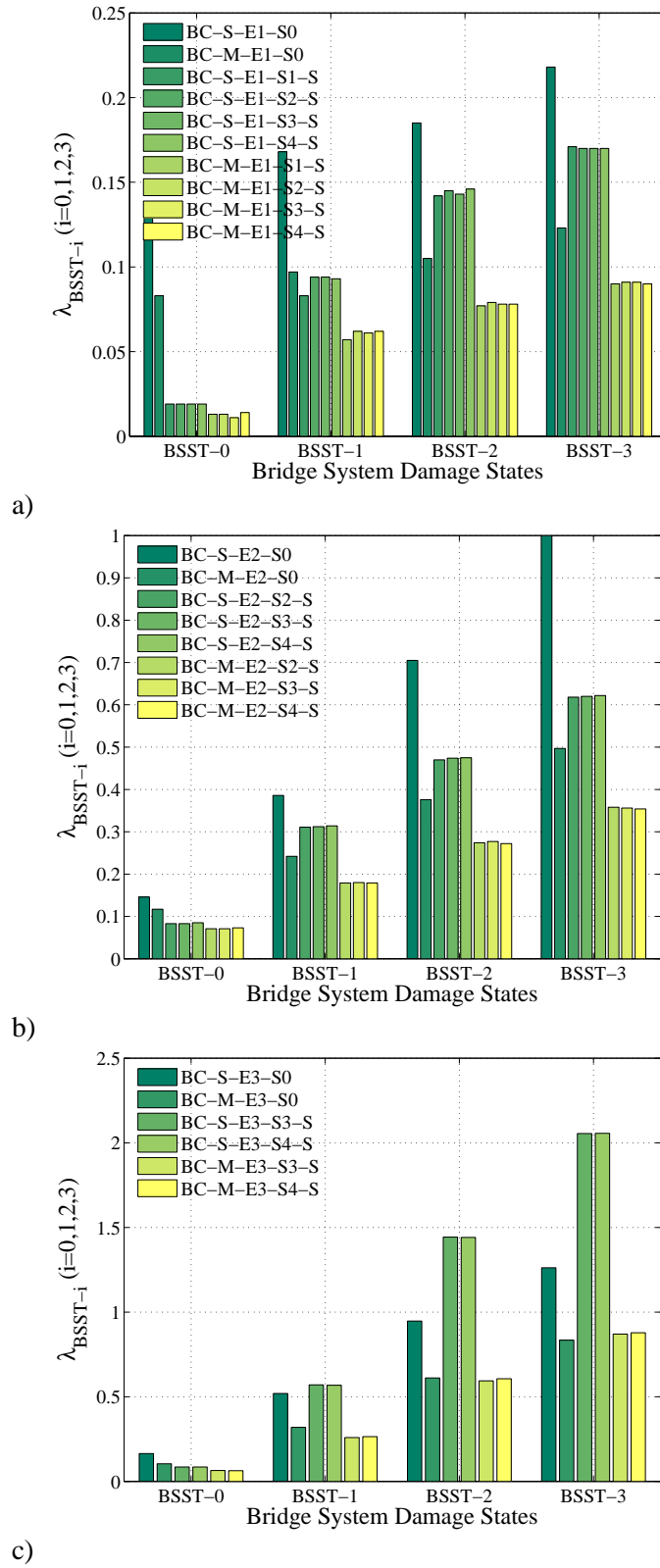


Figure 6.6: Plot of median values of system fragility for a) pre 1971, b) 1971-1990, and c) post 1990 design era

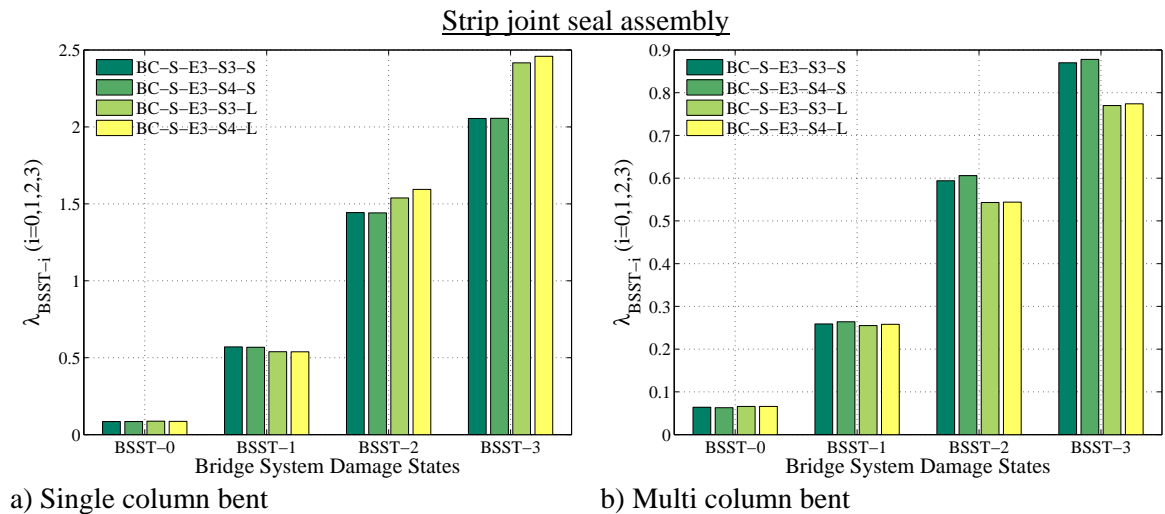
6.2.4 Effect of Gap Size on the Fragility of Post 1990 MSCC-BG bridges

In order to determine the effect of the gap between the deck and abutment backwall on the vulnerability of the bridge system, fragility curves are developed for post 1990 MSCC-BG bridges with seat abutments using two ranges of gap sizes. NLTHA was conducted on two sets of 320 bridge models, the first set comprising of a small gap, denoted by S, between the deck and the abutment backwall which is considered as a uniform random variable between 0 and 1.5 in and a second set consisting of a larger gap, denoted by L, between the deck and the abutment backwall, also modeled as a uniform random number between 1.5 and 6.0 in. It must be noted that the gap size depends on the movement rating (MR) of the joint and further dictates the type of joint seal mechanism in place. Smaller gaps have Type A and B joint sealants while the larger ones have a joint seal assembly in place (either strip or modular type). Extensive details about the MR, gaps and joint seal types were provided in section 3.5.6 of Chapter 3. The comparison of gap sizes, therefore, takes into account the change in dynamic characteristics of the bridge as well as the contribution of joint seal components with different capacity definitions.

Figure 6.7 shows the comparison of median fragilities for post 1990 MSCC-BG bridges with small gap and larger gap, consisting of strip and modular joint seal assemblies. The median and dispersion values are reported in Table 6.6. The following inferences can be drawn by looking at Figure 6.7 and Table 6.6:

- The median values and dispersion for both strip and modular joint assemblies are similar across damage states for both SCBs and MCBs. This is due to the fact the joint seal does not dominate the vulnerability at the BSST-0 and -1 damage states for either case. This indicates that joints may be broadly classified based on the gap as small and large and significant additional effort is not required to further classify the gaps based on the seal mechanism.

- Bridges with large gaps and SCBs are less vulnerable when compared to small gaps. The reduced vulnerability of the abutment seat in the case of larger gaps may be attributed to the abutments not being engaged in this case. However, the trend is reversed in the case of MCBs where bridges with small gaps are less vulnerable when compared to those with large gaps. In this case, the higher vulnerability of the larger gaps may be attributed to the contribution of piles, which attract a major proportion of the force in comparison to the backfill soil. This can further be understood by a quick inspection of the component fragility curves shown in Figure 6.8, which shows the system and component level fragility curves for MSCC-BG-S-E3-S4-L and MSCC-BG-M-E3-S4-L with modular joint assembly. It is evident that in the case of MCBs, the relative contribution of abutment seat to the overall system vulnerability is much higher when compared to that in the case of SCBs, and also MCBs with smaller gaps.
- The investigation of the effect of joint gap size or MR of the joint reinforces the need to capture this attribute in order to obtain reasonable estimates of the system vulnerability. Attributing similar fragilities to either joint gap size may lead to underestimation or overestimation of the vulnerability depending on the bent type in the bridge.



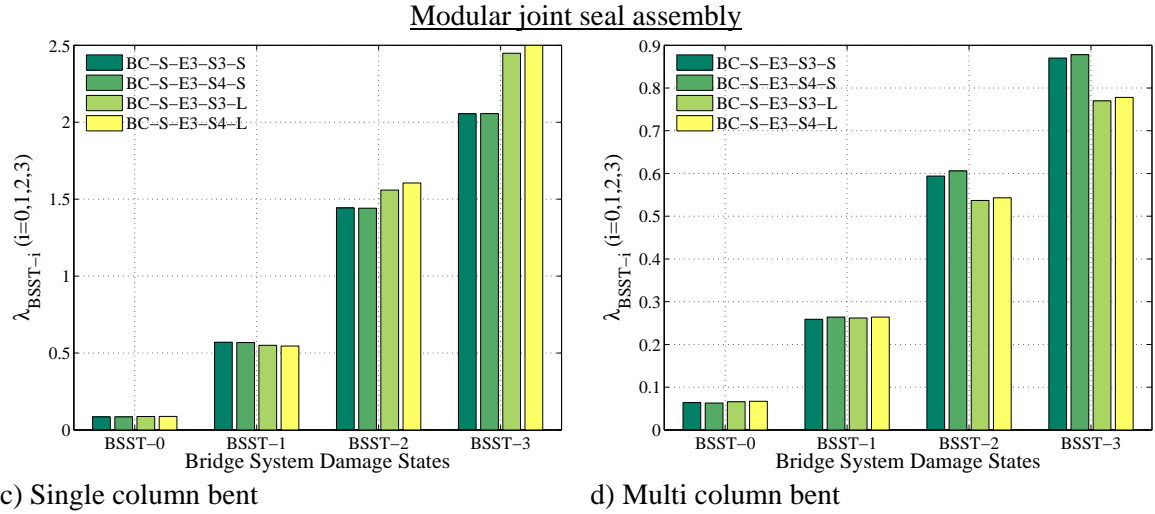
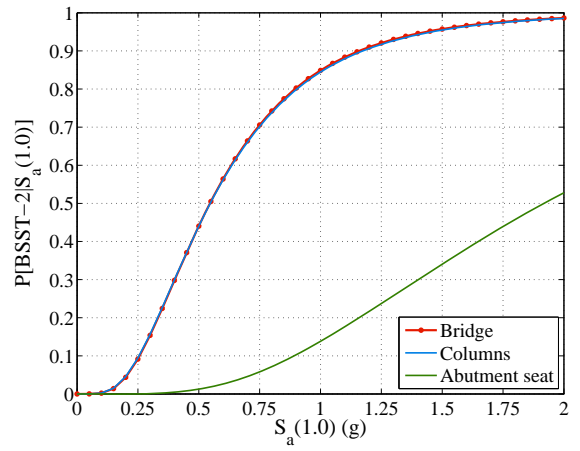
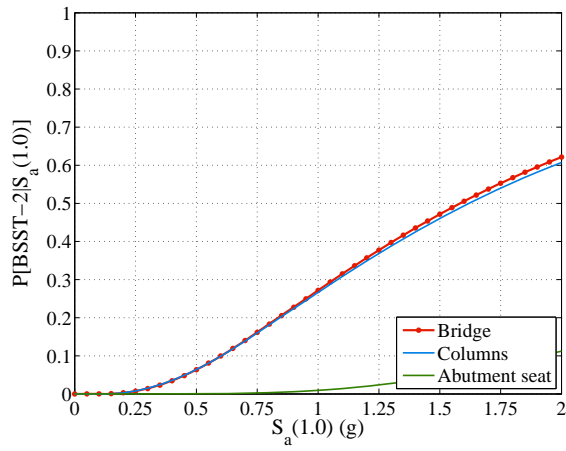
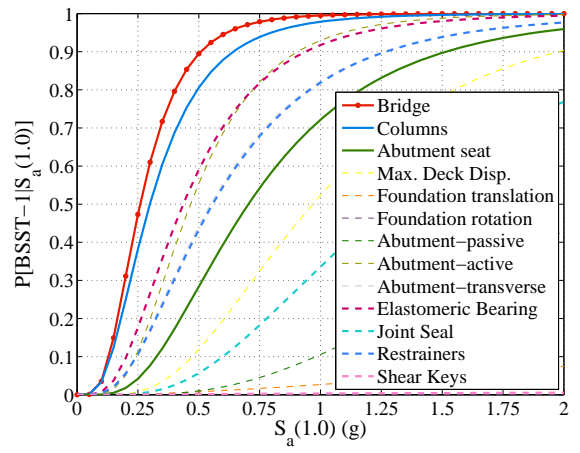
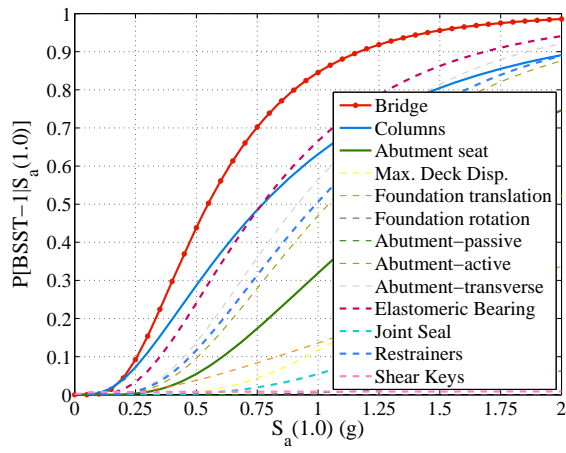
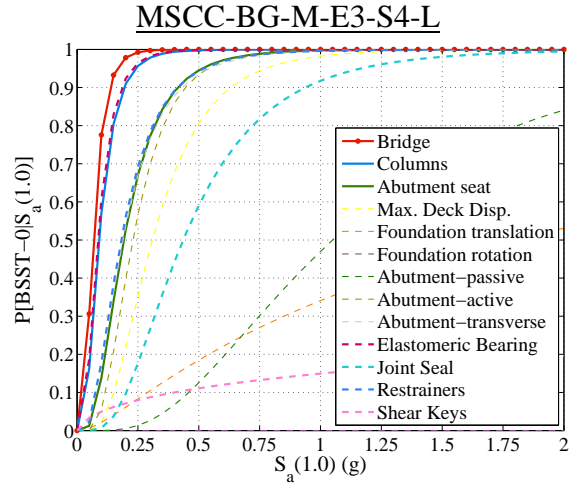
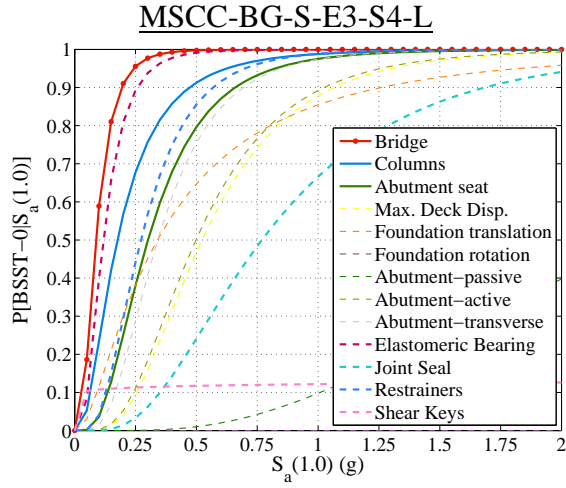


Figure 6.7: Comparison of median values for bridge fragility curves for post 1990 MSCC-BG bridges with small and large gaps installed with different joint seal units

Table 6.6: System fragilities for post 1990 designed MSCC-BG bridges with strip and modular joint seat assemblies

Seismic performance sub-bin	BSST-0		BSST-1		BSST-2		BSST-3		ζ^*
	λ	ζ	λ	ζ	λ	ζ	λ	ζ	
<u>Strip assembly</u>									
MSCC-BG-S-E3-S3-L	0.09	0.61	0.54	0.58	1.54	0.74	2.42	0.74	0.67
MSCC-BG-S-E3-S4-L	0.09	0.60	0.54	0.58	1.59	0.76	2.46	0.74	0.67
MSCC-BG-M-E3-S3-L	0.07	0.55	0.26	0.53	0.54	0.59	0.77	0.58	0.56
MSCC-BG-M-E3-S4-L	0.07	0.55	0.26	0.54	0.54	0.59	0.77	0.59	0.56
<u>Modular assembly</u>									
MSCC-BG-S-E3-S3-L	0.09	0.62	0.55	0.60	1.56	0.73	2.45	0.75	0.67
MSCC-BG-S-E3-S4-L	0.09	0.64	0.55	0.59	1.61	0.76	2.50	0.77	0.69
MSCC-BG-M-E3-S3-L	0.07	0.54	0.26	0.54	0.54	0.58	0.77	0.58	0.56
MSCC-BG-M-E3-S4-L	0.07	0.56	0.26	0.55	0.54	0.59	0.78	0.59	0.57



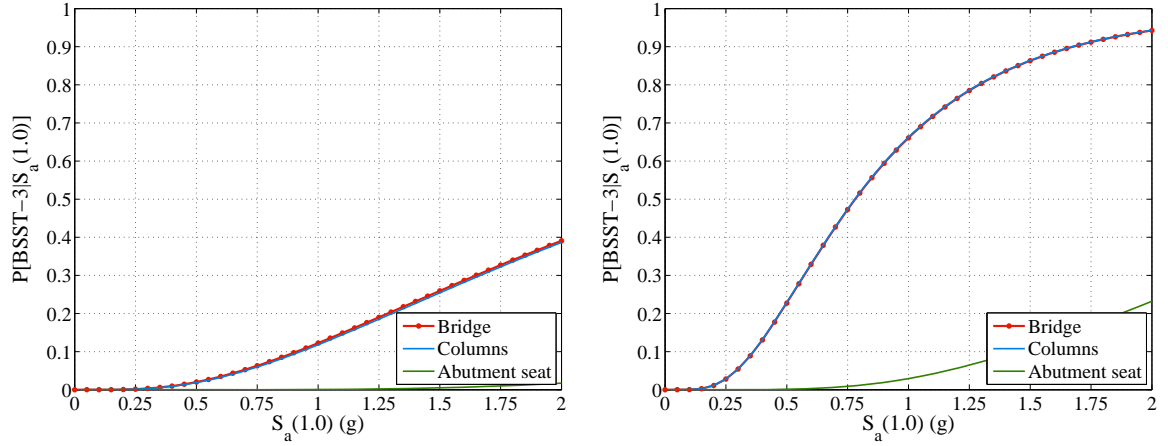


Figure 6.8: System and component level fragility curves for post 1990 MSCC-BG bridges with SCB and MCB equipped with modular joint seal assembly systems

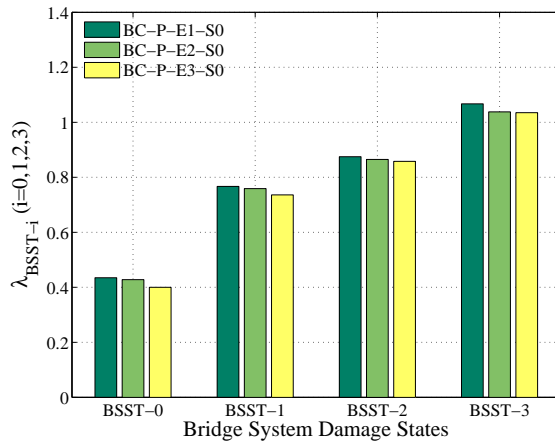
6.3 Multispan Continuous Concrete Tee-girder Bridges

This section presents the results of fragility analysis of MSCC-TG bridges with MCB alone consisting of both integral pile columns (P) and traditional circular columns (M) with seat and diaphragm abutments. Table 6.7 lists the median, λ , and dispersion, ζ , values for the SPS considered along with an average dispersion, ζ^* . A comparison of median fragilities for integral pile columns and MCB in bridges with diaphragm and seat abutments is shown in Figure 6.9. Table 6.8 lists the most vulnerable component for the SPS considered in this bridge class.

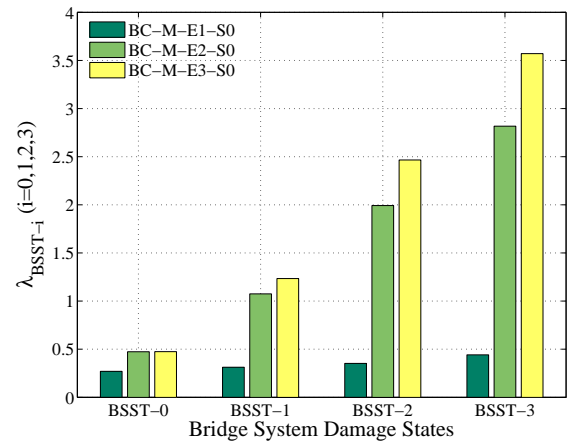
Table 6.7: Multispan continuous concrete Tee-girder bridge fragilities

Seismic performance sub-bin	BSST-0		BSST-1		BSST-2		BSST-3		ζ^*
	λ	ζ	λ	ζ	λ	ζ	λ	ζ	
<u>Pre 1971 design era</u>									
MSCC-TG-P-E1-S0	0.44	0.55	0.77	0.65	0.88	0.68	1.07	0.68	0.64
MSCC-TG-M-E1-S0	0.27	0.56	0.31	0.57	0.35	0.57	0.44	0.57	0.57
MSCC-TG-P-E1-S1	0.06	0.37	0.12	0.40	0.20	0.42	0.28	0.44	0.41
MSCC-TG-P-E1-S2	0.08	0.36	0.23	0.42	0.31	0.51	0.37	0.53	0.45
MSCC-TG-P-E1-S3	0.08	0.37	0.23	0.43	0.32	0.55	0.38	0.56	0.48
MSCC-TG-P-E1-S4	0.08	0.35	0.23	0.43	0.32	0.57	0.38	0.58	0.48
MSCC-TG-M-E1-S1	0.07	0.51	0.14	0.55	0.23	0.56	0.30	0.55	0.54
MSCC-TG-M-E1-S2	0.10	0.50	0.24	0.58	0.27	0.62	0.34	0.64	0.59
MSCC-TG-M-E1-S3	0.10	0.50	0.24	0.57	0.28	0.64	0.34	0.65	0.59
MSCC-TG-M-E1-S4	0.10	0.49	0.24	0.58	0.28	0.64	0.34	0.64	0.59
<u>1971-1990 design era</u>									
MSCC-TG-P-E2-S0	0.43	0.48	0.76	0.56	0.87	0.60	1.04	0.60	0.56
MSCC-TG-M-E2-S0	0.47	0.51	1.08	0.56	1.99	0.59	2.82	0.51	0.54
MSCC-TG-P-E2-S2	0.09	0.57	0.28	0.60	0.38	0.68	0.47	0.71	0.64
MSCC-TG-P-E2-S3	0.09	0.57	0.28	0.60	0.39	0.72	0.47	0.73	0.65
MSCC-TG-P-E2-S4	0.09	0.57	0.28	0.60	0.39	0.73	0.46	0.73	0.66
MSCC-TG-M-E2-S2	0.12	0.46	0.41	0.47	0.79	0.49	1.12	0.49	0.48
MSCC-TG-M-E2-S3	0.12	0.46	0.41	0.47	1.06	0.52	1.52	0.52	0.49
MSCC-TG-M-E2-S4	0.12	0.46	0.40	0.46	1.20	0.55	1.71	0.55	0.51
<u>Post 1990 design era</u>									
MSCC-TG-P-E3-S0	0.40	0.48	0.74	0.57	0.86	0.63	1.04	0.63	0.57
MSCC-TG-M-E3-S0	0.48	0.47	1.23	0.49	2.47	0.64	3.57	0.40	0.50
MSCC-TG-P-E3-S3	0.07	0.39	0.26	0.43	0.43	0.54	0.54	0.57	0.49
MSCC-TG-P-E3-S4	0.07	0.39	0.25	0.42	0.44	0.58	0.54	0.60	0.50
MSCC-TG-M-E3-S3	0.11	0.44	0.39	0.46	1.20	0.48	1.72	0.48	0.46
MSCC-TG-M-E3-S4	0.11	0.44	0.39	0.45	1.55	0.47	2.23	0.49	0.46

Diaphragm Abutments

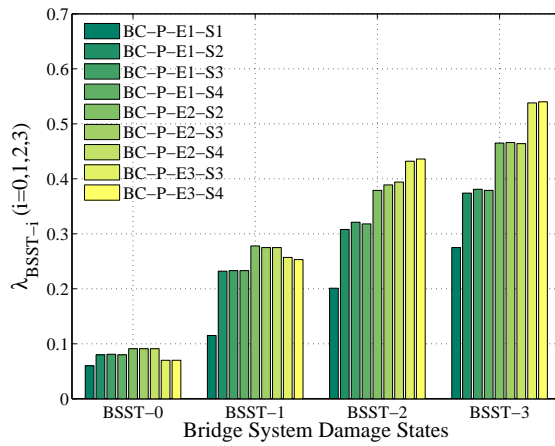


a) Integral pile column

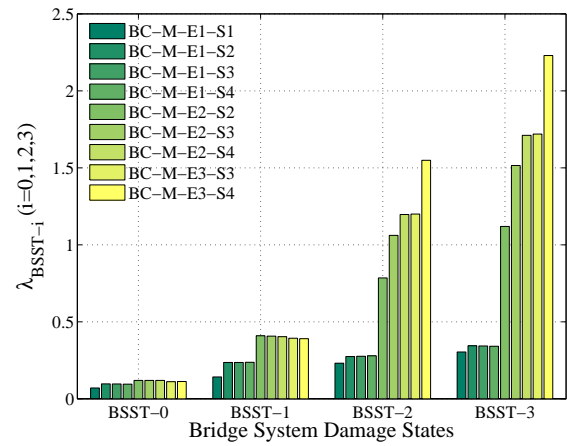


b) Regular multi column bents

Seat Abutments



c) Integral pile column



d) Regular multi column bents

Figure 6.9: Comparison of median values of system fragility for MSCC-TG bridge class

Table 6.8: List of the most vulnerable component across damage states for the SPS in MSCC-TG bridge class

Seismic performance sub-bin	BSST-0	BSST-1	BSST-2	BSST-3
<u>Diaphragm Abutments</u>				
MSCC-TG-P-E1-S0	Deck disp.	Columns	Columns	Columns
MSCC-TG-P-E2-S0	Deck disp.	Columns	Columns	Columns
MSCC-TG-P-E3-S0	Deck disp.	Columns	Columns	Columns
MSCC-TG-M-E1-S0	Columns	Columns	Columns	Columns
MSCC-TG-M-E2-S0	Columns	Columns	Columns	Columns
MSCC-TG-M-E3-S0	Columns	Columns	Columns	Columns
<u>Seat Abutments</u>				
MSCC-TG-P-E1-S1	Abut seat	Abut seat	Abut seat	Abut seat
MSCC-TG-P-E1-S2	Joint seal	Columns	Columns	Columns
MSCC-TG-P-E1-S3	Joint seal	Columns	Columns	Columns
MSCC-TG-P-E1-S4	Joint seal	Columns	Columns	Columns
MSCC-TG-M-E1-S1	Abut seat	Abut seat	Columns	Columns
MSCC-TG-M-E1-S2	Joint seal	Columns	Columns	Columns
MSCC-TG-M-E1-S3	Joint seal	Columns	Columns	Columns
MSCC-TG-M-E1-S4	Joint seal	Columns	Columns	Columns
MSCC-TG-P-E2-S2	Joint seal	Abut seat	Columns	Columns
MSCC-TG-P-E2-S3	Joint seal	Abut seat	Columns	Columns
MSCC-TG-P-E2-S4	Joint seal	Abut seat	Columns	Columns
MSCC-TG-M-E2-S2	Joint seal	Abut seat	Abut seat	Abut seat
MSCC-TG-M-E2-S3	Joint seal	Abut seat	Columns	Columns
MSCC-TG-M-E2-S4	Joint seal	Abut seat	Columns	Columns
MSCC-TG-P-E3-S3	Joint seal	Abut seat	Columns	Columns
MSCC-TG-P-E3-S4	Joint seal	Abut seat	Columns	Columns
MSCC-TG-M-E3-S3	Joint seal	Abut seat	Abut seat	Abut seat
MSCC-TG-M-E3-S4	Joint seal	Abut seat	Abut seat	Abut seat

6.3.1 Trends based on Diaphragm Abutments

The following are some of the conclusions and inferences that can be drawn for MSCC-TG bridges with diaphragm abutments:

- The median fragilities for integral pile columns are very similar across the design eras (Figure 6.9(a)). This is due to the fact that there has been no evolution in the standard pile details through the design eras unlike traditional MCBs with circular columns which saw a radical shift in the design philosophy from brittle to ductile

behavior. This suggests that a single set of fragilities may be employed for MSCC-TG with integral pile columns and diaphragm abutments irrespective of the time of construction of the bridge.

- Contrasting the case of integral pile columns, the vulnerability of traditional MCBs reduces with the progression of design eras, as expected (Figure 6.9(b)).
- Pre 1971 design era bridges with integral pile columns are less vulnerable when compared to bridges with traditional MCBs. This may be attributed to the slightly better confinement in the former (reinforced and prestressed piles) when compared to traditional circular columns with very little confinement and hence minimal ductility capacity, which is characteristic of this design era columns.
- On the other hand, traditional MCBs in the 1971-1990 and post 1990 era bridges are less vulnerable when compared to integral pile columns. This underscores the effectiveness of the shift in design philosophy towards energy dissipation in the latter design eras.
- The difference in vulnerability of integral pile columns versus traditional MCBs underscores the necessity to capture this attribute which is not done to date in the NBI.

6.3.2 Trends based on Seat Abutments

- Traditional MCBs with seat type abutments have a tremendous reduction in their vulnerability with the evolution of seat ranges and column design philosophy (Figure 6.9(d)). The enhanced ductility capacity of the modern day columns coupled with generous seat width makes these much less vulnerable when compared to the pre 1971 bridges.
- Bridges with integral pile columns do not see a major reduction in system vulnerability with the evolution of seat widths (Figure 6.9(c)). Although abutment seats are primary components along with columns, the benefit of a larger seat

width is masked by the dominance of the brittle integral pile columns to the system vulnerability. Neglecting the subtle differences in the median fragilities, a single set of fragility curves can be used for MSCC-TG-P across the design eras for all ranges of seat widths, thereby reducing the effort to capture these attributes.

- Integral pile columns and traditional MCBs have similar fragilities in the pre 1971 design era, although integral pile columns are slightly less vulnerable. This is due to similar response characteristics and limited ductility capacity of either of them.
- However, in the latter two design eras, traditional MCBs are far less vulnerable when compared to integral pile columns. As stated previously, this once again stresses the need to capture the type of column in the bridge to obtain reasonable estimates of the vulnerability.

6.3.3 Trends based on Design Era

The plot of median fragilities based on design era is shown in Figure 6.10. The observations can be summarized as below:

- Across design eras, it is observed that irrespective of the column type, diaphragm abutments are less vulnerable when compared to seat abutments.
- In the pre-1971 design era, integral pile columns are less vulnerable when compared to traditional MCBs due to slightly better confinement in the former when compared to the latter. In the case of seat abutments, it is seen that there is insignificant reduction in the vulnerability of the bridge system beyond the 12-18 inch seat range (S2) for both integral pile columns and traditional MCBs. This is indicated by the similar values of median fragilities for seat ranges S2 through S4 across all damage states. It can therefore be concluded that the most effective technique would be to focus on retrofitting the columns once the seat has been increased to at least the 12 – 18 inch (S2) range. The results suggest that the

columns govern the overall vulnerability with seats increased to categories S2 through S4. This does not imply that shorter seat widths are just as effective or that seats do not contribute to the vulnerability. Improvement in the performance of columns by retrofitting or replacement of the non-ductile columns with ductile ones, will demonstrate the impact of increasing the seat width potentially.

- In the 1971-1990 and post 1990 design eras, traditional MCBs are less vulnerable when compared to integral pile columns due to enhanced energy dissipation and ductile characteristics. Unlike the situation in the pre 1971 era bridges, the vulnerability of traditional MCBs is reduced with an increase in the seat width. This is due to the relatively larger contribution of the abutment seat to the overall vulnerability in the latter design eras when compared to the pre 1971 design era where columns dominate the vulnerability almost entirely. This is illustrated in Figure 6.11. Unlike the case of MSCC-BG and MSCC-SL bridges, where columns dominate the vulnerability with the provision of increased seat widths beyond a certain range, the situation is not the same in the case of MSCC-TG bridges, where the provision of increased seat widths (S1 through S4) leads to a reduction in vulnerability successively. This necessitates the need to capture not only the presence of seat abutments in this bridge class, but also specific information regarding the actual seat width range, in order to obtain reliable estimates of the vulnerability.
- The median fragilities across seat ranges (S2 through S4) is similar for bridges with integral pile columns in the 1971-1990 and post 1990 design eras. This once again serves as an indicator to target the retrofit prioritization efforts towards columns to see the potential benefit of increased seat widths and reduced bridge system vulnerability.
- The percentage reduction in vulnerability between diaphragm and seat abutments for integral pile columns and traditional MCBs not consistent across the design

eras. Table 6.9 reports the percentage reduction in the vulnerability of diaphragm abutments in comparison to seat abutments for the two column types across the three design eras. Clearly it is seen that the trends are different for integral pile columns and traditional MCBs. This may be attributed to several factors such as change in the dynamic characteristics of the bridges, bridge geometry, end conditions of the column, relative vulnerability between bridge components, to mention a few.

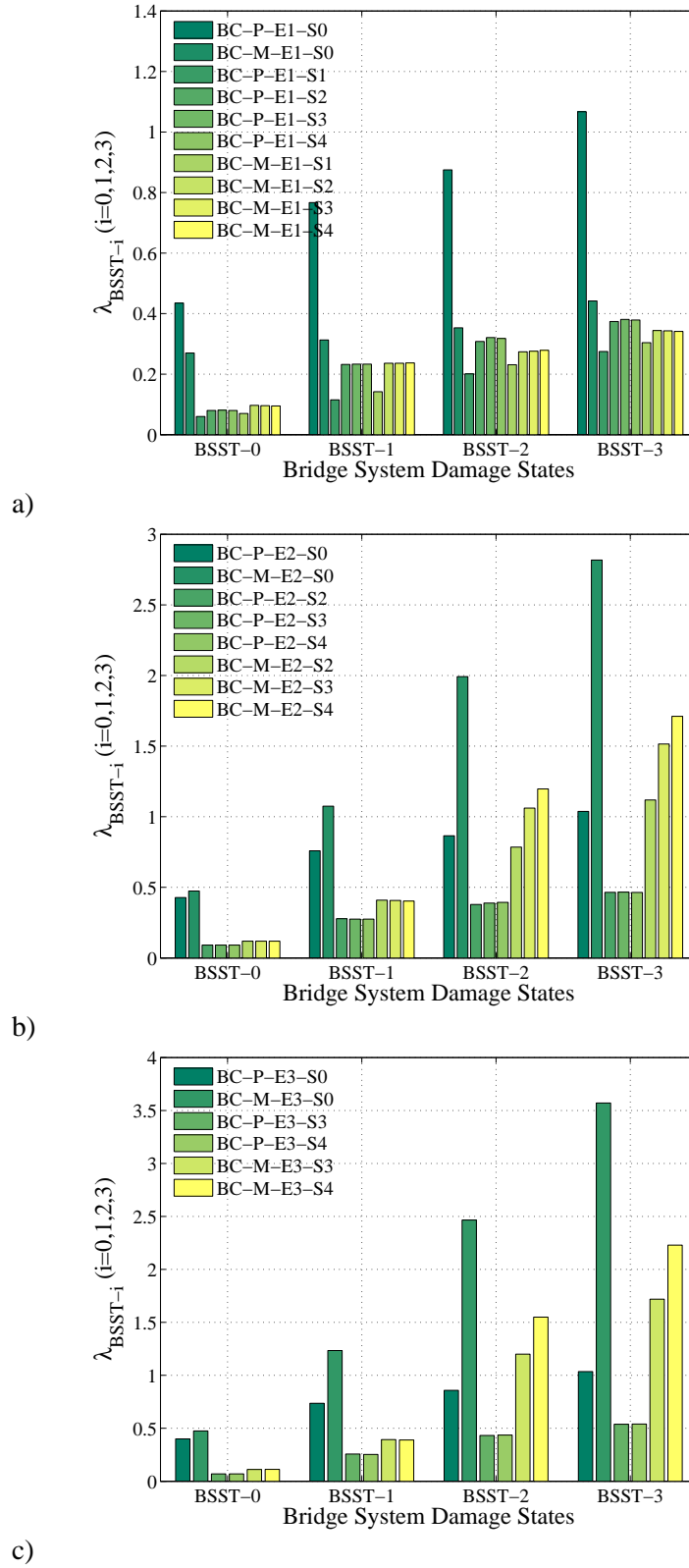


Figure 6.10: Plot of median values of system fragility across damage states for MSCC-TG bridges designed a) pre 1971, b) 1971-1990, and c) post 1990

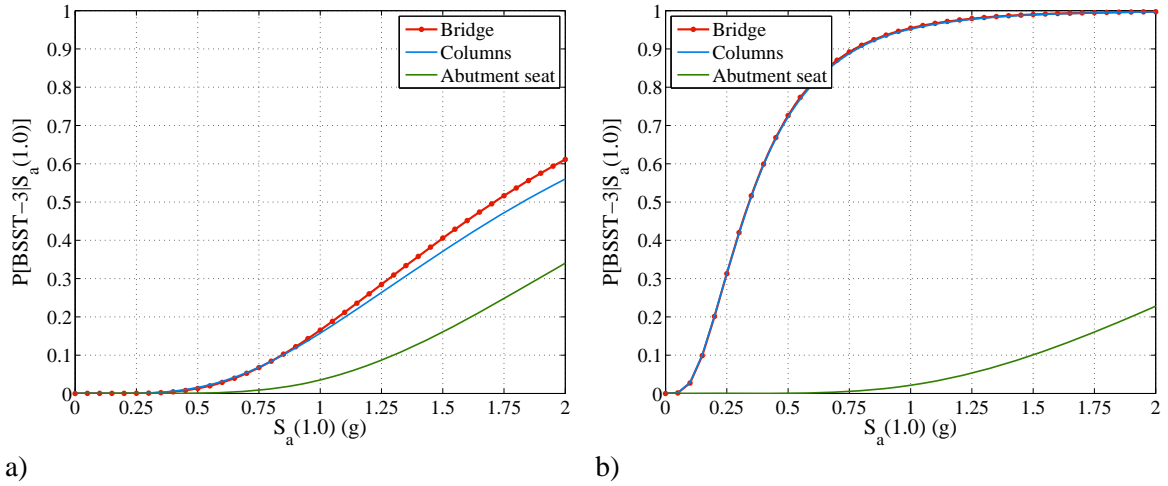


Figure 6.11: System and component fragility curves for a) MSCC-TG-M-E2-S4, and b) MSCC-TG-M-E1-S4

Table 6.9: Percentage reduction in vulnerability of diaphragm abutments with respect to seat abutments in MSCC-TG bridges

Design era	Bent (column) type	
	Integral pile columns	Traditional MCBs
Pre 1971	182%	29%
1971-1990	121%	65%
Post 1990	93%	60%

6.4 Multispan Continuous Concrete I-girder Bridges

Component and system level fragility curves are developed for MSCC-IG bridges with diaphragm and seat abutments, single and multi-column bents across the three significant design eras considered in this study. Table 6.10 lists the median, λ , and dispersion, ζ , values for the SPS considered along with an average dispersion, ζ^* . The following sub-sections provide discussion about the observed trends based on a number of criteria.

Table 6.10: Multispan continuous concrete I-girder bridge fragilities

Seismic performance sub-bin	BSST-0		BSST-1		BSST-2		BSST-3		ζ^*
	λ	ζ	λ	ζ	λ	ζ	λ	ζ	
<u>Pre 1971 design era</u>									
MSCC-IG-S-E1-S0	0.12	0.56	0.33	0.58	0.47	0.76	0.54	0.75	0.66
MSCC-IG-M-E1-S0	0.09	0.58	0.22	0.63	0.27	0.71	0.33	0.71	0.66
MSCC-IG-S-E1-S1	0.05	0.54	0.16	0.56	0.37	0.55	0.52	0.54	0.55
MSCC-IG-S-E1-S2	0.07	0.49	0.29	0.48	0.49	0.56	0.57	0.56	0.52
MSCC-IG-S-E1-S3	0.07	0.50	0.29	0.48	0.49	0.57	0.57	0.57	0.53
MSCC-IG-S-E1-S4	0.07	0.50	0.29	0.49	0.49	0.57	0.57	0.57	0.53
MSCC-IG-M-E1-S1	0.06	0.44	0.13	0.47	0.19	0.49	0.23	0.50	0.47
MSCC-IG-M-E1-S2	0.07	0.45	0.18	0.49	0.21	0.55	0.25	0.55	0.51
MSCC-IG-M-E1-S3	0.07	0.45	0.18	0.50	0.21	0.56	0.25	0.56	0.52
MSCC-IG-M-E1-S4	0.07	0.45	0.18	0.50	0.21	0.56	0.25	0.56	0.52
<u>1971-1990 design era</u>									
MSCC-IG-S-E2-S0	0.09	0.59	0.24	0.61	0.68	0.91	0.88	0.91	0.75
MSCC-IG-M-E2-S0	0.11	0.52	0.35	0.50	0.76	0.58	1.02	0.59	0.55
MSCC-IG-S-E2-S2	0.04	0.53	0.15	0.54	0.31	0.55	0.46	0.55	0.54
MSCC-IG-S-E2-S3	0.04	0.52	0.15	0.55	0.51	0.55	0.73	0.55	0.54
MSCC-IG-S-E2-S4	0.04	0.52	0.16	0.55	0.67	0.56	0.97	0.56	0.55
MSCC-IG-M-E2-S2	0.06	0.43	0.21	0.45	0.42	0.46	0.62	0.45	0.45
MSCC-IG-M-E2-S3	0.06	0.43	0.21	0.44	0.58	0.46	0.84	0.48	0.45
MSCC-IG-M-E2-S4	0.06	0.42	0.21	0.43	0.66	0.49	0.93	0.50	0.46
<u>Post 1990 design era</u>									
MSCC-IG-S-E3-S0	0.05	0.81	0.19	0.78	2.15	0.99	3.28	0.94	0.88
MSCC-IG-M-E3-S0	0.10	0.56	0.37	0.54	1.59	0.64	2.24	0.64	0.59
MSCC-IG-S-E3-S3	0.03	0.65	0.18	0.66	0.56	0.74	0.93	0.74	0.72
MSCC-IG-S-E3-S4	0.03	0.67	0.18	0.67	0.84	0.74	1.40	0.74	0.73
MSCC-IG-M-E3-S3	0.08	0.39	0.28	0.41	0.72	0.45	1.04	0.46	0.44
MSCC-IG-M-E3-S4	0.08	0.39	0.28	0.41	0.96	0.45	1.38	0.45	0.44

6.4.1 Trends based on Diaphragm Abutments

The plot of median values of system fragility for MSCC-IG bridges with diaphragm abutments across the three design eras is shown in Figure 6.12. The trends observed in this case are very similar to those observed in the case of MSCC-BG bridge class and can be summarized as below.

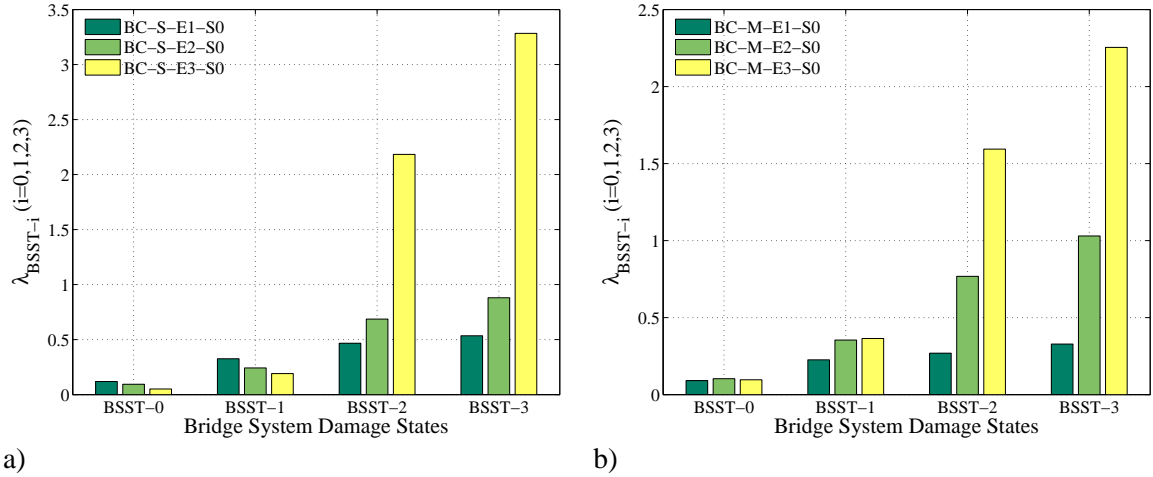


Figure 6.12: Plot of median fragilities for MSCC-IG with diaphragm abutments consisting of a) single column bents, b) multi column bents, across design eras

- The vulnerability of bridges decreases with the progression of the design era, which reinforces the effectiveness of the ductile design philosophy.
- SCBs are less vulnerable when compared to MCBs with diaphragm abutments. MSCC-IG bridges with diaphragm abutments and MCBs are 39%, 13% and 27% more vulnerable when compared to their SCB counterparts in the pre 1971, 1971-1990 and post 1990 design eras, respectively.
- This study recommends the need to capture the type of bent in the bridge owing to the differences in the median values and dispersions characterizing the system fragility due to this attribute.

6.4.2 Trends based on Seat Abutments

Figure 6.13 shows the comparison of median fragilities for I-girder bridge class with seat type abutments across the design eras considered in this study.

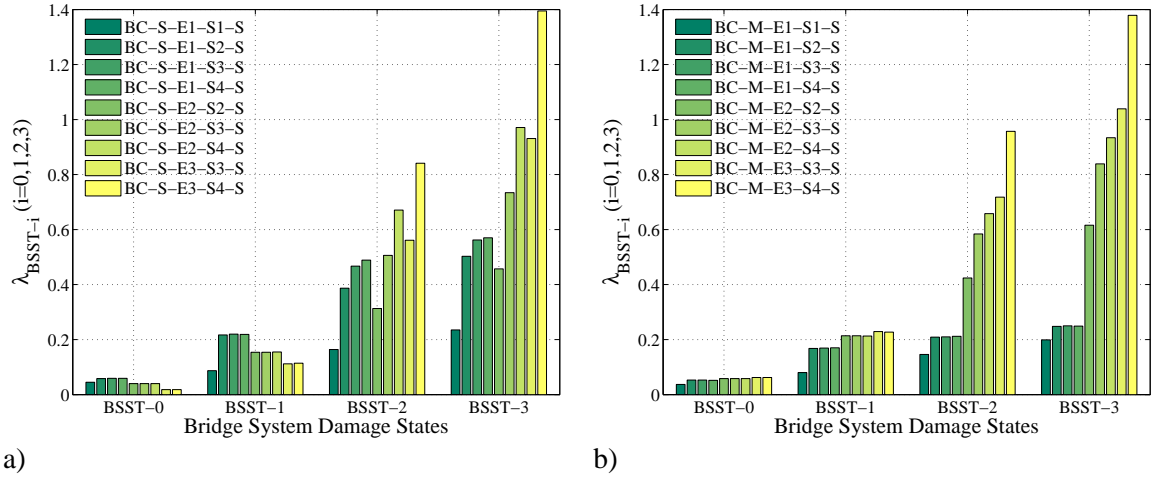


Figure 6.13: Plot of median fragilities for MSCC-IG with seat type abutments consisting of a) single column bents, b) multi column bents, across design eras

The important observations are summarized below.

- Akin to the case of diaphragm abutments, the vulnerability of bridges (both SCB and MCB) reduces across the design eras. However, in the case of seat abutments, it is seen that MCBs are less vulnerable when compared to the SCBs.
- In the pre 1971 design era it is seen that the median fragilities are similar for seat ranges S2 thru S4 and these are less vulnerable when compared to S1 as expected. This establishes the potential impact of increasing the seat widths beyond the S2 (12 – 18 in) range and focusing on modifying the response of columns in an attempt to reduce the overall vulnerability of the bridge system.
- However in the 1971-1990 and post 1990 design eras, there is a reduction in the vulnerability with the progression of seat ranges S2 through S4. This is due to the fact that the relative contribution of the abutment seat to the overall vulnerability is higher in these cases when compared to the situation in the pre 1971 designed bridges, where columns dominate the overall vulnerability.

- The results presented in this section underscore the importance of capturing attributes such as the bent type and type of abutment in order to obtain reliable estimates of the overall vulnerability of the bridge system.

Table 6.11 lists the most vulnerable component for the MSCC-IG bridge class and the different SPS associated with it.

Table 6.11: Details of the most vulnerable component for MSCC-IG bridge class

Seismic performance sub-bin	BSST-0	BSST-1	BSST-2	BSST-3
MSCC-IG-S-E1-S0	Bearings	Bearings	Columns	Columns
MSCC-IG-M-E1-S0	Bearings	Columns	Columns	Columns
MSCC-IG-S-E1-S1	Abut seat	Abut seat	Columns	Columns
MSCC-IG-S-E1-S2	Joint seal	Abut seat	Abut seat	Columns
MSCC-IG-S-E1-S3	Joint seal	Abut seat	Columns	Columns
MSCC-IG-S-E1-S4	Joint seal	Abut seat	Columns	Columns
MSCC-IG-M-E1-S1	Abut seat	Abut seat	Abut seat	Abut seat
MSCC-IG-M-E1-S2	Joint seal	Columns	Columns	Columns
MSCC-IG-M-E1-S3	Joint seal	Columns	Columns	Columns
MSCC-IG-M-E1-S4	Joint seal	Columns	Columns	Columns
MSCC-IG-S-E2-S0	Bearings	Bearings	Columns	Columns
MSCC-IG-M-E2-S0	Bearings	Bearings	Columns	Columns
MSCC-IG-S-E2-S2	Joint seal	Abut seat	Abut seat	Abut seat
MSCC-IG-S-E2-S3	Joint seal	Abut seat	Abut seat	Abut seat
MSCC-IG-S-E2-S4	Joint seal	Abut seat	Abut seat	Abut seat
MSCC-IG-M-E2-S2	Joint seal	Abut seat	Abut seat	Abut seat
MSCC-IG-M-E2-S3	Joint seal	Abut seat	Columns	Columns
MSCC-IG-M-E2-S4	Joint seal	Abut seat	Columns	Columns
MSCC-IG-S-E3-S0	Bearings	Bearings	Columns	Columns
MSCC-IG-M-E3-S0	Bearings	Bearings	Columns	Columns
MSCC-IG-S-E3-S3	Joint seal	Abut seat	Abut seat	Abut seat
MSCC-IG-S-E3-S4	Joint seal	Abut seat	Abut seat	Abut seat
MSCC-IG-M-E3-S3	Joint seal	Abut seat	Abut seat	Abut seat
MSCC-IG-M-E3-S4	Joint seal	Abut seat	Abut seat	Abut seat

6.4.3 Trends based on Design Era

The median values of system fragility curves for MSCC-IG bridges with SCBs and MCBs, seat and diaphragm abutments based on the design era are shown in Figure 6.14.

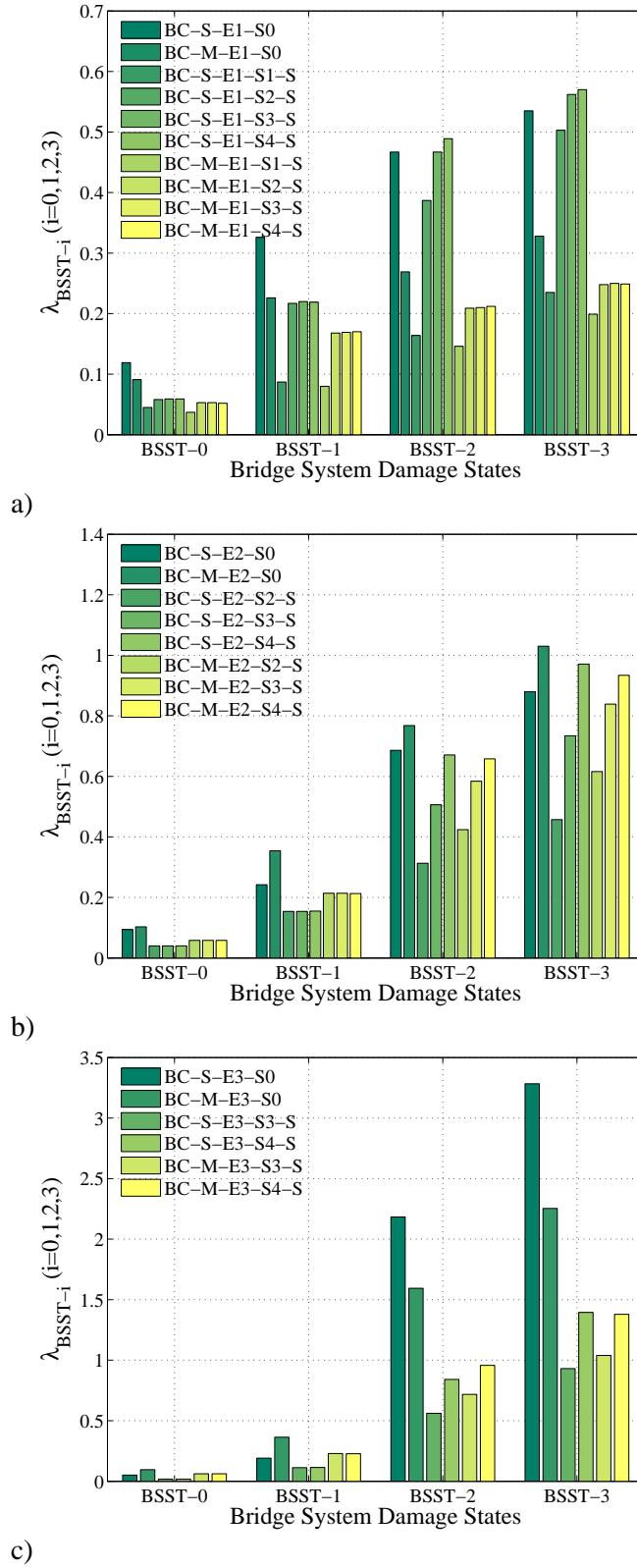


Figure 6.14: Plot of median fragilities for MSCC-IG bridges designed in the a) pre 1971, b) 1971-1990, and c) post 1990 era

- Clearly, the vulnerability of the I-girder bridges reduces with the evolution of column design philosophy and seat widths moving from pre 1971 through 1971-1990 and post 1990 eras.
- MCBs and diaphragm abutments are less vulnerable when compared to MCBs and seat type abutments. However, the trend is quite complex in the case of SCBs where the seat abutments are less vulnerable when compared to diaphragm abutments in the pre 1971 and 1971-1990 design eras. However, SCBs and diaphragm abutments are less vulnerable when compared to SCBs and seat abutments in the post 1990 design era.

6.5 HAZUS Comparison

A detailed discussion about the assumptions, methodology and limitations of the HAZUS fragilities (HAZUS-MH, 2011) were discussed in Chapter 2. HAZUS fragilities were developed by synthesizing the information from the NBI alone unlike the present study where extensive data from bridge plans and in-house databases and the evolution of seismic design philosophy at the component level was used to supplement the information from NBI to obtain seismic performance sub-bins with similar characteristics. As was demonstrated in Chapter 5 and proceeding sections in this chapter, this led to significant variability in the median fragilities across design eras. Further, significant variation was seen with the SPS for the same design era. Despite the differences between the present study and HAZUS methodology, discussed previously, there are a couple of similarities. $S_a(I.0)$ is used as the intensity measure in both cases and so is the number of damage states characterizing the bridge system vulnerability. Although the vulnerability of bridges is governed by that of the columns alone in the case of HAZUS, the column damage state threshold values are chosen and the damage state descriptions are defined keeping in view the anticipated damage to the other bridge components and the HAZUS damage indicators are defined in Table 6.12.

Table 6.12: HAZUS damage state definitions (HAZUS-MH, 2011)

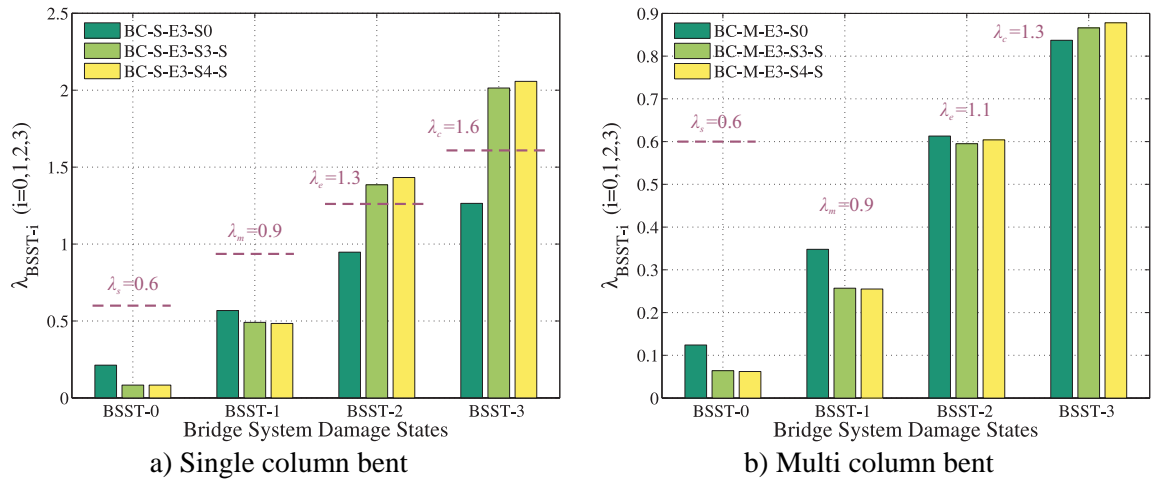
Damage state	Notation	Description
None	ds ₁	None
Slight	ds ₂	Minor spalling to the column requiring no more than cosmetic repair; minor cracking to the deck; minor cracking and spalling to the abutment; cracks in shear keys at the abutment
Moderate	ds ₃	Moderate cracking (shear cracks) and spalling to the columns but is still structurally sound; moderate (< 2 in) movement of the abutment; extensive cracking and spalling of the shear keys; moderate settlement of the approach slab
Extensive	ds ₄	Shear failure of the column causing strength degradation without collapse and columns is structurally unsafe; significant residual movement of superstructure-bent cap connection; vertical offset of the abutment; major settlement of the approach slab; shear key failure at the abutments
Complete	ds ₅	Collapse of the column; loss of bearing support in the connection leading to unseating and imminent deck collapse; foundation failure leading to titling of the superstructure

The HAZUS median fragilities (λ_s , λ_m , λ_e , λ_c , corresponding to slight, moderate, extensive, and complete damage states, respectively) and dispersion (β_{ds}) are documented in Table 6.13. A single value of dispersion equal to 0.6 is prescribed across all the bridge classes. The equivalent bridge class notations between HAZUS and the present study are also noted to facilitate comparison. Figure 6.15 shows a plot of median values for MSCC-BG bridge class with single columns bents in the post 1990 design era and the HAZUS fragilities for illustrative purposes.

Table 6.13: Median values and dispersion for the HAZUS fragilities

Bridge class notation		Median fragilities				β_{ds}
Present study	HAZUS	λ_s	λ_m	λ_e	λ_c	
MSCC-BG-S-E1-SX	HWB8/HWB20	0.35	0.45	0.55	0.80	0.60
MSCC-BG-S-E2/3-SX	HWB9/HWB21	0.60	0.90	1.30	1.60	0.60
MSCC-TG-P/M-E1-SX	HWB10/HWB22	0.60	0.90	1.10	1.50	0.60
MSCC-IG-S/M-E1-SX						
MSCC-BG-M-E1-SX						
MSCC-SL-P-EX-SX						
MSCC-TG-P/M-E2/3-SX	HWB11/HWB23	0.90	0.90	1.10	1.50	0.60
MSCC-IG-S/M-E2/3-SX						
MSCC-BG-M-E2/3-SX						

Note: X stands for all possible combinations pertinent to the attribute under consideration

**Figure 6.15:** Comparison of median values of system fragility for MSCC-BG-S-E3 based on the present study and HAZUS

The following are some of the trends based on comparison:

- Bridges with diaphragm abutments are found to be more vulnerable than predicted by HAZUS, which does not distinguish this feature. The degree of vulnerability is higher for MCBs when compared to SCBs.
- Bridges with seat abutments and SCBs are more vulnerable relative to HAZUS at the BSST-0 and BSST-1 damage states while the trend reverses for the BSST-2

and -3 damage states where HAZUS predicts the bridge class to be more vulnerable.

- Bridges with seat abutments and MCBs are found to be more vulnerable than predicted by HAZUS.

The procedure of comparing the median values of the fragility at the system level is repeated for all of the bridge classes and the respective SPS across the design eras and the trends are summarized below. The percentage change in median values with respect to HAZUS is calculated in each case where a positive change in the median value indicates a less vulnerable bridge while a negative value indicates a more vulnerable bridge. These values are reported in Appendix E. In all cases, the bridges in this study are found to be more vulnerable than that predicted by HAZUS for the lower bridge system damage states, BSST-0 and BSST-1. This is mainly due to the contribution of the secondary components which account for the vulnerability at these lower damage states, which are perceived to necessitate repair.

- MSCC-BG bridges with SCBs and MCBs having both seat and diaphragm abutments in the pre 1971 and 1971-1990 design eras are more vulnerable than that predicted by HAZUS. The change in median values is very high for BSST-0 and -1 damage states when compared to the higher damage states in the bridge. In the post 1990 design era, MSCC-BG bridges with diaphragm abutments are more vulnerable than that predicted by HAZUS. The same is the case with MCBs and seat abutments. However, based on the results of this study, SCBs and seat abutments are less vulnerable than that predicted by HAZUS for the higher damage states BSST-2, and BSST-3. The dispersions obtained from the present study are close to the HAZUS values but are systematically lower for all the bridge classes considered in this study.
- The fragilities for MSCC-SL bridge class indicate that they are more vulnerable than those presented by HAZUS. The percentage change in the median values is

as high as 50% for the higher bridge damage states. The average dispersion is about 0.7 which is roughly 17% higher than the HAZUS prescribed value.

- MSCC-TG bridges with integral pile columns and traditional MCBs in the pre 1971 design era are more vulnerable than that predicted by HAZUS. In the 1971-1990 and post 1990 design eras, traditional MCBs are less vulnerable than that predicted by HAZUS. However, the integral pile columns in the 1971-1990 and post 1990 design eras are much more vulnerable (about 60% lower median value of the fragilities) than that predicted by HAZUS. The dispersions for this bridge class are generally found to be lower than that predicted by HAZUS, particularly for the integral pile columns.
- The results from this study indicate that MSCC-IG bridges in the pre 1971 design era are more vulnerable than that predicted by HAZUS. However, the SCBs in the 1971-1990 and post 1990 are less vulnerable and the percentage change in median values is as high as 160% in the case of MSCC-IG-S-E3-S4. The MCBs in the 1971-1990 design era are more vulnerable than that predicted by HAZUS, however, the trend is reversed in the case of post 1990 design era MCBs. In short, the post 1990 bridge fragilities from this study reveal much lower vulnerability than that predicted by HAZUS. The dispersions calculated in this study are lower than that proposed in HAZUS in a majority of the SPS for this bridge class.

6.6 Closure

Bridge component and system level seismic fragility curves are generated and presented for four multispan continuous concrete bridge classes with several seismic performance sub-bins across three significant design eras considered in this study. The curves are generated using Monte Carlo simulation by comparing realizations of the joint probabilistic seismic demand models with realizations of the capacity models, discussed in the previous chapter.

The following are some of the significant findings of this chapter:

- The vulnerability of all the bridge classes reduced with the evolution of column and ductile design philosophy and seat widths across the design eras considered.
- MSCC-BG bridges are the most fragile in the pre 1971 design era in comparison to the other bridge classes considered in this study. The multi column bents (MCB) are more vulnerable when compared to the single column bents (SCB).
- In the 1971-1990 design era, MSCC-BG bridges with MCBs and diaphragm abutments are the most vulnerable bridges followed by their seat abutment counterparts. MSCC-IG bridges with diaphragm abutments are the most vulnerable considering SCBs.
- MSCC-TG bridges with integral pile columns and seat abutments are the most fragile among the modern day bridges followed by MSCC-BG bridges with MCBs and diaphragm abutments.
- Across bridge classes and design eras, in general it was seen that SCBs and diaphragm abutments are relatively less vulnerable when compared to MCBs and seat abutments, barring a few exceptions.
- Comparison with HAZUS fragilities revealed the wide disparity between the results of the present study and the values prescribed in HAZUS. The results from this study indicate that a majority of the SPS in the pre 1971 and 1971-1990 design eras are more vulnerable than that predicted by HAZUS. However, the SPS in modern day bridges are less vulnerable than predicted by HAZUS in a majority of cases. Discrepancies with HAZUS are likely due to the mechanical analyses technique used to define component response distributions, system reliability definition, capacity models or damage state definitions, to mention a few.

CHAPTER 7

CONCLUSIONS AND FUTURE WORK

7.1 Summary and Conclusions

Quantification of the seismic performance of engineered structures using metrics that are readily understood and deployed by engineers, stake holders and policy makers in the decision-making framework is the fundamental aim of performance-based earthquake engineering. Bridges form the critical link in the highway infrastructure system and play a significant role in post earthquake response and recovery. Vulnerability estimation as well as quantitative and qualitative assessment of the seismic risk to highway bridges is therefore crucial in obtaining reliable estimates of the resilience of highway transportation systems. Fragility curves, which furnish the probabilities of exceeding user specified damage states or performance levels as a function of a ground motion intensity measure, have found widespread use in the area of seismic risk assessment. With the increased awareness of the high seismic hazard in California, potential vulnerabilities associated with the bridge classes and the high investments required for new construction, maintenance and retrofit, reliable estimation and quantification of the seismic risk is important which requires sufficiently accurate and reliable fragility relationships, which is the main objective of this study.

The 1971 San Fernando, 1989 Loma Prieta, and 1994 Northridge earthquakes in California motivated significant research on the seismic response, analysis, and design philosophy of bridges. These earthquakes resulted in collapse or major damage to many bridges that were at least nominally designed for seismic forces. Following the San Fernando earthquake, which exposed major deficiencies in bridges at that time, the elastic bridge design philosophy was significantly modified with a major focus on ductility and

inelasticity and special attention to detailing aspects. The Loma Prieta and Northridge earthquakes furthered this approach when significant damage was observed in bridges constructed prior to 1971. A majority of the bridges constructed after 1971 performed relatively well demonstrating the superiority of the improved design and retrofitting philosophy. In line with the temporal evolution of seismic design philosophy marked by the three design eras, pre 1971, 1971-1990, and post 1990, this study is devoted to developing fragility relationships for multispan concrete bridge classes in California capturing the unique design and detailing attributes pertinent to them.

A major task in the current research was to seek an understanding of the highway bridge inventory and capture the trends pertaining to the changes in design and detailing aspects of various bridge components across the three design eras. These include dimensions and reinforcement layout in columns, chronology of seat widths at the abutments and the bent, abutment types, foundation types, pile classes, restrainers and shear key attributes, to mention a few. Four multispan bridges classes, box-girders (MSCC-BG), slabs (MSCC-SL), Tee-girders (MSCC-TG) and I-girders (MSCC-IG) were identified and used for the development of fragility curves. In addition to the basic geometric information, such as span length, deck width, column height, and number of spans made available through the National Bridge Inventory (NBI), extensive details about the aforementioned bridge components and their respective evolutionary design features were obtained based on an extensive review of bridge plans and the California Department of Transportation (Caltrans) in-house databases. The characterization of this type of variability and its incorporation into the fragility formulation not only makes the resulting fragility models applicable to a wide geographic area, but also leads to the creation of improved bridge class sub-bins with consistent performance.

Three dimensional parameterized stochastic finite element models were developed using the finite element platform, OpenSEES. The models incorporate a high degree of detail with respect to the component modeling strategies and their ability to

capture damage due to the imposed seismic demand. Deterministic analyses of the bridge models were conducted to be used as a sanity check and study the relative response of bridge components to suggest criticalities and dynamic characteristics. An important conclusion was that columns are not always the critical components as perceived by some of the previous researchers. Significant damage can be expected to other components such as abutments, shear keys, and elastomeric bearing pads and neglect of these components in determining the vulnerability of the bridge system might not be appropriate. This is particularly important when using fragility curves for determining post earthquake repair and retrofit strategies, as in the present case, where exclusion of components other than columns might lead to damage in them being undetected.

A multiphase framework for the development of analytical fragility curves was described. Details about various parts of the framework including assembly of a ground motion suite, conducting nonlinear time history analysis (NLTHA), development of probabilistic seismic demand models (PSDM), definition of capacity models (or limit state models), formulation of component and bridge system level fragility curves was presented. A suite of 320 ground motions, 160 unscaled and 160 scaled (factor of two) ground motions assembled by Baker et al. (2011) were used in conducting NLTHA on bridge models capturing a wide range of geometric and material uncertainties, to aid in the development of PSDMs. In order to identify the optimal intensity measure (IM) to characterize component demands, an investigation was conducted on four commonly adopted and hazard computable IMs: peak ground acceleration, PGA, spectral acceleration (S_a) at 0.2 sec period, $S_a(0.2)$, $S_a(0.3)$ and $S_a(1.0)$. Metrics such as efficiency, practicality, sufficiency, and proficiency were tested and $S_a(1.0)$ was identified as the optimal IM for probabilistic seismic demand modeling and fragility analysis of typical classes of California bridges.

A significant contribution of the present study was providing damage state definitions for the components derived in such a way that they align with the Caltrans

design and operational experience. This will facilitate the application of the generated fragility curves in assessing repair and operational consequences in the aftermath of an earthquake, which is the intent of the present research. Components were grouped as primary and secondary in such a way that the component level damage has similar consequences at the bridge system level in terms of closure and repair implications. Threshold values of engineering demand parameters (EDPs) consistent with those used in the formulation of PSDMs, were identified by drawing upon the literature and expertise of Caltrans design and maintenance professionals to describe the capacity models. Typical repair strategies and visible damage patterns consistent with the EDP threshold limit states values were also identified to facilitate correlation and observations in the field. Bridge component and system level fragility curves were obtained for the bridge classes and their respective seismic performance sub-bins based on the convolution of the demand and capacity models. Specifically system level fragility relationships were developed using Monte Carlo simulations and joint probabilistic seismic demand models (JPSDMs) with correlation between components considered.

Many of the key contributions of the study lie in the insights gleaned from the fragility analysis of the California bridge classes across the three design eras. The following are some of the notable findings from the fragility analysis:

- The vulnerability of all the bridge classes reduced with the evolution of column design philosophy and progressively increasing seat widths across the design eras considered.
- Multispan continuous concrete box-girder bridges with multi column bents (MCBs) and seat abutments were the most fragile in the pre 1971 design era, while MSCC-BG bridges with MCBs and diaphragm abutments are the most fragile in the 1971-1990 design era. MSCC-TG bridges with integral pile column bents and seat abutments are the most vulnerable among the modern day bridge classes.

- Across bridge classes and design eras, it was revealed that single column bents (SCBs) and diaphragm abutments are the least vulnerable.
- Comparison with HAZUS fragilities revealed the wide disparity between the results of the present study and the values prescribed in HAZUS. The results from this study indicate that a majority of the seismic performance sub-bins in the pre 1971 and 1971-1990 design eras are more vulnerable than that predicted by HAZUS. However, the seismic performance sub-bins in modern day bridge classes are less vulnerable than predicted by HAZUS in a majority of cases. Discrepancies with HAZUS are likely due to the structural modeling and analyses techniques used in the demand analysis, system reliability definition, capacity models or damage state definitions, to mention a few.

The results from this research across bridge classes underscored the necessity to capture various attributes that are not currently documented in the NBI or the state databases. Clearly, the evolution of seismic design philosophy had a profound impact on the reduction of vulnerability in the modern day bridges in comparison to their pre 1971 counterparts by as high as 60% in some cases. This stresses the need to capture unique design details and sub-bin bridge classes beyond their current classification in the NBI and HAZUS. Several other attributes such as the type of abutment (diaphragm versus seat), type of bent (single versus multi-column), foundation type (pile shafts versus pile group with a pile cap), and range of seat widths significantly affected the vulnerability. This stresses the need to capture these attributes in the NBI and state databases in order to be able to better classify the bridge classes akin to the classification in the present study and obtain reliable estimates of the vulnerability.

7.2 Research Impact

This study presented a rigorous probabilistic performance assessment framework to develop analytical seismic fragility curves for common concrete bridge classes in California. This resulted in a significant number of contributions which are as follows:

- An enhanced understanding of the evolution of seismic design philosophy along with a capture of trends in the design and detailing of several bridge components such as columns, seat widths, abutment and foundation types, and superstructure to substructure connectivity issues, over three significant design eras: pre 1971, 1971-1990, and post 1990 separated by the historic 1971 San Fernando and 1989 Loma Prieta California earthquakes.
- Modeling considerations and detailed formulations of three dimensional nonlinear finite element bridge models depicting the common Californian bridge classes. Extensive details regarding the variability in geometric and material properties across the bridge classes based on extensive review of bridge plans and Caltrans in-house databases.
- A detailed perspective on the component level damage states along with threshold values of engineering demand parameters, visible damage indicators, repair strategies and their implications on the bridge system level repair and traffic consequences consistent with Caltrans' perspective. This is particularly relevant in the field of post-earthquake inspection and management, where fragility curves are used in risk assessment and situational awareness packages such as ShakeCast or REDARS.
- Development of fragility curves considering the vulnerability of multiple components will facilitate stake holders and decision makers in the prioritization and selection of retrofit strategies based on performance metrics or cost-effectiveness strategies.

- The first systematic approach in sub-binning bridge classes based on the evolution of seismic design philosophy and developed fragility curves for each of these sub-bins considering variations in the bent type, abutment type, and range of seat widths. This leads to the development of improved sub-bins within a bridge class with consistent design and performance features in contrast to some of the previous studies that combine all the characteristics into a single bridge class.
- Fragility analysis reveal significant differences in vulnerability across the design era based sub-bins for the same bridge class. Further, differences are observed within the same sub-bin for attributes such as bent, abutment, and foundation types, to mention a few. This underscores the necessity to account for the creation of sub-bins based on design features as well as accounting for various attributes such as bent, abutment and foundation type.

7.3 Recommendations for Future Work

There are several potential arenas in which the present research can be extended.

A few of these are described below:

- This study looked at the vulnerability assessment of straight and non-skewed bridges with a fixed number of spans (equal to the mode statistic obtained from the inventory analysis of the NBI data). HAZUS-MH provides median value modification factors to account for the effect of skew and number of spans and these were based on simplified static analyses. This warrants a thorough investigation, validation, and if necessary a revision to these equations by incorporating dynamic effects and three dimensional modeling strategies. Also the effect of curvature on the median fragilities should be studied, since a majority of highway interchanges have curved superstructure configurations.
- A majority of bridges with more than five spans have in-span hinges which lead to significant differences in the bridge dynamic behavior. Bridges with

intermediate hinges have evolved in their design philosophy which is unique in its consideration of balanced frame design approaches. This study should be extended to bridges with intermediate hinges and equations should be developed to modify the median fragilities akin to the modification factors for skew and number of spans.

- The sub-binning strategy should be extended to steel bridge classes capturing the evolution of seismic design philosophy in the design and detailing of steel connections, intermediate diaphragm and steel bearings, to mention a few in addition to the components captured in the present study.
- Bridge foundations and abutments may be founded on liquefiable soil and significant damage can be seen in regions with high seismic hazard. Methodologies incorporating the effect of liquefaction and ground deformation hazard through the use of macro-elements or p-y soil springs should be integrated in the fragility formulation presented in this study.
- Another area of bridge system investigations identified is a rational evaluation of costs and benefits of enhanced performance bridge structural elements and response modification devices such as base isolators, elastomeric isolation bearings, column retrofits, to mention a few. Rigorous application of the framework across the sub-bins with the potential retrofits against a complete bridge replacement using modern day design principles would enable a direct comparison of the total life cycle costs of new designs to their retrofit counterparts. Such comparisons will facilitate the understanding of effectiveness of new designs as well as the identification of new technologies and potential retrofits aimed at improved bridge performance and cost effectiveness.
- Another important aspect that deserves attention is the loss of capacity of bridge components resulting from degradation or cumulative damage due to repeated seismic events. This is of particular relevance in geographical areas where

bridges experience several mainshock-aftershock sequences, where no research is done considering the cumulative effect of multiple shocks on the load carrying capacity of bridges and this deserves a thorough investigation.

- In line with the preceding discussion, it is fairly important to consider deterioration in the component capacities due to factors such as aging and deterioration due to spalling of reinforced concrete, build of debris leading to corrosion of bridge components such as steel bearings, corrosion of the column longitudinal reinforcement etc. This is of particular significance now that more than one half of the nations' bridges are approaching the end of their design life and nearly a quarter need significant retrofit or replacement to eliminate the existing deficiencies according to published reports from the American Society of Civil Engineers (ASCE, 2009).

APPENDIX A

COMPONENT ATTRIBUTES AND MODELING ASSUMPTIONS

This Appendix is devoted to presenting details for the bridge classes to aid in the development of finite element models used for fragility analysis. The details are obtained based on an extensive review of bridge plans across the three significant design eras chosen in this study, and Caltrans in-house documents. Section A.1 presents details about attributes that are common to all bridge classes. For every bridge class, a table of modeling assumptions along with specific bridge component information is presented in the subsequent sections.

A.1 Attributes Common to all Bridge Classes

Details such the spacing of the abutment piles, soil profiles adopted in the determination of foundation translation and rotational springs are common to all the bridge classes and these are documented in this section.

A.1.1 Common Soil Profiles

The soil profile changes vastly over a wide geographic area and the stiffness of the foundation translation and rotational springs depends on the soil profile at a particular location. In order to obtain realistic estimates of bridge performance within a class, it is imperative to capture a wide range of soil profiles. Other factors such as the type of foundation system, end conditions of the columns (pinned vs. restrained) and column details (size and reinforcement) affect the stiffness of the foundation springs. The different foundation systems and the soil profiles are modeled and analyzed in LPILE and Table 5.2 in Chapter 5 summarized the parameters for the truncated normal distribution

describing the stiffness of the foundation translation and rotational springs. Typical soil profiles considered in the calculation of stiffnesses are presented in Table A.1.

Table A.1: Soil profiles considered in the stiffness calculations

Foundation type		<u>Integral pile columns</u>			
Soil profile		Soft	Depth of water table – 3 ft		
Description	Depth (ft)	Soil type	S_u (psf)*	ϕ^*	γ (psf)*
	0 – 7	Clay	300	-	95
	7 – 17	Clay	600	-	100
	17 – 24	Sand	-	37	129
Soil profile		Stiff	Depth of water table – 30 ft		
Description	Depth (ft)	Soil type	S_u (psf)	ϕ	γ (psf)
	0 – 15	Sand	0	38	127
	15 – 43	Sand	0	40	130
Foundation type		<u>Spread footing (pile cap) with piles</u>			
Soil profile		Soft	Depth of water table – 3 ft		
Description	Depth (ft)	Soil type	S_u (psf)	ϕ	γ (psf)
	0 – 7	Clay	300	-	95
	7 – 17	Clay	600	-	100
	17 – 24	Sand	-	37	129
	24 – 48	Clay	1500	-	110
	48 – 58	Sand	-	36	130
	58 – 85	Sand	-	39	130
Soil profile		Stiff	Depth of water table – 30 ft		
Description	Depth (ft)	Soil type	S_u (psf)	ϕ	γ (psf)
	0 – 15	Sand	0	36	127
	15 – 41	Sand	0	38	130
	41 – 85	Sand	0	42	130

* S_u denotes the undrained shear strength, ϕ the angle of internal friction, and γ the unit weight

A.1.2 Typical Footing Configurations

Details of the typical footing configuration based on the soil profile and bridge column framing into it is described in Table A.2. It must be noted that MSCC-SL bridges employ integral pile columns. MSCC-TG bridges also employ integral pile columns in addition to traditional multi column bents (MCBs). Standard pile details were provided in section 4.3.2.1 (also see Figure 4.23) of Chapter 4. However, in the case of MSCC-BG and MSCC-IG bridges with MCBs, the foundation consists of a pile cap with a group of

piles underneath the columns. The same is the case with MSCC-IG with SCBs. MSCC-BG bridges with SCBs employ pile shafts as well as a system of pile cap and a group of piles. Details are presented in Table A.2.

Table A.2: Details of foundation systems

Bridge class	Column details	Soil profile	Foundation details
MSCC-BG MSCC-IG	6 ft dia. column – 1% long. steel	Soft	14 ft × 14 ft pile cap with 8 nos. of 24-in precast prestressed piles
		Stiff	15 ft × 15 ft pile cap with 16 nos. of 16-in precast prestressed piles
MSCC-BG MSCC-IG	6 ft dia. column – 3% long. steel	Soft	18 ft × 18 ft pile cap with 9 nos. of 24-in precast prestressed piles
		Stiff	16 ft × 14 ft pile cap with 20 nos. of 16-in precast prestressed piles
MSCC-BG MSCC-IG MSCC-TG	3 ft dia. column – 1.5% long. steel	Soft	9 ft × 9 ft pile cap with 6 nos. of 14×89 steel H section piles
		Stiff	10 ft × 10 ft pile cap with 6 nos. of 10-in cast-in-place concrete piles

A.1.3 Spacing of the Abutment Piles

Bridge Design Aids (BDA) 4-10 (2009) gives details about the pile spacing (shown in Figure A.1) depending on the pile class, typical bridge layout and support type (shown in Figure A.2), and span length.

ABUTMENT		Support Type	Length of Span "L"															
			16	18	20	22	24	26	28	30	32	34	36	38	40	42	44	
45T Pile Spacing*	I		9	8 3/4	8 1/2	8 1/4	8	8	7 3/4	7 1/2	7 1/4	7	6 3/4	6 1/2	6 1/4	6	5 3/4	
70T Pile Spacing*	I								12	11 1/2	11 1/4	11	10 1/2	10	9 3/4	9 1/4	9	
45T Pile Spacing*	IV		9 3/4	9 1/2	9 1/4	9	8 3/4	8 3/4	8 1/2	8 1/4	8	8	7 3/4	7 1/2	7 1/4	7	6 3/4	
70T Pile Spacing*	IV																	
45T Pile Spacing*	VII		8 1/2	8	7 3/4	7 1/2	7 1/4	7	6 3/4	6 1/2	6 1/4	6	5 3/4	5 1/2	5 1/4	5	4 3/4	
70T Pile Spacing*	VII					11 3/4	11 1/2	11	10 1/2	10	9 3/4	9 1/4	9	8 1/2	8	7 3/4	7 1/4	

Figure A.1: Typical abutment pile spacing (BDA 4-10, 2009)

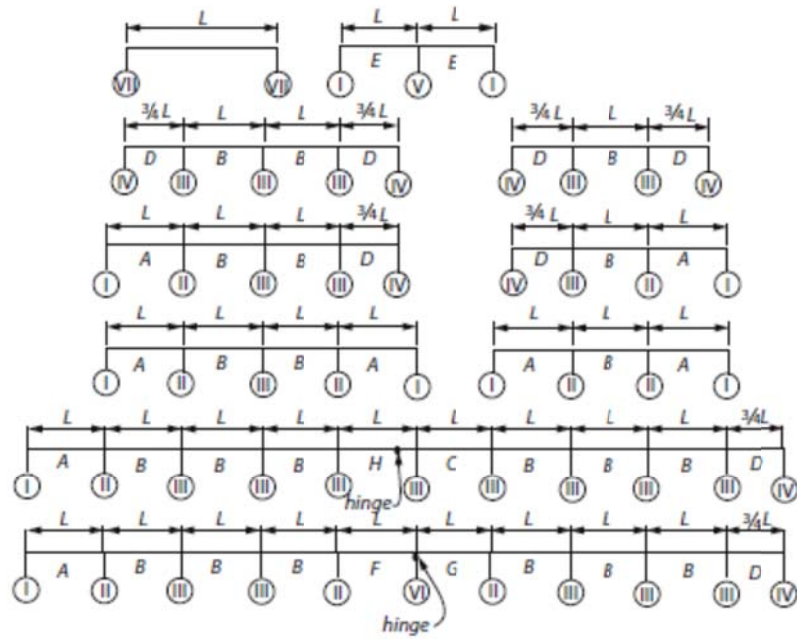


Figure A.2: Typical bridge layout to determine support type (BDA 4-10, 2009)

A.2 Multispan Continuous Concrete Box-girder Bridges

Table A.3: Bridge component details for MSCC-BG bridge class and its seismic performance sub-bins

Attribute	MSCC-BG bridge class		
	Pre 1971	1971-1990	Post 1990
<u>Superstructure</u>			
Number of spans	2	2	2
	This is the mode statistic based on inventory analysis		
Center span (ft)	90.0 – 180.0	90.0 – 180.0	90.0 – 180.0
Center/Edge span length	1.0	1.0	1.0
Deck width(ft)			
Minimum	25	30	30
Maximum	60	120	130
<u>Box-girder details</u>			
Top flange thickness (in)	See Table A.4		
	Note that this value can be decided only after determining the number of boxes and c/c spacing		
Bottom flange thickness	6.0	6.5	7.0
Wall thickness (in)	12.0	12.0	12.0
Overall girder depth	Proportioned based on typical depth-to-span ratios: Cast-in-place reinforced concrete: 0.055 Cast-in-place prestressed concrete: 0.04		
Min. number of boxes	3	3	3
Max. number of boxes	5	12	15
Number of boxes	See Table A.5		
	Having picked the number of boxes based on bridge width, the girder c/c distance is picked from Table A.1		
<u>Elastomeric bearing pad</u>			
Span ≤ 130 ft	14'' × 14'' × 2.5''	14'' × 14'' × 2.5''	14'' × 14'' × 2.5''
Span > 130 ft	20'' × 14'' × 2.5''	20'' × 14'' × 2.5''	20'' × 14'' × 2.5''
<u>Columns</u>			
<u>Diameter (ft)</u>			
Single column bent	6	6	7
Multi column bent	4	5	5 (2, 3, 4 col/bent) 4 (5 col/bent)
Long. reinf. ratio (%)	1.4 – 2.4	1.0 – 3.7	1.0 – 3.5
Tran. reinf. ratio (%)	#4 @ 12 in. o.c.	0.3 – 0.9	0.4 – 1.7
Number of columns per bent	See Table A.5		
<u>Foundation</u>			
Single column bent	Pile shaft + Pile cap with pile group	Pile shaft + Pile cap with pile group	Pile shaft + Pile cap with pile group
Multi column bent	Pile cap with pile group	Pile cap with pile group	Pile cap with pile group
	See Table 5.2 in Chapter 5 for foundation spring stiffnesses		

Abutments			
Backwall height (ft)	3.50 – 8.50	3.50 – 8.50	3.50 – 8.50
Pile spacing	See Figure A.2	See Figure A.2	See Figure A.2

Table A.4: Box-girder cell center-to-center spacing and deck slab thickness (MTD 10-20, 2008)

Reinforced concrete box-girders

REINFORCED CONCRETE BOX & STEEL GIRDERS w/ flange width >12" and < 24"						
"S"	"F"	Dimension	Transverse Bars	"D" Bars	"G" Bars	
Girder CL to CL Spacing	Top Slab Thickness	"F"	Size Spacing ¹	#5 Bars	#4 Bars	
4'-0"	7"	6"	#5 12"	3	2	
4'-3"	7"	6"	#5 12"	3	2	
4'-6"	7"	6"	#5 12"	3	2	
4'-9"	7"	7"	#5 12"	3	2	
5'-0"	7"	7"	#5 12"	4	2	
5'-3"	7"	7"	#5 12"	4	3	
5'-6"	7"	8"	#5 12"	4	3	
5'-9"	7"	8"	#5 11"	4	3	
6'-0"	7 1/8"	9"	#5 11"	5	3	
6'-3"	7 1/8"	9"	#5 11"	5	3	
6'-6"	7 1/4"	9"	#5 11"	5	3	
6'-9"	7 3/8"	10"	#5 11"	5	3	
7'-0"	7 1/2"	10"	#5 10"	6	3	
7'-3"	7 1/2"	11"	#5 10"	6	3	
7'-6"	7 5/8"	11"	#5 10"	6	3	
7'-9"	7 3/4"	11"	#5 10"	6	3	
8'-0"	7 3/4"	1'-0"	#5 10"	7	3	
8'-3"	7 7/8"	1'-0"	#5 10"	7	4	
8'-6"	8"	1'-1"	#5 10"	7	4	
8'-9"	8 1/8"	1'-1"	#5 10"	7	4	
9'-0"	8 1/8"	1'-1"	#5 10"	7	4	
9'-3"	8 1/4"	1'-2"	#5 10"	8	4	
9'-6"	8 3/8"	1'-2"	#5 10"	8	4	
9'-9"	8 3/8"	1'-2"	#5 10"	8	4	
10'-0"	8 1/2"	1'-3"	#6 12"	10	4	
10'-3"	8 5/8"	1'-3"	#6 11"	11	4	
10'-6"	8 5/8"	1'-4"	#6 11"	11	4	
10'-9"	8 3/4"	1'-4"	#6 11"	11	4	
11'-0"	8 7/8"	1'-4"	#6 11"	11	4	
11'-3"	8 7/8"	1'-5"	#6 11"	12	5	
11'-6"	9"	1'-5"	#6 11"	12	5	
11'-9"	9 1/8"	1'-6"	#6 11"	12	5	
12'-0"	9 1/8"	1'-6"	#6 10"	13	5	
12'-3"	9 1/4"	1'-6"	#6 10"	13	5	
12'-6"	9 3/8"	1'-7"	#6 10"	13	5	
12'-9"	9 1/2"	1'-7"	#6 10"	14	5	
13'-0"	9 1/2"	1'-7"	#6 10"	14	5	
13'-3"	9 5/8"	1'-8"	#6 10"	14	5	
13'-6"	9 3/4"	1'-8"	#6 10"	14	5	
13'-9"	9 3/4"	1'-9"	#6 10"	14	5	
14'-0"	9 7/8"	1'-9"	#6 10"	14	5	
14'-3"	10"	1'-9"	#6 10"	14	5	
14'-6"	10 1/8"	1'-10"	#6 10"	15	5	
14'-9"	10 1/4"	1'-10"	#6 10"	15	5	
15'-0"	10 3/8"	1'-11"	#6 10"	15	5	

Prestressed concrete box-girders

CIP PRESTRESSED BOX, PRECAST-I, & STEEL GIRDERS w/ flange width >=24"						
"S"	"F"	Dimension	Transverse Bars	"D" Bars	"G" Bars	
Girder CL to CL Spacing	Top Slab Thickness	"F"	Size Spacing ¹	#5 Bars	#4 Bars	
4'-0"	7"	5"	#5 12"	3	2	
4'-3"	7"	5"	#5 12"	3	2	
4'-6"	7"	6"	#5 12"	3	2	
4'-9"	7"	6"	#5 12"	3	2	
5'-0"	7"	6"	#5 12"	3	2	
5'-3"	7"	7"	#5 12"	3	2	
5'-6"	7"	7"	#5 12"	4	2	
5'-9"	7"	7"	#5 12"	4	3	
6'-0"	7"	8"	#5 12"	4	3	
6'-3"	7"	8"	#5 12"	4	3	
6'-6"	7 1/8"	9"	#5 12"	4	3	
6'-9"	7 1/8"	9"	#5 11"	5	3	
7'-0"	7 1/4"	9"	#5 11"	5	3	
7'-3"	7 3/8"	10"	#5 11"	5	3	
7'-6"	7 1/2"	10"	#5 11"	5	3	
7'-9"	7 1/2"	11"	#5 11"	5	3	
8'-0"	7 5/8"	11"	#5 11"	6	3	
8'-3"	7 3/4"	11"	#5 11"	6	3	
8'-6"	7 3/4"	1'-0"	#5 11"	6	3	
8'-9"	7 7/8"	1'-0"	#5 11"	6	4	
9'-0"	8"	1'-1"	#5 11"	6	4	
9'-3"	8 1/8"	1'-1"	#5 11"	7	4	
9'-6"	8 1/8"	1'-1"	#5 11"	7	4	
9'-9"	8 1/4"	1'-2"	#5 10"	8	4	
10'-0"	8 3/8"	1'-2"	#5 10"	8	4	
10'-3"	8 3/8"	1'-2"	#5 10"	8	4	
10'-6"	8 1/2"	1'-3"	#5 10"	8	4	
10'-9"	8 5/8"	1'-3"	#5 10"	8	4	
11'-0"	8 5/8"	1'-4"	#6 11"	11	4	
11'-3"	8 3/4"	1'-4"	#6 11"	11	4	
11'-6"	8 7/8"	1'-4"	#6 11"	11	4	
11'-9"	8 7/8"	1'-5"	#6 11"	12	5	
12'-0"	9"	1'-5"	#6 11"	12	5	
12'-3"	9 1/8"	1'-6"	#6 11"	12	5	
12'-6"	9 1/8"	1'-6"	#6 11"	12	5	
12'-9"	9 1/4"	1'-6"	#6 11"	12	5	
13'-0"	9 3/8"	1'-7"	#6 10"	13	5	
13'-3"	9 1/2"	1'-7"	#6 10"	14	5	
13'-6"	9 1/2"	1'-7"	#6 10"	14	5	
13'-9"	9 5/8"	1'-8"	#6 10"	14	5	
14'-0"	9 3/4"	1'-8"	#6 10"	14	5	
14'-3"	9 3/4"	1'-9"	#6 10"	14	5	
14'-6"	9 7/8"	1'-9"	#6 10"	14	5	
14'-9"	10"	1'-9"	#6 10"	14	5	
15'-0"	10 1/8"	1'-10"	#6 10"	15	5	

Table A.5: Number of cells in the box-girder and number of columns per bent as a function of deck width for MSCC-BG bridges

a) Pre 1971 design era			b) 1971-1990 design era		
# boxes	# columns	Width range (ft)	# boxes	# columns	Width range (ft)
3	1	Upto 40	3	1	Upto 40
5	2	> 40	5	2	40 – 60
			7	3	60 – 80
			9	3	80 – 100
			11	4	> 100

c) Post 1990 design era		
# boxes	# columns	Width range (ft)
3	1	Upto 40
5	2	40 – 60
7	3	60 – 80
9	4	80 – 100
11	5	100 – 120
15	5	> 120

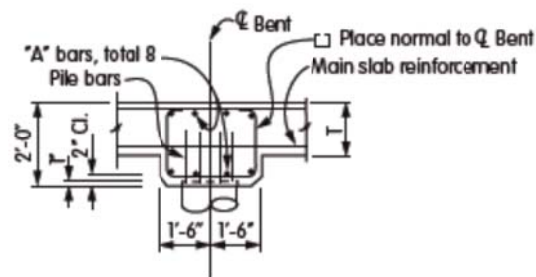
A.3 Multispan Continuous Concrete Slab Bridges

Table A.6: Bridge component details for MSCC-SL bridge class

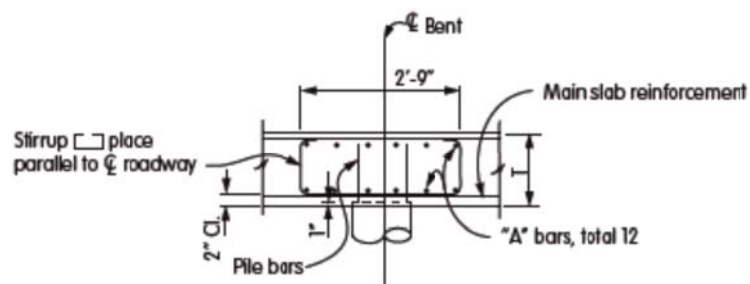
Attribute	Values
<u>Superstructure</u>	
# of spans	3
Center span (ft)	16.0 – 50.0
Center/Edge span length	1.2
Deck width (ft)	≥ 35.0
Slab thickness	$Thickness = \max\left[\frac{S + 10}{30}, 0.542\right]$
S is the maximum span length (ft)	
This is tabulated in Figure A.3	
Elastomeric bearing pads	16" \times 12" \times 1.5"
<u>Columns</u>	
Integral pile columns – See section 4.3.2.1 in Chapter 4 for details	
Center-to-center spacing	See Figure A.1
Number of columns per bent	$Number\ of\ columns / bent = \frac{Width - 2y}{pile\ spacing} + 1$
y is the edge distance and is assumed to be 0.4 \times pile spacing	
Bent cap details	The presence of bent cap depends on the span length. Details about the bent cap dimensions and the reinforcement layout is shown in Figure A.4.
<u>Foundation</u>	
Integral pile columns	
<u>Abutments</u>	
Backwall height (ft)	3.5 – 8.5
Pile spacing	See Figure A.2

L=Length of Span			16'	18'	20'	22'	24'	26'	28'	30'	32'	34'	36'	38'	40'	42'	44'	
REINFORCEMENT	Top of Slab bars	Ⓐ	Size	#7	#7	#7	#7	#8	#8	#8	#9	#9	#9	#10	#10	#10	#10	
		Length(l)	34.0'	38.0'	42.0'	46.0'	50.0'	54.0'	58.0'	74.0'	78.0'	82.0'	90.0'	94.0'	98.0'	102'	106'	
		Ⓑ	Size	#7	#7	#7	#7	#7	#8	#8	#8	#9	#9	#9	#10	#10	#10	#10
		Length	12.0'	13.0'	15.0'	16.0'	17.0'	18.0'	19.0'	15.0'	16.0'	17.0'	18.0'	19.0'	20.0'	20.0'	21.0'	
		Xb	6.0'	6.5'	7.5'	8.0'	8.5'	9.0'	9.5'	7.5'	8.0'	8.5'	9.0'	9.5'	10.0'	10.0'	10.5'	
		Ⓒ	Size	#7	#7	#7	#7	#7	#7	#8	#8	#8	#9	#9	#9	#9	#9	#10
	Bottom of Slab bars	Length	6.0'	6.0'	6.0'	7.0'	7.0'	8.0'	8.0'	9.0'	11.0'	11.0'	11.0'	11.0'	12.0'	12.0'	14.0'	
		Xc	3.0'	3.0'	3.0'	3.5'	3.5'	4.0'	4.0'	4.5'	5.5'	5.5'	5.5'	5.5'	6.0'	6.0'	7.0'	
		Ⓓ	Size	#7	#7	#7	#8	#8	#8	#8	#8	#9	#9	#9	#9	#9	#9	#9
		Length(l)	36.0'	40.0'	44.0'	48.0'	52.0'	56.0'	60.0'	68.0'	72.0'	78.0'	82.0'	86.0'	90.0'	94.0'	98.0'	
		Ⓔ	Size	#7	#7	#7	#7	#7	#8	#8	#8	#8	#8	#8	#9	#9	#9	#9
		Length	16.5'	18.0'	20.0'	19.5'	21.0'	23.0'	24.5'	26.0'	27.5'	29.5'	31.0'	32.5'	34.5'	36.0'	37.5'	
		Xe	0.5'	1.0'	1.0'	3.5'	4.0'	4.0'	4.5'	5.0'	5.5'	5.5'	6.0'	6.5'	6.5'	7.0'	7.5'	
		Ⓕ	Size	#7	#7	#7	#7	#7	#7	#7	#8	#8	#8	#8	#8	#8	#9	#9
		Length	12.0'	13.0'	14.5'	15.5'	17.0'	18.0'	19.0'	20.5'	22.0'	23.0'	24.5'	26.0'	27.5'	28.5'	30.0'	
X†	3.5'	4.5'	5.0'	5.5'	6.0'	6.5'	7.0'	8.0'	8.5'	9.0'	9.5'	10.0'	10.5'	11.0'	11.5'			
Distribution Steel			Size	#5	#5	#5	#5	#5	#5	#5	#5	#5	#5	#5	#5	#5		
Top of Slab			Spacing	12"	12"	12"	12"	12"	12"	12"	12"	12"	12"	12"	12"	12"		
Transverse Reinforcement			Size	#4	#4	#4	#4	#4	#4	#4	#4	#5	#5	#5	#5	#5		
T= Thickness of Slab(2)			Spacing	18"	18"	18"	15"	15"	15"	12"	12"	18"	18"	15"	15"	15"		
T= Thickness of Slab(2)				10 1/8"	11 1/8"	12"	13"	14"	14 1/2"	15 1/2"	16"	17"	18"	18 1/2"	19 1/4"	20"	21"	
Approximate quantities per foot of width			Concrete (ft³)	14.7	18.0	20.8	24.6	28.9	32.3	37.1	41.0	46.4	52.1	56.7	63.0	67.9	83.9	
			Steel (lbs)	125	138	152	176	205	235	253	306	331	373	425	472	496	560	
Camber at Mid-Span				.01'	.01'	.02'	.02'	.03'	.03'	.04'	.05'	.05'	.06'	.07'	.08'	.09'	.10'	

Figure A.3: Deck slab thickness for MSCC-SL bridges as a function of span length (BDA 4-10, 2009)



a) Bent cap – spans ≤ 28 ft



b) Bent cap – spans > 28 ft

		Support Type	Length of Span "L"															
			16	18	20	22	24	26	28	30	32	34	36	38	40	42	44	
BENT CAP	45T Pile Spacing*	II	7 1/2	7 1/4	6 1/2	6	5 3/4	5 1/4	5	4 3/4	4 1/2	4 1/4	4					
	"A" bars (Skew 0-20)	II	#7	#7	#7	#7	#7	#7	#7	#6	#7	#6	#6					
	"A" bars (Skew 21-35)	II	#8	#8	#7	#7	#7	#7	#7	#6	#7	#7	#6					
	"A" bars (Skew 36-50)	II	#8	#8	#8	#8	#8	#8	#8	#7	#7	#7	#7					
	Stirrup Spacing	II	#5@12	#5@12	#5@12	#5@12	#5@12	#5@12	#5@12	#5@6	#5@7	#5@7	#5@9					
	70T Pile Spacing*	II	12	11 1/4	10 1/4	9 1/2	8 3/4	8 1/4	7 3/4	7 1/2	7	6 1/2	6	5 3/4	5 1/2	5	4 3/4	
	"A" bars (Skew 0-20)	II	#8	#8	#8	#8	#8	#8	#8	#8	#7	#7	#7	#7	#7	#7	#7	
	"A" bars (Skew 21-35)	II	#9	#9	#8	#8	#8	#8	#8	#8	#8	#8	#7	#7	#7	#7	#7	
	"A" bars (Skew 36-50)	II	#10	#10	#10	#9	#9	#9	#9	#9	#9	#9	#8	#8	#8	#7	#8	
	Stirrup Spacing	II	#5@8	#5@8	#5@8	#5@7	#5@7	#5@7	#5@7	#6@6	#5@4	#5@4	#5@5	#5@6	#5@7	#5@9	#5@10	
	45T Pile Spacing*	III	8 1/4	7 3/4	7 1/2	7	6 1/2	6	5 3/4	5 1/2	5 1/4	5	4 3/4	4 1/2	4			
	"A" bars (Skew 0-20)	III	#7	#7	#7	#7	#7	#7	#7	#7	#6	#7	#6	#6	#6			
	"A" bars (Skew 21-35)	III	#8	#8	#8	#8	#8	#8	#7	#7	#7	#7	#7	#6	#6			
	"A" bars (Skew 36-50)	III	#8	#8	#8	#8	#8	#8	#8	#8	#7	#7	#7	#7	#7			
	Stirrup Spacing	III	#5@12	#5@12	#5@12	#5@12	#5@12	#5@12	#5@12	#5@6	#5@7	#5@8	#5@10	#5@11	#5@12			
	70T Pile Spacing*	III		11 3/4	10 3/4	10	9 1/2	9	8 1/2	8	7 3/4	7 1/4	6 3/4	6 1/4	6	5 1/2		
	"A" bars (Skew 0-20)	III		#8	#8	#8	#8	#8	#8	#8	#8	#7	#7	#7	#7	#7	#7	
	"A" bars (Skew 21-35)	III		#9	#9	#8	#8	#8	#8	#9	#8	#8	#8	#7	#7	#8	#7	
	"A" bars (Skew 36-50)	III		#10	#10	#9	#9	#9	#9	#10	#9	#9	#9	#8	#8	#8	#8	
	Stirrup Spacing	III		#5@8	#5@8	#5@8	#5@8	#5@7	#5@7	#6@6	#5@4	#5@4	#5@5	#5@5	#5@7	#5@8	#5@10	
	45T Pile Spacing*	V	7 1/2	6 3/4	6 1/4	5 3/4	5 1/2	5	4 3/4	4 1/2	4 1/4							
	"A" bars (Skew 0-20)	V	#7	#7	#7	#7	#7	#7	#7	#7	#6	#6						
	"A" bars (Skew 21-35)	V	#8	#7	#7	#7	#7	#7	#7	#7	#6	#7						
	"A" bars (Skew 36-50)	V	#8	#8	#8	#8	#8	#8	#8	#8	#7	#7						
	Stirrup Spacing	V	#5@12	#5@12	#5@12	#5@12	#5@12	#5@12	#5@12	#5@6	#5@7							
	70T Pile Spacing*	V	11 1/2	10 1/2	10	9	8 1/2	8	7 1/2	7	6 1/2	6	5 3/4	5 1/4	5	4 3/4	4 1/4	
	"A" bars (Skew 0-20)	V	#8	#8	#8	#8	#8	#8	#8	#8	#8	#7	#7	#7	#7	#7	#6	
	"A" bars (Skew 21-35)	V	#9	#8	#8	#8	#8	#8	#8	#8	#8	#7	#7	#7	#7	#7	#7	
	"A" bars (Skew 36-50)	V	#10	#10	#9	#9	#9	#9	#9	#9	#9	#8	#8	#8	#7	#8	#8	
	Stirrup Spacing	V	#5@8	#5@8	#5@8	#5@7	#5@7	#5@7	#5@7	#6@6	#5@4	#5@4	#5@5	#5@6	#5@8	#5@9	#5@10	
	45T Pile Spacing*	VI	9 1/4	8 3/4	8 1/4	7 3/4	7 1/2	7	6 1/2	6 1/4	5 3/4	5 1/2	5 1/4	4 3/4	4 1/2	4 1/4	4	
	"A" bars (Skew 0-20)	VI	#7	#7	#7	#7	#7	#7	#7	#7	#6	#7	#6	#6	#6	#5	#5	
	"A" bars (Skew 21-35)	VI	#8	#8	#8	#8	#8	#8	#7	#7	#7	#7	#7	#6	#6	#6	#6	
	"A" bars (Skew 36-50)	VI	#8	#8	#8	#8	#8	#8	#8	#8	#7	#7	#7	#7	#7	#7	#7	
	Stirrup Spacing	VI	#5@12	#5@12	#5@12	#5@12	#5@12	#5@12	#5@12	#5@6	#5@9	#5@10	#5@12	#5@12	#5@12	#5@12	#5@12	
	70T Pile Spacing*	VI					11 1/2	11	10 1/4	9 3/4	9	8 1/2	8 1/4	7 1/2	7 1/4	6 3/4	6 1/2	
	"A" bars (Skew 0-20)	VI					#8	#8	#8	#8	#8	#8	#7	#7	#7	#7	#7	
	"A" bars (Skew 21-35)	VI					#9	#9	#8	#9	#8	#8	#8	#7	#7	#8	#7	
	"A" bars (Skew 36-50)	VI					#10	#10	#9	#10	#9	#9	#9	#8	#8	#8	#8	
	Stirrup Spacing	VI					#5@8	#5@8	#5@8	#5@4	#5@4	#5@5	#5@5	#5@6	#5@7	#5@9	#5@10	

c) Bent cap longitudinal and transverse reinforcement

Figure A.4: Bent cap details in MSCC-SL bridges as a function of span length (BDA 4-10, 2009)

A.4 Multispan Continuous Concrete Tee-girder Bridges

Table A.7: Bridge component details for MSCC-TG bridge class and the respective seismic performance sub-bins

Attribute	MSCC-TG bridge class		
	Pre 1971	1971-1990	Post 1990
<u>Superstructure</u>			
Number of spans	3	3	3
Center span (ft)	40.0 – 130.0	40.0 – 130.0	40.0 – 130.0
Center/Edge span length	1.4	1.4	1.33
Deck width (ft)	30.0 – 80.0	30.0 – 80.0	30.0 – 80.0
Deck slab thickness (in)	7.0	7.0	7.0
Number of Tee girders	See Table A.8	See Table A.8	See Table A.8
Tee girder details			
Width (in)	12.0	12.0	12.0
Depth (in)	Proportioned based on typical superstructure depth to span ratio of 0.065		
Elastomeric bearing pads			
Span \leq 100 ft	16" \times 12" \times 1.5"	16" \times 12" \times 1.5"	16" \times 12" \times 1.5"
Span > 100 ft	20" \times 14" \times 2.0"	20" \times 14" \times 2.0"	20" \times 14" \times 2.0"
<u>Columns</u>			
Diameter (ft)			
Traditional multi column bent	3.0	3.0	3.0
Integral pile columns	Integral pile columns – See section 4.3.2.1 in Chapter 4 for all details		
Traditional multi column bents			
Long. reinf. ratio (%)	1.08 – 3.61	1.18 – 5.31	1.49 – 5.35
Trans. reinf. ratio (%)	#4 @ 12 in.	0.31 – 1.07	0.31 – 1.61
Number of columns per bent			
Integral pile columns	Same procedure as in MSCC-SL bridges (see Table A.6)		
Traditional multi column bent	See Table A.8	See Table A.8	See Table A.8
<u>Foundation</u>			
Integral pile column	Integral pile column	Integral pile column	Integral pile column
Traditional multi column bent	Pile cap with pile group See Table 5.2 in Chapter 5 for foundation spring stiffnesses	Pile cap with pile group	Pile cap with pile group
<u>Abutments</u>			
Backwall height (ft)	3.50 – 8.50	3.50 – 8.50	3.50 – 8.50
Pile spacing	See Figure A.2	See Figure A.2	See Figure A.2

Table A.8: Number of superstructure girders and number of columns per bent as a function of deck width for MSCC-TG bridges

# columns	# girders	Width range (ft)
2	7	Upto 45
3	9	45 – 60
4	9	> 60

A.4 Multispan Continuous Concrete I-girder Bridges

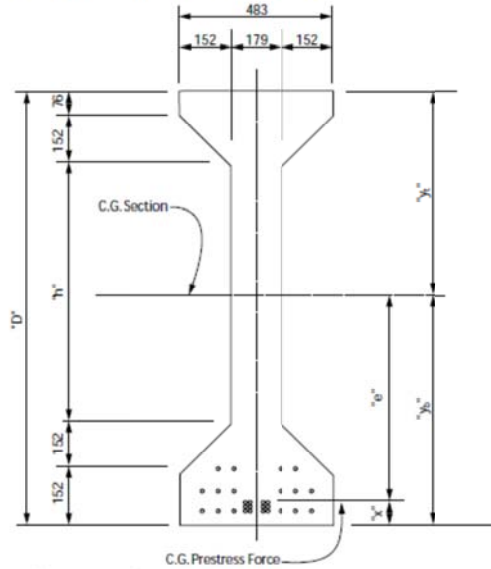
Table A.9: Bridge component details for MSCC-IG bridge class and the respective seismic performance sub-bins

Attribute	MSCC-IG bridge class		
	Pre 1971	1971-1990	Post 1990
<u>Superstructure</u>			
Number of spans	3	3	3
	This is the mode statistic based on inventory analysis		
Center span (ft)	40.0 – 150.0	40.0 – 150.0	40.0 – 150.0
Center/Edge span length	1.4	1.4	1.33
Deck slab thickness (in)			
Standard I girder	7.5	7.5	7.5
Bulb Tee girder	7.0	7.0	7.0
Number of I-girders	See Table A.10	See Table A.10	See Table A.10
Girder type and dimensions	The choice of girder type and dimension is based on superstructure depth to span ratio – 0.05 for I-girders and 0.045 for Bulb-Tee girders See Figure A.5		
Girder spacing	1.5 times the superstructure depth		
Elastomeric bearing pad			
Span ≤ 50 ft	14" x 10" x 1"	14" x 10" x 1"	14" x 10" x 1"
50 ft < Span ≤ 100 ft	16" x 12" x 1.5"	16" x 12" x 1.5"	16" x 12" x 1.5"
Span > 100 ft	20" x 14" x 2"	20" x 14" x 2"	20" x 14" x 2"
<u>Columns</u>			
Diameter (ft)			
Single column bent	6	6	6
Multi column bent	3	3	3
Long. reinf. ratio (%)	1.08 – 3.61	1.18 – 5.31	1.49 – 5.35
Trans. reinf. ratio (%)	#4 @ 12 in. o.c.	0.31 – 1.07	0.31 – 1.61
Number of columns per bent	See Table A.10	See Table A.10	See Table A.10
<u>Foundation</u>			
Single column bent	Pile cap with pile group	Pile cap with pile group	Pile cap with pile group
Multi column bent	Pile cap with pile group	Pile cap with pile group	Pile cap with pile group
<u>Abutments</u>			
Backwall height (ft)	3.50 – 8.50	3.50 – 8.50	3.50 – 8.50
Pile spacing	See Figure A.2	See Figure A.2	See Figure A.2

Table A.10: Number of superstructure girders and number of columns per bent as a function of deck width for MSCC-IG bridges

# columns	# girders	Width range (ft)
1	5	Upto 45
2	7	45 – 60
3, 4	9	> 60

Caltrans Standard “I” Girder

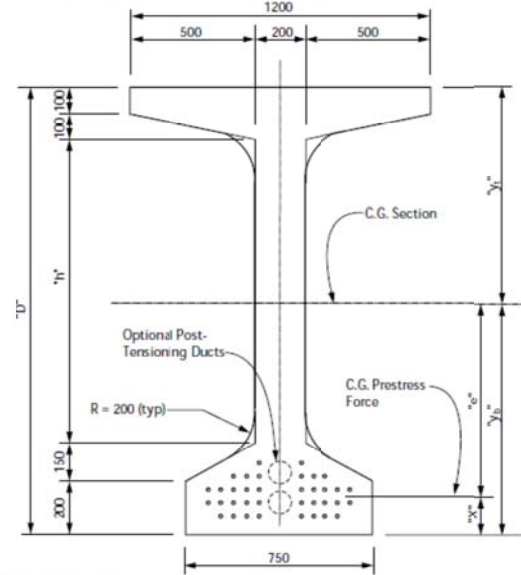


Section Properties

"D" (mm)	"h" (mm)	Area (mm ²)	I (mm ⁴)	y _B (mm)	y _T (mm)	S _B (mm ³)	S _T (mm ³)	r (mm)	Force (N/m)	Mass (Kg/m)
914	382	279 200	26 200 E6	435	479	60.3 E6	54.7 E6	306	6589	671
1067	535	306 500	39 800 E6	508	559	18.3 E6	71.1 E6	360	7221	736
1219	687	333 700	56 800 E6	580	639	17.9 E6	89.0 E6	413	7864	802
1372	840	361 000	77 800 E6	654	718	118.9 E6	108.4 E6	464	8509	867
1524	992	388 300	102 900 E6	728	796	141.4 E6	129.3 E6	515	9152	933
1676	1144	415 600	132 600 E6	802	874	155.3 E6	151.6 E6	565	9796	998

a) Caltrans Standard I-girder

Caltrans Standard “Bulb-Tee” Girder



Section Properties

"D" (mm)	"h" (mm)	Area (mm ²)	I (mm ⁴)	y _B (mm)	y _T (mm)	S _B (mm ³)	S _T (mm ³)	r (mm)	Force (N/m)	Mass (Kg/m)
1400	850	506 500	155 400 E6	721	679	215.5 E6	228.8 E6	510	14 060	1433
1550	1000	626 500	201 200 E6	795	755	253.0 E6	266.5 E6	562	14 770	1508
1700	1150	656 700	254 200 E6	870	830	292.1 E6	306.2 E6	622	15 480	1577
1850	1300	686 100	314 500 E6	945	905	333.0 E6	347.5 E6	677	16 180	1650
2000	1450	716 300	382 600 E6	1019	981	375.4 E6	390.0 E6	731	16 890	1722
2150	1600	746 500	458 800 E6	1094	1056	419.4 E6	434.5 E6	784	17 600	1794

b) Caltrans Standard Bulb-Tee girder

Figure A.5: Standard I-girders used in the California MSCC-IG bridges

APPENDIX B

PROBABILISTIC SEISMIC DEMAND MODELS AND CORRELATION MATRICES

The formulation of the probabilistic seismic demand model (PSDM) was described in section 5.3 of Chapter 5. The model parameters, a and b , describing the median demand and the coefficient of determination, R^2 , of the linear fit are tabulated and presented in this Appendix. The dispersion, $\beta_{D|IM}$, characterizing the distribution of median demand is also tabulated across bridge classes and seismic performance sub-bins. Further, correlation coefficients are evaluated based on the simulation results in order to assemble the covariance matrix in the system fragility formulation. Specifically, correlation between the peak component demands are estimated from an analysis of the simulation results of the nonlinear time history analyses. These correlations have previously been found to be relatively consistent across all the ground motion intensities, and hence a single correlation matrix and covariance matrix is assembled for fragility analysis. The correlation coefficients of the natural logarithm of the component demands across bridge classes and the respective seismic performance sub-bins are also documented.

Table B.1: PSDMs for multispan continuous concrete box-girder bridge class and the respective seismic performance sub-bins

$\ln(EDP)$	$\ln(a)$	b	β_{DIM}	R^2	$\ln(EDP)$	$\ln(a)$	b	β_{DIM}	R^2
<u>MSCC-BG-S-E1-S0</u>					<u>MSCC-BG-M-E1-S0</u>				
$\ln(\mu_\phi)$	1.85	1.09	0.54	0.81	$\ln(\mu_\phi)$	2.72	1.21	0.50	0.83
$\ln(\delta_{deck})$	1.82	0.99	0.41	0.86	$\ln(\delta_{deck})$	2.64	1.19	0.52	0.81
$\ln(\delta_{fnd})$	0.21	0.68	0.49	0.67	$\ln(\delta_{fnd})$	-1.11	0.49	0.96	0.18
$\ln(\theta_{pile})$	-5.21	0.76	0.41	0.78	$\ln(\theta_{pile})$	-2.92	1.22	0.52	0.82
$\ln(\delta_p)$	1.29	0.92	0.48	0.79	$\ln(\delta_p)$	2.05	1.15	0.51	0.82
$\ln(\delta_a)$	1.29	0.90	0.48	0.78	$\ln(\delta_a)$	2.06	1.14	0.50	0.82
$\ln(\delta_t)$	1.79	1.02	0.42	0.86	$\ln(\delta_t)$	2.62	1.23	0.53	0.82
<u>MSCC-BG-S-E1-SX</u>					<u>MSCC-BG-M-E1-SX</u>				
$\ln(\mu_\phi)$	2.16	1.12	0.48	0.86	$\ln(\mu_\phi)$	3.26	1.28	0.67	0.76
$\ln(\delta_{seat})$	1.41	0.74	0.33	0.86	$\ln(\delta_{seat})$	2.12	0.91	0.42	0.76
$\ln(\delta_{deck})$	1.96	0.87	0.39	0.84	$\ln(\delta_{deck})$	3.10	1.25	0.60	0.79
$\ln(\delta_{fnd})$	0.25	0.49	0.49	0.53	$\ln(\delta_{fnd})$	-0.98	0.44	0.86	0.18
$\ln(\theta_{pile})$	-5.04	0.67	0.39	0.76	$\ln(\theta_{pile})$	-2.49	1.22	0.58	0.79
$\ln(\delta_p)$	1.24	1.29	0.73	0.78	$\ln(\delta_p)$	1.68	1.29	0.59	0.80
$\ln(\delta_a)$	1.84	1.22	0.58	0.83	$\ln(\delta_a)$	2.57	1.39	0.48	0.88
$\ln(\delta_t)$	2.85	0.94	1.24	0.38	$\ln(\delta_t)$	3.47	1.09	0.99	0.51
$\ln(\delta_{brng})$	2.55	0.65	0.91	0.38	$\ln(\delta_{brng})$	2.95	0.69	0.69	0.51
$\ln(\delta_{seal})$	1.41	0.74	0.33	0.38	$\ln(\delta_{seal})$	2.12	0.91	0.42	0.51
$\ln(\delta_{rest})$	1.38	0.75	0.35	0.38	$\ln(\delta_{rest})$	2.11	0.95	0.43	0.51
$\ln(\delta_{key})$	-0.10	0.31	0.54	0.38	$\ln(\delta_{key})$	-0.14	0.22	0.59	0.51
<u>MSCC-BG-S-E2-S0</u>					<u>MSCC-BG-M-E2-S0</u>				
$\ln(\mu_\phi)$	1.61	1.02	0.62	0.68	$\ln(\mu_\phi)$	2.54	1.31	0.66	0.79
$\ln(\delta_{deck})$	1.85	0.99	0.40	0.83	$\ln(\delta_{deck})$	2.40	1.15	0.55	0.81
$\ln(\delta_{fnd})$	0.25	0.70	0.47	0.63	$\ln(\delta_{fnd})$	-0.41	0.68	0.73	0.47
$\ln(\theta_{pile})$	-5.27	0.72	0.31	0.81	$\ln(\theta_{pile})$	-3.19	1.19	0.55	0.82
$\ln(\delta_p)$	1.44	1.04	0.47	0.80	$\ln(\delta_p)$	1.93	1.15	0.47	0.86
$\ln(\delta_a)$	1.45	1.03	0.47	0.80	$\ln(\delta_a)$	1.94	1.14	0.47	0.86
$\ln(\delta_t)$	1.77	0.99	0.41	0.83	$\ln(\delta_t)$	2.30	1.14	0.58	0.79
<u>MSCC-BG-S-E2-SX</u>					<u>MSCC-BG-M-E2-SX</u>				
$\ln(\mu_\phi)$	2.24	1.32	0.58	0.81	$\ln(\mu_\phi)$	3.02	1.37	0.81	0.74
$\ln(\delta_{seat})$	1.41	0.76	0.37	0.81	$\ln(\delta_{seat})$	1.97	0.93	0.37	0.74
$\ln(\delta_{deck})$	2.11	1.00	0.36	0.86	$\ln(\delta_{deck})$	2.83	1.21	0.64	0.78
$\ln(\delta_{fnd})$	0.60	0.73	0.47	0.67	$\ln(\delta_{fnd})$	-0.36	0.59	0.72	0.41
$\ln(\theta_{pile})$	-5.00	0.75	0.29	0.84	$\ln(\theta_{pile})$	-2.77	1.23	0.62	0.79
$\ln(\delta_p)$	1.45	1.70	0.69	0.84	$\ln(\delta_p)$	1.77	1.60	0.91	0.75
$\ln(\delta_a)$	1.76	1.49	0.54	0.86	$\ln(\delta_a)$	2.37	1.48	0.54	0.88
$\ln(\delta_t)$	1.57	1.50	0.86	0.72	$\ln(\delta_t)$	2.66	1.68	0.97	0.75
$\ln(\delta_{brng})$	1.66	0.86	0.37	0.72	$\ln(\delta_{brng})$	1.98	0.92	0.36	0.75
$\ln(\delta_{seal})$	1.41	0.76	0.37	0.72	$\ln(\delta_{seal})$	1.97	0.93	0.37	0.75
$\ln(\delta_{rest})$	1.40	0.78	0.36	0.72	$\ln(\delta_{rest})$	1.95	0.95	0.39	0.75
$\ln(\delta_{key})$	-0.48	0.11	0.78	0.72	$\ln(\delta_{key})$	-0.31	0.26	0.66	0.75

<u>MSCC-BG-S-E3-S0</u>					<u>MSCC-BG-M-E3-S0</u>				
$ln(\mu_\phi)$	2.15	1.41	0.44	0.91	$ln(\mu_\phi)$	2.72	1.30	0.64	0.79
$ln(\delta_{deck})$	1.80	1.03	0.31	0.91	$ln(\delta_{deck})$	2.54	1.17	0.56	0.80
$ln(\delta_{fnd})$	0.48	0.79	0.38	0.79	$ln(\delta_{fnd})$	-0.44	0.69	0.76	0.44
$ln(\theta_{pile})$	-4.99	0.94	0.32	0.89	$ln(\theta_{pile})$	-3.03	1.19	0.58	0.79
$ln(\delta_p)$	1.32	1.01	0.39	0.86	$ln(\delta_p)$	2.03	1.20	0.41	0.89
$ln(\delta_a)$	1.33	0.99	0.39	0.85	$ln(\delta_a)$	2.03	1.18	0.41	0.89
$ln(\delta_t)$	1.75	1.03	0.35	0.89	$ln(\delta_t)$	2.46	1.17	0.60	0.77
<u>MSCC-BG-S-E3-SX-S</u>					<u>MSCC-BG-M-E3-SX-S</u>				
$ln(\mu_\phi)$	1.66	1.14	0.41	0.87	$ln(\mu_\phi)$	2.62	1.09	0.57	0.77
$ln(\delta_{seat})$	1.16	0.67	0.26	0.87	$ln(\delta_{seat})$	2.04	0.95	0.47	0.77
$ln(\delta_{deck})$	1.81	0.83	0.28	0.89	$ln(\delta_{deck})$	2.42	0.96	0.42	0.82
$ln(\delta_{fnd})$	0.47	0.46	0.40	0.55	$ln(\delta_{fnd})$	-0.35	0.68	0.72	0.46
$ln(\theta_{pile})$	-5.13	0.72	0.26	0.87	$ln(\theta_{pile})$	-3.10	1.00	0.40	0.85
$ln(\delta_p)$	1.04	1.05	0.68	0.68	$ln(\delta_p)$	1.58	1.34	0.87	0.70
$ln(\delta_a)$	1.21	0.96	0.51	0.75	$ln(\delta_a)$	2.39	1.44	0.64	0.83
$ln(\delta_t)$	1.32	1.04	0.67	0.68	$ln(\delta_t)$	2.30	1.37	0.78	0.74
$ln(\delta_{brng})$	1.52	0.78	0.30	0.68	$ln(\delta_{brng})$	2.03	0.91	0.43	0.74
$ln(\delta_{seal})$	1.16	0.67	0.26	0.68	$ln(\delta_{seal})$	2.04	0.95	0.47	0.74
$ln(\delta_{rest})$	1.16	0.67	0.26	0.68	$ln(\delta_{rest})$	2.06	0.97	0.46	0.74
$ln(\delta_{key})$	-0.53	0.17	0.75	0.68	$ln(\delta_{key})$	-0.38	0.14	0.62	0.74
<u>MSCC-BG-S-E3-SX-L</u>					<u>MSCC-BG-M-E3-SX-L</u>				
$ln(\mu_\phi)$	1.63	0.94	0.63	0.66	$ln(\mu_\phi)$	2.77	1.15	0.59	0.79
$ln(\delta_{seat})$	1.44	0.70	0.27	0.66	$ln(\delta_{seat})$	2.09	0.86	0.39	0.79
$ln(\delta_{deck})$	1.93	0.84	0.31	0.86	$ln(\delta_{deck})$	2.52	0.96	0.41	0.84
$ln(\delta_{fnd})$	0.68	0.63	0.54	0.55	$ln(\delta_{fnd})$	-0.37	0.64	0.84	0.36
$ln(\theta_{pile})$	-4.97	0.64	0.33	0.75	$ln(\theta_{pile})$	-3.03	1.00	0.42	0.85
$ln(\delta_p)$	-0.13	1.41	0.88	0.70	$ln(\delta_p)$	1.02	1.58	0.96	0.73
$ln(\delta_a)$	1.33	1.33	0.66	0.79	$ln(\delta_a)$	2.44	1.39	0.63	0.83
$ln(\delta_t)$	1.51	1.40	0.69	0.79	$ln(\delta_t)$	2.16	1.30	0.76	0.73
$ln(\delta_{brng})$	1.58	0.74	0.28	0.79	$ln(\delta_{brng})$	2.09	0.85	0.37	0.73
$ln(\delta_{seal})$	1.44	0.70	0.27	0.79	$ln(\delta_{seal})$	2.09	0.86	0.39	0.73
$ln(\delta_{rest})$	1.39	0.76	0.26	0.79	$ln(\delta_{rest})$	1.90	0.87	0.44	0.73
$ln(\delta_{kev})$	-0.74	0.03	0.91	0.79	$ln(\delta_{kev})$	-0.34	0.19	0.62	0.73

Table B.2: PSDMs for multispan continuous concrete slab bridge class and the respective seismic performance sub-bins

$\ln(EDP)$	$\ln(a)$	b	$\beta_{D IM}$	R^2	$\ln(EDP)$	$\ln(a)$	b	$\beta_{D IM}$	R^2
<u>MSCC-SL-P-EX-S0</u>					<u>MSCC-SL-P-EX-SX</u>				
$\ln(\mu_\phi)$	-0.02	0.83	0.41	0.80	$\ln(\mu_\phi)$	0.60	0.97	0.63	0.68
$\ln(\delta_{deck})$	1.48	0.77	0.47	0.73	$\ln(\delta_{seat})$	1.89	0.78	0.63	0.68
$\ln(\delta_{fnd})$	-0.26	0.62	0.72	0.45	$\ln(\delta_{deck})$	2.24	1.01	0.43	0.83
$\ln(\theta_{pile})$	-4.01	0.77	0.40	0.80	$\ln(\delta_{fnd})$	0.63	0.94	0.87	0.52
$\ln(\delta_p)$	1.16	0.75	0.46	0.73	$\ln(\theta_{pile})$	-3.42	0.96	0.40	0.84
$\ln(\delta_a)$	1.16	0.75	0.46	0.73	$\ln(\delta_p)$	0.77	0.57	0.31	0.77
$\ln(\delta_i)$	1.34	0.77	0.44	0.76	$\ln(\delta_a)$	1.98	0.96	0.45	0.81
$\ln(\mu_\phi)$	-0.02	0.83	0.41	0.80	$\ln(\delta_i)$	-1.02	0.19	0.53	0.10
					$\ln(\delta_{brng})$	2.16	1.20	0.42	0.10
					$\ln(\delta_{seat})$	1.89	0.78	0.63	0.10

Table B.3: PSDMs for multispan continuous concrete Tee-girder bridge class and the respective seismic performance sub-bins

$\ln(EDP)$	$\ln(a)$	b	$\beta_{D IM}$	R^2	$\ln(EDP)$	$\ln(a)$	b	$\beta_{D IM}$	R^2
<u>MSCC-TG-P-E1-S0</u>					<u>MSCC-TG-M-E1-S0</u>				
$\ln(\mu_\phi)$	0.12	0.91	0.51	0.79	$\ln(\mu_\phi)$	0.86	0.83	0.33	0.84
$\ln(\delta_{deck})$	1.96	0.88	0.28	0.92	$\ln(\delta_{deck})$	1.63	0.85	0.36	0.82
$\ln(\delta_{fnd})$	-0.58	0.66	0.67	0.51	$\ln(\delta_{fnd})$	-2.38	0.70	0.44	0.67
$\ln(\theta_{pile})$	-4.07	0.81	0.29	0.90	$\ln(\theta_{pile})$	-3.70	0.80	0.49	0.70
$\ln(\delta_p)$	0.21	0.73	0.62	0.58	$\ln(\delta_p)$	-0.30	0.56	0.44	0.54
$\ln(\delta_a)$	0.21	0.73	0.62	0.58	$\ln(\delta_a)$	-0.30	0.55	0.45	0.52
$\ln(\delta_t)$	-0.59	0.69	0.57	0.61	$\ln(\delta_t)$	-0.73	0.70	0.44	0.63
<u>MSCC-TG-P-E1-SX</u>					<u>MSCC-TG-M-E1-SX</u>				
$\ln(\mu_\phi)$	1.21	1.06	0.52	0.77	$\ln(\mu_\phi)$	1.10	0.85	0.43	0.78
$\ln(\delta_{seat})$	2.45	1.14	0.31	0.77	$\ln(\delta_{seat})$	1.93	1.01	0.42	0.78
$\ln(\delta_{deck})$	2.43	0.96	0.30	0.90	$\ln(\delta_{deck})$	1.93	0.91	0.40	0.83
$\ln(\delta_{fnd})$	0.06	0.82	0.58	0.63	$\ln(\delta_{fnd})$	-2.18	0.69	0.65	0.49
$\ln(\theta_{pile})$	-3.46	0.93	0.41	0.82	$\ln(\theta_{pile})$	-3.66	0.86	0.37	0.82
$\ln(\delta_p)$	0.35	0.36	0.35	0.47	$\ln(\delta_p)$	1.12	0.70	0.31	0.82
$\ln(\delta_a)$	2.17	1.04	0.35	0.89	$\ln(\delta_a)$	1.13	0.70	0.31	0.81
$\ln(\delta_t)$	-2.75	0.12	0.20	0.21	$\ln(\delta_t)$	-2.71	0.16	0.20	0.34
$\ln(\delta_{brng})$	2.45	1.14	0.31	0.21	$\ln(\delta_{brng})$	1.93	1.01	0.42	0.34
$\ln(\delta_{seal})$	2.45	1.14	0.31	0.21	$\ln(\delta_{seal})$	1.93	1.01	0.42	0.34
<u>MSCC-TG-P-E2-S0</u>					<u>MSCC-TG-M-E2-S0</u>				
$\ln(\mu_\phi)$	0.14	0.99	0.47	0.79	$\ln(\mu_\phi)$	0.61	0.93	0.42	0.84
$\ln(\delta_{deck})$	2.02	0.92	0.27	0.91	$\ln(\delta_{deck})$	1.71	1.00	0.37	0.89
$\ln(\delta_{fnd})$	-0.32	1.02	0.56	0.76	$\ln(\delta_{fnd})$	-1.82	0.90	0.74	0.62
$\ln(\theta_{pile})$	-3.83	0.95	0.31	0.90	$\ln(\theta_{pile})$	-3.64	0.95	0.69	0.68
$\ln(\delta_p)$	0.45	0.89	0.60	0.65	$\ln(\delta_p)$	-0.29	0.75	0.53	0.64
$\ln(\delta_a)$	0.45	0.89	0.60	0.65	$\ln(\delta_a)$	-0.28	0.76	0.53	0.65
$\ln(\delta_t)$	0.00	1.09	0.61	0.72	$\ln(\delta_t)$	-0.45	0.98	0.48	0.77
<u>MSCC-TG-P-E2-SX</u>					<u>MSCC-TG-M-E2-SX</u>				
$\ln(\mu_\phi)$	0.96	1.03	0.67	0.70	$\ln(\mu_\phi)$	1.00	1.01	0.49	0.77
$\ln(\delta_{seat})$	2.32	1.14	0.57	0.70	$\ln(\delta_{seat})$	2.02	1.14	0.45	0.77
$\ln(\delta_{deck})$	2.38	1.00	0.45	0.82	$\ln(\delta_{deck})$	1.94	0.98	0.46	0.78
$\ln(\delta_{fnd})$	-0.18	0.75	0.86	0.43	$\ln(\delta_{fnd})$	-1.84	0.57	0.76	0.31
$\ln(\theta_{pile})$	-3.56	0.92	0.52	0.76	$\ln(\theta_{pile})$	-3.56	1.00	0.42	0.82
$\ln(\delta_p)$	0.53	0.55	0.32	0.74	$\ln(\delta_p)$	1.15	0.79	0.34	0.82
$\ln(\delta_a)$	1.97	1.03	0.58	0.76	$\ln(\delta_a)$	1.17	0.79	0.35	0.82
$\ln(\delta_t)$	-2.71	0.18	0.23	0.38	$\ln(\delta_t)$	-2.64	0.22	0.22	0.46
$\ln(\delta_{brng})$	2.32	1.14	0.57	0.38	$\ln(\delta_{brng})$	2.02	1.14	0.45	0.46
$\ln(\delta_{seal})$	2.32	1.14	0.57	0.38	$\ln(\delta_{seal})$	2.02	1.14	0.45	0.46
<u>MSCC-TG-P-E3-S0</u>					<u>MSCC-TG-M-E3-S0</u>				
$\ln(\mu_\phi)$	0.15	0.97	0.49	0.76	$\ln(\mu_\phi)$	0.64	0.96	0.33	0.88
$\ln(\delta_{deck})$	2.21	1.04	0.32	0.91	$\ln(\delta_{deck})$	1.60	0.85	0.34	0.84
$\ln(\delta_{fnd})$	-0.40	0.92	0.64	0.66	$\ln(\delta_{fnd})$	-2.05	0.63	0.59	0.51

$\ln(\theta_{pile})$	-3.90	0.94	0.36	0.87	$\ln(\theta_{pile})$	-3.64	0.91	0.45	0.79
$\ln(\delta_p)$	0.51	0.94	0.58	0.72	$\ln(\delta_p)$	-0.38	0.61	0.48	0.57
$\ln(\delta_a)$	0.51	0.94	0.58	0.72	$\ln(\delta_a)$	-0.36	0.61	0.47	0.59
$\ln(\delta_t)$	-0.19	0.93	0.67	0.64	$\ln(\delta_t)$	-0.57	0.85	0.46	0.73
<u>MSCC-TG-P-E3-SX</u>					<u>MSCC-TG-M-E3-SX</u>				
$\ln(\mu_\phi)$	0.72	0.87	0.39	0.80	$\ln(\mu_\phi)$	1.16	1.07	0.46	0.83
$\ln(\delta_{seat})$	2.34	1.04	0.31	0.80	$\ln(\delta_{seat})$	2.07	1.14	0.42	0.83
$\ln(\delta_{deck})$	2.37	0.89	0.25	0.92	$\ln(\delta_{deck})$	2.08	1.09	0.41	0.87
$\ln(\delta_{fnd})$	-0.45	0.79	0.63	0.60	$\ln(\delta_{fnd})$	-1.62	0.77	0.59	0.60
$\ln(\theta_{pile})$	-3.66	0.84	0.29	0.89	$\ln(\theta_{pile})$	-3.53	1.02	0.38	0.87
$\ln(\delta_p)$	0.42	0.54	0.35	0.70	$\ln(\delta_p)$	1.13	0.85	0.36	0.84
$\ln(\delta_a)$	2.08	1.01	0.38	0.87	$\ln(\delta_a)$	1.15	0.85	0.36	0.84
$\ln(\delta_t)$	-2.66	0.13	0.19	0.23	$\ln(\delta_t)$	-2.81	0.13	0.23	0.24
$\ln(\delta_{brng})$	2.34	1.04	0.31	0.23	$\ln(\delta_{brng})$	2.07	1.14	0.42	0.24
$\ln(\delta_{seal})$	2.34	1.04	0.31	0.23	$\ln(\delta_{seal})$	2.07	1.14	0.42	0.24

Table B.4: PSDMs for multispan continuous concrete I-girder bridge class and the respective seismic performance sub-bins

$\ln(EDP)$	$\ln(a)$	b	$\beta_{D IM}$	R^2	$\ln(EDP)$	$\ln(a)$	b	$\beta_{D IM}$	R^2
<u>MSCC-IG-S-E1-S0</u>					<u>MSCC-IG-M-E1-S0</u>				
$\ln(\mu_\phi)$	1.02	1.35	0.96	0.67	$\ln(\mu_\phi)$	1.23	0.93	0.56	0.73
$\ln(\delta_{deck})$	2.50	1.11	0.51	0.83	$\ln(\delta_{deck})$	2.20	0.89	0.37	0.86
$\ln(\delta_{fnd})$	0.08	1.20	0.85	0.67	$\ln(\delta_{fnd})$	-1.35	0.51	0.71	0.33
$\ln(\theta_{pile})$	-5.38	0.95	0.69	0.67	$\ln(\theta_{pile})$	-3.71	0.87	0.43	0.80
$\ln(\delta_p)$	-0.51	0.58	0.36	0.67	$\ln(\delta_p)$	-0.05	0.91	0.43	0.79
$\ln(\delta_a)$	-0.48	0.46	0.36	0.55	$\ln(\delta_a)$	0.01	0.82	0.44	0.75
$\ln(\delta_t)$	0.19	0.66	0.52	0.61	$\ln(\delta_t)$	0.10	0.72	0.43	0.70
$\ln(\delta_{brng})$	2.61	1.22	0.57	0.61	$\ln(\delta_{brng})$	2.28	0.95	0.45	0.70
$\ln(\delta_{rest})$	0.26	0.48	0.36	0.61	$\ln(\delta_{rest})$	0.07	0.30	0.28	0.70
$\ln(\delta_{key})$	-0.32	0.54	0.55	0.61	$\ln(\delta_{key})$	-0.80	0.24	0.39	0.70
<u>MSCC-IG-S-E1-SX</u>					<u>MSCC-IG-M-E1-SX</u>				
$\ln(\mu_\phi)$	0.84	1.17	0.56	0.84	$\ln(\mu_\phi)$	1.64	1.05	0.46	0.82
$\ln(\delta_{seat})$	1.17	0.67	0.28	0.84	$\ln(\delta_{seat})$	2.15	1.08	0.37	0.82
$\ln(\delta_{deck})$	2.75	1.09	0.39	0.91	$\ln(\delta_{deck})$	2.59	0.93	0.34	0.87
$\ln(\delta_{fnd})$	-0.18	0.92	0.54	0.76	$\ln(\delta_{fnd})$	-1.48	0.69	0.64	0.51
$\ln(\theta_{pile})$	-5.41	0.85	0.39	0.84	$\ln(\theta_{pile})$	-3.33	0.95	0.37	0.85
$\ln(\delta_p)$	0.06	1.06	0.47	0.86	$\ln(\delta_p)$	0.20	0.93	0.43	0.81
$\ln(\delta_a)$	-0.04	1.06	0.42	0.88	$\ln(\delta_a)$	-0.10	0.89	0.42	0.80
$\ln(\delta_t)$	1.35	1.60	0.86	0.83	$\ln(\delta_t)$	1.10	0.93	0.57	0.72
$\ln(\delta_{brng})$	2.66	1.09	0.42	0.83	$\ln(\delta_{brng})$	2.49	0.99	0.36	0.72
$\ln(\delta_{seal})$	1.17	0.67	0.28	0.83	$\ln(\delta_{seal})$	2.15	1.08	0.37	0.72
$\ln(\delta_{rest})$	0.80	0.57	0.29	0.83	$\ln(\delta_{rest})$	0.22	0.51	0.31	0.72
$\ln(\delta_{key})$	-0.21	0.53	0.48	0.83	$\ln(\delta_{key})$	-1.18	0.14	0.46	0.72
<u>MSCC-IG-S-E2-S0</u>					<u>MSCC-IG-M-E2-S0</u>				
$\ln(\mu_\phi)$	1.79	1.40	1.22	0.54	$\ln(\mu_\phi)$	1.58	1.21	0.62	0.81
$\ln(\delta_{deck})$	3.09	1.24	0.59	0.80	$\ln(\delta_{deck})$	2.24	0.96	0.33	0.90
$\ln(\delta_{fnd})$	1.17	1.52	0.95	0.68	$\ln(\delta_{fnd})$	-1.14	0.70	0.73	0.48
$\ln(\theta_{pile})$	-4.66	1.16	0.85	0.62	$\ln(\theta_{pile})$	-3.45	1.01	0.45	0.85
$\ln(\delta_p)$	-0.09	0.82	0.40	0.79	$\ln(\delta_p)$	-0.16	0.83	0.48	0.74
$\ln(\delta_a)$	-0.38	0.64	0.36	0.73	$\ln(\delta_a)$	-0.12	0.73	0.47	0.70
$\ln(\delta_t)$	1.21	1.18	0.55	0.79	$\ln(\delta_t)$	0.25	0.76	0.45	0.72
$\ln(\delta_{brng})$	3.36	1.42	0.77	0.79	$\ln(\delta_{brng})$	2.33	1.03	0.42	0.72
$\ln(\delta_{rest})$	0.44	0.55	0.27	0.79	$\ln(\delta_{rest})$	0.05	0.33	0.28	0.72
$\ln(\delta_{key})$	-0.54	0.51	0.48	0.79	$\ln(\delta_{key})$	-0.67	0.32	0.39	0.72
<u>MSCC-IG-S-E2-S0</u>					<u>MSCC-IG-M-E2-S0</u>				
$\ln(\mu_\phi)$	1.02	1.09	0.67	0.73	$\ln(\mu_\phi)$	1.61	1.03	0.44	0.83
$\ln(\delta_{seat})$	1.51	0.81	0.33	0.73	$\ln(\delta_{seat})$	2.24	1.12	0.34	0.83
$\ln(\delta_{deck})$	3.04	1.02	0.45	0.84	$\ln(\delta_{deck})$	2.71	1.00	0.34	0.90
$\ln(\delta_{fnd})$	0.09	0.72	0.72	0.49	$\ln(\delta_{fnd})$	-1.71	0.36	0.62	0.26
$\ln(\theta_{pile})$	-5.18	0.76	0.40	0.79	$\ln(\theta_{pile})$	-3.19	1.02	0.32	0.91
$\ln(\delta_p)$	0.46	1.16	0.58	0.80	$\ln(\delta_p)$	0.18	0.92	0.35	0.87
$\ln(\delta_a)$	0.09	1.04	0.59	0.74	$\ln(\delta_a)$	-0.15	0.87	0.37	0.84

$ln(\delta_t)$	2.00	1.71	0.86	0.81	$ln(\delta_t)$	1.63	1.24	0.67	0.77
$ln(\delta_{brng})$	3.03	1.07	0.48	0.81	$ln(\delta_{brng})$	2.67	1.09	0.37	0.77
$ln(\delta_{seal})$	1.51	0.81	0.33	0.81	$ln(\delta_{seal})$	2.24	1.12	0.34	0.77
$ln(\delta_{rest})$	1.10	0.72	0.37	0.81	$ln(\delta_{rest})$	0.26	0.52	0.22	0.77
$ln(\delta_{key})$	-0.15	0.63	0.45	0.81	$ln(\delta_{key})$	-1.27	0.15	0.46	0.77
<u>MSCC-IG-S-E3-S0</u>					<u>MSCC-IG-M-E3-S0</u>				
$ln(\mu_\phi)$	1.18	1.07	1.08	0.50	$ln(\mu_\phi)$	1.53	1.18	0.67	0.76
$ln(\delta_{deck})$	2.83	1.03	0.52	0.81	$ln(\delta_{deck})$	2.29	0.98	0.38	0.87
$ln(\delta_{fnd})$	0.65	0.89	0.92	0.50	$ln(\delta_{fnd})$	-0.90	0.65	0.72	0.43
$ln(\theta_{pile})$	-4.84	0.84	0.77	0.55	$ln(\theta_{pile})$	-3.41	0.98	0.49	0.79
$ln(\delta_p)$	-0.12	0.73	0.50	0.65	$ln(\delta_p)$	-0.17	0.77	0.43	0.72
$ln(\delta_a)$	-0.31	0.56	0.50	0.50	$ln(\delta_a)$	-0.01	0.76	0.43	0.72
$ln(\delta_t)$	1.06	0.89	0.66	0.64	$ln(\delta_t)$	0.19	0.74	0.50	0.65
$ln(\delta_{brng})$	3.11	1.05	0.80	0.64	$ln(\delta_{brng})$	2.40	1.03	0.47	0.65
$ln(\delta_{rest})$	0.38	0.43	0.27	0.64	$ln(\delta_{rest})$	0.18	0.37	0.28	0.65
$ln(\delta_{key})$	-0.33	0.42	0.48	0.64	$ln(\delta_{key})$	-0.85	0.26	0.44	0.65
<u>MSCC-IG-S-E3-SX</u>					<u>MSCC-IG-M-E3-SX</u>				
$ln(\mu_\phi)$	0.41	0.77	0.55	0.62	$ln(\mu_\phi)$	1.50	1.08	0.39	0.87
$ln(\delta_{seat})$	1.43	0.82	0.29	0.62	$ln(\delta_{seat})$	2.26	1.12	0.34	0.87
$ln(\delta_{deck})$	2.90	0.92	0.45	0.76	$ln(\delta_{deck})$	2.66	0.98	0.35	0.88
$ln(\delta_{fnd})$	-0.06	0.23	0.44	0.17	$ln(\delta_{fnd})$	-1.44	0.57	0.67	0.38
$ln(\theta_{pile})$	-5.51	0.36	0.31	0.53	$ln(\theta_{pile})$	-3.19	1.03	0.36	0.89
$ln(\delta_p)$	0.07	1.10	0.50	0.81	$ln(\delta_p)$	0.20	0.93	0.38	0.85
$ln(\delta_a)$	-0.26	0.92	0.53	0.72	$ln(\delta_a)$	-0.17	0.84	0.36	0.83
$ln(\delta_t)$	1.75	1.26	0.86	0.70	$ln(\delta_t)$	1.69	1.30	0.74	0.77
$ln(\delta_{brng})$	2.77	0.80	0.48	0.70	$ln(\delta_{brng})$	2.66	1.11	0.38	0.77
$ln(\delta_{seal})$	1.43	0.82	0.29	0.70	$ln(\delta_{seal})$	2.26	1.12	0.34	0.77
$ln(\delta_{rest})$	1.00	0.74	0.26	0.70	$ln(\delta_{rest})$	0.26	0.53	0.24	0.77
$ln(\delta_{key})$	-0.57	0.29	0.44	0.70	$ln(\delta_{key})$	-1.16	0.21	0.49	0.77

Table B.5: Correlation Coefficients of the component demands of multispan continuous concrete box-girder bridge class and the respective seismic performance sub-bins
MSCC-BG-S-E1-S0

	$\ln(\mu_\phi)$	$\ln(\delta_{deck})$	$\ln(\delta_{fnd})$	$\ln(\theta_{pile})$	$\ln(\delta_p)$	$\ln(\delta_a)$	$\ln(\delta_t)$
$\ln(\mu_\phi)$	1.00	0.95	0.75	0.91	0.88	0.88	0.94
$\ln(\delta_{deck})$	0.95	1.00	0.85	0.93	0.94	0.94	0.98
$\ln(\delta_{fnd})$	0.75	0.85	1.00	0.84	0.79	0.79	0.84
$\ln(\theta_{pile})$	0.91	0.93	0.84	1.00	0.87	0.87	0.92
$\ln(\delta_p)$	0.88	0.94	0.79	0.87	1.00	1.00	0.90
$\ln(\delta_a)$	0.88	0.94	0.79	0.87	1.00	1.00	0.90
$\ln(\delta_t)$	0.94	0.98	0.84	0.92	0.90	0.90	1.00

MSCC-BG-M-E1-S0

	$\ln(\mu_\phi)$	$\ln(\delta_{deck})$	$\ln(\delta_{fnd})$	$\ln(\theta_{pile})$	$\ln(\delta_p)$	$\ln(\delta_a)$	$\ln(\delta_t)$
$\ln(\mu_\phi)$	1.00	0.98	0.70	0.98	0.82	0.83	0.98
$\ln(\delta_{deck})$	0.98	1.00	0.75	1.00	0.81	0.81	1.00
$\ln(\delta_{fnd})$	0.70	0.75	1.00	0.75	0.53	0.53	0.75
$\ln(\theta_{pile})$	0.98	1.00	0.75	1.00	0.80	0.80	0.99
$\ln(\delta_p)$	0.82	0.81	0.53	0.80	1.00	1.00	0.80
$\ln(\delta_a)$	0.83	0.81	0.53	0.80	1.00	1.00	0.80
$\ln(\delta_t)$	0.98	1.00	0.75	0.99	0.80	0.80	1.00

MSCC-BG-S-E1-SX

	$\ln(\mu_\phi)$	$\ln(\delta_{seat})$	$\ln(\delta_{deck})$	$\ln(\delta_{fnd})$	$\ln(\theta_{pile})$	$\ln(\delta_p)$	$\ln(\delta_a)$	$\ln(\delta_t)$	$\ln(\delta_{brng})$	$\ln(\delta_{seal})$	$\ln(\delta_{rest})$	$\ln(\delta_{key})$
$\ln(\mu_\phi)$	1.00	0.87	0.95	0.68	0.88	0.84	0.86	0.59	0.57	0.87	0.84	0.31
$\ln(\delta_{seat})$	0.87	1.00	0.91	0.72	0.86	0.89	0.94	0.56	0.56	1.00	0.99	0.25
$\ln(\delta_{deck})$	0.95	0.91	1.00	0.80	0.93	0.89	0.91	0.68	0.68	0.91	0.89	0.27
$\ln(\delta_{fnd})$	0.68	0.72	0.80	1.00	0.85	0.78	0.78	0.65	0.65	0.72	0.73	0.29
$\ln(\theta_{pile})$	0.88	0.86	0.93	0.85	1.00	0.88	0.88	0.63	0.64	0.86	0.86	0.33
$\ln(\delta_p)$	0.84	0.89	0.89	0.78	0.88	1.00	0.97	0.65	0.65	0.89	0.90	0.27
$\ln(\delta_a)$	0.86	0.94	0.91	0.78	0.88	0.97	1.00	0.64	0.63	0.94	0.94	0.26
$\ln(\delta_t)$	0.59	0.56	0.68	0.65	0.63	0.65	0.64	1.00	0.97	0.56	0.57	0.10
$\ln(\delta_{brng})$	0.57	0.56	0.68	0.65	0.64	0.65	0.63	0.97	1.00	0.56	0.58	0.10
$\ln(\delta_{seal})$	0.87	1.00	0.91	0.72	0.86	0.89	0.94	0.56	0.56	1.00	0.99	0.25
$\ln(\delta_{rest})$	0.84	0.99	0.89	0.73	0.86	0.90	0.94	0.57	0.58	0.99	1.00	0.27
$\ln(\delta_{key})$	0.31	0.25	0.27	0.29	0.33	0.27	0.26	0.10	0.10	0.25	0.27	1.00

MSCC-BG-M-E1-SX

	$\ln(\mu_\phi)$	$\ln(\delta_{seat})$	$\ln(\delta_{deck})$	$\ln(\delta_{fnd})$	$\ln(\theta_{pile})$	$\ln(\delta_p)$	$\ln(\delta_a)$	$\ln(\delta_t)$	$\ln(\delta_{brng})$	$\ln(\delta_{seal})$	$\ln(\delta_{rest})$	$\ln(\delta_{key})$
$\ln(\mu_\phi)$	1.00	0.77	0.98	0.72	0.98	0.73	0.78	0.87	0.77	0.77	0.77	0.23
$\ln(\delta_{seat})$	0.77	1.00	0.78	0.49	0.77	0.81	0.93	0.65	0.65	1.00	0.98	0.17
$\ln(\delta_{deck})$	0.98	0.78	1.00	0.74	1.00	0.75	0.78	0.90	0.78	0.78	0.78	0.20
$\ln(\delta_{fnd})$	0.72	0.49	0.74	1.00	0.74	0.47	0.49	0.71	0.68	0.49	0.50	0.04
$\ln(\theta_{pile})$	0.98	0.77	1.00	0.74	1.00	0.73	0.77	0.90	0.77	0.77	0.77	0.20
$\ln(\delta_p)$	0.73	0.81	0.75	0.47	0.73	1.00	0.93	0.66	0.61	0.81	0.82	0.22
$\ln(\delta_a)$	0.78	0.93	0.78	0.49	0.77	0.93	1.00	0.67	0.64	0.93	0.92	0.21
$\ln(\delta_t)$	0.87	0.65	0.90	0.71	0.90	0.66	0.67	1.00	0.90	0.65	0.65	0.15
$\ln(\delta_{brng})$	0.77	0.65	0.78	0.68	0.77	0.61	0.64	0.90	1.00	0.65	0.65	0.09
$\ln(\delta_{seal})$	0.77	1.00	0.78	0.49	0.77	0.81	0.93	0.65	0.65	1.00	0.98	0.17
$\ln(\delta_{rest})$	0.77	0.98	0.78	0.50	0.77	0.82	0.92	0.65	0.65	0.98	1.00	0.17
$\ln(\delta_{key})$	0.23	0.17	0.20	0.04	0.20	0.22	0.21	0.15	0.09	0.17	0.17	1.00

MSCC-BG-S-E2-S0

	$\ln(\mu_\phi)$	$\ln(\delta_{deck})$	$\ln(\delta_{fnd})$	$\ln(\theta_{pile})$	$\ln(\delta_p)$	$\ln(\delta_a)$	$\ln(\delta_t)$
$\ln(\mu_\phi)$	1.00	0.92	0.64	0.87	0.80	0.80	0.92
$\ln(\delta_{deck})$	0.92	1.00	0.81	0.94	0.92	0.92	0.99
$\ln(\delta_{fnd})$	0.64	0.81	1.00	0.85	0.73	0.73	0.81
$\ln(\theta_{pile})$	0.87	0.94	0.85	1.00	0.84	0.84	0.93
$\ln(\delta_p)$	0.80	0.92	0.73	0.84	1.00	1.00	0.87
$\ln(\delta_a)$	0.80	0.92	0.73	0.84	1.00	1.00	0.87
$\ln(\delta_t)$	0.92	0.99	0.81	0.93	0.87	0.87	1.00

MSCC-BG-M-E2-S0

	$\ln(\mu_\phi)$	$\ln(\delta_{deck})$	$\ln(\delta_{fnd})$	$\ln(\theta_{pile})$	$\ln(\delta_p)$	$\ln(\delta_a)$	$\ln(\delta_t)$
$\ln(\mu_\phi)$	1.00	0.98	0.77	0.98	0.81	0.81	0.97
$\ln(\delta_{deck})$	0.98	1.00	0.82	1.00	0.81	0.81	1.00
$\ln(\delta_{fnd})$	0.77	0.82	1.00	0.80	0.63	0.63	0.82
$\ln(\theta_{pile})$	0.98	1.00	0.80	1.00	0.80	0.80	0.99
$\ln(\delta_p)$	0.81	0.81	0.63	0.80	1.00	1.00	0.79
$\ln(\delta_a)$	0.81	0.81	0.63	0.80	1.00	1.00	0.79
$\ln(\delta_t)$	0.97	1.00	0.82	0.99	0.79	0.79	1.00

MSCC-BG-S-E2-SX

	$\ln(\mu_\phi)$	$\ln(\delta_{seat})$	$\ln(\delta_{deck})$	$\ln(\delta_{fnd})$	$\ln(\theta_{pile})$	$\ln(\delta_p)$	$\ln(\delta_a)$	$\ln(\delta_t)$	$\ln(\delta_{brng})$	$\ln(\delta_{seal})$	$\ln(\delta_{rest})$	$\ln(\delta_{key})$
$\ln(\mu_\phi)$	1.00	0.83	0.94	0.73	0.92	0.82	0.86	0.82	0.89	0.83	0.84	0.09
$\ln(\delta_{seat})$	0.83	1.00	0.90	0.77	0.84	0.88	0.96	0.75	0.96	1.00	1.00	0.03
$\ln(\delta_{deck})$	0.94	0.90	1.00	0.89	0.96	0.90	0.94	0.90	0.93	0.90	0.91	0.10
$\ln(\delta_{fnd})$	0.73	0.77	0.89	1.00	0.87	0.81	0.83	0.80	0.77	0.77	0.76	0.16
$\ln(\theta_{pile})$	0.92	0.84	0.96	0.87	1.00	0.88	0.91	0.89	0.88	0.84	0.84	0.04
$\ln(\delta_p)$	0.82	0.88	0.90	0.81	0.88	1.00	0.96	0.82	0.86	0.88	0.89	0.04
$\ln(\delta_a)$	0.86	0.96	0.94	0.83	0.91	0.96	1.00	0.83	0.92	0.96	0.96	0.04
$\ln(\delta_t)$	0.82	0.75	0.90	0.80	0.89	0.82	0.83	1.00	0.80	0.75	0.76	0.05
$\ln(\delta_{brng})$	0.89	0.96	0.93	0.77	0.88	0.86	0.92	0.80	1.00	0.96	0.96	0.06
$\ln(\delta_{seal})$	0.83	1.00	0.90	0.77	0.84	0.88	0.96	0.75	0.96	1.00	1.00	0.03
$\ln(\delta_{rest})$	0.84	1.00	0.91	0.76	0.84	0.89	0.96	0.76	0.96	1.00	1.00	0.03
$\ln(\delta_{key})$	0.09	0.03	0.10	0.16	0.04	0.04	0.04	0.05	0.06	0.03	0.03	1.00

MSCC-BG-M-E2-SX

	$\ln(\mu_\phi)$	$\ln(\delta_{seat})$	$\ln(\delta_{deck})$	$\ln(\delta_{fnd})$	$\ln(\theta_{pile})$	$\ln(\delta_p)$	$\ln(\delta_a)$	$\ln(\delta_t)$	$\ln(\delta_{brng})$	$\ln(\delta_{seal})$	$\ln(\delta_{rest})$	$\ln(\delta_{key})$
$\ln(\mu_\phi)$	1.00	0.81	0.98	0.79	0.98	0.69	0.80	0.95	0.82	0.81	0.80	0.15
$\ln(\delta_{seat})$	0.81	1.00	0.80	0.61	0.80	0.78	0.93	0.80	0.99	1.00	0.99	0.26
$\ln(\delta_{deck})$	0.98	0.80	1.00	0.82	1.00	0.68	0.80	0.97	0.81	0.80	0.79	0.14
$\ln(\delta_{fnd})$	0.79	0.61	0.82	1.00	0.81	0.54	0.63	0.80	0.61	0.61	0.59	0.18
$\ln(\theta_{pile})$	0.98	0.80	1.00	0.81	1.00	0.68	0.80	0.96	0.81	0.80	0.79	0.14
$\ln(\delta_p)$	0.69	0.78	0.68	0.54	0.68	1.00	0.91	0.71	0.78	0.78	0.79	0.18
$\ln(\delta_a)$	0.80	0.93	0.80	0.63	0.80	0.91	1.00	0.81	0.93	0.93	0.93	0.21
$\ln(\delta_t)$	0.95	0.80	0.97	0.80	0.96	0.71	0.81	1.00	0.80	0.80	0.78	0.11
$\ln(\delta_{brng})$	0.82	0.99	0.81	0.61	0.81	0.78	0.93	0.80	1.00	0.99	0.99	0.26
$\ln(\delta_{seal})$	0.81	1.00	0.80	0.61	0.80	0.78	0.93	0.80	0.99	1.00	0.99	0.26
$\ln(\delta_{rest})$	0.80	0.99	0.79	0.59	0.79	0.79	0.93	0.78	0.99	0.99	1.00	0.26
$\ln(\delta_{key})$	0.15	0.26	0.14	0.18	0.14	0.18	0.21	0.11	0.26	0.26	0.26	1.00

MSCC-BG-S-E3-S0

	$\ln(\mu_\varphi)$	$\ln(\delta_{deck})$	$\ln(\delta_{fnd})$	$\ln(\theta_{pile})$	$\ln(\delta_p)$	$\ln(\delta_a)$	$\ln(\delta_t)$
$\ln(\mu_\varphi)$	1.00	0.90	0.66	0.88	0.86	0.86	0.91
$\ln(\delta_{deck})$	0.90	1.00	0.86	0.96	0.91	0.91	0.99
$\ln(\delta_{fnd})$	0.66	0.86	1.00	0.86	0.72	0.72	0.87
$\ln(\theta_{pile})$	0.88	0.96	0.86	1.00	0.87	0.86	0.95
$\ln(\delta_p)$	0.86	0.91	0.72	0.87	1.00	1.00	0.88
$\ln(\delta_a)$	0.86	0.91	0.72	0.86	1.00	1.00	0.88
$\ln(\delta_t)$	0.91	0.99	0.87	0.95	0.88	0.88	1.00

MSCC-BG-M-E3-S0

	$\ln(\mu_\varphi)$	$\ln(\delta_{deck})$	$\ln(\delta_{fnd})$	$\ln(\theta_{pile})$	$\ln(\delta_p)$	$\ln(\delta_a)$	$\ln(\delta_t)$
$\ln(\mu_\varphi)$	1.00	0.98	0.83	0.98	0.84	0.84	0.98
$\ln(\delta_{deck})$	0.98	1.00	0.85	1.00	0.82	0.82	1.00
$\ln(\delta_{fnd})$	0.83	0.85	1.00	0.84	0.70	0.70	0.85
$\ln(\theta_{pile})$	0.98	1.00	0.84	1.00	0.82	0.82	0.99
$\ln(\delta_p)$	0.84	0.82	0.70	0.82	1.00	1.00	0.80
$\ln(\delta_a)$	0.84	0.82	0.70	0.82	1.00	1.00	0.80
$\ln(\delta_t)$	0.98	1.00	0.85	0.99	0.80	0.80	1.00

MSCC-BG-S-E3-SX-S

	$\ln(\mu_\varphi)$	$\ln(\delta_{seat})$	$\ln(\delta_{deck})$	$\ln(\delta_{fnd})$	$\ln(\theta_{pile})$	$\ln(\delta_p)$	$\ln(\delta_a)$	$\ln(\delta_t)$	$\ln(\delta_{brng})$	$\ln(\delta_{seal})$	$\ln(\delta_{rest})$	$\ln(\delta_{key})$
$\ln(\mu_\varphi)$	1.00	0.86	0.91	0.53	0.89	0.75	0.82	0.80	0.87	0.86	0.86	0.11
$\ln(\delta_{seat})$	0.86	1.00	0.92	0.68	0.88	0.75	0.86	0.81	0.92	1.00	1.00	0.27
$\ln(\delta_{deck})$	0.91	0.92	1.00	0.77	0.93	0.84	0.92	0.87	0.98	0.92	0.92	0.28
$\ln(\delta_{fnd})$	0.53	0.68	0.77	1.00	0.76	0.62	0.68	0.71	0.77	0.68	0.68	0.41
$\ln(\theta_{pile})$	0.89	0.88	0.93	0.76	1.00	0.76	0.84	0.85	0.89	0.88	0.88	0.21
$\ln(\delta_p)$	0.75	0.75	0.84	0.62	0.76	1.00	0.96	0.79	0.78	0.75	0.75	0.16
$\ln(\delta_a)$	0.82	0.86	0.92	0.68	0.84	0.96	1.00	0.81	0.86	0.86	0.86	0.24
$\ln(\delta_t)$	0.80	0.81	0.87	0.71	0.85	0.79	0.81	1.00	0.86	0.81	0.81	0.04
$\ln(\delta_{brng})$	0.87	0.92	0.98	0.77	0.89	0.78	0.86	0.86	1.00	0.92	0.92	0.33
$\ln(\delta_{seal})$	0.86	1.00	0.92	0.68	0.88	0.75	0.86	0.81	0.92	1.00	1.00	0.27
$\ln(\delta_{rest})$	0.86	1.00	0.92	0.68	0.88	0.75	0.86	0.81	0.92	1.00	1.00	0.27
$\ln(\delta_{key})$	0.11	0.27	0.28	0.41	0.21	0.16	0.24	0.04	0.33	0.27	0.27	1.00

MSCC-BG-M-E3-SX-S

	$\ln(\mu_\varphi)$	$\ln(\delta_{seat})$	$\ln(\delta_{deck})$	$\ln(\delta_{fnd})$	$\ln(\theta_{pile})$	$\ln(\delta_p)$	$\ln(\delta_a)$	$\ln(\delta_t)$	$\ln(\delta_{brng})$	$\ln(\delta_{seal})$	$\ln(\delta_{rest})$	$\ln(\delta_{key})$
$\ln(\mu_\varphi)$	1.00	0.84	0.97	0.77	0.98	0.64	0.81	0.95	0.85	0.84	0.84	0.09
$\ln(\delta_{seat})$	0.84	1.00	0.84	0.65	0.83	0.80	0.96	0.82	0.99	1.00	1.00	0.10
$\ln(\delta_{deck})$	0.97	0.84	1.00	0.80	1.00	0.64	0.80	0.97	0.85	0.84	0.84	0.11
$\ln(\delta_{fnd})$	0.77	0.65	0.80	1.00	0.78	0.52	0.63	0.79	0.65	0.65	0.65	0.19
$\ln(\theta_{pile})$	0.98	0.83	1.00	0.78	1.00	0.63	0.79	0.97	0.84	0.83	0.83	0.10
$\ln(\delta_p)$	0.64	0.80	0.64	0.52	0.63	1.00	0.91	0.68	0.79	0.80	0.81	0.09
$\ln(\delta_a)$	0.81	0.96	0.80	0.63	0.79	0.91	1.00	0.81	0.95	0.96	0.97	0.10
$\ln(\delta_t)$	0.95	0.82	0.97	0.79	0.97	0.68	0.81	1.00	0.83	0.82	0.82	0.08
$\ln(\delta_{brng})$	0.85	0.99	0.85	0.65	0.84	0.79	0.95	0.83	1.00	0.99	0.99	0.10
$\ln(\delta_{seal})$	0.84	1.00	0.84	0.65	0.83	0.80	0.96	0.82	0.99	1.00	1.00	0.10
$\ln(\delta_{rest})$	0.84	1.00	0.84	0.65	0.83	0.81	0.97	0.82	0.99	1.00	1.00	0.10
$\ln(\delta_{key})$	0.09	0.10	0.11	0.19	0.10	0.09	0.10	0.08	0.10	0.10	0.10	1.00

MSCC-BG-S-E3-SX-L

	$\ln(\mu_\varphi)$	$\ln(\delta_{\text{seal}})$	$\ln(\delta_{\text{deck}})$	$\ln(\delta_{\text{find}})$	$\ln(\theta_{\text{pile}})$	$\ln(\delta_p)$	$\ln(\delta_a)$	$\ln(\delta_t)$	$\ln(\delta_{\text{brng}})$	$\ln(\delta_{\text{seal}})$	$\ln(\delta_{\text{rest}})$	$\ln(\delta_{\text{key}})$
$\ln(\mu_\varphi)$	1.00	0.74	0.86	0.57	0.87	0.70	0.76	0.80	0.81	0.74	0.76	0.08
$\ln(\delta_{\text{seal}})$	0.74	1.00	0.95	0.85	0.90	0.89	0.96	0.81	0.98	1.00	0.97	0.01
$\ln(\delta_{\text{deck}})$	0.86	0.95	1.00	0.84	0.95	0.91	0.95	0.90	0.97	0.95	0.93	0.06
$\ln(\delta_{\text{find}})$	0.57	0.85	0.84	1.00	0.82	0.74	0.81	0.79	0.86	0.85	0.82	0.02
$\ln(\theta_{\text{pile}})$	0.87	0.90	0.95	0.82	1.00	0.81	0.89	0.87	0.92	0.90	0.88	0.02
$\ln(\delta_p)$	0.70	0.89	0.91	0.74	0.81	1.00	0.95	0.80	0.87	0.89	0.84	0.13
$\ln(\delta_a)$	0.76	0.96	0.95	0.81	0.89	0.95	1.00	0.81	0.94	0.96	0.94	0.03
$\ln(\delta_t)$	0.80	0.81	0.90	0.79	0.87	0.80	0.81	1.00	0.84	0.81	0.80	0.24
$\ln(\delta_{\text{brng}})$	0.81	0.98	0.97	0.86	0.92	0.87	0.94	0.84	1.00	0.98	0.95	0.04
$\ln(\delta_{\text{seal}})$	0.74	1.00	0.95	0.85	0.90	0.89	0.96	0.81	0.98	1.00	0.97	0.01
$\ln(\delta_{\text{rest}})$	0.76	0.97	0.93	0.82	0.88	0.84	0.94	0.80	0.95	0.97	1.00	0.03
$\ln(\delta_{\text{key}})$	0.08	0.01	0.06	0.02	0.02	0.13	0.03	0.24	0.04	0.01	0.03	1.00

MSCC-BG-M-E3-SX-L

	$\ln(\mu_\varphi)$	$\ln(\delta_{\text{seal}})$	$\ln(\delta_{\text{deck}})$	$\ln(\delta_{\text{find}})$	$\ln(\theta_{\text{pile}})$	$\ln(\delta_p)$	$\ln(\delta_a)$	$\ln(\delta_t)$	$\ln(\delta_{\text{brng}})$	$\ln(\delta_{\text{seal}})$	$\ln(\delta_{\text{rest}})$	$\ln(\delta_{\text{key}})$
$\ln(\mu_\varphi)$	1.00	0.76	0.98	0.73	0.98	0.74	0.78	0.96	0.77	0.76	0.75	0.17
$\ln(\delta_{\text{seal}})$	0.76	1.00	0.76	0.53	0.75	0.83	0.95	0.76	1.00	1.00	0.97	0.20
$\ln(\delta_{\text{deck}})$	0.98	0.76	1.00	0.76	1.00	0.73	0.77	0.97	0.76	0.76	0.75	0.14
$\ln(\delta_{\text{find}})$	0.73	0.53	0.76	1.00	0.75	0.49	0.55	0.74	0.54	0.53	0.51	0.16
$\ln(\theta_{\text{pile}})$	0.98	0.75	1.00	0.75	1.00	0.73	0.76	0.97	0.75	0.75	0.74	0.14
$\ln(\delta_p)$	0.74	0.83	0.73	0.49	0.73	1.00	0.91	0.74	0.83	0.83	0.82	0.18
$\ln(\delta_a)$	0.78	0.95	0.77	0.55	0.76	0.91	1.00	0.78	0.95	0.95	0.93	0.18
$\ln(\delta_t)$	0.96	0.76	0.97	0.74	0.97	0.74	0.78	1.00	0.76	0.76	0.74	0.08
$\ln(\delta_{\text{brng}})$	0.77	1.00	0.76	0.54	0.75	0.83	0.95	0.76	1.00	1.00	0.96	0.19
$\ln(\delta_{\text{seal}})$	0.76	1.00	0.76	0.53	0.75	0.83	0.95	0.76	1.00	1.00	0.97	0.20
$\ln(\delta_{\text{rest}})$	0.75	0.97	0.75	0.51	0.74	0.82	0.93	0.74	0.96	0.97	1.00	0.18
$\ln(\delta_{\text{key}})$	0.17	0.20	0.14	0.16	0.14	0.18	0.18	0.08	0.19	0.20	0.18	1.00

Table B.6: Correlation Coefficients of the component demands of multispan continuous concrete slab bridge class and the respective seismic performance sub-bins

MSCC-SL-P-EX-S0

	$\ln(\mu_\phi)$	$\ln(\delta_{deck})$	$\ln(\delta_{fnd})$	$\ln(\theta_{pile})$	$\ln(\delta_p)$	$\ln(\delta_a)$	$\ln(\delta_t)$
$\ln(\mu_\phi)$	1.00	0.87	0.63	0.88	0.80	0.80	0.85
$\ln(\delta_{deck})$	0.87	1.00	0.92	0.96	0.95	0.95	0.97
$\ln(\delta_{fnd})$	0.63	0.92	1.00	0.84	0.89	0.89	0.89
$\ln(\theta_{pile})$	0.88	0.96	0.84	1.00	0.91	0.91	0.94
$\ln(\delta_p)$	0.80	0.95	0.89	0.91	1.00	1.00	0.90
$\ln(\delta_a)$	0.80	0.95	0.89	0.91	1.00	1.00	0.90
$\ln(\delta_t)$	0.85	0.97	0.89	0.94	0.90	0.90	1.00

MSCC-SL-P-EX-SX

	$\ln(\mu_\phi)$	$\ln(\delta_{seat})$	$\ln(\delta_{deck})$	$\ln(\delta_{fnd})$	$\ln(\theta_{pile})$	$\ln(\delta_p)$	$\ln(\delta_a)$	$\ln(\delta_t)$	$\ln(\delta_{brng})$	$\ln(\delta_{seal})$
$\ln(\mu_\phi)$	1.00	0.81	0.91	0.76	0.92	0.39	0.88	0.09	0.91	0.81
$\ln(\delta_{seat})$	0.81	1.00	0.84	0.75	0.83	0.44	0.85	0.17	0.82	1.00
$\ln(\delta_{deck})$	0.91	0.84	1.00	0.92	0.96	0.62	0.98	0.36	0.96	0.84
$\ln(\delta_{fnd})$	0.76	0.75	0.92	1.00	0.90	0.60	0.91	0.56	0.82	0.75
$\ln(\theta_{pile})$	0.92	0.83	0.96	0.90	1.00	0.47	0.93	0.20	0.94	0.83
$\ln(\delta_p)$	0.39	0.44	0.62	0.60	0.47	1.00	0.64	0.62	0.56	0.44
$\ln(\delta_a)$	0.88	0.85	0.98	0.91	0.93	0.64	1.00	0.38	0.94	0.85
$\ln(\delta_t)$	0.09	0.17	0.36	0.56	0.20	0.62	0.38	1.00	0.21	0.17
$\ln(\delta_{brng})$	0.91	0.82	0.96	0.82	0.94	0.56	0.94	0.21	1.00	0.82
$\ln(\delta_{seal})$	0.81	1.00	0.84	0.75	0.83	0.44	0.85	0.17	0.82	1.00

Table B.7: Correlation Coefficients of the component demands of multispan continuous concrete Tee-girder bridge class and the respective seismic performance sub-bins

MSCC-TG-P-E1-S0

	$\ln(\mu_\phi)$	$\ln(\delta_{deck})$	$\ln(\delta_{fnd})$	$\ln(\theta_{pile})$	$\ln(\delta_p)$	$\ln(\delta_a)$	$\ln(\delta_t)$
$\ln(\mu_\phi)$	1.00	0.89	0.37	0.86	0.70	0.70	0.72
$\ln(\delta_{deck})$	0.89	1.00	0.60	0.96	0.75	0.75	0.77
$\ln(\delta_{fnd})$	0.37	0.60	1.00	0.65	0.58	0.58	0.57
$\ln(\theta_{pile})$	0.86	0.96	0.65	1.00	0.80	0.80	0.82
$\ln(\delta_p)$	0.70	0.75	0.58	0.80	1.00	1.00	0.89
$\ln(\delta_a)$	0.70	0.75	0.58	0.80	1.00	1.00	0.89
$\ln(\delta_t)$	0.72	0.77	0.57	0.82	0.89	0.89	1.00

MSCC-TG-M-E1-S0

	$\ln(\mu_\phi)$	$\ln(\delta_{deck})$	$\ln(\delta_{fnd})$	$\ln(\theta_{pile})$	$\ln(\delta_p)$	$\ln(\delta_a)$	$\ln(\delta_t)$
$\ln(\mu_\phi)$	1.00	0.95	0.72	0.81	0.71	0.71	0.76
$\ln(\delta_{deck})$	0.95	1.00	0.64	0.81	0.77	0.77	0.76
$\ln(\delta_{fnd})$	0.72	0.64	1.00	0.59	0.52	0.52	0.66
$\ln(\theta_{pile})$	0.81	0.81	0.59	1.00	0.67	0.67	0.64
$\ln(\delta_p)$	0.71	0.77	0.52	0.67	1.00	1.00	0.84
$\ln(\delta_a)$	0.71	0.77	0.52	0.67	1.00	1.00	0.84
$\ln(\delta_t)$	0.76	0.76	0.66	0.64	0.84	0.84	1.00

MSCC-TG-P-E1-SX

	$\ln(\mu_\phi)$	$\ln(\delta_{seat})$	$\ln(\delta_{deck})$	$\ln(\delta_{fnd})$	$\ln(\theta_{pile})$	$\ln(\delta_p)$	$\ln(\delta_a)$	$\ln(\delta_t)$	$\ln(\delta_{brng})$	$\ln(\delta_{seal})$
$\ln(\mu_\phi)$	1.00	0.80	0.86	0.69	0.95	0.41	0.74	0.26	0.80	0.80
$\ln(\delta_{seat})$	0.80	1.00	0.96	0.59	0.82	0.61	0.96	0.40	1.00	1.00
$\ln(\delta_{deck})$	0.86	0.96	1.00	0.70	0.90	0.58	0.90	0.44	0.96	0.96
$\ln(\delta_{fnd})$	0.69	0.59	0.70	1.00	0.81	0.36	0.51	0.25	0.59	0.59
$\ln(\theta_{pile})$	0.95	0.82	0.90	0.81	1.00	0.49	0.75	0.31	0.82	0.82
$\ln(\delta_p)$	0.41	0.61	0.58	0.36	0.49	1.00	0.62	0.22	0.61	0.61
$\ln(\delta_a)$	0.74	0.96	0.90	0.51	0.75	0.62	1.00	0.41	0.96	0.96
$\ln(\delta_t)$	0.26	0.40	0.44	0.25	0.31	0.22	0.41	1.00	0.40	0.40
$\ln(\delta_{brng})$	0.80	1.00	0.96	0.59	0.82	0.61	0.96	0.40	1.00	1.00
$\ln(\delta_{seal})$	0.80	1.00	0.96	0.59	0.82	0.61	0.96	0.40	1.00	1.00

MSCC-TG-M-E1-SX

	$\ln(\mu_\phi)$	$\ln(\delta_{seat})$	$\ln(\delta_{deck})$	$\ln(\delta_{fnd})$	$\ln(\theta_{pile})$	$\ln(\delta_p)$	$\ln(\delta_a)$	$\ln(\delta_t)$	$\ln(\delta_{brng})$	$\ln(\delta_{seal})$
$\ln(\mu_\phi)$	1.00	0.97	0.97	0.73	0.98	0.78	0.78	0.49	0.97	0.97
$\ln(\delta_{seat})$	0.97	1.00	1.00	0.73	0.99	0.80	0.80	0.44	1.00	1.00
$\ln(\delta_{deck})$	0.97	1.00	1.00	0.73	0.99	0.79	0.79	0.47	1.00	1.00
$\ln(\delta_{fnd})$	0.73	0.73	0.73	1.00	0.74	0.53	0.53	0.32	0.73	0.73
$\ln(\theta_{pile})$	0.98	0.99	0.99	0.74	1.00	0.79	0.79	0.46	0.99	0.99
$\ln(\delta_p)$	0.78	0.80	0.79	0.53	0.79	1.00	1.00	0.54	0.80	0.80
$\ln(\delta_a)$	0.78	0.80	0.79	0.53	0.79	1.00	1.00	0.54	0.80	0.80
$\ln(\delta_t)$	0.49	0.44	0.47	0.32	0.46	0.54	0.54	1.00	0.44	0.44
$\ln(\delta_{brng})$	0.97	1.00	1.00	0.73	0.99	0.80	0.80	0.44	1.00	1.00
$\ln(\delta_{seal})$	0.97	1.00	1.00	0.73	0.99	0.80	0.80	0.44	1.00	1.00

MSCC-TG-P-E2-S0

	$\ln(\mu_\phi)$	$\ln(\delta_{deck})$	$\ln(\delta_{fnd})$	$\ln(\theta_{pile})$	$\ln(\delta_p)$	$\ln(\delta_a)$	$\ln(\delta_t)$
$\ln(\mu_\phi)$	1.00	0.83	0.56	0.84	0.72	0.72	0.75
$\ln(\delta_{deck})$	0.83	1.00	0.80	0.95	0.74	0.74	0.80
$\ln(\delta_{fnd})$	0.56	0.80	1.00	0.84	0.61	0.61	0.63
$\ln(\theta_{pile})$	0.84	0.95	0.84	1.00	0.78	0.78	0.81
$\ln(\delta_p)$	0.72	0.74	0.61	0.78	1.00	1.00	0.85
$\ln(\delta_a)$	0.72	0.74	0.61	0.78	1.00	1.00	0.85
$\ln(\delta_t)$	0.75	0.80	0.63	0.81	0.85	0.85	1.00

MSCC-TG-M-E2-S0

	$\ln(\mu_\phi)$	$\ln(\delta_{deck})$	$\ln(\delta_{fnd})$	$\ln(\theta_{pile})$	$\ln(\delta_p)$	$\ln(\delta_a)$	$\ln(\delta_t)$
$\ln(\mu_\phi)$	1.00	0.93	0.67	0.78	0.64	0.65	0.78
$\ln(\delta_{deck})$	0.93	1.00	0.65	0.75	0.74	0.74	0.87
$\ln(\delta_{fnd})$	0.67	0.65	1.00	0.79	0.23	0.23	0.40
$\ln(\theta_{pile})$	0.78	0.75	0.79	1.00	0.35	0.35	0.50
$\ln(\delta_p)$	0.64	0.74	0.23	0.35	1.00	1.00	0.84
$\ln(\delta_a)$	0.65	0.74	0.23	0.35	1.00	1.00	0.84
$\ln(\delta_t)$	0.78	0.87	0.40	0.50	0.84	0.84	1.00

MSCC-TG-P-E2-SX

	$\ln(\mu_\phi)$	$\ln(\delta_{seat})$	$\ln(\delta_{deck})$	$\ln(\delta_{fnd})$	$\ln(\theta_{pile})$	$\ln(\delta_p)$	$\ln(\delta_a)$	$\ln(\delta_t)$	$\ln(\delta_{brng})$	$\ln(\delta_{seal})$
$\ln(\mu_\phi)$	1.00	0.96	0.97	0.83	0.97	0.44	0.95	0.42	0.96	0.96
$\ln(\delta_{seat})$	0.96	1.00	0.99	0.85	0.96	0.59	0.98	0.48	1.00	1.00
$\ln(\delta_{deck})$	0.97	0.99	1.00	0.86	0.97	0.55	0.97	0.51	0.99	0.99
$\ln(\delta_{fnd})$	0.83	0.85	0.86	1.00	0.90	0.47	0.83	0.41	0.85	0.85
$\ln(\theta_{pile})$	0.97	0.96	0.97	0.90	1.00	0.48	0.95	0.44	0.96	0.96
$\ln(\delta_p)$	0.44	0.59	0.55	0.47	0.48	1.00	0.55	0.60	0.59	0.59
$\ln(\delta_a)$	0.95	0.98	0.97	0.83	0.95	0.55	1.00	0.44	0.98	0.98
$\ln(\delta_t)$	0.42	0.48	0.51	0.41	0.44	0.60	0.44	1.00	0.48	0.48
$\ln(\delta_{brng})$	0.96	1.00	0.99	0.85	0.96	0.59	0.98	0.48	1.00	1.00
$\ln(\delta_{seal})$	0.96	1.00	0.99	0.85	0.96	0.59	0.98	0.48	1.00	1.00

MSCC-TG-M-E2-SX

	$\ln(\mu_\phi)$	$\ln(\delta_{seat})$	$\ln(\delta_{deck})$	$\ln(\delta_{fnd})$	$\ln(\theta_{pile})$	$\ln(\delta_p)$	$\ln(\delta_a)$	$\ln(\delta_t)$	$\ln(\delta_{brng})$	$\ln(\delta_{seal})$
$\ln(\mu_\phi)$	1.00	0.96	0.96	0.65	0.97	0.76	0.77	0.57	0.96	0.96
$\ln(\delta_{seat})$	0.96	1.00	0.99	0.63	0.99	0.80	0.80	0.54	1.00	1.00
$\ln(\delta_{deck})$	0.96	0.99	1.00	0.63	0.99	0.77	0.77	0.54	0.99	0.99
$\ln(\delta_{fnd})$	0.65	0.63	0.63	1.00	0.63	0.49	0.49	0.42	0.63	0.63
$\ln(\theta_{pile})$	0.97	0.99	0.99	0.63	1.00	0.78	0.78	0.53	0.99	0.99
$\ln(\delta_p)$	0.76	0.80	0.77	0.49	0.78	1.00	1.00	0.62	0.80	0.80
$\ln(\delta_a)$	0.77	0.80	0.77	0.49	0.78	1.00	1.00	0.63	0.80	0.80
$\ln(\delta_t)$	0.57	0.54	0.54	0.42	0.53	0.62	0.63	1.00	0.54	0.54
$\ln(\delta_{brng})$	0.96	1.00	0.99	0.63	0.99	0.80	0.80	0.54	1.00	1.00
$\ln(\delta_{seal})$	0.96	1.00	0.99	0.63	0.99	0.80	0.80	0.54	1.00	1.00

MSCC-TG-P-E3-S0

	$\ln(\mu_\phi)$	$\ln(\delta_{deck})$	$\ln(\delta_{fnd})$	$\ln(\theta_{pile})$	$\ln(\delta_p)$	$\ln(\delta_a)$	$\ln(\delta_t)$
$\ln(\mu_\phi)$	1.00	0.87	0.50	0.85	0.74	0.74	0.71
$\ln(\delta_{deck})$	0.87	1.00	0.74	0.97	0.83	0.83	0.85
$\ln(\delta_{fnd})$	0.50	0.74	1.00	0.77	0.68	0.68	0.65
$\ln(\theta_{pile})$	0.85	0.97	0.77	1.00	0.85	0.85	0.85
$\ln(\delta_p)$	0.74	0.83	0.68	0.85	1.00	1.00	0.87
$\ln(\delta_a)$	0.74	0.83	0.68	0.85	1.00	1.00	0.87
$\ln(\delta_t)$	0.71	0.85	0.65	0.85	0.87	0.87	1.00

MSCC-TG-M-E3-S0

	$\ln(\mu_\phi)$	$\ln(\delta_{deck})$	$\ln(\delta_{fnd})$	$\ln(\theta_{pile})$	$\ln(\delta_p)$	$\ln(\delta_a)$	$\ln(\delta_t)$
$\ln(\mu_\phi)$	1.00	0.93	0.66	0.83	0.72	0.72	0.84
$\ln(\delta_{deck})$	0.93	1.00	0.73	0.88	0.75	0.75	0.83
$\ln(\delta_{fnd})$	0.66	0.73	1.00	0.65	0.61	0.61	0.59
$\ln(\theta_{pile})$	0.83	0.88	0.65	1.00	0.72	0.71	0.75
$\ln(\delta_p)$	0.72	0.75	0.61	0.72	1.00	1.00	0.82
$\ln(\delta_a)$	0.72	0.75	0.61	0.71	1.00	1.00	0.82
$\ln(\delta_t)$	0.84	0.83	0.59	0.75	0.82	0.82	1.00

MSCC-TG-P-E3-SX

	$\ln(\mu_\phi)$	$\ln(\delta_{seat})$	$\ln(\delta_{deck})$	$\ln(\delta_{fnd})$	$\ln(\theta_{pile})$	$\ln(\delta_p)$	$\ln(\delta_a)$	$\ln(\delta_t)$	$\ln(\delta_{brng})$	$\ln(\delta_{seal})$
$\ln(\mu_\phi)$	1.00	0.88	0.89	0.37	0.88	0.65	0.86	0.37	0.88	0.88
$\ln(\delta_{seat})$	0.88	1.00	0.98	0.62	0.95	0.67	0.95	0.45	1.00	1.00
$\ln(\delta_{deck})$	0.89	0.98	1.00	0.63	0.96	0.68	0.92	0.46	0.98	0.98
$\ln(\delta_{fnd})$	0.37	0.62	0.63	1.00	0.64	0.49	0.56	0.44	0.62	0.62
$\ln(\theta_{pile})$	0.88	0.95	0.96	0.64	1.00	0.70	0.89	0.40	0.95	0.95
$\ln(\delta_p)$	0.65	0.67	0.68	0.49	0.70	1.00	0.67	0.41	0.67	0.67
$\ln(\delta_a)$	0.86	0.95	0.92	0.56	0.89	0.67	1.00	0.46	0.95	0.95
$\ln(\delta_t)$	0.37	0.45	0.46	0.44	0.40	0.41	0.46	1.00	0.45	0.45
$\ln(\delta_{brng})$	0.88	1.00	0.98	0.62	0.95	0.67	0.95	0.45	1.00	1.00
$\ln(\delta_{seal})$	0.88	1.00	0.98	0.62	0.95	0.67	0.95	0.45	1.00	1.00

MSCC-TG-M-E3-SX

	$\ln(\mu_\phi)$	$\ln(\delta_{seat})$	$\ln(\delta_{deck})$	$\ln(\delta_{fnd})$	$\ln(\theta_{pile})$	$\ln(\delta_p)$	$\ln(\delta_a)$	$\ln(\delta_t)$	$\ln(\delta_{brng})$	$\ln(\delta_{seal})$
$\ln(\mu_\phi)$	1.00	0.96	0.95	0.69	0.98	0.78	0.78	0.45	0.96	0.96
$\ln(\delta_{seat})$	0.96	1.00	1.00	0.70	0.99	0.82	0.82	0.49	1.00	1.00
$\ln(\delta_{deck})$	0.95	1.00	1.00	0.69	0.99	0.81	0.81	0.50	1.00	1.00
$\ln(\delta_{fnd})$	0.69	0.70	0.69	1.00	0.69	0.62	0.62	0.47	0.70	0.70
$\ln(\theta_{pile})$	0.98	0.99	0.99	0.69	1.00	0.81	0.81	0.49	0.99	0.99
$\ln(\delta_p)$	0.78	0.82	0.81	0.62	0.81	1.00	1.00	0.53	0.82	0.82
$\ln(\delta_a)$	0.78	0.82	0.81	0.62	0.81	1.00	1.00	0.53	0.82	0.82
$\ln(\delta_t)$	0.45	0.49	0.50	0.47	0.49	0.53	0.53	1.00	0.49	0.49
$\ln(\delta_{brng})$	0.96	1.00	1.00	0.70	0.99	0.82	0.82	0.49	1.00	1.00
$\ln(\delta_{seal})$	0.96	1.00	1.00	0.70	0.99	0.82	0.82	0.49	1.00	1.00

Table B.8: Correlation Coefficients of the component demands of multispan continuous concrete I-girder bridge class and the respective seismic performance sub-bins

MSCC-IG-S-E1-S0

	$\ln(\mu_\phi)$	$\ln(\delta_{deck})$	$\ln(\delta_{fnd})$	$\ln(\theta_{pile})$	$\ln(\delta_p)$	$\ln(\delta_a)$	$\ln(\delta_t)$	$\ln(\delta_{brng})$	$\ln(\delta_{rest})$	$\ln(\delta_{key})$
$\ln(\mu_\phi)$	1.00	0.90	0.91	0.98	0.70	0.64	0.83	0.94	0.73	0.37
$\ln(\delta_{deck})$	0.90	1.00	0.89	0.90	0.78	0.75	0.89	0.98	0.79	0.35
$\ln(\delta_{fnd})$	0.91	0.89	1.00	0.96	0.71	0.66	0.83	0.91	0.71	0.27
$\ln(\theta_{pile})$	0.98	0.90	0.96	1.00	0.72	0.66	0.83	0.94	0.71	0.32
$\ln(\delta_p)$	0.70	0.78	0.71	0.72	1.00	0.93	0.75	0.76	0.68	0.29
$\ln(\delta_a)$	0.64	0.75	0.66	0.66	0.93	1.00	0.75	0.72	0.70	0.30
$\ln(\delta_t)$	0.83	0.89	0.83	0.83	0.75	0.75	1.00	0.90	0.69	0.30
$\ln(\delta_{brng})$	0.94	0.98	0.91	0.94	0.76	0.72	0.90	1.00	0.77	0.37
$\ln(\delta_{rest})$	0.73	0.79	0.71	0.71	0.68	0.70	0.69	0.77	1.00	0.29
$\ln(\delta_{key})$	0.37	0.35	0.27	0.32	0.29	0.30	0.30	0.37	0.29	1.00

MSCC-IG-M-E1-S0

	$\ln(\mu_\phi)$	$\ln(\delta_{deck})$	$\ln(\delta_{fnd})$	$\ln(\theta_{pile})$	$\ln(\delta_p)$	$\ln(\delta_a)$	$\ln(\delta_t)$	$\ln(\delta_{brng})$	$\ln(\delta_{rest})$	$\ln(\delta_{key})$
$\ln(\mu_\phi)$	1.00	0.83	0.66	0.95	0.66	0.68	0.80	0.87	0.64	0.26
$\ln(\delta_{deck})$	0.83	1.00	0.56	0.87	0.78	0.78	0.87	0.95	0.67	0.37
$\ln(\delta_{fnd})$	0.66	0.56	1.00	0.67	0.35	0.38	0.48	0.64	0.48	0.14
$\ln(\theta_{pile})$	0.95	0.87	0.67	1.00	0.70	0.72	0.82	0.92	0.70	0.26
$\ln(\delta_p)$	0.66	0.78	0.35	0.70	1.00	0.97	0.80	0.69	0.60	0.42
$\ln(\delta_a)$	0.68	0.78	0.38	0.72	0.97	1.00	0.83	0.69	0.60	0.41
$\ln(\delta_t)$	0.80	0.87	0.48	0.82	0.80	0.83	1.00	0.83	0.55	0.38
$\ln(\delta_{brng})$	0.87	0.95	0.64	0.92	0.69	0.69	0.83	1.00	0.70	0.28
$\ln(\delta_{rest})$	0.64	0.67	0.48	0.70	0.60	0.60	0.55	0.70	1.00	0.27
$\ln(\delta_{key})$	0.26	0.37	0.14	0.26	0.42	0.41	0.38	0.28	0.27	1.00

MSCC-IG-S-E1-SX

	$\ln(\mu_\phi)$	$\ln(\delta_{seat})$	$\ln(\delta_{deck})$	$\ln(\delta_{fnd})$	$\ln(\theta_{pile})$	$\ln(\delta_p)$	$\ln(\delta_a)$	$\ln(\delta_t)$	$\ln(\delta_{brng})$	$\ln(\delta_{seat})$	$\ln(\delta_{rest})$	$\ln(\delta_{key})$
$\ln(\mu_\phi)$	1.00	0.70	0.94	0.84	0.97	0.77	0.77	0.85	0.94	0.70	0.62	0.54
$\ln(\delta_{seat})$	0.70	1.00	0.74	0.53	0.68	0.91	0.92	0.68	0.74	1.00	0.97	0.62
$\ln(\delta_{deck})$	0.94	0.74	1.00	0.84	0.93	0.80	0.80	0.87	0.99	0.74	0.69	0.58
$\ln(\delta_{fnd})$	0.84	0.53	0.84	1.00	0.89	0.67	0.65	0.73	0.86	0.53	0.48	0.44
$\ln(\theta_{pile})$	0.97	0.68	0.93	0.89	1.00	0.76	0.76	0.84	0.94	0.68	0.62	0.55
$\ln(\delta_p)$	0.77	0.91	0.80	0.67	0.76	1.00	0.98	0.70	0.80	0.91	0.85	0.61
$\ln(\delta_a)$	0.77	0.92	0.80	0.65	0.76	0.98	1.00	0.72	0.81	0.92	0.87	0.63
$\ln(\delta_t)$	0.85	0.68	0.87	0.73	0.84	0.70	0.72	1.00	0.88	0.68	0.66	0.52
$\ln(\delta_{brng})$	0.94	0.74	0.99	0.86	0.94	0.80	0.81	0.88	1.00	0.74	0.69	0.57
$\ln(\delta_{seat})$	0.70	1.00	0.74	0.53	0.68	0.91	0.92	0.68	0.74	1.00	0.97	0.62
$\ln(\delta_{rest})$	0.62	0.97	0.69	0.48	0.62	0.85	0.87	0.66	0.69	0.97	1.00	0.55
$\ln(\delta_{key})$	0.54	0.62	0.58	0.44	0.55	0.61	0.63	0.52	0.57	0.62	0.55	1.00

MSCC-IG-M-E1-SX

	$\ln(\mu_\phi)$	$\ln(\delta_{seat})$	$\ln(\delta_{deck})$	$\ln(\delta_{fnd})$	$\ln(\theta_{pile})$	$\ln(\delta_p)$	$\ln(\delta_a)$	$\ln(\delta_t)$	$\ln(\delta_{brng})$	$\ln(\delta_{seat})$	$\ln(\delta_{rest})$	$\ln(\delta_{key})$
$\ln(\mu_\phi)$	1.00	0.84	0.91	0.62	0.93	0.77	0.76	0.72	0.89	0.84	0.79	0.20
$\ln(\delta_{seat})$	0.84	1.00	0.93	0.58	0.93	0.87	0.86	0.65	0.92	1.00	0.80	0.27
$\ln(\delta_{deck})$	0.91	0.93	1.00	0.66	0.97	0.83	0.81	0.74	0.98	0.93	0.82	0.24
$\ln(\delta_{fnd})$	0.62	0.58	0.66	1.00	0.68	0.56	0.56	0.55	0.67	0.58	0.59	0.26
$\ln(\theta_{pile})$	0.93	0.93	0.97	0.68	1.00	0.84	0.83	0.71	0.96	0.93	0.83	0.24

$\ln(\delta_p)$	0.77	0.87	0.83	0.56	0.84	1.00	0.95	0.62	0.81	0.87	0.82	0.27
$\ln(\delta_a)$	0.76	0.86	0.81	0.56	0.83	0.95	1.00	0.59	0.79	0.86	0.81	0.24
$\ln(\delta_t)$	0.72	0.65	0.74	0.55	0.71	0.62	0.59	1.00	0.77	0.65	0.52	0.09
$\ln(\delta_{brng})$	0.89	0.92	0.98	0.67	0.96	0.81	0.79	0.77	1.00	0.92	0.79	0.21
$\ln(\delta_{seai})$	0.84	1.00	0.93	0.58	0.93	0.87	0.86	0.65	0.92	1.00	0.80	0.27
$\ln(\delta_{rest})$	0.79	0.80	0.82	0.59	0.83	0.82	0.81	0.52	0.79	0.80	1.00	0.23
$\ln(\delta_{key})$	0.20	0.27	0.24	0.26	0.24	0.27	0.24	0.09	0.21	0.27	0.23	1.00

MSCC-IG-S-E2-S0

	$\ln(\mu_\phi)$	$\ln(\delta_{deck})$	$\ln(\delta_{fnd})$	$\ln(\theta_{pile})$	$\ln(\delta_p)$	$\ln(\delta_a)$	$\ln(\delta_t)$	$\ln(\delta_{brng})$	$\ln(\delta_{rest})$	$\ln(\delta_{key})$
$\ln(\mu_\phi)$	1.00	0.66	0.91	0.91	0.97	0.71	0.63	0.89	0.95	0.66
$\ln(\delta_{deck})$	0.66	1.00	0.82	0.76	0.73	0.85	0.80	0.77	0.78	1.00
$\ln(\delta_{fnd})$	0.91	0.82	1.00	0.94	0.95	0.86	0.79	0.92	0.98	0.82
$\ln(\theta_{pile})$	0.91	0.76	0.94	1.00	0.97	0.78	0.69	0.89	0.95	0.76
$\ln(\delta_p)$	0.97	0.73	0.95	0.97	1.00	0.76	0.66	0.91	0.97	0.73
$\ln(\delta_a)$	0.71	0.85	0.86	0.78	0.76	1.00	0.93	0.84	0.82	0.85
$\ln(\delta_t)$	0.63	0.80	0.79	0.69	0.66	0.93	1.00	0.73	0.73	0.80
$\ln(\delta_{brng})$	0.89	0.77	0.92	0.89	0.91	0.84	0.73	1.00	0.94	0.77
$\ln(\delta_{rest})$	0.95	0.78	0.98	0.95	0.97	0.82	0.73	0.94	1.00	0.78
$\ln(\delta_{key})$	0.66	1.00	0.82	0.76	0.73	0.85	0.80	0.77	0.78	1.00

MSCC-IG-M-E2-S0

	$\ln(\mu_\phi)$	$\ln(\delta_{deck})$	$\ln(\delta_{fnd})$	$\ln(\theta_{pile})$	$\ln(\delta_p)$	$\ln(\delta_a)$	$\ln(\delta_t)$	$\ln(\delta_{brng})$	$\ln(\delta_{rest})$	$\ln(\delta_{key})$
$\ln(\mu_\phi)$	1.00	0.64	0.87	0.69	0.96	0.67	0.67	0.77	0.92	0.64
$\ln(\delta_{deck})$	0.64	1.00	0.68	0.49	0.68	0.68	0.70	0.58	0.69	1.00
$\ln(\delta_{fnd})$	0.87	0.68	1.00	0.64	0.90	0.75	0.75	0.86	0.96	0.68
$\ln(\theta_{pile})$	0.69	0.49	0.64	1.00	0.73	0.38	0.39	0.51	0.73	0.49
$\ln(\delta_p)$	0.96	0.68	0.90	0.73	1.00	0.68	0.67	0.78	0.95	0.68
$\ln(\delta_a)$	0.67	0.68	0.75	0.38	0.68	1.00	0.96	0.82	0.70	0.68
$\ln(\delta_t)$	0.67	0.70	0.75	0.39	0.67	0.96	1.00	0.84	0.70	0.70
$\ln(\delta_{brng})$	0.77	0.58	0.86	0.51	0.78	0.82	0.84	1.00	0.82	0.58
$\ln(\delta_{rest})$	0.92	0.69	0.96	0.73	0.95	0.70	0.70	0.82	1.00	0.69
$\ln(\delta_{key})$	0.64	1.00	0.68	0.49	0.68	0.68	0.70	0.58	0.69	1.00

MSCC-IG-S-E2-SX

	$\ln(\mu_\phi)$	$\ln(\delta_{seai})$	$\ln(\delta_{deck})$	$\ln(\delta_{fnd})$	$\ln(\theta_{pile})$	$\ln(\delta_p)$	$\ln(\delta_a)$	$\ln(\delta_t)$	$\ln(\delta_{brng})$	$\ln(\delta_{seai})$	$\ln(\delta_{rest})$	$\ln(\delta_{key})$
$\ln(\mu_\phi)$	1.00	0.71	0.91	0.81	0.96	0.69	0.66	0.81	0.91	0.71	0.72	0.43
$\ln(\delta_{seai})$	0.71	1.00	0.77	0.61	0.74	0.90	0.88	0.74	0.77	1.00	0.94	0.63
$\ln(\delta_{deck})$	0.91	0.77	1.00	0.86	0.93	0.75	0.74	0.85	0.99	0.77	0.79	0.52
$\ln(\delta_{fnd})$	0.81	0.61	0.86	1.00	0.88	0.54	0.51	0.74	0.87	0.61	0.66	0.49
$\ln(\theta_{pile})$	0.96	0.74	0.93	0.88	1.00	0.69	0.65	0.78	0.93	0.74	0.74	0.41
$\ln(\delta_p)$	0.69	0.90	0.75	0.54	0.69	1.00	0.96	0.73	0.74	0.90	0.85	0.57
$\ln(\delta_a)$	0.66	0.88	0.74	0.51	0.65	0.96	1.00	0.71	0.72	0.88	0.85	0.57
$\ln(\delta_t)$	0.81	0.74	0.85	0.74	0.78	0.73	0.71	1.00	0.85	0.74	0.73	0.55
$\ln(\delta_{brng})$	0.91	0.77	0.99	0.87	0.93	0.74	0.72	0.85	1.00	0.77	0.79	0.55
$\ln(\delta_{seai})$	0.71	1.00	0.77	0.61	0.74	0.90	0.88	0.74	0.77	1.00	0.94	0.63
$\ln(\delta_{rest})$	0.72	0.94	0.79	0.66	0.74	0.85	0.85	0.73	0.79	0.94	1.00	0.59
$\ln(\delta_{key})$	0.43	0.63	0.52	0.49	0.41	0.57	0.57	0.55	0.55	0.63	0.59	1.00

MSCC-IG-M-E2-SX

	$\ln(\mu_\varphi)$	$\ln(\delta_{\text{seat}})$	$\ln(\delta_{\text{deck}})$	$\ln(\delta_{\text{fnd}})$	$\ln(\theta_{\text{pile}})$	$\ln(\delta_p)$	$\ln(\delta_a)$	$\ln(\delta_i)$	$\ln(\delta_{\text{brng}})$	$\ln(\delta_{\text{seal}})$	$\ln(\delta_{\text{rest}})$	$\ln(\delta_{\text{key}})$
$\ln(\mu_\varphi)$	1.00	0.75	0.84	0.55	0.89	0.76	0.75	0.77	0.85	0.75	0.69	0.18
$\ln(\delta_{\text{seat}})$	0.75	1.00	0.90	0.36	0.89	0.87	0.86	0.66	0.89	1.00	0.85	0.25
$\ln(\delta_{\text{deck}})$	0.84	0.90	1.00	0.52	0.96	0.83	0.81	0.80	0.98	0.90	0.81	0.17
$\ln(\delta_{\text{fnd}})$	0.55	0.36	0.52	1.00	0.54	0.41	0.36	0.58	0.54	0.36	0.33	0.13
$\ln(\theta_{\text{pile}})$	0.89	0.89	0.96	0.54	1.00	0.82	0.81	0.79	0.97	0.89	0.81	0.21
$\ln(\delta_p)$	0.76	0.87	0.83	0.41	0.82	1.00	0.95	0.68	0.81	0.87	0.81	0.25
$\ln(\delta_a)$	0.75	0.86	0.81	0.36	0.81	0.95	1.00	0.67	0.80	0.86	0.79	0.25
$\ln(\delta_i)$	0.77	0.66	0.80	0.58	0.79	0.68	0.67	1.00	0.81	0.66	0.61	0.03
$\ln(\delta_{\text{brng}})$	0.85	0.89	0.98	0.54	0.97	0.81	0.80	0.81	1.00	0.89	0.80	0.19
$\ln(\delta_{\text{seal}})$	0.75	1.00	0.90	0.36	0.89	0.87	0.86	0.66	0.89	1.00	0.85	0.25
$\ln(\delta_{\text{rest}})$	0.69	0.85	0.81	0.33	0.81	0.81	0.79	0.61	0.80	0.85	1.00	0.24
$\ln(\delta_{\text{key}})$	0.18	0.25	0.17	0.13	0.21	0.25	0.25	0.03	0.19	0.25	0.24	1.00

MSCC-IG-S-E3-S0

	$\ln(\mu_\varphi)$	$\ln(\delta_{\text{deck}})$	$\ln(\delta_{\text{fnd}})$	$\ln(\theta_{\text{pile}})$	$\ln(\delta_p)$	$\ln(\delta_a)$	$\ln(\delta_i)$	$\ln(\delta_{\text{brng}})$	$\ln(\delta_{\text{rest}})$	$\ln(\delta_{\text{key}})$
$\ln(\mu_\varphi)$	1.00	0.64	0.89	0.89	0.98	0.53	0.47	0.86	0.95	0.64
$\ln(\delta_{\text{deck}})$	0.64	1.00	0.78	0.66	0.69	0.78	0.80	0.79	0.74	1.00
$\ln(\delta_{\text{fnd}})$	0.89	0.78	1.00	0.89	0.92	0.72	0.65	0.92	0.98	0.78
$\ln(\theta_{\text{pile}})$	0.89	0.66	0.89	1.00	0.94	0.60	0.51	0.84	0.92	0.66
$\ln(\delta_p)$	0.98	0.69	0.92	0.94	1.00	0.58	0.52	0.88	0.97	0.69
$\ln(\delta_a)$	0.53	0.78	0.72	0.60	0.58	1.00	0.94	0.72	0.64	0.78
$\ln(\delta_i)$	0.47	0.80	0.65	0.51	0.52	0.94	1.00	0.69	0.57	0.80
$\ln(\delta_{\text{brng}})$	0.86	0.79	0.92	0.84	0.88	0.72	0.69	1.00	0.92	0.79
$\ln(\delta_{\text{rest}})$	0.95	0.74	0.98	0.92	0.97	0.64	0.57	0.92	1.00	0.74
$\ln(\delta_{\text{key}})$	0.64	1.00	0.78	0.66	0.69	0.78	0.80	0.79	0.74	1.00

MSCC-IG-M-E3-S0

	$\ln(\mu_\varphi)$	$\ln(\delta_{\text{deck}})$	$\ln(\delta_{\text{fnd}})$	$\ln(\theta_{\text{pile}})$	$\ln(\delta_p)$	$\ln(\delta_a)$	$\ln(\delta_i)$	$\ln(\delta_{\text{brng}})$	$\ln(\delta_{\text{rest}})$	$\ln(\delta_{\text{key}})$
$\ln(\mu_\varphi)$	1.00	0.66	0.90	0.75	0.96	0.72	0.72	0.80	0.93	0.66
$\ln(\delta_{\text{deck}})$	0.66	1.00	0.74	0.53	0.72	0.65	0.68	0.62	0.74	1.00
$\ln(\delta_{\text{fnd}})$	0.90	0.74	1.00	0.67	0.91	0.79	0.80	0.85	0.96	0.74
$\ln(\theta_{\text{pile}})$	0.75	0.53	0.67	1.00	0.75	0.54	0.53	0.58	0.73	0.53
$\ln(\delta_p)$	0.96	0.72	0.91	0.75	1.00	0.72	0.72	0.79	0.96	0.72
$\ln(\delta_a)$	0.72	0.65	0.79	0.54	0.72	1.00	0.95	0.81	0.75	0.65
$\ln(\delta_i)$	0.72	0.68	0.80	0.53	0.72	0.95	1.00	0.85	0.75	0.68
$\ln(\delta_{\text{brng}})$	0.80	0.62	0.85	0.58	0.79	0.81	0.85	1.00	0.82	0.62
$\ln(\delta_{\text{rest}})$	0.93	0.74	0.96	0.73	0.96	0.75	0.75	0.82	1.00	0.74
$\ln(\delta_{\text{key}})$	0.66	1.00	0.74	0.53	0.72	0.65	0.68	0.62	0.74	1.00

MSCC-IG-S-E3-SX

	$\ln(\mu_\varphi)$	$\ln(\delta_{\text{seat}})$	$\ln(\delta_{\text{deck}})$	$\ln(\delta_{\text{fnd}})$	$\ln(\theta_{\text{pile}})$	$\ln(\delta_p)$	$\ln(\delta_a)$	$\ln(\delta_i)$	$\ln(\delta_{\text{brng}})$	$\ln(\delta_{\text{seal}})$	$\ln(\delta_{\text{rest}})$	$\ln(\delta_{\text{key}})$
$\ln(\mu_\varphi)$	1.00	0.63	0.83	0.60	0.88	0.56	0.58	0.67	0.84	0.63	0.67	0.39
$\ln(\delta_{\text{seat}})$	0.63	1.00	0.70	0.38	0.59	0.86	0.80	0.61	0.68	1.00	0.94	0.48
$\ln(\delta_{\text{deck}})$	0.83	0.70	1.00	0.69	0.87	0.58	0.58	0.65	0.99	0.70	0.72	0.37
$\ln(\delta_{\text{fnd}})$	0.60	0.38	0.69	1.00	0.82	0.29	0.30	0.49	0.73	0.38	0.40	0.20
$\ln(\theta_{\text{pile}})$	0.88	0.59	0.87	0.82	1.00	0.51	0.52	0.63	0.89	0.59	0.62	0.40
$\ln(\delta_p)$	0.56	0.86	0.58	0.29	0.51	1.00	0.94	0.62	0.56	0.86	0.80	0.40
$\ln(\delta_a)$	0.58	0.80	0.58	0.30	0.52	0.94	1.00	0.63	0.56	0.80	0.77	0.37
$\ln(\delta_i)$	0.67	0.61	0.65	0.49	0.63	0.62	0.63	1.00	0.66	0.61	0.65	0.30

$\ln(\delta_{brng})$	0.84	0.68	0.99	0.73	0.89	0.56	0.56	0.66	1.00	0.68	0.70	0.35
$\ln(\delta_{seal})$	0.63	1.00	0.70	0.38	0.59	0.86	0.80	0.61	0.68	1.00	0.94	0.48
$\ln(\delta_{rest})$	0.67	0.94	0.72	0.40	0.62	0.80	0.77	0.65	0.70	0.94	1.00	0.50
$\ln(\delta_{key})$	0.39	0.48	0.37	0.20	0.40	0.40	0.37	0.30	0.35	0.48	0.50	1.00

MSCC-IG-M-E3-SX

	$\ln(\mu_\phi)$	$\ln(\delta_{seal})$	$\ln(\delta_{deck})$	$\ln(\delta_{fnd})$	$\ln(\theta_{pile})$	$\ln(\delta_p)$	$\ln(\delta_a)$	$\ln(\delta_i)$	$\ln(\delta_{brng})$	$\ln(\delta_{seal})$	$\ln(\delta_{rest})$	$\ln(\delta_{key})$
$\ln(\mu_\phi)$	1.00	0.78	0.85	0.54	0.88	0.72	0.73	0.77	0.85	0.78	0.70	0.24
$\ln(\delta_{seal})$	0.78	1.00	0.90	0.45	0.91	0.87	0.87	0.73	0.89	1.00	0.82	0.22
$\ln(\delta_{deck})$	0.85	0.90	1.00	0.59	0.96	0.79	0.79	0.82	0.98	0.90	0.81	0.20
$\ln(\delta_{fnd})$	0.54	0.45	0.59	1.00	0.57	0.43	0.40	0.57	0.61	0.45	0.56	0.16
$\ln(\theta_{pile})$	0.88	0.91	0.96	0.57	1.00	0.80	0.81	0.81	0.96	0.91	0.81	0.22
$\ln(\delta_p)$	0.72	0.87	0.79	0.43	0.80	1.00	0.96	0.66	0.78	0.87	0.78	0.21
$\ln(\delta_a)$	0.73	0.87	0.79	0.40	0.81	0.96	1.00	0.67	0.77	0.87	0.76	0.19
$\ln(\delta_i)$	0.77	0.73	0.82	0.57	0.81	0.66	0.67	1.00	0.86	0.73	0.68	0.14
$\ln(\delta_{brng})$	0.85	0.89	0.98	0.61	0.96	0.78	0.77	0.86	1.00	0.89	0.80	0.19
$\ln(\delta_{seal})$	0.78	1.00	0.90	0.45	0.91	0.87	0.87	0.73	0.89	1.00	0.82	0.22
$\ln(\delta_{rest})$	0.70	0.82	0.81	0.56	0.81	0.78	0.76	0.68	0.80	0.82	1.00	0.31
$\ln(\delta_{key})$	0.24	0.22	0.20	0.16	0.22	0.21	0.19	0.14	0.19	0.22	0.31	1.00

APPENDIX C

OPTIMAL INTENSITY MEASURE INVESTIGATION

This appendix presents the results from the investigation of optimal intensity measures across the bridge classes and seismic performance sub-bins considered in this study. This was detailed in section 5.4 of Chapter 5. Efficiency, practicality, proficiency, and sufficiency are some of the essential properties of an optimal IM and the results are presented in Table C.1.

Table C.1: Investigation of efficiency, proficiency, practicality and sufficiency properties to investigate optimality of intensity measures

Bridge class	SPS	IM	Column curvature ductility, μ_ϕ								Abutment seat displacement, δ_{seat}							
			$\log(a)$	b	R^2	β_{DIM}	ζ	p_M	p_R	p_ε	$\log(a)$	b	R^2	β_{DIM}	ζ	p_M	p_R	p_ε
MSCC-BG-S	E1-S0	PGA	2.28	1.28	0.82	0.53	0.41	0.84	0.12	0.91								
		S _{a-0.3}	1.20	1.24	0.79	0.56	0.45	0.53	0.56	0.77								
		S _{a-0.2}	1.28	1.29	0.72	0.67	0.52	0.66	0.83	0.39								
		S _{a-1.0}	1.85	1.09	0.81	0.54	0.49	0.66	0.54	0.73								
	E1-SX	PGA	2.27	1.09	0.74	0.60	0.55	0.31	0.93	0.95	1.52	0.75	0.70	0.45	0.60	0.69	0.31	0.01
		S _{a-0.3}	1.42	1.11	0.70	0.66	0.59	1.00	0.52	0.01	0.95	0.75	0.69	0.45	0.60	0.16	1.00	0.76
		S _{a-0.2}	1.37	1.03	0.64	0.70	0.68	0.54	0.32	0.59	0.88	0.69	0.60	0.51	0.74	0.22	0.76	0.60
		S _{a-1.0}	2.16	1.12	0.86	0.48	0.43	0.44	0.36	0.23	1.41	0.74	0.85	0.33	0.45	0.87	0.79	0.66
	E2-S0	PGA	1.87	1.09	0.61	0.66	0.61	0.29	0.67	0.42								
		S _{a-0.3}	0.93	1.22	0.57	0.74	0.60	0.55	0.22	0.67								
		S _{a-0.2}	0.98	0.98	0.46	0.77	0.79	0.31	0.24	0.24								
		S _{a-1.0}	1.61	1.02	0.68	0.62	0.61	0.21	0.96	0.08								
	E2-SX	PGA	2.41	1.14	0.72	0.64	0.56	0.36	0.28	0.56	1.53	0.72	0.63	0.47	0.65	0.70	0.61	0.65
		S _{a-0.3}	1.34	1.21	0.76	0.62	0.52	0.66	0.62	0.25	0.95	0.79	0.63	0.52	0.66	0.72	0.29	0.18
		S _{a-0.2}	1.46	1.16	0.62	0.79	0.68	0.54	0.64	0.07	0.93	0.74	0.59	0.52	0.70	0.09	0.09	0.11
		S _{a-1.0}	2.24	1.32	0.81	0.58	0.44	0.27	0.08	0.22	1.41	0.76	0.77	0.37	0.49	0.54	0.06	0.96
	E3-S0	PGA	2.21	1.33	0.84	0.52	0.39	0.50	0.68	0.25								
		S _{a-0.3}	0.96	1.22	0.79	0.58	0.48	0.76	0.89	0.74								
		S _{a-0.2}	1.09	1.30	0.73	0.68	0.52	0.24	0.48	0.98								
		S _{a-1.0}	2.15	1.41	0.91	0.44	0.31	0.96	0.93	0.89								
	E3-SX	PGA	2.14	1.32	0.86	0.41	0.31	0.63	0.85	0.03	1.38	0.77	0.69	0.39	0.51	0.25	0.43	0.44
		S _{a-0.3}	1.05	1.29	0.75	0.57	0.45	0.08	0.02	0.09	0.76	0.72	0.71	0.36	0.50	0.29	0.04	0.15
		S _{a-0.2}	1.00	1.28	0.70	0.62	0.48	0.28	0.12	0.79	0.75	0.71	0.57	0.46	0.64	0.50	0.45	0.51
		S _{a-1.0}	1.66	1.14	0.87	0.41	0.37	0.33	0.01	0.53	1.16	0.67	0.85	0.26	0.38	0.81	0.13	0.00

MSCC-BG-M	E1-S0	PGA	2.63	1.11	0.57	0.81	0.73	0.75	0.36	0.21								
		S _{a-0.3}	1.67	1.09	0.55	0.82	0.75	0.31	0.53	0.70								
		S _{a-0.2}	1.56	0.90	0.41	0.91	1.00	0.02	0.72	0.90								
		S _{a-1.0}	2.72	1.21	0.83	0.50	0.41	0.64	0.90	0.33								
	E1-SX	PGA	3.30	1.20	0.53	0.90	0.75	0.70	0.82	0.64	2.23	0.91	0.57	0.61	0.67	0.76	0.64	0.11
		S _{a-0.3}	2.21	1.14	0.50	0.93	0.81	0.64	0.82	0.62	1.44	0.88	0.56	0.61	0.70	0.60	0.25	0.58
		S _{a-0.2}	2.24	1.08	0.38	1.03	0.95	0.37	0.78	0.31	1.46	0.85	0.43	0.71	0.84	0.44	0.01	0.12
		S _{a-1.0}	3.26	1.28	0.76	0.67	0.53	0.02	0.38	0.55	2.12	0.91	0.80	0.42	0.46	0.12	1.00	0.87
	E2-S0	PGA	2.74	1.37	0.66	0.85	0.62	0.09	0.34	0.12								
		S _{a-0.3}	1.61	1.35	0.62	0.93	0.69	0.75	0.38	0.49								
		S _{a-0.2}	1.53	1.24	0.52	1.01	0.81	0.78	0.58	0.18								
		S _{a-1.0}	2.54	1.31	0.79	0.66	0.50	0.80	0.49	0.08								
	E2-SX	PGA	3.06	1.35	0.55	1.02	0.75	0.72	0.99	0.17	2.07	0.96	0.68	0.54	0.56	0.70	0.44	0.12
		S _{a-0.3}	1.97	1.33	0.54	1.03	0.77	0.49	0.83	0.02	1.25	0.89	0.64	0.56	0.62	0.93	0.24	0.45
		S _{a-0.2}	1.87	1.20	0.42	1.16	0.97	0.43	0.93	0.48	1.23	0.85	0.53	0.65	0.77	0.44	0.24	0.67
		S _{a-1.0}	3.02	1.37	0.74	0.81	0.59	0.56	0.77	0.16	1.97	0.93	0.86	0.37	0.40	0.80	0.26	0.10
	E3-S0	PGA	3.15	1.52	0.67	0.83	0.55	0.62	0.36	0.18								
		S _{a-0.3}	1.86	1.42	0.63	0.87	0.62	0.99	0.44	0.14								
		S _{a-0.2}	1.78	1.27	0.56	0.89	0.70	0.04	0.32	0.30								
		S _{a-1.0}	2.72	1.30	0.79	0.64	0.49	0.65	0.43	0.76								
	E3-SX	PGA	2.61	1.04	0.51	0.82	0.79	0.91	0.86	0.07	2.14	0.97	0.62	0.65	0.67	0.62	0.12	0.89
		S _{a-0.3}	1.78	1.02	0.48	0.89	0.87	0.11	0.41	0.69	1.34	0.95	0.65	0.62	0.65	0.92	0.52	0.56
		S _{a-0.2}	1.72	0.95	0.39	0.96	1.01	0.22	0.65	0.77	1.28	0.88	0.51	0.73	0.84	0.97	0.52	0.02
		S _{a-1.0}	2.62	1.09	0.77	0.57	0.52	0.67	0.82	0.81	2.04	0.95	0.79	0.47	0.49	0.02	0.83	0.69
MSCC-SL-P	EX-S0	PGA	0.19	0.95	0.75	0.46	0.49	0.78	0.00	0.00								
		S _{a-0.3}	-0.53	1.01	0.78	0.45	0.45	1.00	0.02	0.00								

EX-SX	S _{a-0.2}	-0.60	0.89	0.65	0.53	0.59	0.82	0.01	0.00									
	S _{a-1.0}	-0.02	0.83	0.80	0.41	0.50	0.58	0.09	0.00									
	PGA	0.69	0.98	0.54	0.75	0.77	0.39	0.04	0.06	2.06	0.80	0.48	0.68	0.85	0.28	0.06	0.95	
	S _{a-0.3}	-0.12	0.97	0.54	0.74	0.76	0.81	0.05	0.00	1.39	0.78	0.48	0.67	0.87	0.68	0.58	0.83	
	S _{a-0.2}	-0.17	0.88	0.42	0.84	0.95	0.48	0.17	0.31	1.42	0.76	0.43	0.70	0.92	0.62	0.11	0.25	
	S _{a-1.0}	0.60	0.97	0.68	0.63	0.65	0.56	0.03	0.00	1.89	0.78	0.58	0.63	0.81	0.40	0.92	0.87	
MSCC-TG-P	E1-S0	PGA	0.51	1.11	0.78	0.54	0.49	0.76	0.02	0.19								
		S _{a-0.3}	-0.46	1.00	0.74	0.52	0.53	0.41	0.20	0.01								
		S _{a-0.2}	-0.43	1.05	0.72	0.59	0.56	0.62	0.07	0.03								
		S _{a-1.0}	0.12	0.91	0.79	0.51	0.55	0.04	0.16	0.00								
	E1-SX	PGA	1.41	1.09	0.66	0.61	0.56	1.00	0.71	0.91	2.78	1.23	0.78	0.52	0.42	0.41	0.27	0.84
		S _{a-0.3}	0.44	1.06	0.66	0.62	0.59	0.26	0.80	0.66	1.64	1.15	0.79	0.50	0.44	0.13	0.40	0.04
		S _{a-0.2}	0.44	0.96	0.56	0.66	0.68	0.05	0.69	0.19	1.61	1.06	0.68	0.61	0.58	0.83	0.34	0.87
		S _{a-1.0}	1.21	1.06	0.77	0.52	0.49	0.03	0.65	0.23	2.45	1.14	0.92	0.31	0.27	0.61	0.84	0.69
	E2-S0	PGA	0.17	0.89	0.65	0.54	0.61	0.28	0.90	0.36								
		S _{a-0.3}	-0.52	0.95	0.70	0.54	0.57	0.75	0.60	0.40								
		S _{a-0.2}	-0.55	0.88	0.63	0.55	0.63	0.40	0.62	0.70								
		S _{a-1.0}	0.14	0.99	0.79	0.47	0.48	0.84	0.36	0.00								
	E2-SX	PGA	1.17	1.09	0.61	0.75	0.69	0.66	0.53	0.74	2.59	1.19	0.70	0.68	0.57	0.92	0.73	0.25
		S _{a-0.3}	0.28	1.09	0.60	0.76	0.70	0.74	0.92	0.07	1.60	1.19	0.70	0.68	0.57	0.56	0.45	0.86
		S _{a-0.2}	0.24	0.98	0.52	0.80	0.81	0.75	0.60	0.15	1.56	1.08	0.58	0.79	0.73	0.29	0.63	0.29
		S _{a-1.0}	0.96	1.03	0.70	0.67	0.65	0.93	0.30	0.11	2.32	1.14	0.80	0.57	0.50	0.24	0.25	0.11
	E3-S0	PGA	0.33	0.99	0.71	0.56	0.56	0.94	0.01	0.02								
		S _{a-0.3}	-0.52	0.98	0.70	0.55	0.56	0.94	0.01	0.31								
		S _{a-0.2}	-0.48	0.97	0.70	0.53	0.55	0.93	0.00	0.00								
		S _{a-1.0}	0.15	0.97	0.76	0.49	0.51	0.92	0.03	0.00								
	E3-SX	PGA	0.84	0.88	0.64	0.52	0.59	0.91	0.10	0.00	2.64	1.14	0.79	0.46	0.41	0.34	0.50	0.32

		S _{a-0.3}	0.14	0.89	0.69	0.48	0.54	0.56	0.45	0.57	1.70	1.21	0.82	0.46	0.38	0.28	0.70	0.93
		S _{a-0.2}	0.10	0.80	0.55	0.57	0.71	0.56	0.35	0.15	1.71	1.16	0.73	0.56	0.48	0.57	0.99	0.43
		S _{a-1.0}	0.72	0.87	0.80	0.39	0.45	0.04	0.86	0.05	2.34	1.04	0.92	0.31	0.30	0.45	0.36	0.65
MSCC-TG-M	E1-S0	PGA	0.99	0.91	0.78	0.39	0.43	0.54	0.04	0.33								
		S _{a-0.3}	0.28	0.93	0.78	0.40	0.43	0.97	0.17	0.63								
		S _{a-0.2}	0.22	0.92	0.70	0.44	0.48	0.83	0.01	0.01								
		S _{a-1.0}	0.86	0.83	0.84	0.33	0.40	0.50	0.03	0.00								
	E1-SX	PGA	1.33	0.96	0.73	0.46	0.48	0.84	0.01	0.17	2.17	1.11	0.79	0.46	0.41	0.94	0.63	0.00
		S _{a-0.3}	0.50	0.95	0.66	0.53	0.56	0.90	0.20	0.96	1.22	1.06	0.69	0.57	0.54	0.42	0.31	0.23
		S _{a-0.2}	0.51	0.89	0.61	0.56	0.63	0.06	0.14	0.98	1.28	1.06	0.68	0.57	0.54	0.24	0.61	0.52
		S _{a-1.0}	1.10	0.85	0.78	0.43	0.50	0.99	0.63	0.64	1.93	1.01	0.82	0.42	0.42	0.84	0.14	0.16
	E2-S0	PGA	0.92	1.16	0.86	0.39	0.33	0.34	0.61	0.90								
		S _{a-0.3}	0.07	1.20	0.86	0.40	0.33	0.03	0.66	0.20								
		S _{a-0.2}	0.05	1.12	0.76	0.50	0.45	0.03	0.64	0.09								
		S _{a-1.0}	0.61	0.93	0.84	0.42	0.45	0.82	0.48	0.33								
	E2-SX	PGA	1.09	1.03	0.63	0.59	0.58	0.78	0.85	0.92	2.09	1.18	0.70	0.59	0.51	0.41	0.02	0.09
		S _{a-0.3}	0.19	1.01	0.62	0.62	0.61	0.85	0.36	0.54	1.08	1.14	0.70	0.59	0.52	0.92	0.94	0.49
		S _{a-0.2}	0.19	0.96	0.52	0.69	0.72	0.59	0.70	0.38	1.06	1.10	0.64	0.63	0.57	0.99	0.25	0.51
		S _{a-1.0}	1.00	1.01	0.77	0.49	0.49	0.88	0.17	0.02	2.02	1.14	0.83	0.45	0.39	0.13	0.81	0.14
	E3-S0	PGA	0.87	1.02	0.84	0.35	0.35	0.95	0.84	0.01								
		S _{a-0.3}	0.03	1.03	0.86	0.35	0.34	0.31	0.22	0.00								
		S _{a-0.2}	-0.05	0.94	0.74	0.44	0.47	0.54	0.47	0.09								
		S _{a-1.0}	0.64	0.96	0.88	0.33	0.34	0.95	0.19	0.00								
	E3-SX	PGA	1.20	1.02	0.76	0.48	0.47	0.23	0.59	0.82	2.21	1.15	0.80	0.50	0.44	0.77	0.97	0.79
		S _{a-0.3}	0.32	0.98	0.72	0.56	0.58	0.68	0.94	0.51	1.18	1.10	0.77	0.56	0.51	0.72	0.21	0.15
		S _{a-0.2}	0.29	0.88	0.63	0.59	0.67	0.01	0.21	0.03	1.17	1.03	0.70	0.61	0.60	0.08	0.42	0.52
		S _{a-1.0}	1.16	1.07	0.83	0.46	0.43	0.11	0.92	0.34	2.07	1.14	0.88	0.42	0.37	0.74	0.58	0.07

MSCC-IG-S																		
MSCC-IG-S	E1-S0	PGA	1.22	1.72	0.67	0.99	0.58	0.94	0.36	0.95								
		S _{a-0.3}	-0.07	1.70	0.64	1.02	0.60	0.19	0.64	0.40								
		S _{a-0.2}	-0.21	1.78	0.65	1.00	0.56	0.30	0.41	0.48								
		S _{a-1.0}	1.02	1.35	0.67	0.96	0.71	0.59	0.69	0.62								
	E1-SX	PGA	0.91	1.09	0.72	0.66	0.61	0.04	0.22	0.79	1.43	0.81	0.87	0.29	0.36	0.01	0.53	0.06
		S _{a-0.3}	-0.07	1.13	0.77	0.59	0.52	0.16	0.79	0.44	0.76	0.78	0.83	0.33	0.42	0.00	0.18	0.13
		S _{a-0.2}	0.02	1.11	0.74	0.63	0.57	0.08	0.63	0.40	0.75	0.72	0.77	0.37	0.52	0.19	0.13	0.10
		S _{a-1.0}	0.84	1.17	0.84	0.56	0.48	0.63	0.66	0.26	1.17	0.67	0.88	0.28	0.42	0.01	0.23	0.37
	E2-S0	PGA	2.02	1.77	0.65	1.22	0.69	0.18	0.77	0.10								
		S _{a-0.3}	0.66	1.85	0.66	1.20	0.65	0.00	0.74	0.16								
		S _{a-0.2}	0.57	1.83	0.69	1.15	0.63	0.03	0.86	0.80								
		S _{a-1.0}	1.79	1.40	0.54	1.22	0.87	0.32	0.73	0.03								
	E2-SX	PGA	1.16	1.26	0.63	0.78	0.62	0.18	0.51	0.17	1.56	0.86	0.76	0.40	0.47	0.64	0.83	0.47
		S _{a-0.3}	0.18	1.08	0.55	0.84	0.78	0.60	0.16	0.23	0.84	0.81	0.75	0.40	0.50	0.91	0.10	0.04
		S _{a-0.2}	0.36	1.11	0.61	0.73	0.66	0.53	0.25	0.82	0.83	0.85	0.74	0.42	0.50	0.97	0.82	0.23
		S _{a-1.0}	1.02	1.09	0.73	0.67	0.61	0.08	0.81	0.38	1.51	0.81	0.85	0.33	0.41	0.55	0.06	0.83
	E3-S0	PGA	1.27	1.12	0.39	1.13	1.01	0.30	0.94	0.51								
		S _{a-0.3}	0.39	1.20	0.47	1.03	0.86	0.35	0.77	0.04								
		S _{a-0.2}	0.46	0.96	0.33	1.02	1.07	0.16	0.00	0.47								
		S _{a-1.0}	1.18	1.07	0.50	1.08	1.02	0.22	0.76	0.95								
	E3-SX	PGA	0.51	0.81	0.57	0.59	0.72	0.53	0.58	0.08	1.56	0.84	0.83	0.32	0.38	0.13	0.83	0.27
		S _{a-0.3}	-0.12	0.74	0.53	0.56	0.75	0.68	0.96	0.06	0.89	0.81	0.81	0.33	0.41	0.49	0.59	0.25
		S _{a-0.2}	-0.10	0.75	0.51	0.57	0.76	0.77	0.64	0.62	0.89	0.84	0.80	0.34	0.41	0.02	0.91	0.36
		S _{a-1.0}	0.41	0.77	0.62	0.55	0.71	0.56	0.69	0.60	1.43	0.82	0.89	0.29	0.35	0.64	0.55	0.49
MSCC-IG-M	E1-S0	PGA	1.44	1.04	0.66	0.62	0.60	0.28	0.05	0.09								
		S _{a-0.3}	0.58	0.98	0.68	0.59	0.61	0.05	0.22	0.79								

E1-SX	S _{a-0.2}	0.68	1.05	0.65	0.64	0.61	0.44	0.34	0.90	2.37	1.10	0.73	0.56	0.50	0.27	0.32	0.37
	S _{a-1.0}	1.23	0.93	0.73	0.56	0.61	0.82	0.28	0.88								
	PGA	1.74	0.92	0.65	0.55	0.59	0.54	0.11	0.12								
	S _{a-0.3}	0.91	0.91	0.66	0.55	0.61	0.90	0.72	0.08								
	S _{a-0.2}	0.91	0.78	0.49	0.64	0.81	0.55	0.44	0.71								
E2-S0	S _{a-1.0}	1.64	1.05	0.82	0.46	0.44	0.50	0.00	0.85	2.15	1.08	0.89	0.37	0.34	0.25	0.07	0.07
	PGA	1.95	1.40	0.74	0.69	0.49	0.79	0.15	0.91								
	S _{a-0.3}	0.73	1.31	0.72	0.71	0.54	0.55	0.12	0.01								
	S _{a-0.2}	0.76	1.25	0.66	0.75	0.60	0.72	0.07	0.24								
	S _{a-1.0}	1.58	1.21	0.81	0.62	0.51	0.83	0.10	0.20								
E2-SX	PGA	1.64	0.99	0.75	0.47	0.47	0.59	0.53	0.41	2.57	1.23	0.85	0.42	0.34	0.47	0.67	0.96
	S _{a-0.3}	0.90	1.09	0.74	0.52	0.48	0.14	0.47	0.31								
	S _{a-0.2}	0.85	0.94	0.65	0.58	0.61	0.92	0.33	0.81								
	S _{a-1.0}	1.61	1.03	0.83	0.44	0.43	0.84	0.72	0.29								
	PGA	1.76	1.32	0.74	0.70	0.53	0.07	0.27	0.00								
E3-S0	S _{a-0.3}	0.74	1.41	0.76	0.69	0.49	0.48	0.52	0.44	2.24	1.12	0.92	0.34	0.30	0.75	0.42	0.43
	S _{a-0.2}	0.75	1.42	0.72	0.70	0.49	0.57	0.59	0.57								
	S _{a-1.0}	1.53	1.18	0.76	0.67	0.56	0.05	0.69	0.77								
	PGA	1.62	1.07	0.76	0.49	0.46	0.95	0.73	0.54								
	S _{a-0.3}	0.73	1.16	0.78	0.51	0.44	0.68	0.08	0.53								
E3-SX	S _{a-0.2}	0.71	1.04	0.68	0.58	0.55	0.49	0.77	0.22	1.38	1.09	0.74	0.52	0.48	0.73	0.50	0.30
	S _{a-1.0}	1.50	1.08	0.87	0.39	0.37	0.92	0.02	0.53								
	PGA	1.62	1.07	0.76	0.49	0.46	0.95	0.73	0.54								

The shaded quantities represent the most efficient (lower $\beta_{D|IM}$), practical (higher b), proficient (lower ζ), and sufficient (higher p_M, p_R, p_e)

APPENDIX D

COMPONENT FRAGILITY CURVES FOR BRIDGE CLASSES AND SEISMIC PERFORMANCE SUB-BINS

Chapter 6 presented the approach for developing fragility curves for the components that contribute to the vulnerability of bridge classes and their respective seismic performance sub-bins. The median and dispersion (logarithmic standard deviation) for the components across the four damage states is documented in the subsequent tables. The median value is in units of acceleration due to gravity, g . When the component median fragility value is greater than 5.0, the corresponding median and dispersion values are reported as 99.0 and 0.00, respectively, to indicate that the contribution of the component to the system vulnerability is negligible.

Table D.1: Component level fragility relationships for multispan continuous concrete box-girder bridge class and the respective seismic performance sub-bins

Bridge class (CBC + SPS)	CDT-0		CDT-1		CDT-2		CDT-3	
	λ	ζ	λ	ζ	λ	ζ	λ	ζ
<u>Pre 1971 design era</u>								
MSCC-BG-S-E1-S0								
Column	0.15	0.59	0.17	0.59	0.18	0.59	0.22	0.59
Deck-max	0.64	0.54	1.95	0.54				
Fnd-tran	0.74	0.88	5.66	0.88				
Fnd-rot	99.0	0.00	99.0	0.00				
Abt-Pass	0.81	0.65	3.01	0.65				
Abt-Act	0.38	0.66	1.11	0.66				
Abt-tran	0.17	0.54	0.67	0.54				
MSCC-BG-M-E1-S0								
Column	0.09	0.51	0.10	0.51	0.11	0.51	0.12	0.51
Deck-max	0.35	0.52	0.88	0.52				
Fnd-tran	99.0	0.00	99.0	0.00				
Fnd-rot	99.0	0.00	99.0	0.00				
Abt-Pass	0.44	0.54	1.24	0.54				
Abt-Act	0.24	0.54	0.56	0.54				
Abt-tran	0.12	0.51	0.37	0.51				
MSCC-BG-S-E1-S1								
Column	0.12	0.53	0.13	0.53	0.14	0.53	0.17	0.53
Abt-seat	0.01	1.49	0.02	1.49	0.06	1.49	0.11	1.49
Deck-max	0.51	0.60	1.82	0.60				
Fnd-tran	0.60	1.24	99.0	0.00				
Fnd-rot	99.0	0.00	99.0	0.00				
Abt-Pass	0.90	0.63	2.28	0.63				
Abt-Act	0.31	0.56	0.69	0.56				
Abt-tran	0.05	1.38	0.21	1.38				
Bearing	0.02	1.49	0.17	1.49				
Joint Seal	0.01	1.49	99.0	0.00				
Restrainer	0.27	0.66	1.01	0.66				
Shear key	99.0	0.00	99.0	0.00				
MSCC-BG-S-E1-S2								
MSCC-BG-S-E1-S3								
MSCC-BG-S-E1-S4								
Column	0.12	0.53	0.13	0.53	0.14	0.53	0.17	0.53
Abt-seat	0.02	1.49	0.11	1.49	0.31	1.49	0.58	1.49
Deck-max	0.51	0.60	1.82	0.60				
Fnd-tran	0.60	1.24	99.0	0.00				
Fnd-rot	99.0	0.00	99.0	0.00				
Abt-Pass	0.90	0.63	2.28	0.63				
Abt-Act	0.31	0.56	0.69	0.56				
Abt-tran	0.05	1.38	0.21	1.38				
Bearing	0.02	1.49	0.17	1.49				
Joint Seal	0.01	1.49	99.0	0.00				

Restrainer	0.27	0.66	99.0	0.00				
Shear key	99.0	0.00	99.0	0.00				

MSCC-BG-M-E1-S1

Column	0.07	0.59	0.07	0.59	0.08	0.59	0.09	0.59
Abt-seat	0.01	1.11	0.01	1.11	0.04	1.11	0.07	1.11
Deck-max	0.26	0.56	0.61	0.56				
Fnd-tran	99.0	0.00	99.0	0.00				
Fnd-rot	99.0	0.00	99.0	0.00				
Abt-Pass	0.64	0.53	1.62	0.53				
Abt-Act	0.21	0.43	0.43	0.43				
Abt-tran	0.04	0.96	0.15	0.96				
Bearing	0.01	1.11	0.11	1.11				
Joint Seal	0.01	1.11	99.0	0.00				
Restrainer	0.17	0.58	0.47	0.58				
Shear key	99.0	0.00	99.0	0.00				

MSCC-BG-M-E1-S2

MSCC-BG-M-E1-S3

MSCC-BG-M-E1-S4

Column	0.07	0.59	0.07	0.59	0.08	0.59	0.09	0.59
Abt-seat	0.01	1.11	0.07	1.11	0.40	1.11	0.71	1.11
Deck-max	0.26	0.56	0.61	0.56				
Fnd-tran	99.0	0.00	99.0	0.00				
Fnd-rot	99.0	0.00	99.0	0.00				
Abt-Pass	0.64	0.53	1.62	0.53				
Abt-Act	0.21	0.43	0.43	0.43				
Abt-tran	0.04	0.96	0.15	0.96				
Bearing	0.01	1.11	0.11	1.11				
Joint Seal	0.01	1.11	99.0	0.00				
Restrainer	0.17	0.58	0.47	0.58				
Shear key	99.0	0.00	99.0	0.00				

1971-1990 design era

MSCC-BG-S-E2-S0

Column	0.21	0.70	0.41	0.70	0.70	0.70	1.00	0.70
Deck-max	0.63	0.54	1.91	0.54				
Fnd-tran	0.70	0.84	5.01	0.84				
Fnd-rot	99.0	0.00	99.0	0.00				
Abt-Pass	0.72	0.57	2.29	0.57				
Abt-Act	0.36	0.57	0.94	0.57				
Abt-tran	0.17	0.54	0.68	0.54				

MSCC-BG-M-E2-S0

Column	0.14	0.57	0.25	0.57	0.38	0.57	0.49	0.57
Deck-max	0.41	0.56	1.08	0.56				
Fnd-tran	1.82	1.19	99.0	0.00				
Fnd-rot	99.0	0.00	99.0	0.00				
Abt-Pass	0.48	0.51	1.38	0.51				
Abt-Act	0.26	0.51	0.61	0.51				

Abt-tran	0.13	0.60	0.45	0.60				
MSCC-BG-S-E2-S2								
MSCC-BG-S-E2-S3								
MSCC-BG-S-E2-S4								
Column	0.18	0.51	0.31	0.51	0.47	0.51	0.62	0.51
Abt-seat	0.14	0.60	0.52	0.60	2.12	0.60	3.40	0.60
Deck-max	0.48	0.50	1.45	0.50				
Fnd-tran	0.44	0.80	2.95	0.80				
Fnd-rot	99.0	0.00	99.0	0.00				
Abt-Pass	0.81	0.45	1.65	0.45				
Abt-Act	0.40	0.43	0.78	0.43				
Abt-tran	0.35	0.62	0.88	0.62				
Bearing	0.14	0.60	0.73	0.60				
Joint Seal	0.10	0.60	99.0	0.00				
Restrainer	0.28	0.65	0.98	0.65				
Shear key	99.0	0.00	99.0	0.00				
MSCC-BG-M-E2-S2								
MSCC-BG-M-E2-S3								
MSCC-BG-M-E2-S4								
Column	0.11	0.64	0.18	0.64	0.28	0.64	0.36	0.64
Abt-seat	0.12	0.55	0.38	0.55	2.05	0.55	3.19	0.55
Deck-max	0.30	0.60	0.75	0.60				
Fnd-tran	1.82	1.35	99.0	0.00				
Fnd-rot	99.0	0.00	99.0	0.00				
Abt-Pass	0.66	0.61	1.40	0.61				
Abt-Act	0.26	0.44	0.51	0.44				
Abt-tran	0.21	0.61	0.47	0.61				
Bearing	0.12	0.55	0.53	0.55				
Joint Seal	0.09	0.55	99.0	0.00				
Restrainer	0.20	0.55	0.55	0.55				
Shear key	99.0	0.00	99.0	0.00				
Post 1990 design era								
MSCC-BG-S-E3-S0								
Column	0.22	0.40	0.58	0.40	0.95	0.40	1.26	0.40
Deck-max	0.67	0.45	1.95	0.45				
Fnd-tran	0.55	0.65	3.16	0.65				
Fnd-rot	99.0	0.00	99.0	0.00				
Abt-Pass	0.80	0.52	2.64	0.52				
Abt-Act	0.39	0.53	1.06	0.53				
Abt-tran	0.18	0.48	0.70	0.48				
MSCC-BG-M-E3-S0								
Column	0.12	0.56	0.36	0.56	0.61	0.56	0.84	0.56
Deck-max	0.37	0.56	0.95	0.56				
Fnd-tran	1.89	1.21	99.0	0.00				
Fnd-rot	99.0	0.00	99.0	0.00				
Abt-Pass	0.46	0.45	1.26	0.45				

Abt-Act	0.25	0.45	0.58	0.45
Abt-tran	0.12	0.59	0.40	0.59

MSCC-BG-S-E3-S3

MSCC-BG-S-E3-S4

Column	0.23	0.48	0.78	0.48	1.44	0.48	2.06	0.48
Abt-seat	0.14	0.60	0.58	0.60	4.21	0.60	7.07	0.60
Deck-max	0.60	0.54	2.26	0.54				
Fnd-tran	0.36	1.15	99.0	0.00				
Fnd-rot	99.0	0.00	99.0	0.00				
Abt-Pass	1.06	0.73	3.35	0.73				
Abt-Act	0.43	0.65	1.21	0.65				
Abt-tran	0.28	0.73	1.07	0.73				
Bearing	0.14	0.60	0.85	0.60				
Joint Seal	0.10	0.60	99.0	0.00				
Restrainer	0.33	0.65	1.41	0.65				
Shear key	99.0	0.00	99.0	0.00				

MSCC-BG-M-E3-S3

MSCC-BG-M-E3-S4

Column	0.09	0.61	0.32	0.61	0.61	0.61	0.88	0.61
Abt-seat	0.11	0.61	0.36	0.61	1.95	0.61	3.04	0.61
Deck-max	0.34	0.57	1.07	0.57				
Fnd-tran	1.68	1.18	99.0	0.00				
Fnd-rot	99.0	0.00	99.0	0.00				
Abt-Pass	0.70	0.70	1.71	0.70				
Abt-Act	0.25	0.51	0.50	0.51				
Abt-tran	0.19	0.63	0.51	0.63				
Bearing	0.11	0.61	0.49	0.61				
Joint Seal	0.08	0.61	99.0	0.00				
Restrainer	0.18	0.60	0.50	0.60				
Shear key	99.0	0.00	99.0	0.00				

Table D.2: Component level fragility relationships for multispan continuous concrete slab bridge class and the respective seismic performance sub-bins

Bridge class (CBC + SPS)	CDT-0		CDT-1		CDT-2		CDT-3	
	λ	ζ	λ	ζ	λ	ζ	λ	ζ
MSCC-SL-P-EX-S0								
Column	0.79	0.65	0.91	0.65	1.03	0.65	1.28	0.65
Deck-max	0.88	0.76	3.65	0.76				
Fnd-tran	1.52	1.29	99.0	0.00				
Fnd-rot	99.0	0.00	99.0	0.00				
Abt-Pass	0.92	0.78	4.60	0.78				
Abt-Act	0.77	0.64	2.23	0.64				
Abt-tran	0.18	0.73	1.06	0.73				
MSCC-SL-P-EX-S1								
Column	0.43	0.74	0.49	0.74	0.54	0.74	0.65	0.74
Abt-seat	0.09	0.46	0.17	0.46	0.30	0.46	0.42	0.46
Deck-max	0.43	0.55	1.28	0.55				
Fnd-tran	0.51	0.99	2.24	0.99				
Fnd-rot	99.0	0.00	99.0	0.00				
Abt-Pass	1.77	0.81	99.0	0.00				
Abt-Act	1.68	0.84	99.0	0.00				
Abt-tran	99.0	0.00	99.0	0.00				
Bearing	0.17	0.46	0.53	0.46				
Joint Seal	0.13	0.46	99.0	0.00				
MSCC-SL-P-EX-S2								
MSCC-SL-P-EX-S3								
MSCC-SL-P-EX-S4								
Column	0.43	0.74	0.49	0.74	0.54	0.74	0.65	0.74
Abt-seat	0.17	0.46	0.42	0.46	1.49	0.46	2.09	0.46
Deck-max	0.43	0.55	1.28	0.55				
Fnd-tran	0.51	0.99	2.24	0.99				
Fnd-rot	99.0	0.00	99.0	0.00				
Abt-Pass	1.77	0.81	99.0	0.00				
Abt-Act	1.68	0.84	99.0	0.00				
Abt-tran	99.0	0.00	99.0	0.00				
Bearing	0.17	0.46	0.53	0.46				
Joint Seal	0.13	0.46	99.0	0.00				

Table D.3: Component level fragility relationships for multispan continuous concrete Tee-girder bridge class and the respective seismic performance sub-bins

Bridge class (CBC + SPS)	CDT-0		CDT-1		CDT-2		CDT-3	
	λ	ζ	λ	ζ	λ	ζ	λ	ζ
<u>Pre 1971 design era</u>								
MSCC-TG-P-E1-S0								
MSCC-TG-P-E2-S0								
MSCC-TG-P-E3-S0								
Column	0.69	0.67	0.78	0.67	0.88	0.67	1.07	0.67
Deck-max	0.52	0.51	1.82	0.51				
Fnd-tran	2.41	1.14	99.0	0.00				
Fnd-rot	99.0	0.00	99.0	0.00				
Abt-Pass	3.42	0.98	99.0	0.00				
Abt-Act	99.0	0.00	99.0	0.00				
Abt-tran	2.34	0.97	99.0	0.00				
MSCC-TG-M-E1-S0								
Column	0.27	0.58	0.32	0.58	0.36	0.58	0.45	0.58
Deck-max	0.75	0.59	2.74	0.59				
Fnd-tran	99.0	0.00	99.0	0.00				
Fnd-rot	99.0	0.00	99.0	0.00				
Abt-Pass	99.0	0.00	99.0	0.00				
Abt-Act	3.82	1.01	99.0	0.00				
Abt-tran	2.84	0.81	99.0	0.00				
MSCC-TG-P-E1-S1								
Column	0.26	0.59	0.29	0.59	0.32	0.59	0.38	0.59
Abt-seat	0.06	0.41	0.12	0.41	0.21	0.41	0.31	0.41
Deck-max	0.34	0.48	1.06	0.48				
Fnd-tran	0.93	0.82	4.98	0.82				
Fnd-rot	99.0	0.00	99.0	0.00				
Abt-Pass	99.0	0.00	99.0	0.00				
Abt-Act	2.90	0.65	99.0	0.00				
Abt-tran	99.0	0.00	99.0	0.00				
Bearing	0.12	0.41	0.39	0.41				
Joint Seal	0.09	0.41	99.0	0.00				
MSCC-TG-P-E1-S2								
MSCC-TG-P-E1-S3								
MSCC-TG-P-E1-S4								
Column	0.26	0.59	0.29	0.59	0.32	0.59	0.38	0.59
Abt-seat	0.12	0.41	0.31	0.41	0.88	0.41	1.25	0.41
Deck-max	0.34	0.48	1.06	0.48				
Fnd-tran	0.93	0.82	4.98	0.82				
Fnd-rot	99.0	0.00	99.0	0.00				
Abt-Pass	99.0	0.00	99.0	0.00				
Abt-Act	2.90	0.65	99.0	0.00				
Abt-tran	99.0	0.00	99.0	0.00				
Bearing	0.12	0.41	0.39	0.41				
Joint Seal	0.09	0.41	99.0	0.00				

MSCC-TG-M-E1-S1

Column	0.21	0.65	0.24	0.65	0.28	0.65	0.34	0.65
Abt-seat	0.08	0.54	0.15	0.54	0.30	0.54	0.44	0.54
Deck-max	0.55	0.58	1.84	0.58				
Fnd-tran	99.0	0.00	99.0	0.00				
Fnd-rot	99.0	0.00	99.0	0.00				
Abt-Pass	0.97	0.67	99.0	0.00				
Abt-Act	1.15	0.53	99.0	0.00				
Abt-tran	99.0	0.00	99.0	0.00				
Bearing	0.15	0.54	0.58	0.54				
Joint Seal	0.11	0.54	99.0	0.00				

MSCC-TG-M-E1-S2

MSCC-TG-M-E1-S3

MSCC-TG-M-E1-S4

Column	0.21	0.65	0.24	0.65	0.28	0.65	0.34	0.65
Abt-seat	0.15	0.54	0.44	0.54	2.01	0.54	2.99	0.54
Deck-max	0.55	0.58	1.84	0.58				
Fnd-tran	99.0	0.00	99.0	0.00				
Fnd-rot	99.0	0.00	99.0	0.00				
Abt-Pass	0.97	0.67	99.0	0.00				
Abt-Act	1.15	0.53	99.0	0.00				
Abt-tran	99.0	0.00	99.0	0.00				
Bearing	0.15	0.54	0.58	0.54				
Joint Seal	0.11	0.54	99.0	0.00				

1971-1990 design era

MSCC-TG-M-E2-S0

Column	0.52	0.59	1.09	0.59	2.00	0.59	2.93	0.59
Deck-max	0.72	0.51	2.17	0.51				
Fnd-tran	99.0	0.00	99.0	0.00				
Fnd-rot	99.0	0.00	99.0	0.00				
Abt-Pass	99.0	0.00	99.0	0.00				
Abt-Act	3.47	0.93	99.0	0.00				
Abt-tran	1.59	0.61	99.0	0.00				

MSCC-TG-P-E2-S2

MSCC-TG-P-E2-S3

MSCC-TG-P-E2-S4

Column	0.31	0.74	0.35	0.74	0.39	0.74	0.47	0.74
Abt-seat	0.13	0.59	0.34	0.59	0.99	0.59	1.41	0.59
Deck-max	0.37	0.57	1.11	0.57				
Fnd-tran	1.28	1.24	99.0	0.00				
Fnd-rot	99.0	0.00	99.0	0.00				
Abt-Pass	2.78	0.86	99.0	0.00				
Abt-Act	2.42	0.57	6.46	0.57				
Abt-tran	99.0	0.00	99.0	0.00				
Bearing	0.13	0.59	0.44	0.59				
Joint Seal	0.10	0.59	99.0	0.00				

MSCC-TG-M-E2-S2

Column	0.37	0.60	0.74	0.60	1.28	0.60	1.83	0.60
Abt-seat	0.17	0.50	0.45	0.50	0.82	0.50	1.17	0.50
Deck-max	0.57	0.59	1.75	0.59				
Fnd-tran	99.0	0.00	99.0	0.00				
Fnd-rot	99.0	0.00	99.0	0.00				
Abt-Pass	0.94	0.62	4.33	0.62				
Abt-Act	0.90	0.44	1.73	0.44				
Abt-tran	99.0	0.00	99.0	0.00				
Bearing	0.17	0.50	0.58	0.50				
Joint Seal	0.13	0.50	99.0	0.00				

MSCC-TG-M-E2-S3

Column	0.37	0.60	0.74	0.60	1.28	0.60	1.83	0.60
Abt-seat	0.17	0.50	0.45	0.50	1.28	0.50	1.83	0.50
Deck-max	0.57	0.59	1.75	0.59				
Fnd-tran	99.0	0.00	99.0	0.00				
Fnd-rot	99.0	0.00	99.0	0.00				
Abt-Pass	0.94	0.62	4.33	0.62				
Abt-Act	0.90	0.44	1.73	0.44				
Abt-tran	99.0	0.00	99.0	0.00				
Bearing	0.17	0.50	0.58	0.50				
Joint Seal	0.13	0.50	99.0	0.00				

MSCC-TG-M-E2-S4

Column	0.37	0.60	0.74	0.60	1.28	0.60	1.83	0.60
Abt-seat	0.17	0.50	0.45	0.50	1.72	0.50	2.45	0.50
Deck-max	0.57	0.59	1.75	0.59				
Fnd-tran	99.0	0.00	99.0	0.00				
Fnd-rot	99.0	0.00	99.0	0.00				
Abt-Pass	0.94	0.62	4.33	0.62				
Abt-Act	0.90	0.44	1.73	0.44				
Abt-tran	99.0	0.00	99.0	0.00				
Bearing	0.17	0.50	0.58	0.50				
Joint Seal	0.13	0.50	99.0	0.00				

Post 1990 design era

MSCC-TG-M-E3-S0

Column	0.51	0.50	2.18	0.50	4.48	0.50	6.84	0.50
Deck-max	0.78	0.57	2.84	0.57				
Fnd-tran	99.0	0.00	99.0	0.00				
Fnd-rot	99.0	0.00	99.0	0.00				
Abt-Pass	99.0	0.00	99.0	0.00				
Abt-Act	4.02	0.90	99.0	0.00				
Abt-tran	1.94	0.68	99.0	0.00				

MSCC-TG-P-E3-S3

MSCC-TG-P-E3-S4

Column	0.34	0.60	0.39	0.60	0.44	0.60	0.54	0.60
--------	------	------	------	------	------	------	------	------

Abt-seat	0.11	0.45	0.30	0.45	1.34	0.45	1.97	0.45
Deck-max	0.33	0.48	1.14	0.48				
Fnd-tran	1.77	0.92	99.0	0.00				
Fnd-rot	99.0	0.00	99.0	0.00				
Abt-Pass	3.52	0.92	99.0	0.00				
Abt-Act	2.88	0.66	99.0	0.00				
Abt-tran	99.0	0.00	99.0	0.00				
Bearing	0.11	0.45	0.40	0.45				
Joint Seal	0.08	0.45	99.0	0.00				

MSCC-TG-M-E3-S3

Column	0.34	0.54	1.24	0.54	2.36	0.54	3.44	0.54
Abt-seat	0.16	0.48	0.42	0.48	1.22	0.48	1.75	0.48
Deck-max	0.53	0.49	1.46	0.49				
Fnd-tran	99.0	0.00	99.0	0.00				
Fnd-rot	99.0	0.00	99.0	0.00				
Abt-Pass	0.96	0.59	3.98	0.59				
Abt-Act	1.24	0.52	2.57	0.52				
Abt-tran	99.0	0.00	99.0	0.00				
Bearing	0.16	0.48	0.55	0.48				
Joint Seal	0.13	0.48	99.0	0.00				

MSCC-TG-M-E3-S4

Column	0.34	0.54	1.24	0.54	2.36	0.54	3.44	0.54
Abt-seat	0.16	0.48	0.42	0.48	1.64	0.48	2.35	0.48
Deck-max	0.53	0.49	1.46	0.49				
Fnd-tran	99.0	0.00	99.0	0.00				
Fnd-rot	99.0	0.00	99.0	0.00				
Abt-Pass	0.96	0.59	3.98	0.59				
Abt-Act	1.24	0.52	2.57	0.52				
Abt-tran	99.0	0.00	99.0	0.00				
Bearing	0.16	0.48	0.55	0.48				
Joint Seal	0.13	0.48	99.0	0.00				

Table D.4: Component level fragility relationships for multispan continuous concrete I-girder bridge class and the respective seismic performance sub-bins

Bridge class (CBC + SPS)	CDT-0		CDT-1		CDT-2		CDT-3	
	λ	ζ	λ	ζ	λ	ζ	λ	ζ
<u>Pre 1971 design era</u>								
MSCC-IG-S-E1-S0								
Column	0.40	0.76	0.44	0.76	0.47	0.76	0.54	0.76
Deck-max	0.37	0.56	0.98	0.56				
Fnd-tran	0.94	0.77	2.99	0.77				
Fnd-rot	99.0	0.00	99.0	0.00				
Abt-Pass	99.0	0.00	99.0	0.00				
Abt-Act	99.0	0.00	99.0	0.00				
Abt-tran	0.75	0.95	6.13	0.95				
Bearing	0.12	0.55	0.37	0.55				
Restrainer	1.35	1.06	99.0	0.00				
Shear key	3.89	1.22	99.0	0.00				
MSCC-IG-M-E1-S0								
Column	0.21	0.71	0.24	0.71	0.27	0.71	0.32	0.71
Deck-max	0.40	0.57	1.38	0.57				
Fnd-tran	99.0	0.00	99.0	0.00				
Fnd-rot	99.0	0.00	99.0	0.00				
Abt-Pass	3.54	0.62	99.0	0.00				
Abt-Act	1.62	0.68	99.0	0.00				
Abt-tran	0.87	0.77	99.0	0.00				
Bearing	0.09	0.59	0.39	0.59				
Restrainer	3.05	1.49	99.0	0.00				
Shear key	99.0	0.00	99.0	0.00				
MSCC-IG-S-E1-S1								
Column	0.40	0.57	0.45	0.57	0.49	0.57	0.57	0.57
Abt-seat	0.05	0.50	0.09	0.50	0.16	0.50	0.24	0.50
Deck-max	0.29	0.48	0.79	0.48				
Fnd-tran	1.21	0.70	99.0	0.00				
Fnd-rot	99.0	0.00	99.0	0.00				
Abt-Pass	2.66	0.55	99.0	0.00				
Abt-Act	1.52	0.52	3.84	0.52				
Abt-tran	0.43	0.58	1.02	0.58				
Bearing	0.09	0.50	0.31	0.50				
Joint Seal	0.07	0.50	4.62	0.50				
Restrainer	0.50	0.80	2.83	0.80				
Shear key	3.22	1.13	99.0	0.00				
MSCC-IG-S-E1-S2								
MSCC-IG-S-E1-S3								
MSCC-IG-S-E1-S4								
Column	0.40	0.57	0.45	0.57	0.49	0.57	0.57	0.57
Abt-seat	0.09	0.50	0.24	0.50	0.98	0.50	1.43	0.50
Deck-max	0.29	0.48	0.79	0.48				
Fnd-tran	1.21	0.70	99.0	0.00				

Fnd-rot	99.0	0.00	99.0	0.00
Abt-Pass	2.66	0.55	99.0	0.00
Abt-Act	1.52	0.52	3.84	0.52
Abt-tran	0.43	0.58	1.02	0.58
Bearing	0.09	0.50	0.31	0.50
Joint Seal	0.07	0.50	4.62	0.50
Restrainer	0.50	0.80	2.83	0.80
Shear key	3.22	1.13	99.0	0.00

MSCC-IG-M-E1-S1

Column	0.17	0.55	0.19	0.55	0.21	0.55	0.25	0.55
Abt-seat	0.04	0.51	0.08	0.51	0.16	0.51	0.24	0.51
Deck-max	0.27	0.52	0.89	0.52				
Fnd-tran	99.0	0.00	99.0	0.00				
Fnd-rot	99.0	0.00	99.0	0.00				
Abt-Pass	2.61	0.60	99.0	0.00				
Abt-Act	1.76	0.61	99.0	0.00				
Abt-tran	0.31	0.73	1.36	0.73				
Bearing	0.08	0.51	0.33	0.51				
Joint Seal	0.06	0.51	6.36	0.51				
Restrainer	1.45	0.92	99.0	0.00				
Shear key	99.0	0.00	99.0	0.00				

MSCC-IG-M-E1-S2

MSCC-IG-M-E1-S3

MSCC-IG-M-E1-S4

Column	0.17	0.55	0.19	0.55	0.21	0.55	0.25	0.55
Abt-seat	0.08	0.51	0.24	0.51	0.83	0.51	1.25	0.51
Deck-max	0.27	0.52	0.89	0.52				
Fnd-tran	99.0	0.00	99.0	0.00				
Fnd-rot	99.0	0.00	99.0	0.00				
Abt-Pass	2.61	0.60	99.0	0.00				
Abt-Act	1.76	0.61	99.0	0.00				
Abt-tran	0.31	0.73	1.36	0.73				
Bearing	0.08	0.51	0.33	0.51				
Joint Seal	0.06	0.51	99.0	0.00				
Restrainer	1.45	0.92	99.0	0.00				
Shear key	99.0	0.00	99.0	0.00				

1971-1990 design era

MSCC-IG-S-E2-S0

Column	0.28	0.91	0.46	0.91	0.68	0.91	0.88	0.91
Deck-max	0.25	0.55	0.61	0.55				
Fnd-tran	0.46	0.67	1.15	0.67				
Fnd-rot	99.0	0.00	99.0	0.00				
Abt-Pass	4.24	0.64	99.0	0.00				
Abt-Act	3.41	0.78	99.0	0.00				
Abt-tran	0.36	0.55	1.16	0.55				
Bearing	0.10	0.60	0.25	0.60				
Restrainer	0.95	0.79	99.0	0.00				

Shear key	99.0	0.00	99.0	0.00				
MSCC-IG-M-E2-S0								
Column	0.27	0.59	0.48	0.59	0.76	0.59	1.03	0.59
Deck-max	0.41	0.50	1.30	0.50				
Fnd-tran	99.0	0.00	99.0	0.00				
Fnd-rot	99.0	0.00	99.0	0.00				
Abt-Pass	4.54	0.71	99.0	0.00				
Abt-Act	2.04	0.80	99.0	0.00				
Abt-tran	0.72	0.75	4.44	0.75				
Bearing	0.11	0.53	0.40	0.53				
Restrainer	2.88	1.34	99.0	0.00				
Shear key	99.0	0.00	99.0	0.00				
MSCC-IG-S-E2-S2								
Column	0.39	0.69	0.74	0.69	1.24	0.69	1.72	0.69
Abt-seat	0.06	0.56	0.17	0.56	0.32	0.56	0.46	0.56
Deck-max	0.20	0.56	0.58	0.56				
Fnd-tran	0.89	1.11	99.0	0.00				
Fnd-rot	99.0	0.00	99.0	0.00				
Abt-Pass	1.74	0.59	4.91	0.59				
Abt-Act	1.35	0.66	3.46	0.66				
Abt-tran	0.31	0.54	0.70	0.54				
Bearing	0.06	0.56	0.22	0.56				
Joint Seal	0.05	0.56	3.34	0.56				
Restrainer	0.38	0.70	1.49	0.70				
Shear key	2.39	0.90	99.0	0.00				
MSCC-IG-S-E2-S3								
Column	0.39	0.69	0.74	0.69	1.24	0.69	1.72	0.69
Abt-seat	0.06	0.56	0.17	0.56	0.51	0.56	0.74	0.56
Deck-max	0.20	0.56	0.58	0.56				
Fnd-tran	0.89	1.11	99.0	0.00				
Fnd-rot	99.0	0.00	99.0	0.00				
Abt-Pass	1.74	0.59	4.91	0.59				
Abt-Act	1.35	0.66	3.46	0.66				
Abt-tran	0.31	0.54	0.70	0.54				
Bearing	0.06	0.56	0.22	0.56				
Joint Seal	0.05	0.56	3.34	0.56				
Restrainer	0.38	0.70	1.49	0.70				
Shear key	2.39	0.90	99.0	0.00				
MSCC-IG-S-E2-S4								
Column	0.39	0.69	0.74	0.69	1.24	0.69	1.72	0.69
Abt-seat	0.06	0.56	0.17	0.56	0.70	0.56	1.02	0.56
Deck-max	0.20	0.56	0.58	0.56				
Fnd-tran	0.89	1.11	99.0	0.00				
Fnd-rot	99.0	0.00	99.0	0.00				
Abt-Pass	1.74	0.59	4.91	0.59				
Abt-Act	1.35	0.66	3.46	0.66				

Abt-tran	0.31	0.54	0.70	0.54
Bearing	0.06	0.56	0.22	0.56
Joint Seal	0.05	0.56	3.34	0.56
Restrainer	0.38	0.70	1.49	0.70
Shear key	2.39	0.90	99.0	0.00

MSCC-IG-M-E2-S2

Column	0.21	0.55	0.41	0.55	0.71	0.55	1.00	0.55
Abt-seat	0.09	0.47	0.24	0.47	0.45	0.47	0.65	0.47
Deck-max	0.26	0.49	0.80	0.49				
Fnd-tran	99.0	0.00	99.0	0.00				
Fnd-rot	99.0	0.00	99.0	0.00				
Abt-Pass	2.72	0.54	99.0	0.00				
Abt-Act	1.89	0.59	99.0	0.00				
Abt-tran	0.27	0.61	0.82	0.61				
Bearing	0.09	0.47	0.31	0.47				
Joint Seal	0.07	0.47	4.57	0.47				
Restrainer	1.33	0.79	99.0	0.00				
Shear key	99.0	0.00	99.0	0.00				

MSCC-IG-M-E2-S3

Column	0.21	0.55	0.41	0.55	0.71	0.55	1.00	0.55
Abt-seat	0.09	0.47	0.24	0.47	0.71	0.47	1.04	0.47
Deck-max	0.26	0.49	0.80	0.49				
Fnd-tran	99.0	0.00	99.0	0.00				
Fnd-rot	99.0	0.00	99.0	0.00				
Abt-Pass	2.72	0.54	99.0	0.00				
Abt-Act	1.89	0.59	99.0	0.00				
Abt-tran	0.27	0.61	0.82	0.61				
Bearing	0.09	0.47	0.31	0.47				
Joint Seal	0.07	0.47	4.57	0.47				
Restrainer	1.33	0.79	99.0	0.00				
Shear key	99.0	0.00	99.0	0.00				

MSCC-IG-M-E2-S4

Column	0.21	0.55	0.41	0.55	0.71	0.55	1.00	0.55
Abt-seat	0.09	0.47	0.24	0.47	0.97	0.47	1.41	0.47
Deck-max	0.26	0.49	0.80	0.49				
Fnd-tran	99.0	0.00	99.0	0.00				
Fnd-rot	99.0	0.00	99.0	0.00				
Abt-Pass	2.72	0.54	99.0	0.00				
Abt-Act	1.89	0.59	99.0	0.00				
Abt-tran	0.27	0.61	0.82	0.61				
Bearing	0.09	0.47	0.31	0.47				
Joint Seal	0.07	0.47	4.57	0.47				
Restrainer	1.33	0.79	99.0	0.00				
Shear key	99.0	0.00	99.0	0.00				

Post 1990 design era
MSCC-IG-S-E3-S0

Column	0.33	1.07	1.21	1.07	2.32	1.07	3.39	1.07
Deck-max	0.24	0.62	0.71	0.62				
Fnd-tran	0.48	1.10	2.29	1.10				
Fnd-rot	99.0	0.00	99.0	0.00				
Abt-Pass	99.0	0.00	99.0	0.00				
Abt-Act	3.56	1.09	99.0	0.00				
Abt-tran	0.31	0.84	1.45	0.84				
Bearing	0.05	0.83	0.19	0.83				
Restrainer	1.06	1.03	99.0	0.00				
Shear key	99.0	0.00	99.0	0.00				

MSCC-IG-M-E3-S0

Column	0.27	0.64	0.89	0.64	1.59	0.64	2.25	0.64
Deck-max	0.40	0.53	1.22	0.53				
Fnd-tran	4.00	1.23	99.0	0.00				
Fnd-rot	99.0	0.00	99.0	0.00				
Abt-Pass	99.0	0.00	99.0	0.00				
Abt-Act	1.73	0.73	99.0	0.00				
Abt-tran	0.78	0.83	99.0	0.00				
Bearing	0.10	0.57	0.37	0.57				
Restrainer	1.84	1.20	99.0	0.00				
Shear key	99.0	0.00	99.0	0.00				

MSCC-IG-S-E3-S3

Column	0.59	0.84	3.55	0.84	99.0	0.00	99.0	0.00
Abt-seat	0.03	0.74	0.12	0.74	0.56	0.74	0.93	0.74
Deck-max	0.20	0.62	0.64	0.62				
Fnd-tran	1.31	2.43	99.0	0.00				
Fnd-rot	99.0	0.00	99.0	0.00				
Abt-Pass	2.56	0.56	99.0	0.00				
Abt-Act	2.07	0.69	99.0	0.00				
Abt-tran	0.25	0.74	0.75	0.74				
Bearing	0.03	0.74	0.18	0.74				
Joint Seal	0.02	0.74	99.0	0.00				
Restrainer	0.45	0.60	1.69	0.60				
Shear key	99.0	0.00	99.0	0.00				

MSCC-IG-S-E3-S4

Column	0.59	0.84	3.55	0.84	99.0	0.00	99.0	0.00
Abt-seat	0.03	0.74	0.12	0.74	0.85	0.74	1.41	0.74
Deck-max	0.20	0.62	0.64	0.62				
Fnd-tran	1.31	2.43	99.0	0.00				
Fnd-rot	99.0	0.00	99.0	0.00				
Abt-Pass	2.56	0.56	99.0	0.00				
Abt-Act	2.07	0.69	99.0	0.00				
Abt-tran	0.25	0.74	0.75	0.74				
Bearing	0.03	0.74	0.18	0.74				
Joint Seal	0.02	0.74	99.0	0.00				
Restrainer	0.45	0.60	1.69	0.60				
Shear key	99.0	0.00	99.0	0.00				

MSCC-IG-M-E3-S3

Column	0.25	0.49	0.90	0.49	1.72	0.49	2.51	0.49
Abt-seat	0.09	0.46	0.25	0.46	0.73	0.46	1.04	0.46
Deck-max	0.27	0.51	0.83	0.51				
Fnd-tran	99.0	0.00	99.0	0.00				
Fnd-rot	99.0	0.00	99.0	0.00				
Abt-Pass	2.64	0.56	99.0	0.00				
Abt-Act	2.00	0.60	99.0	0.00				
Abt-tran	0.27	0.63	0.79	0.63				
Bearing	0.09	0.46	0.32	0.46				
Joint Seal	0.07	0.46	4.44	0.46				
Restrainer	1.33	0.80	99.0	0.00				
Shear key	99.0	0.00	99.0	0.00				

MSCC-IG-M-E3-S4

Column	0.25	0.49	0.90	0.49	1.72	0.49	2.51	0.49
Abt-seat	0.09	0.46	0.25	0.46	0.98	0.46	1.41	0.46
Deck-max	0.27	0.51	0.83	0.51				
Fnd-tran	99.0	0.00	99.0	0.00				
Fnd-rot	99.0	0.00	99.0	0.00				
Abt-Pass	2.64	0.56	99.0	0.00				
Abt-Act	2.00	0.60	99.0	0.00				
Abt-tran	0.27	0.63	0.79	0.63				
Bearing	0.09	0.46	0.32	0.46				
Joint Seal	0.07	0.46	4.44	0.46				
Restrainer	1.33	0.80	99.0	0.00				
Shear key	99.0	0.00	99.0	0.00				

APPENDIX E

COMPARISON OF THE BRIDGE CLASS SYSTEM FRAGILITIES WITH HAZUS

Table E.1: Percentage change in the median values and dispersions of the bridge class fragilities with respect to HAZUS fragilities

Bridge class (CBC + SPS)	BSST median values, λ				ζ^*	% change in λ and ζ				
	0	1	2	3		0	1	2	3	ζ^*
<u>HAZUS fragilities</u>										
MSCC-BG-S-E1	0.35	0.45	0.55	0.80	0.60					
MSCC-BG-S-E2/E3	0.60	0.90	1.30	1.60	0.60					
MSCC-BG-M-E1	0.60	0.90	1.10	1.50	0.60					
MSCC-BG-M-E2/E3	0.90	0.90	1.10	1.50	0.60					
<u>Current study</u>										
MSCC-BG-S-E1-S0	0.13	0.17	0.19	0.22	0.59	-63	-63	-66	-73	-2
MSCC-BG-M-E1-S0	0.08	0.10	0.11	0.12	0.51	-86	-89	-90	-92	-16
MSCC-BG-S-E1-S1	0.02	0.08	0.14	0.17	0.61	-95	-82	-74	-79	2
MSCC-BG-S-E1-S2	0.02	0.09	0.15	0.17	0.64	-95	-79	-74	-79	7
MSCC-BG-S-E1-S3	0.02	0.09	0.14	0.17	0.64	-95	-79	-74	-79	6
MSCC-BG-S-E1-S4	0.02	0.09	0.15	0.17	0.64	-95	-79	-73	-79	6
MSCC-BG-M-E1-S1	0.01	0.06	0.08	0.09	0.63	-98	-94	-93	-94	5
MSCC-BG-M-E1-S2	0.01	0.06	0.08	0.09	0.68	-98	-93	-93	-94	13
MSCC-BG-M-E1-S3	0.01	0.06	0.08	0.09	0.66	-98	-93	-93	-94	11
MSCC-BG-M-E1-S4	0.01	0.06	0.08	0.09	0.66	-98	-93	-93	-94	11
MSCC-BG-S-E2-S0	0.15	0.39	0.71	1.00	0.64	-76	-57	-46	-38	6
MSCC-BG-M-E2-S0	0.12	0.24	0.38	0.50	0.56	-87	-73	-66	-67	-6
MSCC-BG-S-E2-S2	0.08	0.31	0.47	0.62	0.54	-86	-65	-64	-61	-10
MSCC-BG-S-E2-S3	0.08	0.31	0.47	0.62	0.54	-86	-65	-64	-61	-10
MSCC-BG-S-E2-S4	0.09	0.31	0.48	0.62	0.54	-86	-65	-63	-61	-9
MSCC-BG-M-E2-S2	0.07	0.18	0.27	0.36	0.59	-92	-80	-75	-76	-2
MSCC-BG-M-E2-S3	0.07	0.18	0.28	0.36	0.59	-92	-80	-75	-76	-1
MSCC-BG-M-E2-S4	0.07	0.18	0.27	0.35	0.60	-92	-80	-75	-76	0
MSCC-BG-S-E3-S0	0.16	0.52	0.95	1.26	0.40	-73	-42	-27	-21	-34
MSCC-BG-M-E3-S0	0.10	0.32	0.61	0.83	0.54	-88	-65	-44	-44	-10
MSCC-BG-S-E3-S3	0.09	0.57	1.44	2.06	0.51	-86	-37	11	28	-15

MSCC-BG-S-E3-S4	0.09	0.57	1.44	2.06	0.51	-86	-37	11	29	-14
MSCC-BG-M-E3-S3	0.06	0.26	0.59	0.87	0.58	-93	-71	-46	-42	-4
MSCC-BG-M-E3-S4	0.06	0.26	0.61	0.88	0.59	-93	-71	-45	-41	-3

HAZUS fragilities

MSCC-SL	0.60	0.90	1.10	1.50	0.60
---------	------	------	------	------	------

Current study

MSCC-SL-P-S0	0.17	0.70	1.03	1.28	0.66	-72	-22	-6	-15	9
MSCC-SL-P-S1-S	0.03	0.09	0.21	0.34	0.82	-94	-90	-81	-77	37
MSCC-SL-P-S2-S	0.06	0.28	0.48	0.62	0.70	-91	-69	-56	-58	17
MSCC-SL-P-S3-S	0.06	0.29	0.53	0.65	0.70	-91	-68	-52	-57	17
MSCC-SL-P-S4-S	0.06	0.29	0.53	0.65	0.70	-91	-68	-51	-57	16

HAZUS fragilities

MSCC-TG-S/M-E1	0.60	0.90	1.10	1.50	0.60
MSCC-TG-S/M-E2/E3	0.90	0.90	1.10	1.50	0.60

Current study

MSCC-TG-P-E1-S0	0.44	0.77	0.88	1.07	0.64	-28	-15	-20	-29	6
MSCC-TG-M-E1-S0	0.27	0.31	0.35	0.44	0.57	-55	-65	-68	-71	-5
MSCC-TG-P-E1-S1	0.06	0.12	0.20	0.28	0.41	-90	-87	-82	-82	-32
MSCC-TG-P-E1-S2	0.08	0.23	0.31	0.37	0.45	-87	-74	-72	-75	-24
MSCC-TG-P-E1-S3	0.08	0.23	0.32	0.38	0.48	-87	-74	-71	-75	-21
MSCC-TG-P-E1-S4	0.08	0.23	0.32	0.38	0.48	-87	-74	-71	-75	-20
MSCC-TG-M-E1-S1	0.07	0.14	0.23	0.30	0.54	-88	-84	-79	-80	-10
MSCC-TG-M-E1-S2	0.10	0.24	0.27	0.34	0.59	-84	-74	-75	-77	-2
MSCC-TG-M-E1-S3	0.10	0.24	0.28	0.34	0.59	-84	-74	-75	-77	-2
MSCC-TG-M-E1-S4	0.10	0.24	0.28	0.34	0.59	-84	-74	-75	-77	-2

MSCC-TG-P-E2-S0	0.43	0.76	0.87	1.04	0.56	-52	-16	-21	-31	-7
MSCC-TG-M-E2-S0	0.47	1.08	1.99	2.82	0.54	-47	19	81	88	-9
MSCC-TG-P-E2-S2	0.09	0.28	0.38	0.47	0.64	-90	-69	-66	-69	7
MSCC-TG-P-E2-S3	0.09	0.28	0.39	0.47	0.65	-90	-69	-65	-69	9
MSCC-TG-P-E2-S4	0.09	0.28	0.39	0.46	0.66	-90	-69	-64	-69	10
MSCC-TG-M-E2-S2	0.12	0.41	0.79	1.12	0.48	-87	-55	-29	-25	-20
MSCC-TG-M-E2-S3	0.12	0.41	1.06	1.52	0.49	-87	-55	-4	1	-18
MSCC-TG-M-E2-S4	0.12	0.40	1.20	1.71	0.51	-87	-55	9	14	-15

MSCC-TG-P-E3-S0	0.40	0.74	0.86	1.04	0.57	-56	-18	-22	-31	-4
MSCC-TG-M-E3-S0	0.48	1.23	2.47	3.57	0.50	-47	37	124	138	-17
MSCC-TG-P-E3-S3	0.07	0.26	0.43	0.54	0.49	-92	-71	-61	-64	-19
MSCC-TG-P-E3-S4	0.07	0.25	0.44	0.54	0.50	-92	-72	-60	-64	-17

MSCC-TG-M-E3-S3	0.11	0.39	1.20	1.72	0.46	-88	-56	9	15	-23
MSCC-TG-M-E3-S4	0.11	0.39	1.55	2.23	0.46	-88	-57	41	49	-23

HAZUS fragilities

MSCC-IG-S/M-E1	0.60	0.90	1.10	1.50	0.60
MSCC-IG-S/M-E2/E3	0.90	0.90	1.10	1.50	0.60

Current study

MSCC-BG-S-E1-S0	0.12	0.33	0.47	0.54	0.66	-81	-64	-57	-64	11
MSCC-BG-M-E1-S0	0.09	0.22	0.27	0.33	0.66	-85	-75	-76	-78	9
MSCC-BG-S-E1-S1	0.05	0.16	0.37	0.52	0.55	-91	-82	-66	-66	-9
MSCC-BG-S-E1-S2	0.07	0.29	0.49	0.57	0.52	-88	-68	-56	-62	-13
MSCC-BG-S-E1-S3	0.07	0.29	0.49	0.57	0.53	-88	-68	-56	-62	-12
MSCC-BG-S-E1-S4	0.07	0.29	0.49	0.57	0.53	-88	-68	-56	-62	-12
MSCC-BG-M-E1-S1	0.06	0.13	0.19	0.23	0.47	-90	-86	-83	-84	-21
MSCC-BG-M-E1-S2	0.07	0.18	0.21	0.25	0.51	-88	-80	-81	-83	-15
MSCC-BG-M-E1-S3	0.07	0.18	0.21	0.25	0.52	-88	-80	-81	-83	-14
MSCC-BG-M-E1-S4	0.07	0.18	0.21	0.25	0.52	-88	-80	-81	-84	-14

MSCC-BG-S-E2-S0	0.09	0.24	0.68	0.88	0.75	-90	-73	-38	-41	25
MSCC-BG-M-E2-S0	0.11	0.35	0.76	1.02	0.55	-88	-61	-31	-32	-9
MSCC-BG-S-E2-S2	0.06	0.21	1.00	1.49	0.57	-94	-76	-9	-1	-6
MSCC-BG-S-E2-S3	0.06	0.21	1.20	1.68	0.60	-94	-76	9	12	-1
MSCC-BG-S-E2-S4	0.06	0.22	1.24	1.72	0.60	-94	-76	13	14	1
MSCC-BG-M-E2-S2	0.08	0.26	0.56	0.80	0.43	-92	-71	-49	-47	-28
MSCC-BG-M-E2-S3	0.08	0.26	0.67	0.95	0.44	-92	-71	-39	-37	-26
MSCC-BG-M-E2-S4	0.08	0.26	0.69	0.98	0.47	-92	-71	-37	-34	-22

MSCC-BG-S-E3-S0	0.05	0.19	2.15	3.05	0.88	-94	-79	95	103	47
MSCC-BG-M-E3-S0	0.10	0.37	1.59	2.24	0.59	-89	-59	44	49	-1
MSCC-BG-S-E3-S3	0.03	0.18	2.76	3.41	0.66	-97	-80	151	127	10
MSCC-BG-S-E3-S4	0.03	0.18	3.59	3.87	0.75	-97	-80	227	158	25
MSCC-BG-M-E3-S3	0.08	0.28	1.00	1.44	0.41	-91	-69	-9	-4	-32
MSCC-BG-M-E3-S4	0.08	0.28	1.25	1.80	0.41	-91	-69	14	20	-32

The entities shaded in red indicate more vulnerability with respect to HAZUS (negative change in median fragilities) while those shaded in green indicate less vulnerability with respect to HAZUS (positive change in median fragilities).

REFERENCES

- Abrahamson, N., Silva, W. (2008). *Summary of the Abrahamson & Silva NGA Ground-Motion Relations*, Earthquake Spectra, 24(1), pp: 67-97.
- Ang, A. H.-S., Tang, W. H. (1975). *Probability Concepts in Engineering Planning and Design*, Vol. 1, John Wiley and Sons, New York.
- ACI (2008). *Building Code Requirements for Structural Concrete (ACI 318-08) and Commentary*, American Concrete Institute, Farmington Hills, MI.
- ASCE (2009). *ASCE: Infrastructure fact sheet*,
<http://www.infrastructurereportcard.org/sites/default/files/RC2009_bridges.pdf>.
- ATC (1981). *Seismic Design Guidelines for Highway Bridges*, Report No. ATC-6, Applied Technology Council, Redwood City, CA.
- ATC (1985). *Earthquake damage evaluation data for California*, Report No. ATC-13, Applied Technology Council, Redwood City, CA.
- ATC (1991). *Seismic Vulnerability and Impact of Disruption of Lifelines in the Coterminous United States*, Report No. ATC-25, Applied Technology Council, Redwood City, CA.
- ATC (1996). *Improved Seismic Design Criteria for California Bridges: Provisional Recommendations*, Report No. ATC-32, Applied Technology Council, Redwood City, CA.
- ATC (1996). *Seismic Evaluation and Retrofit of Concrete Buildings*, Report No. ATC-40, Applied Technology Council, Redwood City, CA.
- ATC-63 (2008). *Quantification of Building Seismic Performance Factors*. ATC-63/FEMA P695, Applied Technology Council, Redwood City, CA.
- ATC/MCEER (2002). *Comprehensive Specification for the Seismic Design of Bridges*, Report No. NCHRP 471, National Cooperative Highway Research program, Transportation Research Board, Washington, DC.
- Baker, J. W., Cornell, A. C. (2006). *Vector-Valued Ground Motion Intensity Measures for Probabilistic Seismic Demand Analysis*, Report No. PEER 2006/08, Pacific Earthquake Engineering Research Center, University of California, Berkeley, CA.
- Baker, J. W., Ling, T., Shahi, S. K., Jayaram, N. (2011). *New Ground Motion Selection Procedures and Selected Motions for the PEER Transportation Research Program*, Draft Report, Pacific Earthquake Engineering Research Center, University of California, Berkeley, CA.
- Banerjee, S., Shinozuka, M. (2007). *Nonlinear Static Procedure for Seismic Vulnerability Assessment of Bridges*, Computer-Aided Civil and Infrastructure Engineering, 22, pp: 293-305.

- Basoz, N., Kiremidjian, A. S. (1997). *Evaluation of Bridge Damage Data from the Loma Prieta and Northridge CA Earthquakes*, Report No. MCEER-98-0004, MCEER, University at Buffalo, The State University of New York, Buffalo, NY.
- Basoz, N., Mander, J. B. (1999). *Enhancement of the Lifeline Transportation Module in HAZUS*, Report No. Draft #7, National Institute of Building Sciences, Washington, DC.
- Bavirisetty, R., Vinayagamoorthy, M., Duan, L. (2003). *Dynamic Analysis*, Bridge Engineering – Seismic Design, Edited by Wai-Fah Chen and Lian Duan, CRC Press LLC, Boca Raton, FL, ISBN: 0-8493-1683-9/02.
- Bazurro, P., Cornell, A. C. (1994). *Seismic hazard analysis for non-linear structures. I: Methodology*, Journal of Structural Engineering, 120(11), pp: 3320-3344.
- Bazurro, P., Cornell, A. C. (1994). *Seismic hazard analysis for non-linear structures. II: Applications*, Journal of Structural Engineering, 120(11), pp: 3345-3365.
- Bazurro, P., Cornell, A. C. (2002). *Vector-values probabilistic seismic hazard analysis (VP-SHA)*, Proceedings of the 7th U.S. National Conference on Earthquake Engineering, Boston, MA.
- BDA (1988). *Bridge Design Aids*, California Department of Transportation, Sacramento, CA.
- BDA (1989). *Bridge Design Aids*, California Department of Transportation, Sacramento, CA.
- BDA (1995). *Bridge Design Aids*, California Department of Transportation, Sacramento, CA.
- BDA (2004). *Bridge Design Aids*, California Department of Transportation, Sacramento, CA.
- BDA (2009). *Bridge Design Aids*, California Department of Transportation, Sacramento, CA.
- BDS (1990). *Bridge Design Specifications*, California Department of Transportation, Sacramento, CA.
- Berry, M. P., Eberhard, M. O. (2003). *Performance models for flexural damage in reinforced concrete columns*, Report No. 2003/18, Pacific Earthquake Engineering Research Center, University of California, Berkeley, CA.
- Berry, M. P., Eberhard, M. O. (2004). *PEER Structural Performance Database User's Manual*, Pacific Earthquake Engineering Research Center, University of California, Berkeley, CA.
- Bruneau, M., Chang, S. E., Eguchi, R. T., Lee, G. C., O'Rourke, T. D., Reinhorn, A. M., Shinozuka, M., Tierney, K., Wallace, W. A., and Winterfeldt, D. (2003). *A Framework to Quantitatively Assess and Enhance the Seismic Resilience of Communities*, Earthquake Spectra, 19, pp: 733-752.
- BSSC (1997). *NEHRP Guidelines for the seismic rehabilitation of buildings*, Report No. FEMA-273, Building Seismic Safety Council, Washington, DC.

- Bucher, C. G., Bourgund, U. (1990). *A fast and efficient response surface approach for structural reliability problems*, Structural Safety, 7(1), pp: 57-66.
- Caltrans (2007). *Reinforced Concrete Bridge Capacity Assessment Training Manual*, Report submitted to Structure Maintenance and Investigations, California Department of Transportation, Sacramento, CA.
- Caltrans (2008). *Foundation Manual*, Office of Structure Construction, California Department of Transportation, Sacramento, CA.
- Caltrans (2010-2012). *Personal communication with the P266 Fragility Project Advisory Panel members including* Roblee, C., Yashinsky, M., Mahan, M., Shantz, T., Setberg, H., Turner, L., Sahs, S., Adams, D. T., Keever, M. (2011), California Department of Transportation, Sacramento, CA.
- Celik, O. C., Ellingwood, B. R. (2010). *Seismic fragilities for non-ductile reinforced concrete frames – Role of aleatoric and epistemic uncertainties*, Structural Safety, 32, pp: 1-12.
- Chang, G. A., Mander, J. B. (1994). *Seismic Energy Based Fatigue Damage Analysis of Bridge Columns: Part 1 – Evaluation of Seismic Capacity*, Technical Report NCEER-94-0006, State University of New York, Buffalo, NY.
- Chiou, B., Darragh, R., Gregor, N., Silva, W. (2008). *NGA Project Strong-Motion Database*, Earthquake Spectra, 24(1), pp: 23-44.
- Choi, E. (2002). *Seismic analysis and retrofit of Mid-America bridges*, Ph.D. thesis, School of Civil and Environmental Engineering, Georgia Institute of Technology, Georgia.
- Choi, E., DesRoches, R., Nielson, B. G. (2004). *Seismic Fragility of Typical Bridges in Moderate Seismic Zones*, Engineering Structures, 26(2), pp: 187-199.
- Chopra, A. K. (2007). *Dynamics of Structures: Theory and Applications to Earthquake Engineering*, Third Edition, Prentice Hall, NY.
- Cornell, A. C., Krawinkler, H. (2000). *Progress and challenges in seismic performance assessment*, PEER Center News <<http://peer.berkeley.edu/news/2000spring/index.html>>.
- Cornell, A. C., Jayaler, F., Hamburger, R. O., Foutch, A. D. (2002). *Probabilistic Basis for 2000 SAC Federal Emergency Management Agency Steel Moment Frame Guidelines*, Journal of Structural Engineering, 128(4), pp: 526-533.
- Der Kiureghian, A. (1981). *A Response Spectrum Method for Random Vibration Analysis of MDF Systems*, Earthquake Engineering and Structural Dynamics, 9, pp: 419-435.
- Der Kiureghian, A. (2002). *Bayesian Methods for Seismic Fragility Assessment of Lifeline Components*, Acceptable Risk Processes: Lifelines and Natural Hazards, Monograph No. 21, A. D. Kiureghian ed., Technical Council for Lifeline Earthquake Engineering, ASCE, Reston, VA.
- Duan, L., Li, F. (2003). *Seismic Design Philosophies and Performance-Based Design Criteria*, Bridge Engineering – Seismic Design, Edited by Wai-Fah Chen and Lian Duan, CRC Press LLC, Boca Raton, FL, ISBN: 0-8493-1683-9/02.

- Duenas-Osorio, L., Padgett, J. E. (2011). *Seismic Reliability Assessment of Bridges with User-Defined System Failure Events*, Journal of Engineering Mechanics, 137(10), pp: 680-690.
- Dutta, A. (1999). *On Energy Based Seismic Analysis and Design of Highway Bridges*, Ph.D. Thesis, University at Buffalo, The State University of New York, Buffalo, NY.
- Ellingwood, B. R., Hwang, H. (1985). *Probabilistic Descriptions of Resistance of Safety-Related Structures in Nuclear Plants*, Nuclear Engineering and Design, 88(2), 169-178.
- Ellingwood, B. R., Wen, Y.-K. (2005). *Risk-Benefit-Based Design Decisions for Low-Probability/High Consequence Earthquake Events in Mid-America*, Progress on Structural Engineering and Materials, 7(2), pp: 56-70.
- Elnashai, A., Borzi, B., Vlachos, S. (2004). *Deformation-Based Vulnerability Functions for RC Bridges*, Structural Engineering and Mechanics, 17(2), pp: 215-244.
- Fajfar, P. (2000). *A nonlinear analysis method for performance-based seismic design*, Earthquake Spectra, 16(3), pp: 573-592.
- Fang, J., Li, Q., Jeary, A., Liu, D. (1999). *Damping of Tall Buildings: Its Evaluation and Probabilistic Characteristics*, Structural Design of Tall Buildings, 8(2), pp: 145-153.
- FEMA-273 (1997). *NEHRP Guidelines for the Seismic Rehabilitation of Buildings*, Report No. FEMA-273, Building Seismic Safety Council Seismic Rehabilitation Project, Federal Emergency Management Agency, Washington, DC,
- FEMA-350 (2000). *Recommended seismic design criteria for new steel moment-frame buildings*, Report No. FEMA-350, SAC Joint Venture, Federal Emergency Management Agency, Washington, DC.
- FEMA-351 (2000). *Recommended seismic evaluation and upgrade criteria for existing welded steel moment-frame buildings*, Report No. FEMA-351, SAC Joint Venture, Federal Emergency Management Agency, Washington, DC.
- FEMA (2006). *FEMA 454: Designing for Earthquakes: A Manual for Architects*, Federal Emergency Management Agency, U.S. Department of Homeland Security, Washington, DC.
- FHWA (2010). *Conditions and Performance Report*, U.S. Department of Transportation, Federal Highway Administration, Washington, DC.
- Filippou, F. C., Popov, E. P., Bertero, V. V. (1983). *Effects of Bond Deterioration on Hysteretic Behavior of Reinforced Concrete Joints*, Report No. EERC 83-19, Earthquake Engineering Research Center, University of California, Berkeley, CA.
- Gardoni, P., Der Kiureghian, A., Mosalam, K. M. (2002). *Probabilistic capacity models and fragility estimates for reinforced concrete columns based on experimental observations*, Journal of Engineering Mechanics, 128(10), pp: 1024-1038.

- Gardoni, P., Mosalam, K. M., Der Kiureghian, A. (2003). *Probabilistic seismic demand models and fragility estimates for RC bridges*, Journal of Earthquake Engineering, 7(1), pp: 79-106.
- Ghosh, J., Padgett, J. E., Duenas-Osorio, L. (2012). *Comparative Assessment of Different Surrogate Modeling Strategies with Application to Aging Bridge Seismic Fragility Analysis*, Proceedings of the 2012 Joint Conference of the Engineering Mechanics Institute and the 11th ASCE Joint Specialty Conference on Probabilistic Mechanics and Structural Reliability, Notre Dame, IN.
- Giovenale, P., Cornell, A. C., Esteva, L. (2004). *Comparing the adequacy of alternate ground motion intensity measures for the estimation of structural responses*, Earthquake Engineering and Structural Dynamics, 33(8), pp: 951-979.
- Goel R. K., Chopra, A. K. (1997). *Evaluation of Bridge Abutment Capacity and Stiffness during Earthquake*, Earthquake Spectra, 13(1), pp. 1-21.
- Guan, X. L., Melchers, R. E. (2001). *Effect of response surface parameter variation on structural reliability estimates*, Structural Safety, 23(4), pp: 429-444.
- HAZUS (1997). *Technical Manual*, Federal Emergency Management Agency, Washington DC.
- HAZUS-MH (2011). *Multi-Hazard Loss Estimation Methodology: Earthquake Model HAZUS-MH MR5 Technical Manual*, Federal Emergency Management Agency, Washington DC.
- Hines, W., Montgomery, D., Goldsman, D., Borror, C. (2003). *Probability and Statistics in Engineering*, Wiley, New York.
- Huang, Q., Gardoni, P., Hurlebaus, S. (2010). *Probabilistic Seismic Demand Models and Fragility Estimates for Reinforced Concrete Highway Bridges with One Single-Column Bent*, Journal of Engineering Mechanics, 136(11), pp: 1340-1353.
- Hwang, H., Huo, J. R. (1998). *Probabilistic Seismic Damage Assessment of Highway Bridges*, Proceedings of the 6th U.S. National Conference on Earthquake Engineering, Seattle, WA.
- Hwang, H., Jernigan, J. B., Lin, Y. W. (2000). *Evaluation of seismic damage to Memphis bridges and highway systems*, Journal of Bridge Engineering, 5(4), pp: 322-330.
- Hwang, H., Liu, J., Chiu, Y. (2000a). *Seismic Fragility Analysis of Highway Bridges*, Center for Earthquake Research and Information, The University of Memphis, Memphis, TN.
- Jeong, S. H., Elnashai, A. S. (2007). *Probabilistic Fragility Analysis Parameterized by Fundamental Response Quantities*, Engineering Structures, 29, pp: 1238-1251.
- Kaplan, S., Garrick, B. J. (1981). *On the quantitative definition of risk*, Risk analysis, 1(1), pp: 11-27.
- Keady, K. L., Alameddine F., Sardo, T. E. (2003). *Seismic Retrofit Technology*, Bridge Engineering – Seismic Design, Edited by Wai-Fah Chen and Lian Duan, CRC Press LLC, Boca Raton, FL, ISBN: 0-8493-1683-9/02.

- Kim, S. H., Shinozuka, M. (2004). *Development of fragility curves of bridges retrofitted by column jacketing*, Probabilistic Engineering Mechanics, 19, pp: 105-112.
- Kim, S. H., Mha, H. S., Lee, S. W. (2006). *Effects of bearing damage upon seismic behavior of a multi-span girder bridge*, Engineering Structures, 28(7), pp: 1071-1080.
- Koutsourelakis, P. S. (2010). *Assessing structural vulnerability against earthquakes using multi-dimensional fragility surfaces: A Bayesian framework*, Probabilistic Engineering Mechanics, 25, pp: 49-60.
- Liao, D., Yen, P. W. (2010). *A linkage tool for analyzing earthquake traffic impact in micro level based on seismic risk assessment and traffic simulation*, ACM International Conference Processing Series, 2010, COM. Geo 2010 – 1st International Conference and Exhibition on Computing for Geospatial Research and Application, Washington, DC.
- Lin, K. W., Wald, D. J. (2008). *ShakeCast Manual Open-File Report 2008-1158*, United States Geological Survey, United States Department of Interior, Washington, D.C.
- Lindley, P. B. (1992). *Engineering design with natural rubber*, Malaysia Natural Rubber Producers Research Association, Hertford, England, United Kingdom.
- LPILE (2012). *LPILE v6.0 – A Program for the Analysis and Design of Piles and Drilled Shafts Under Lateral Loads*, Ensoft, Inc. Engineering Software, Austin, Texas.
- Luco, N., Cornell, A. C. (2000). *Effects of connection fractures on SMRF seismic drift demands*, Journal of Structural Engineering, 126, pp: 127-136.
- Luco, N., Cornell, A. C. (2007). *Structure-specific scalar intensity measures for near-source and ordinary earthquake ground motions*, Earthquake Spectra, 23(2), pp:357-392.
- Luna, R., Hoffman, D., Lawrence, W. T. (2008). *Estimation of earthquake loss due to bridge damage in the St. Louis Metropolitan Area. I: Direct losses*, Natural Hazards Review, 9(1), pp: 1-11.
- Lupoi, G., Franchin, P., Lupoi, A., Pinto, P. (2006). *Seismic fragility analysis of structural systems*, Journal of Engineering Mechanics, 132(4), pp: 385-395.
- Mackie, K., Stojadinovic, B. (2001). *Probabilistic seismic demand model for California bridges*, Journal of Bridge Engineering, 6, pp: 468-480.
- Mackie, K., Stojadinovic, B. (2004). *Fragility curves for reinforced concrete highway over-pass bridges*, 13th World Conference on Earthquake Engineering, Vancouver, B.C., Canada.
- Mackie, K., and Stojadinovic, B. (2005). *Fragility Basis for California Highway Overpass Bridge Seismic Decision Making*, PEER Report 2005/02, Pacific Earthquake Engineering Research Center, University of California, Berkeley, CA.
- Mackie, K. R., Wong, J.-M., Stojadinovic, B. (2008). *Integrated Probabilistic Performance-Based Evaluation of Benchmark Reinforced Concrete Bridges*,

Report No. PEER 2007/09, Pacific Earthquake Engineering Research Center, University of California, Berkeley, CA.

- Mackie, K. R., Cronin, K. J., Nielson, B. G. (2011). *Response Sensitivity of Highway Bridges to Randomly Oriented Multi-Component Earthquake Excitation*, Journal of Earthquake Engineering, 15(6), pp: 850-876.
- Mander, J. B., Kim, D. K., Chen, S. S., and Premus, G. J. (1996). *Response of steel bridge bearings to reverse cyclic loading*, Technical Report NCEER-96-0014, NCEER, State University of New York – University at Buffalo, Buffalo, NY.
- Mander, J. B., and Basoz, N. (1999). *Seismic fragility curve theory for highway bridges*, 5th US Conference on Lifeline Earthquake Engineering, Seattle, WA.
- Mander, J. B., Dhakal, R. P., Mashiko, N., Solberg, K. M. (2007). *Incremental dynamic analysis applied to seismic financial risk assessment of bridges*, Engineering Structures, 29, pp: 2662-2672.
- Maroney, B., Ramstad, K., Kutter, B. (1993). *Experimental Testing of Laterally Loaded Large Scale Bridge Abutments*, Structural Engineering in Natural Hazards Mitigation, Irvine, CA, American Society of Civil Engineers.
- Maroney, B., Kutter, B., Romastad, K., Chai, Y. H., Vanderbilt, E. (1994). *Interpretation of Large Scale Bridge Abutment Test Results*, Proceedings of the 3rd Annual Seismic Research Workshop, California Department of Transportation, Sacramento, CA.
- Martin, G. R., Yan, L. (1995). *Modeling Passive Earth Pressure for Bridge Abutments, Earthquake-Induced Movements and Seismic Remediation of Existing Foundations and Abutments*, ASCE 1995 Annual National Convention, Vol. Geotechnical Special Publication 55, San Diego, CA.
- McKay, M. D., Conover, W. J., Beckman, R. J. (1979). *A comparison of three methods for selecting values of input variables in the analysis of output from a computer code*, Technometrics, 21, pp: 239-245.
- McKenna, F., Scott, M., Fenves, G. L. (2010). *Nonlinear Finite-Element Analysis Software Architecture Using Object Composition*, Journal of Computing in Civil Engineering, Vol. 24, No. 1, pp. 95-107.
- Megally, S. H., Silva, P. F., Seible, F. (2002). *Seismic Response of Sacrificial Shear Keys in Bridge Abutments*, Structural Systems Research Project SSRP-2001/24, University of California, San Diego, La Jolla, CA.
- Melchers, R. E. (1999). *Structural Reliability Analysis and Prediction*, John Wiley and Sons, 2nd Edition, ISBN: 978-0471987710.
- Menegotto, M., Pinto, P. E. (1973). *Method of Analysis for Cyclically Loaded Reinforced Concrete Plane Frames Including Changes in Geometry and Non-Elastic Behavior of Elements Under Combined Normal Force and Bending*, Proceedings of the IABSE Symposium on Resistance and Ultimate Deformability of Structures Acted on by Well-Defined Repeated Loads, Lisbon, Portugal, pp: 15-22.

- Moehle, J., Fenves, G., Mayes, R., Priestley, N., Seible, F., Uang, C.-M., Werner, S., Aschheim, M. (1995). *Highway Bridges and Traffic Management*, Earthquake Spectra, 11, pp: 287-372.
- Moehle, J. P., Eberhard, M. O. (2003). *Earthquake Damage to Bridges*, Bridge Engineering – Seismic Design, Edited by Wai-Fah Chen and Lian Duan, CRC Press LLC, Boca Raton, FL, ISBN: 0-8493-1683-9/02.
- Moore, J. E., Kiremidjian, A., Chiu, S. (2000). *Seismic risk model for a designated highway system: Oakland/San Francisco Bay Area*, PEER Report No. 2002/02, U.S.-Japan Workshop on the Effects of Near-Field Earthquake Shaking, Pacific Earthquake Engineering Research Center, University of California, Berkeley, CA.
- MTD 5-1 (1992). *Bridge Memo to Designers (5-1)*, California Department of Transportation, Sacramento, CA.
- MTD 7-1 (1994). *Bridge Memo to Designers (7-1)*, California Department of Transportation, Sacramento, CA.
- MTD 20-4 (1995). *Bridge Memo to Designers (20-4)*, California Department of Transportation, Sacramento, CA.
- MTD 20-1 (1999). *Bridge Memo to Designers (20-1) – Seismic Design Methodology*, California Department of Transportation, Sacramento, CA.
- Mtenga, P. V. (2007). *Elastomeric Bearing Pads under Combined Loading*, Report to the Florida Department of Transportation, Contract No: BC352-16, Tallahassee, FL.
- Muthukumar, S. (2003). *A Contact Element Approach with Hysteresis Damping for the Analysis and Design of Pounding in Bridges*, Ph.D. Dissertation, Georgia Institute of Technology.
- NBI Coding Guide (1995). *Recording and Coding Guide for the Structure Inventory and Appraisal of the Nation's Bridges*, Report No. FHWA-PD-96-001, U.S. Department of Transportation, Federal Highway Administration, Office of Engineering Bridge Division, Washington, DC.
- NBI (2010). *National Bridge Inventory Data*, U.S. Department of Transportation, Federal Highway Administration, Washington, DC, available at: <http://www.fhwa.dot.gov/bridge/nbi/ascii.cfm>.
- Nielson, B. G. (2005). *Analytical Fragility Curves for Highway Bridges in Moderate Seismic Zones*, Ph.D. Dissertation, Georgia Institute of Technology, Atlanta, GA.
- Nielson, B. G., DesRoches, R. (2007). *Analytical Seismic Fragility Curves for Typical Bridges in the Central and Southeastern United States*, Earthquake Spectra, 23, pp: 615-633.
- Padgett, J. E. (2007). *Seismic Vulnerability Assessment of Retrofitted Bridges using Probabilistic Methods*, Ph.D. Dissertation, Georgia Institute of Technology, Atlanta, GA.

- Padgett, J. E., DesRoches, R. (2007). *Bridge Functionality Relationships for Improved Seismic Risk Assessment of Transportation Networks*, Earthquake Spectra, 23(1), pp: 115-130.
- Padgett, J. E., DesRoches, R. (2008). *Methodology for Development of Analytical Fragility Curves for Retrofitted Bridges*, Earthquake Engineering and Structural Dynamics, 37(8), pp: 1157-1174.
- Padgett, J. E., Nielson, B. G., DesRoches, R. (2008). Selection of optimal intensity measures in probabilistic seismic demand models of highway bridge portfolios, Earthquake Engineering and Structural Dynamics, 37(5), pp: 711-725.
- Padgett, J. E., Dennemann, K., Ghosh, J. (2010). *Risk-based seismic life-cycle cost-benefit (LCC-B) analysis for bridge retrofit assessment*, Structural Safety, 32(3), pp: 165-173.
- Pan, Y., Agrawal, A. K., Ghosh, M., Alampalli, S. (2010). *Seismic Fragility of Multispan Simply Supported Steel Highway Bridges in New York State. II: Fragility Analysis, Fragility Curves, and Fragility Surfaces*, Journal of Bridge Engineering, 15(5), pp: 462-472.
- Priestley, M. J. N., Seible, F., Calvi, G. M. (1996). *Seismic Design and Retrofit of Bridges*, John Wiley & Sons, Inc., New York, NY, ISBN: 0-471-57998-X.
- Rajashekhar, M. R., Ellingwood, B. R. (1993). *A new look at the response surface approach for reliability analysis*, Structural Safety, 12(3), pp: 205-220.
- Ramanathan, K., DesRoches, R., Padgett, J. E. (2010). *Analytical Fragility Curves for Multispan Continuous Steel Girder Bridges in Moderate Seismic Zones*, Transportation Research Record: Journal of the Transportation Research Board, 2202, pp: 173-182.
- Ramanathan, K., DesRoches, R., Padgett, J. E. (2012). *A Comparison of Pre- and Post-Seismic Design Considerations in Moderate Seismic Zones through the Fragility Assessment of Multispan Bridge Classes*, Engineering Structures (In Review).
- Rosenblueth, E. (1951). *A Basis for Aseismic Design*, Ph.D. Thesis, University of Illinois, Urbana, IL.
- Sahs, S., Veletzos, M., Panagiotou, M., Restrepo, J. (2008). *Visual Inspection and Capacity Assessment of Earthquake Damaged Reinforced Concrete Bridge Elements: Integrate Research and Deployment Final Report*, California Department of Transportation, Sacramento, CA.
- Saiidi, M., Maragakis, E. A., Feng, S. (1996). *Parameters in Bridge Restrainer Design for Seismic Retrofit*, Journal of Structural Engineering, 122(1), pp. 61-68.
- Saiidi, M., Randall, M., Maragakis, E., Isakovic, T. (2001). *Seismic Restrainer Design Methods for Simply Supported Bridges*, Journal of Bridge Engineering, 6(5), pp. 307-315.
- Scharge, L. (1981). *Anchoring of Bearings by Friction, Joint Sealing and Bearing Systems for Concrete Structures*, World Congress on Joints and Bearings, Vol. 1, American Concrete Institute, Niagara Falls, NY.

- SDC (1990). *Caltrans Structures Seismic Design Reference*, California Department of Transportation, Sacramento, CA.
- SDC (1999). *Seismic Design Criteria*, Version 1, California Department of Transportation, Sacramento, CA.
- SDC (2010). *Seismic Design Criteria*, Version 1.6, California Department of Transportation, Sacramento, CA.
- Shafieezadeh, A., Ramanathan, K., DesRoches, R., Padgett, J. E. (2011). *Fractional order intensity measures for probabilistic seismic demand modeling applied to highway bridges*, Earthquake Engineering and Structural Dynamics, DOI: 10.1002/eqe.1135.
- Shamsabadi, A., Yan, L. (2008). *Closed-Form Force-Displacement Backbone Curves for Bridge Abutment Backfill Systems*, Proceedings of the Geotechnical Earthquake Engineering and Soil Dynamics IV Congress, American Society of Civil Engineers.
- Shantz, T. (2011). *Personal Communication Regarding Modeling the Stiffness for Foundation Translational and Rotational Springs*, California Department of Transportation, Sacramento, CA.
- Shinozuka, M., Feng, M. Q., Kim, H.-K., Kim, S.-H. (2000). *Nonlinear Static Procedure for Fragility Curve Development*, Journal of Engineering Mechanics, 126(12), pp: 1287-1296.
- Shinozuka, M., Feng, M. Q., Kim, H., Uzawa, T. Ueda, T. (2003). *Statistical Analysis of Fragility Curves*, Report No. MCEER-03-0002, MCEER, University at Buffalo, The State University of New York, Buffalo, NY.
- Shome, N., Cornell, A. C. (1999). *Probabilistic Seismic Demand Analysis of Nonlinear Structures*, Reliability of Marine Structures Program Report No. RMS-35, Department of Civil and Environmental Engineering, Stanford University, CA.
- Singhal, A., Kiremidjian, A. S. (1996). *Bayesian updating of fragilities with application to RC frames*, Journal of Structural Engineering, 124(8), pp: 922-929.
- Song, J., Kang, W.-H. (2009). *System reliability and sensitivity under statistical dependence by matrix-based system reliability method*, Structural Safety, 31(2), pp: 148-156.
- Vamvatsikos, D., Cornell, A. C. (2002). *Incremental Dynamic Analysis*, Earthquake Engineering and Structural Dynamics, 31, pp: 491-514.
- Veletzis M. J., Panagiotou, M., Restrepo, J. I. (2006). *Post Seismic Inspection and Capacity Assessment of Reinforced Concrete Bridges*, Report No. SSRP-06/19, Report submitted to the California Department of Transportation, University of California, San Diego, CA.
- Wight, J., MacGregor, J. (2011). *Reinforced Concrete: Mechanics and Design*, 6th Edition, Prentice Hall, ISBN-10: 0132176521, ISBN-13: 9780132176521.

- Werner, S. D., Lavoie, J.-P., Eitzel, C., Cho, S., Huyck, C., Ghosh, S., Eguchi, R. T., Taylor, C. E., Moore II, J. E. (2003). *REDARS 1: Demonstration Software for Seismic Risk Analysis of Highway Systems*, <<http://mceer.buffalo.edu/publications/resacomm/03-SP01/02werner.pdf>>
- Werner, S. D., Taylor, C. E., Sungbin, C., Lavoie, J.-P., Huyck, C. K., Eitzel, C., Eguchi, R. T., Moore, J. E. (2004). *New developments in the seismic risk analysis of highway systems*, Proceedings of the 13th World Conference on Earthquake Engineering, Vancouver, Canada.
- Whitman, R. V., Biggs, J. M., Brennan III, J. E., Cornell, A. C., de Neufville, R. L., Vanmarcke, E. H. (1975). *Seismic Design Decision Analysis*, Journal of Structural Division, 101(ST5), pp: 1067-1084.
- Yamazaki, F., Hamada, T., Motoyama, H., Yamauchi, H. (1999). *Earthquake Damage Assessment of Expressway Bridges in Japan*, Technical Council on Lifeline Earthquake Engineering Monograph, 16, pp: 361-370.
- Yashinsky, M. (1995). *Northridge Earthquake: Lifeline Performance and Post-Earthquake Response*, Technical Council on Lifeline Earthquake Engineering Monograph No. 8, Washington, D.C.
- Yashinsky, M., Karshenas, M. J. (2003) *Fundamentals of Seismic Protection for Bridges*, EERI Monograph #9, Oakland, CA.
- Yu. O., Allen, D. L., and Drnevich, V. P. (1991). *Seismic Vulnerability Assessment of Bridges on Earthquake Priority Routes in Western Kentucky*, 3rd US National Conference on Lifeline Earthquake Engineering, Los Angeles, CA.
- Zhang, J., Huo, Y. (2009). *Evaluating effectiveness and optimum design of isolation devices for highway bridges using the fragility function method*, Engineering Structures, 31, pp: 1648-1660.
- Zhong, J., Gardoni, P., Rosowsky, D., Haukaas, T. (2008). *Probabilistic seismic demand models and fragility estimates for reinforced concrete bridges with two-column bents*, Journal of Engineering Mechanics, 134(6), pp: 495-504.
- Zhou, Y., Banerjee, S., Shinozuka, M. (2010). *Socio-economic effect of seismic retrofit of bridges for highway transportation networks: A pilot study*, Structure and Infrastructure Engineering, 6(1-2), pp: 145-157.

VITA

KARTHIK NARAYAN RAMANATHAN

Karthik Ramanathan was born on December 6, 1984 in Chennai, India and grew up entirely in Hyderabad, India. Upon graduating High School in 2002, he entered Osmania University in Hyderabad. He obtained his Bachelor of Engineering degree in Civil Engineering in 2006. Upon completion of his Bachelor's degree, he continued to graduate school at the University of Pittsburgh pursuing a Master's degree in Civil Engineering with emphasis in Structural Engineering and Mechanics. Having obtained his Master's degree in Spring 2008, he continued to Georgia Institute of Technology to pursue his Doctoral studies in Civil Engineering starting in Fall 2008 with a special emphasis in Earthquake Engineering and minor in Computational Mechanics. He obtained another Master's Degree in Civil Engineering enroute his doctoral degree in Spring 2011.